Electrochemical Studies of Mixed Halo Phosphine/Arsine Osmium (III) Complexes

Nicholas N. Payne

Ph.D. Thesis
University Of Edinburgh
1997

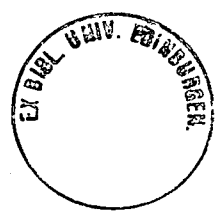

Declaration

Except where specific reference is made to other sources, the work presented in this thesis is the original work of the author. It has not been submitted, in whole or in part for any other degree.

Abstract

A series of complexes of general formula $[OsX_3L_3]$ and $[OsCl_3L_2L']$ where X is a chloride or bromide and L and L' are different tertiary phosphines or arsines have been synthesised. The X-ray diffraction crystal structures of the complexes, *mer*-$[OsCl_3(PMe_2Ph)_3]$, *mer*-$[OsCl_3(PEt_2Ph)_3]$, *mer*-$[OsBr_3(PPr^n_3)_3]$, *mer*-$[OsCl_3(AsMe_2Ph)_3]$, *mer*-$[OsCl_3(PPr^n_2)_2(AsPr^n_3)]$, *mer*-$[OsCl_3(PPr^n_2)_2(PEtPh_2)]$ and *mer*-$[OsCl_3(P(OMe)_2Ph)_2(AsPr^n_3)]$ show them to have slightly distorted octahedral metal environments with the *trans* influence of the Group 15 ligands evident.

The *mer* complexes have been studied electrochemically and all show two one-electron processes; an oxidation and a reduction process. Both couples involve the osmium metal centre. The one electron reduction step is rapidly followed by a chemical reaction resulting in the formation of an electroactive daughter product of general formula $[OsCl_2L_3Y]$ where Y is a neutral coordinating ligand. The chemical reaction has been studied by kinetic and spectrochemical methods. The redox potentials of the *mer* species gives a good linear correlation with Tolmans electronic parameter for the tertiary phosphine. The electronic spectra of the compounds have been recorded and the peaks assigned to specific electronic transitions *via* the use of Extended Hückel Molecular Orbital Calculations. Electrochemical elucidation of these systems have shown that the redox potentials of the complexes are predominately dependent on one ligand namely the phosphine/arsine *trans* to the halide.

The *fac* isomers also show two metal based one-electron couples at very different potentials from the analogous *mer* isomers. The reduction also produces an electroactive daughter product. The oxidation results in the isomerisation of the *fac* isomer to that of the *mer* isomer. The kinetic parameters of the reaction have been measured and a mechanism is proposed for the isomerisation.

Acknowledgements

I have been privileged to have the opportunity to work with many people throughout my Ph.D. here I would like to thank them.

First and foremost I would like to thank my Supervisor, Dr. Lesley J. Yellowlees for her constant enthusiasm, encouragement, support and friendship throughout my four years in the laboratory.

I would like to express my gratitude to Prof. Alan J. Welch of Heriot Watt University for letting me use the EHMO calculation software and for sparing the time to show me how it works. Thanks to Drs. Frank Mabbs and Eric J. McInnes of The University Of Manchester for spending so much time measuring the ESR spectra of my compounds. Although the results are not reported here their efforts are much appreciated. I would also like to thank Dr. Alan Brown for results quoted in Chapter 5.

For their help with the crystallography, thank you to Dr Simon Parsons, Dr Craig Grant and Steven Harris for their patience teaching me the basics. I am grateful to the E.P.S.R.C. for financial support, and the University Of Edinburgh for the use of their facilities. Also thanks to the ERASMUS scheme for three months spent in the University Of Amsterdam and to Rob for making my time there fun.

I am deeply indebted to my parents for their support and encouragement throughout my time at the University Of Edinburgh. Without them I would not be where I am today.

I would like to thank all the people that have made my time at the University of Edinburgh a memorable one, in chemistry namely Ally B, Ally T, Carole, David, Eric, Gideon, Jane, Kathy, Ken, Lorenzo, Massimo, Phil, Ruth and Xiao Ming, whilst "across the road" in Darwin; Anthony, Craig, Darren, Hat and Simone.

Last but no way least, Jo. Thank you for putting up with me for the last year during the writing of this, and for making my life infinitely better.

Table of Contents

List Of Figures

Chapter 1

Chapter 2

Chapter 3

Chapter 4

Chapter 5

Chapter 6

Appendix

List Of Tables

Chapter 1

Chapter 2

Chapter 3

Chapter 4

Chapter 5

Chapter 6

Appendix

Abbreviations

A	Amps
AO	Atomic Orbital
CV	Cyclic Voltammogram
dmf	dimethylformide
E	Potential
EHMO	Extended Hükel Molecular Orbital
EPR	Electron Spin Resonance
Et	ethyl
fac	facial
HOMO	Highest Occupied Molecular Orbital
i	Current
IR	Infra Red
LMCT	Ligand to Metal Charge Transfer
LUMO	Lowest Unoccupied Molecular Orbital
Me	methyl
mer	meridian
MLCT	Metal to Ligand Charge Transfer
MO	Molecular Orbital
NIR	Near Intra Red
NMR	Nuclear Magnetic Resonance
OTE	Optically Transparent Electrode
Ph	phenyl
Pr	propyl
RT	Room Temperature
SOMO	Singly Occupied Molecular Orbital
thf	tetrahydrofuran
UV	Ultra Violet
V	Volts
Vis	Visible

Chapter 1

Introduction of Osmium Halide/Group 15 Complexes

Structure, Electrochemistry and Spectroelectrochemistry of *mer*-$[OsCl_3(PMe_2Ph)_3]$

1.1 Introduction

Coordination compounds of osmium with mixed halide and group 15 ligands were first reported by Nyholm *et. al.*[1] in the 1940's. They synthesised a series of compounds of type $[OsX_3L_3]$ (1) and $[OsX_2L_4]$ (2) (where X was chloride or bromide and L was dimethylphenylarsine). This was followed in the late 1950's with a report on the complexes formed between halo osmium compounds with di(tertiary) arsine ligands.[2]

Analogous phosphine and stibine complexes were not reported until the next decade, with Vaska[3] synthesising complexes of type (1) with bromine and triphenyl-phosphine, -arsine and -stibine. These were followed by the work of Araneo *et. al.*[4] who produced the complex $[OsCl_3(SbPh_3)_3]$. However it was the pioneering work of Chatt *et. al.*[5] that led to a range of mono- and bi-nuclear phosphine and arsine donor ligand complexes being formed.

The first discovered and most stable of these types of compounds were the binuclear species $[Os_2Cl_3(PR_3)_6]^+$ which possess the now well characterised confacial bioctahedral triple halide bridged structure. These complexes have been well studied in this laboratory.[6]

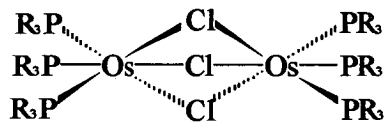

It was not until 1968 that Chatt *et. al.*[7] published details of their first monomeric complexes, of the type (1) and $[OsX_4L_2]$ (3). Reaction of osmium tetroxide in concentrated HX, with a range of phosphine and arsine ligands resulted in a stepwise substitution as shown in Scheme 1.1.

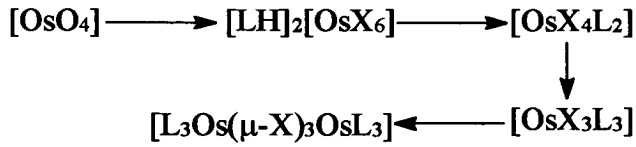

Scheme 1.1

Thus OsO_4 was dissolved in ethanol containing hydrohalic acid to prevent volatilisation by converting the oxide to $[H]_2[OsX_6]$ which was then reacted with

tertiary phosphine or arsine. Complexes of type (**2**) could only be synthesised with less reactive phosphines and arsines.

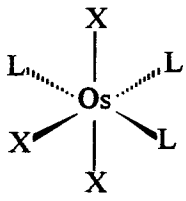

Type 1 - *mer*

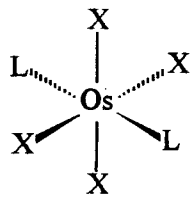

Type 3 - *trans*

The configurations of the complexes formed by Chatt and co-workers, were confirmed by far infra-red studies later that same year, showing that type (**1**) compounds have *mer* and (**3**) have *trans* configurations.[8] The series were also the focus of other studies in the following 3 years.

Hudson and Kennedy[9] recorded the Electron Spin Resonance (ESR) spectra of several low spin d^5 osmium, iridium and ruthenium complexes. The osmium complexes of type *mer*-$[OsX_3L_3]$, where X = Cl, L = PMe_2Ph, $PBu^n{}_2Ph$ and $AsMe_2Ph$; X = Br, L = $PBu^n{}_2Ph$, displayed two distinct peaks in the spectra, although no ligand hyperfine coupling was observed. Hill[10] recorded the single crystal spectrum of *mer*-$[RhCl_3(PEt_2Ph)_3]$ doped with *mer*-$[OsCl_3(PEt_2Ph)_3]$. He reported the principle g-tensor values as 3.32, 1.44 and 0.32, but again no ligand hyperfine was recorded.

The X-Ray Photoelectron Spectra (PES) of type (**1**) and (**3**) complexes were recorded by Leigh and Bremser[11] as part of a study of 25 transition metal complexes. The metal electron binding energies were calculated, but caution was advised by the authors in interpretation of these results. Complexes of type (**1**) and (**3**) where also the focus of a crystallographic study in 1970.[12] The structures of the series $[MCl_4(PMe_2Ph)_2]$, M = W, Re, Os, Ir or Pt and $[MCl_3(PMe_2Ph)_3]$ where M = Re, Os or Ir, were solved and the bond lengths reported and discussed.

The Ultra Violet/Visible (UV/Vis) spectra of the series *mer*-$[MX_3L_3]$ where M = Re, Ru or Os and *trans*-$[MX_4L_2]$ where M = Re, Os, Ir, Pt, were also reported.[13] The lowest energy charge transfer bands were assigned and their energies rationalised by the concept of electronegativity. The magnetic susceptibilities of type (**3**) complexes were recorded and discussed by the same group that year.[14]

Chatt *et. al.*[7] also claimed, that triphenylphosphine was a special case, reacting analogously to the rhenium complex,[15] forming the product $[OsOCl_3(PPh_3)_2]$. This was later found to be in error, when it was discovered that the product was actually a

mixture of $[OsO_2Cl_2(PPh_3)_2]$ and *trans*-$[OsCl_4(PPh_3)_2]$,[16] the former a subject of further study in its own right.[17]

Hoffman and Caulton[18] claimed that changing the solvent from ethanol to a tertiary-butanol/water mixture, produced the 5 coordinate complex $[OsCl_2(PPh_3)_3]$, which is analogous to the bromide complex reported by Vaska.[3] They assigned the configuration of $[OsCl_2(PPh_3)_3]$ as square planar which was later confirmed by X-ray crystallography.[19] It was surmised from this structure that the bulk of the phenyl groups prevented the sixth coordination site from being used. The same coordination structure was found for $[RuCl_2(PPh_3)_2]$ in both solution and solid state.[18,20] The stability in the system arising from either intramolecular blocking of the vacant sixth site by a phenyl ring or an agostic bonding interaction between an ortho hydrogen on the phenyl group and the metal centre.[21]

The bromide analogue of this complex $[OsBr_2\{PPh_3)_3]$ reacted with carboxylic acids, RCO_2H (R is aryl or alkyl), in benzene afford air stable derivatives of type $[OsBr_2(O_2CR)(PPh_3)_2]$.[22] A X-ray crystal structure of one of these complexes was later reported, showing the osmium to be in a slightly distorted octahedral environment with *cis* bromide and *trans* phosphine ligands.[23]

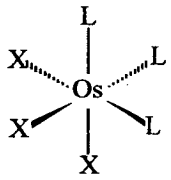

fac isomer

The first facial isomers of $[OsX_3L_3]$were detailed in 1970, by Douglas and Shaw.[24] They were prepared by the reaction of the hydride complex, $[OsH_4L_3]$, with hydrogen chloride gas in methanol. The configuration was confirmed by comparative ir spectroscopy; the *fac*-$[OsCl_3L_3]$ complexes, had virtually identical spectra to the corresponding iridium complexes of the type *fac*-$[IrCl_3L_3]$.[25,26]

In 1967 by Shilov *et al*[27] discovered that the reduction in THF of hexachloroosmate (IV) and osmium tetroxide by hydrazine, yielded dinitrogen containing complexes. There has been considerable interest shown in low valent dinitrogen complexes of osmium. Nitrogen containing complexes of the type $[OsX_2L_3Y]$ where X is chloride or bromide, L is tertiary phosphine or arsine and Y being ammonia or primary amines, where first prepared in 1969.[28] In 1970 Chatt and co-workers[29] published the details of 12 dinitrogen complexes of the type *cis*-$[OsX_2L_3N_2]$, where X is Cl or Br and L is tertiary phosphine or arsine. Such compounds were formed by the reduction of species of type **(1)** under dinitrogen. These were investigated for catalytic behaviour in the reduction of N_2 to ammonia, but unfortunately these studies were

unsuccessful. Within the year other complexes of the type $[OsX_2L_3Y]$ (4) and $[OsX_2L_2Y_2]$ (5) were isolated with other nitrogen containing ligands, including MeCN, PhCN, MeNC, PhNC and also CO.[30]

It was not until 9 years later that further work into this area was detailed in the literature. Srinivasamurthy *et al*[31] detailed the preparation of four chloride and four bromide complexes of type (1) with tertiary arsine ligands. They also detailed analogous reaction with CO to the work of Chatt *et al* above forming the mono and bi-substituted complexes (4) and (5). Later work reported the X-ray crystal structure determination of one of these type (5) complexes, namely $[OsBr_2(CO)_2(PPh_3)_2]$, which showed an octahedral complex with the phosphines *trans* to one another, while the CO and Br are disordered around the other four positions.[32]

Complexes of type (2), are the least studied of this class of compound, with the initial report by Nyholm *et al*[1] Only in the late 1970's were a series of these compounds reported,[33] with the halide being chloride or bromide in conjunction with triphenyl-phosphine, -arsine, -stibine. This was followed 5 years later by the report of the synthesis of *trans*-$[OsCl_2(PMe_3)_4]$ by the reaction of $[OsCl_2(PPh_3)_3]$[18] with PMe_3.[34]

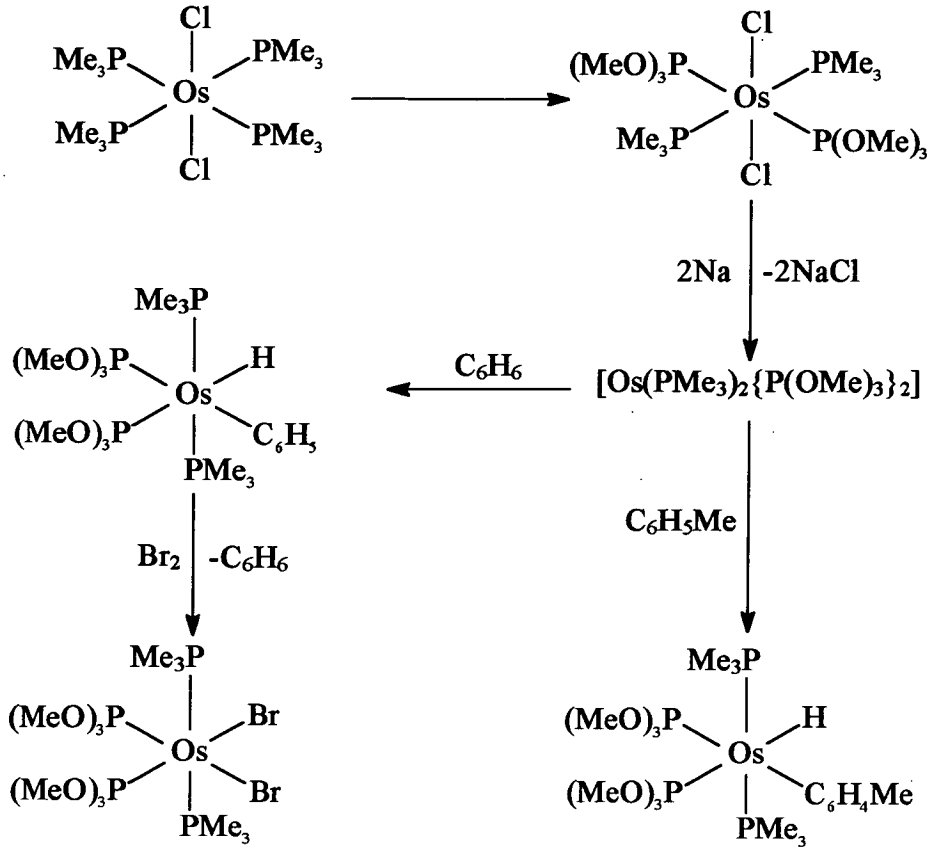

Scheme 1.2

Werner *et al*[35] undertook a detailed study into the reactions of the complex, *trans*-$[OsCl_2(PMe_3)_4]$ during the late 1980's. They showed the reaction of the complex with CO and $P(OMe)_3$ gave mono- and di-substituted derivatives of the type *trans*, *mer*-$[OsCl_2(PMe_3)_3L]$ (L is CO or $P(OMe)_3$) and all *trans*-$[OsCl_2(PMe_3)_2\{P(OMe)_3\}_2]$. The former compound when reduced leads to the addition of an arene (either benzene or toluene) forming the aryl(hydrido) complex (Scheme 1.2). The hydrido(phenyl) complex reacts further with bromine gas to form the first isolated *cis* form of a complex of type (2).

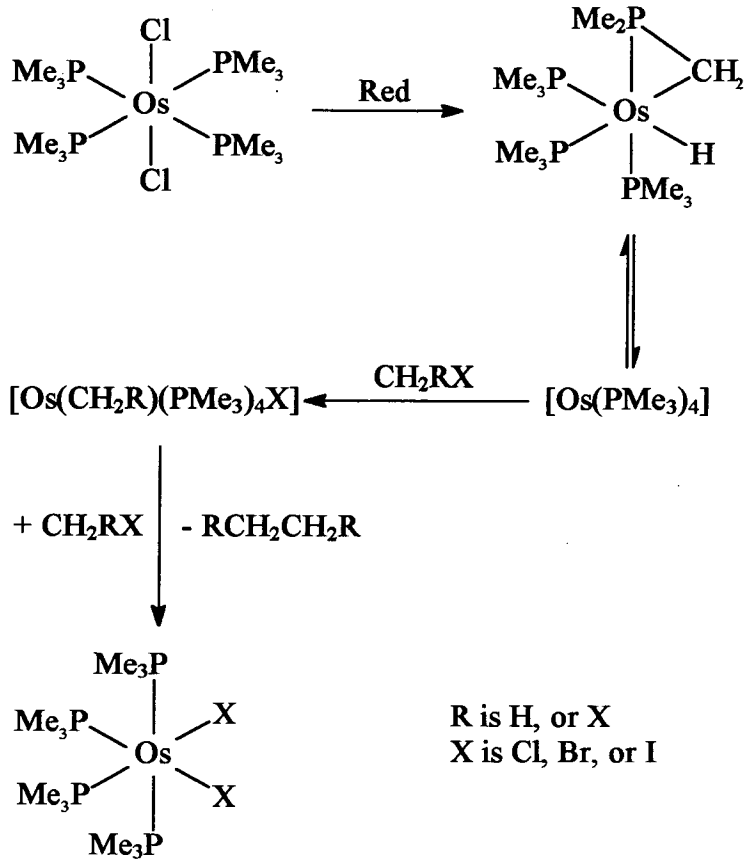

Scheme 1.3

This work was immediately followed by a report that the reduction of *trans*-$[OsCl_2(PMe_3)_4]$ by Na/Hg in the presence of naphthalene produced the complex $[OsH(\eta^2\text{-}CH_2PMe_2)(PMe_3)_3]$ which was believed to be in equilibrium with the isomer $[Os(PMe_3)_4]$.[36] The complex then reacted further with dihalomethanes CH_2X_2 (X is Cl, Br or I) and CH_3I , to form the *cis* isomer of $[OsX_2(PMe_3)_4]$. (See Scheme 1.3).

Two years later Fanwick *et al*[37] reported that the octahalodiosmate(III) anions $[Os_2X_8]^{2-}$ where X is Cl or Br, reacted with monodentate phosphines, for example PMe_3, PEt_3, PMe_2Ph and $PMePh_2$, produced various mononuclear complexes of type (1), (2) and (3). The complexes of type (1) and (3) had been already reported. This was the first report of *trans* bromide complexes of type (2) with phosphines different to PMe_3.

During the late 1980's a series of X-ray crystal structures were reported by Hinckley *et al* with triphenyl Group 15 ligands. The structures of $[OsBr_2(O_2CH_3)(PPh_3)_2]$[23]

and $[OsBr_2(CO)_2(PPh_3)_2]$[32] have already been mentioned earlier. Two others were reported, namely *mer*-$[OsCl_3(SbPh_3)_3]$[38] (Type (1)) and *trans*-$[OsBr_4(AsPh_3)_2]$.[39]

The electrochemistry of this range of compounds has only been reported by Levason *et al* who in a series of papers in the early 1990's studied the complexes of type *trans*-$[OsX_4L_2]$,[40] *mer/fac*-$[OsX_3L_3]$[41] and *trans*-$[OsX_2L_4]$,[42] where X is either chloride or bromide and L is a tertiary phosphine, arsine or stibine. In all studies the reversible electrochemical couples were reported, only passing mention was made to the other observed couples.

The aim of this work is to study further the electrochemistry of the series of compounds *mer/fac*-$[OsX_3L_3]$, where X is chloride or bromide and L is either a tertiary phosphine or arsine. Both reversible and irreversible redox couples will be detailed. There is only one report in the literature of the study of an irreversible electron transfer process occuring with complexes of this type, namely that of mer-$[OsCl_3(PMe_3Ph)_3]$ by this laboratory.[43,44] The structure, electrochemical and spectroelectrochemical study of the complex mer-$[OsCl_3(PMe_3Ph)_3]$ is now described.

1.2 Results and Discussion

1.2.1 Structure of *mer*-[$OsCl_3(PMe_2Ph)_3$]

The X-ray diffraction structure of *mer*-[$OsCl_3(PMe_2Ph)_3$] was redetermined during this study. Suitable crystals were obtained by recrystallisation from an ethanol/conc. HCl mixture. The asymmetric unit of the structure contains two equivalent discrete molecules, (Figure 1.1), selected bond distances and angles are shown in Table 1.1.

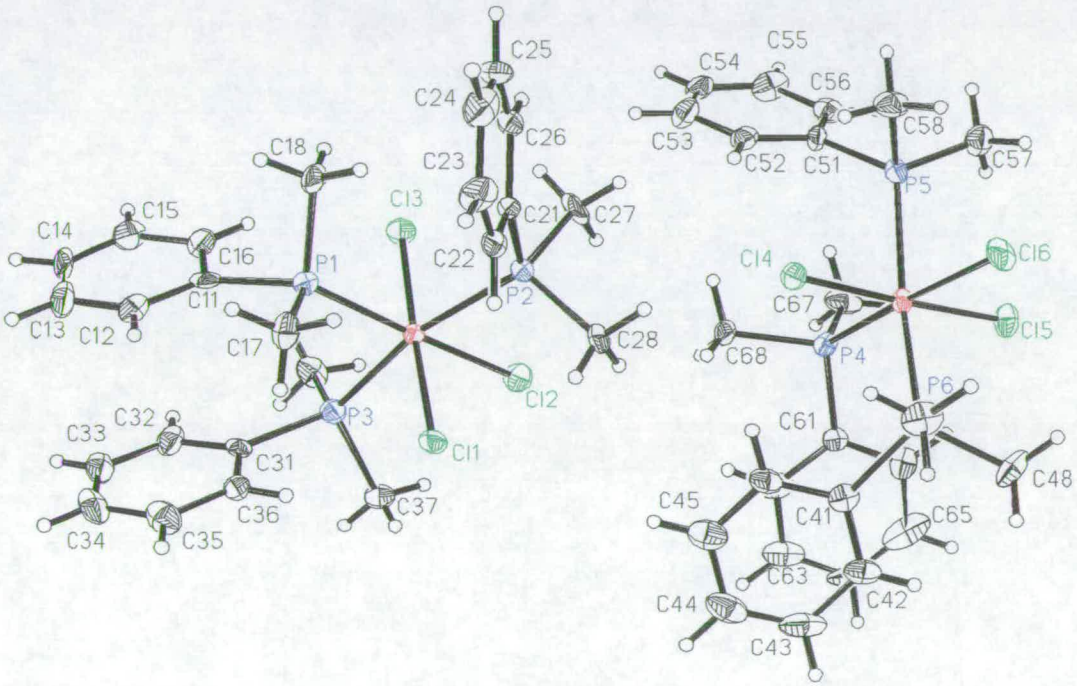

Figure 1.1 - Asymmetric Unit of *mer* - [$OsCl_3(PMe_2Ph)_3$]

Table 1.1 - Selected Bond Distance and Angles for *mer*-$[OsCl_3(PMe_2Ph)_3]$*

Os(1)-Cl(1)	2.351(2)	Os(2)-Cl(4)	2.352(2)
Os(1)-Cl(2)	2.430(2)	Os(2)-Cl(5)	2.360(2)
Os(1)-Cl(3)	2.352(2)	Os(2)-Cl(6)	2.436(2)
Os(1)-P(1)	2.351(2)	Os(2)-P(4)	2.347(2)
Os(1)-P(2)	2.413(2)	Os(2)-P(5)	2.409(2)
Os(1)-P(3)	2.399(2)	Os(2)-P(6)	2.394(2)

P(1)-Os(1)-Cl(1)	93.12(8)	P(1)-Os(1)-Cl(2)	176.84(7)	Cl(5)-Os(2)-P(6)	93.03(8)
P(1)-Os(1)-Cl(3)	88.07(8)	Cl(1)-Os(1)-Cl(2)	89.98(8)	P(4)-Os(2)-P(5)	96.35(8)
Cl(1)-Os(1)-Cl(3)	177.42(8)	Cl(3)-Os(1)-Cl(2)	88.81(8)	Cl(4)-Os(2)-P(5)	87.15(8)
P(1)-Os(1)-P(3)	94.61(8)	P(3)-Os(1)-Cl(2)	86.09(8)	Cl(5)-Os(2)-P(5)	91.17(8)
Cl(1)-Os(1)-P(3)	88.44(8)	P(2)-Os(1)-Cl(2)	81.80(8)	P(6)-Os(2)-P(5)	167.42(8)
Cl(3)-Os(1)-P(3)	93.75(8)	P(4)-Os(2)-Cl(4)	93.65(8)	P(4)-Os(2)-Cl(6)	174.05(9)
P(1)-Os(1)-P(2)	97.71(8)	P(4)-Os(2)-Cl(5)	87.28(9)	Cl(4)-Os(2)-Cl(6)	92.30(8)
Cl(1)-Os(1)-P(2)	87.57(8)	Cl(4)-Os(2)-Cl(5)	178.16(7)	Cl(5)-Os(2)-Cl(6)	86.78(9)
Cl(3)-Os(1)-P(2)	90.00(8)	P(4)-Os(2)-P(6)	95.68(8)	P(6)-Os(2)-Cl(6)	84.58(8)
P(3)-Os(1)-P(2)	167.24(8)	Cl(4)-Os(2)-P(6)	88.46(8)	P(5)-Os(2)-Cl(6)	83.82(8)

Each discrete molecule has a distorted octahedral structure, with the steric bulk of the phosphine ligands distorting the *trans* angle by up to 11° from 180°. The *trans* influence of the phosphine causes the lengthening of the Os-Cl(2) and Os-Cl(6) bond by an average of 0.079Å.

* For Full Details on the Structure and Refinement used see Appendix

1.2.2 Electrochemistry of *mer*-$[OsCl_3(PMe_2Ph)_3]$

The electrochemical response† of *mer*-$[OsCl_3(PMe_2Ph)_3]$ in CH_2Cl_2/0.5M [TBA][BF_4] at room temperature displays two separate electrochemical processes as shown by the cyclic voltammetric behaviour of the complex in Figure 1.2. Coulometric studies and Tafel plot analysis show that both couples involve 1 electron. The oxidation (A in Figure 1.2) is assigned as an Os(III) $\rightarrow$ Os(IV) + e^- electrode process and the reduction (B) as an Os(III) + $e^- \rightarrow$ Os(II) electrode process with a rapid subsequent chemical reaction an ec reaction, forming a product C visable on the 2nd scan.

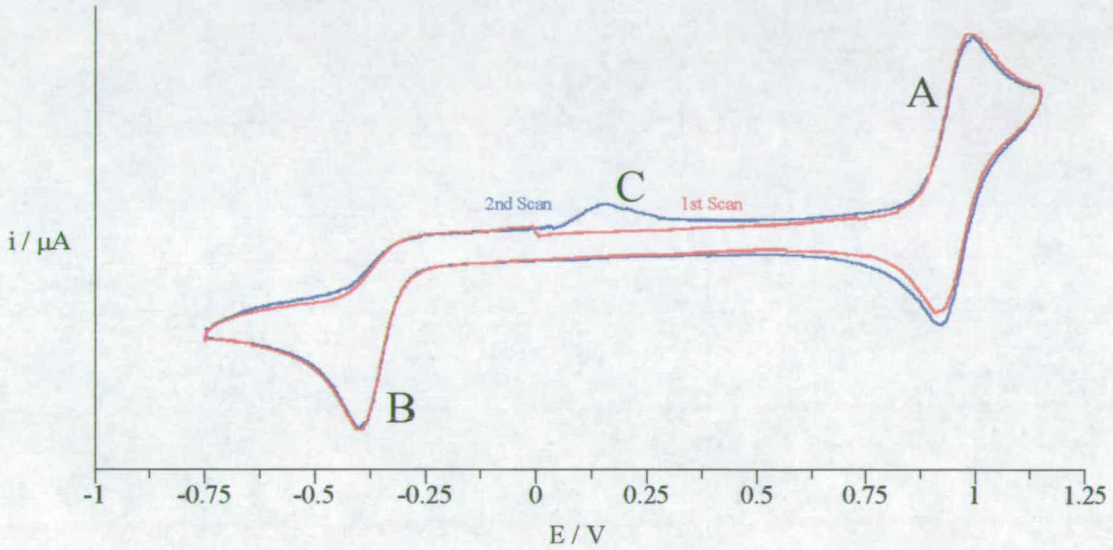

Figure 1.2 - Cyclic Voltammogram of *mer*-$[OsCl_3(PMe_2Ph)_3]$ in CH_2Cl_2/0.5M [TBA][BF_4] at RT at 100mVs^{-1} (*vs.* Ag/AgCl)

At 233K the reduction becomes fully reversible at 100mVs^{-1}, see Figure 1.3 with the ratio of cathodic to anodic peaks, i_p^c:i_p^a, being equal to one, for both oxidation and reduction processes and the peak to peak separation measured as 50mV and 49mV respectively, compared with a theoretical value of 44mV for a Nernstian one electron wave at 233K. Therefore decreasing the temperature stabilises the anion $[OsCl_3(PMe_2Ph)_3]^-$ over the period of the electrochemical experiment (i.e. a matter of a few seconds).

† The electrochemical techniques and equipment employed are described in Chapters 4 and 6 respectively.

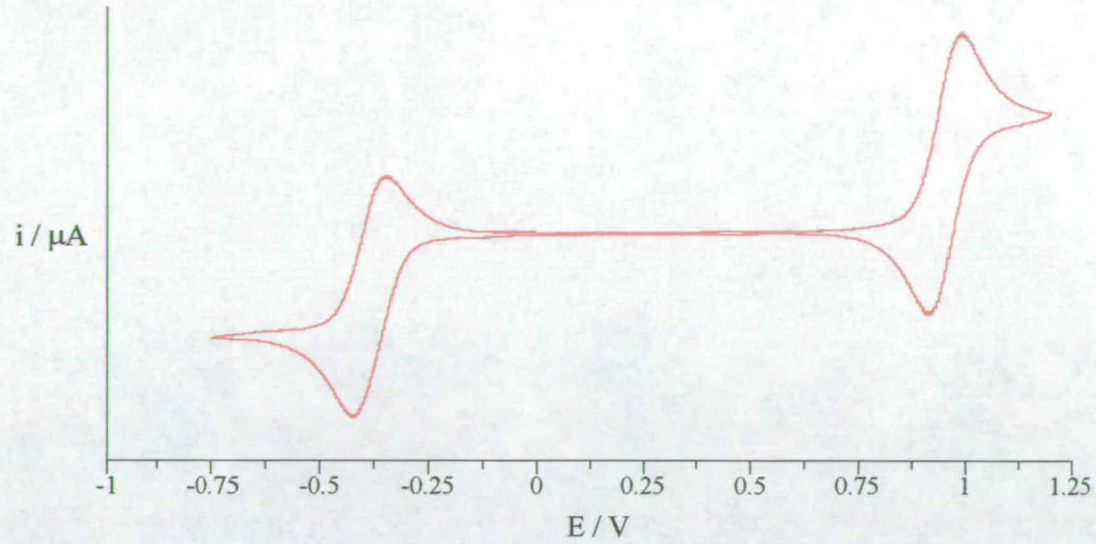

Figure 1.3 - Cyclic Voltammogram of *mer*-$[OsCl_3(PMe_2Ph)_3]$ in CH_2Cl_2/0.5M [TBA][BF_4] at 233K (100 mVs^{-1})

Full characterisation of the anion was achieved by variation of the solvent/electrolyte composition, that is employing $[NR_3Me][BF_4]$ (where R = C_8H_{17} to $C_{10}H_{21}$) as inert electrolyte in CH_2Cl_2. In such a solvent system the fully reversible cyclic voltammetric response of the reduction process could be achieved at room temperature, that is a CV resembling Figure 1.3 could be obtained at room temperature. Bulk electroreduction of the solution yields $[OsCl_3(PMe_2Ph)_3]^-$ and the $^{31}P\{^1H\}$ N.M.R. show the anion to be in the *mer* configuration.[43,44]

Bulk electroreduction of the compound in CH_2Cl_2/0.5M [TBA][BF_4] at room temperature under argon gives a yellowish green coloured solution. The solution shows no sign of $[OsCl_3(PMe_2Ph)_3]$ or $[OsCl_3(PMe_2Ph)_3]^-$ but does contain free chloride and a new Os(II) complex, as evidenced by a new irreversible wave at +1.20V and a reversible oxidation at 0.03V respectively. Thus the following rapid chemical reaction involves the loss of chloride to form $[OsCl_2(PMe_2Ph)_3]$. The exact nature of the five coordinate species is unknown, but the analogous complex $[RuCl_2(PPh_3)_3]$ has square pyramidal co-ordination geometry both in solution and solid state.[18,20]

When the same electrogeneration experiment is carried out in the presence of a neutral coordinating ligand, the 5-coordinate intermediate readily reacted to form a more stable 6-coordinate species. Figure 1.4 shows the cyclic voltammetric response of *mer*-$[OsCl_3(PMe_2Ph)_3]$ in MeCN/0.1M [TBA][BF_4] at room temperature.

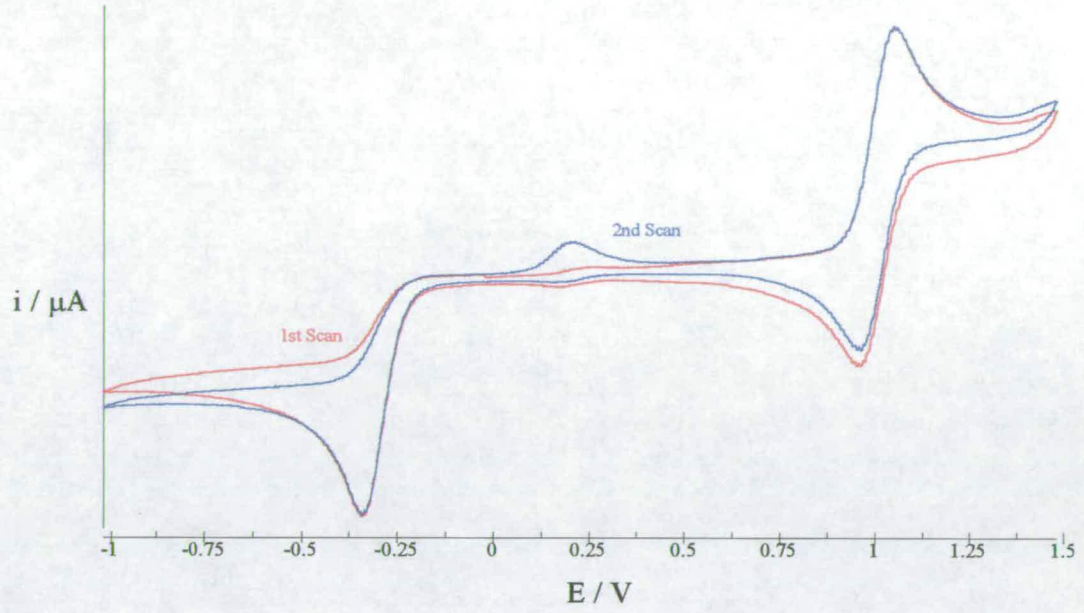

Figure 1.4 - Cyclic Voltammogram of *mer*-$[OsCl_3(PMe_2Ph)_3]$ in MeCN/0.1M [TBA][BF_4] at Room Temperature at 100mVs^{-1}

The second scan, shows a new redox process at 0.25V. The species responsible for this electrochemical is the daughter product of the ec reaction. In acetonitrile the daughter product is the neutral six coordinate complex $[OsCl_2(PMe_2Ph)_3(MeCN)]$. The acetonitrile containing complex can be electrogenerated in bulk. Figure 1.5 shows the resulting electrochemical response of $[OsCl_2(PMe_2Ph)_3(MeCN)]$ in MeCN/0.1M [TBA][BF_4], after removal of free halide with Na[BF_4]. The initial product has been characterised as the *trans* form, by $^{31}P\{^1H\}$ NMR. The *trans*-$[OsCl_2(PMe_2Ph)_3(MeCN)]$ slowly isomerises to the thermodynamically favoured *cis* form which exhibits a very different $^{31}P\{^1H\}$ NMR spectrum from the *trans* isomer. The two isomers are indistinguishable electrochemically.

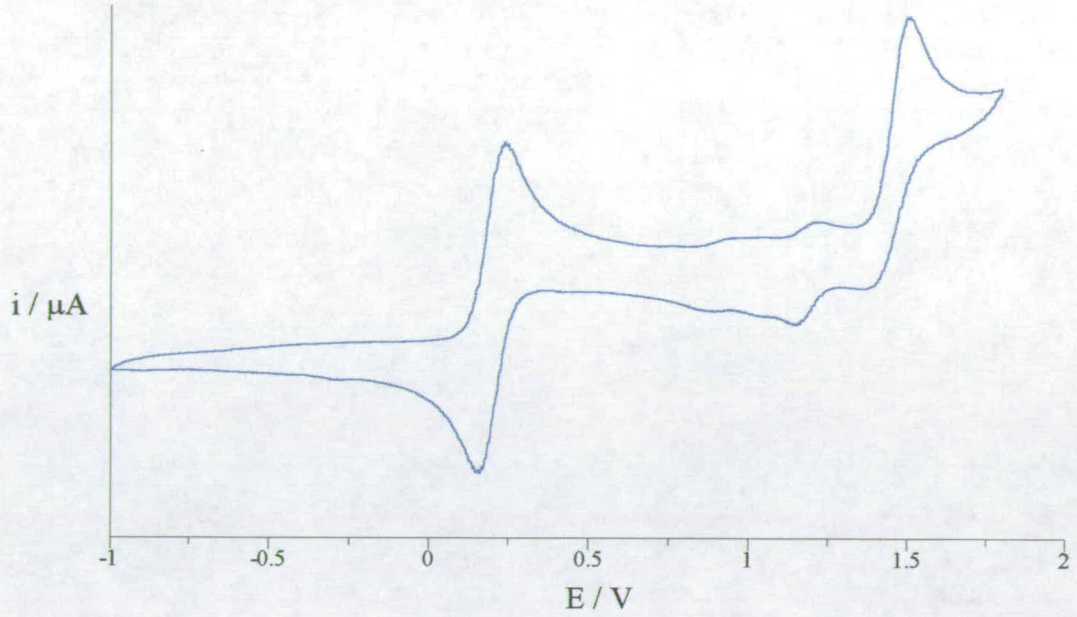

Figure 1.5 - CV of $[OsCl_2(PMe_2Ph)_3(MeCN)]$ in MeCN/0.1M $[TBA][BF_4]$ at RT

Other complexes of the type $[OsCl_2(PMe_2Ph)_3Y]$, where Y = dmf, dmso, PhCN, CO, C_2H_4, N_2 and PMe_2Ph, can readily be prepared from the electrogeneration of *mer*-$[OsCl_3(PMe_2Ph)_3]$ in CH_2Cl_2/0.5M $[TBA][BF_4]$ continuously saturated with the relevant gas or with excess PMe_2Ph added. See Table 1.2 for voltammetric data. Note that the electrode potential for the Os(II)/(Os(III) couple depends on L. As expected the half wave potential shifts to more positive potentials as L becomes a better π-accepting ligand, for example $E_{½}$ = +0.25V when L = MeCN, but $E_{½}$ = +0.83V for L = CO.

Table 1.2 - Electrochemical Data for Derivatives of $[OsCl_3(PMe_2Ph)_3]$[43,44]

Compound	Solvent	$E_{½}$ (Os(II)/Os(III))[a]
trans-$[OsCl_2(PMe_2Ph)_3(MeCN)]$	CH_2Cl_2	0.25V
cis-$[OsCl_2(PMe_2Ph)_3(MeCN)]$	MeCN	0.25V
trans-$[OsCl_2(PMe_2Ph)_3(dmf)]$	CH_2Cl_2	0.02V
cis-$[OsCl_2(PMe_2Ph)_3(dmf)]$	dmf	0.02V
trans-$[OsCl_2(PMe_2Ph)_3(dmso)]$	dmso	0.02V
trans-$[OsCl_2(PMe_2Ph)_3(PhCN)]$	PhCN	0.26V
cis-$[OsCl_2(PMe_2Ph)_3(PhCN)]$	PhCN	0.26V
trans-$[OsCl_2(PMe_2Ph)_3(CO)]$	CH_2Cl_2	0.83V
trans-$[OsCl_2(PMe_2Ph)_3(C_2H_4)]$	CH_2Cl_2	0.54V
trans-$[OsCl_2(PMe_2Ph)_3(N_2)]$	thf	0.16V
trans-$[OsCl_2(PMe_2Ph)_4]$	CH_2Cl_2	0.28V
cis-$[OsCl_2(PMe_2Ph)_4]$	CH_2Cl_2	0.75V

a All values are measured with respect to an Ag/AgCl reference electrode.

In summary, the reduction of *mer*-$[OsCl_3(PMe_2Ph)_3]$ in the presence of a ligand L, produces the complex *trans*-$[OsCl_2(PMe_2Ph)_3(Y)]$, which slowly isomerises to the thermodynamically stable *cis* form, See Scheme 1.4.

If the reduction is carried out in CH_2Cl_2 or thf under argon (i.e. no ligands present), then the final product is the binuclear complex $[Os_2Cl_3(PMe_2Ph)_6]^+$. The mechanism is believed to be via the doubly halide bridged complex $[Os_2Cl_4(PMe_2Ph)_6]$, see Scheme 1.4. The class of compound $[Os_2Cl_3L_6]^+$, where L is either a tertiary phosphine or arsine, has already been well studied in this laboratory.[6]

The reaction described above are examples of redox-induced substitution reactions. Such processes are not well documented in the literature but are worthy of further study. They are an exciting development in the area of clean synthesis especially in the preparation of non-thermodynamically favoured isomers.

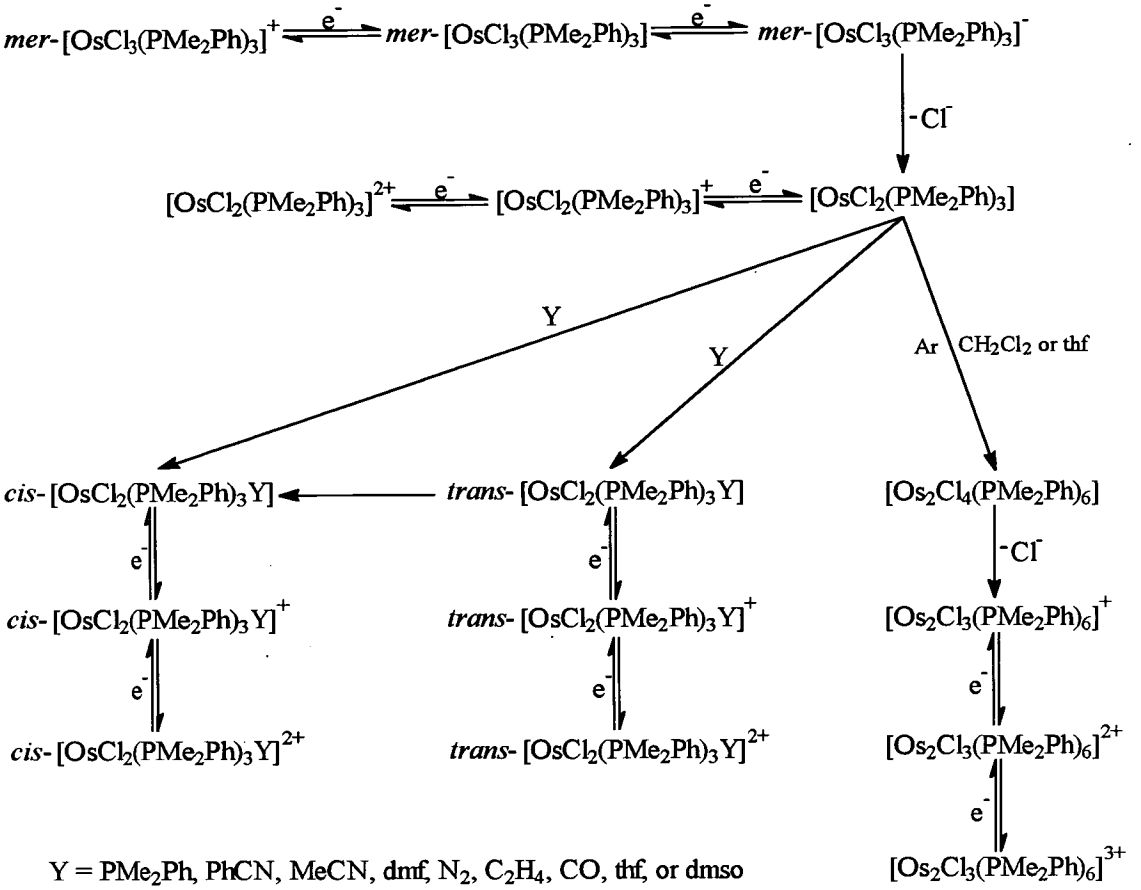

Scheme 1.4 - Reaction of *mer*-$[OsCl_3(PMe_2Ph)_3]$[43,44]

1.2.3 Spectroelectrochemistry of *mer*-$[OsCl_3(PMe_2Ph)_3]$

The electrochemically induced substitution reaction can also be followed by *in situ* Ultra Violet/Visible (UV/Vis) spectroscopy using an Optically Transparent Electrode (O.T.E.).[‡]

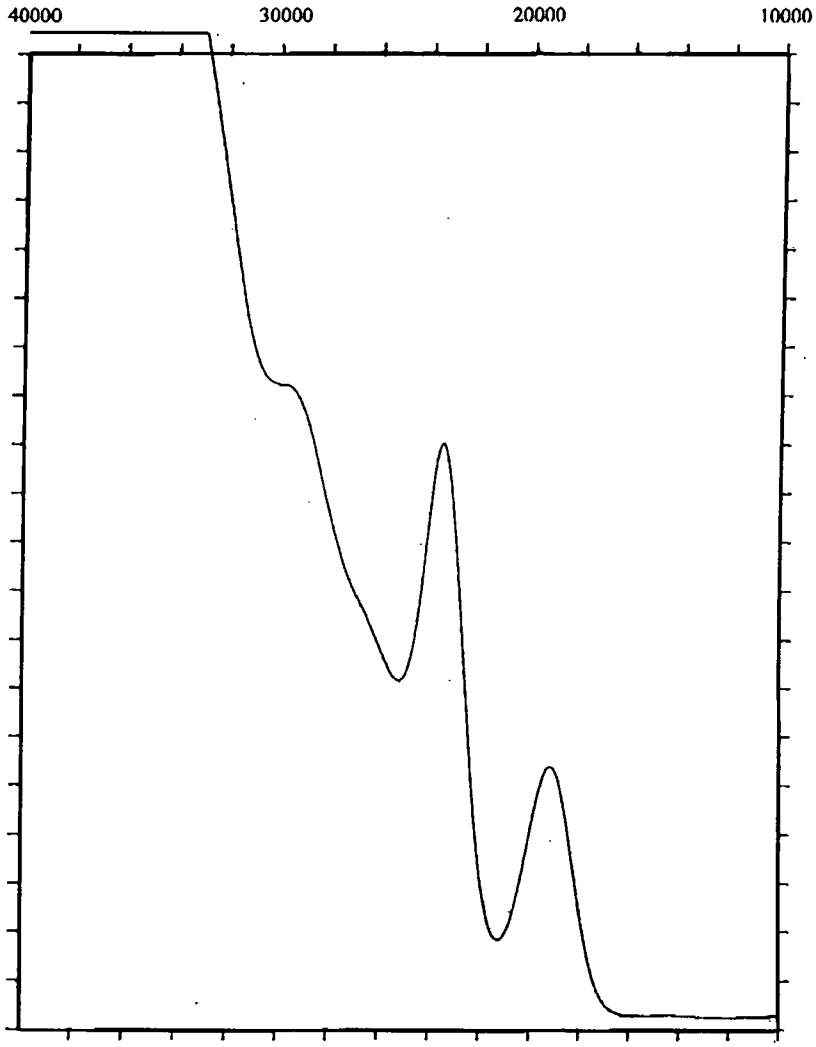

Figure 1.6 - UV/Vis Spectrum Of *mer*-$[OsCl_3(PMe_2Ph)_3]$ in CH_2Cl_2[§]

The UV/Vis spectrum of *mer*-$[OsCl_3(PMe_2Ph)_3]$ is shown in Figure 1.6. The spectrum consist mainly of charge transfer transitions from the full ligand orbitals to

[‡] See Chapter 6 for description and details of equipment used.
[§] Units are in Wavenumbers (cm^{-1}). For list of Molar Extinction Coefficients see Chapter 2.

the vacancy in the metal t_{2g} shell i.e. Ligand to Metal Charge Transfer (LMCT) (See Figure 1.7).

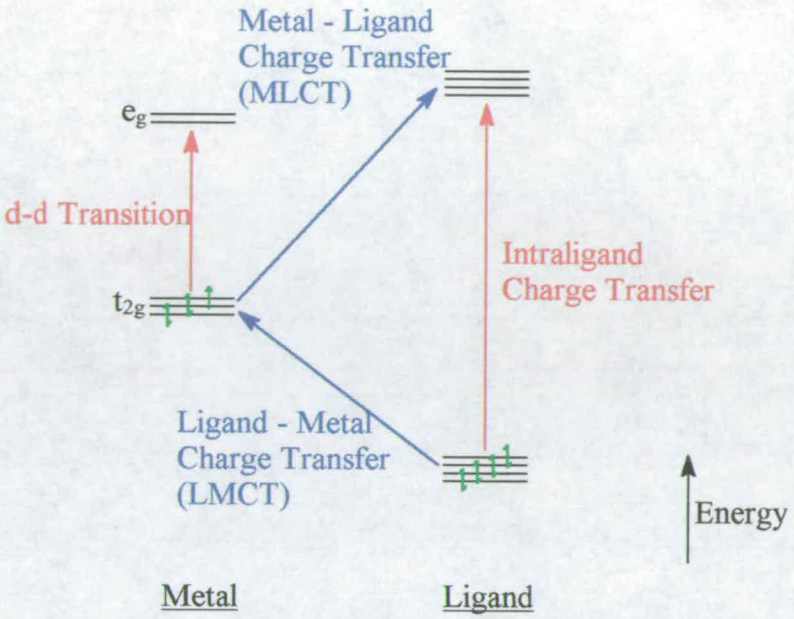

Figure 1.7 - Charge Transfer Pathways in Idealised d^5 Octahedral Complex

To assign the spectrum an Extended Hückel Molecular Orbital (EHMO) calculation was undertaken at Heriot Watt University.** The calculation was carried out on the atomic positions obtained from the X-ray crystal structure, see earlier. The low symmetry of the complex (C_{2v}), results in considerable orbital mixing.

The calculation showed the spectrum was split into three major regions The lowest energy transitions were computed to be from the Molecular Orbitals (MO) based on phosphorus to the Singly Occupied Molecular Orbital (SOMO) in the metal t_{2g} set. The highest energy transitions were assigned as the excitation of electrons from the chloride based MO's (probably π orbitals), to the SOMO. In between these two regions, an area of mixed orbital transitions is observed, from the phosphorus and chloride MO's to the SOMO. The calculation was found to be in good agreement with theoretical model published in 1973 by McCaffery and Rowe, on complexes of the type *mer*-$[OsCl_3L_3]$ where L - tertiary phosphine or arsine.[45]

Therefore the first peak in the spectrum at 19200cm^{-1} ($\varepsilon = 660 M^{-1}cm^{-1}$) was assigned as σ (P)$\rightarrow t_{2g}$(Os). the absorption at 23500cm^{-1} ($\varepsilon = 1440 M^{-1}cm^{-1}$) was assigned to the σ(P) + σ(Cl)$\rightarrow t_{2g}$(Os). The remaining peaks 27000cm^{-1}

** For details of EHMO Calculations see Chapter 6.

($\varepsilon = 1210 M^{-1}cm^{-1}$) and 29400$cm^{-1}$ ($\varepsilon = 1880 M^{-1}cm^{-1}$) were assigned as $\pi(Cl) \rightarrow t_{2g}(Os)$ charge transfers.

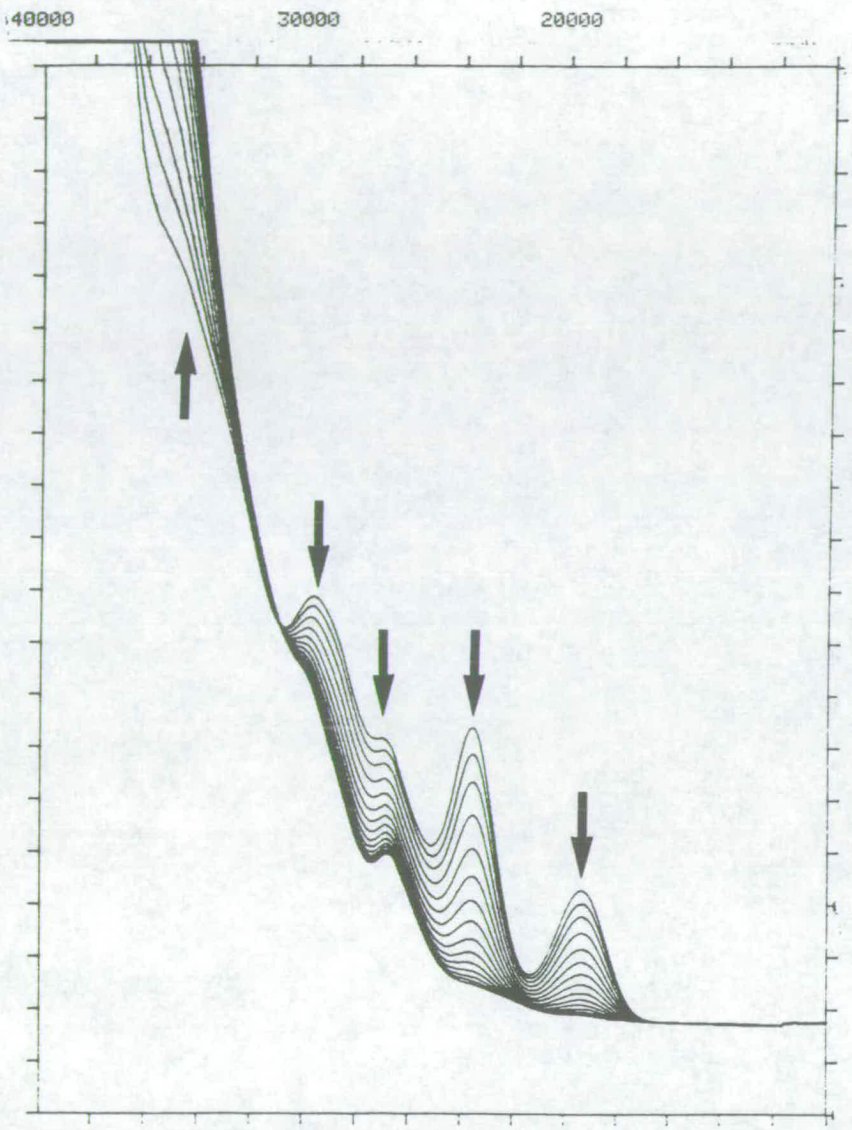

Figure 1.8 - Spectral Changes Accompanying the Reduction of *mer*-$[OsCl_3(PMe_2Ph)_3]$ to *trans*-$[OsCl_2(PMe_2Ph)_3(MeCN)]$ in MeCN/ 0.1M [TBA][BF_4] at RT in an O.T.E. Cell

On reduction to the Os(II) species *trans*-$[OsCl_2(PMe_2Ph)_3(MeCN)]$, Figure 1.8, the LMCT bands collapse due to the filling of the metal t_{2g} set with the addition of the reduction electron. The complete t_{2g} set of orbitals means that LMCT type transitions are forbidden. The π^* orbitals lie at high energy and thus there are no

absorption bands in the visible region, that is the complex *trans*-$[OsCl_2(PMe_2Ph)_3(MeCN)]$ is colourless.

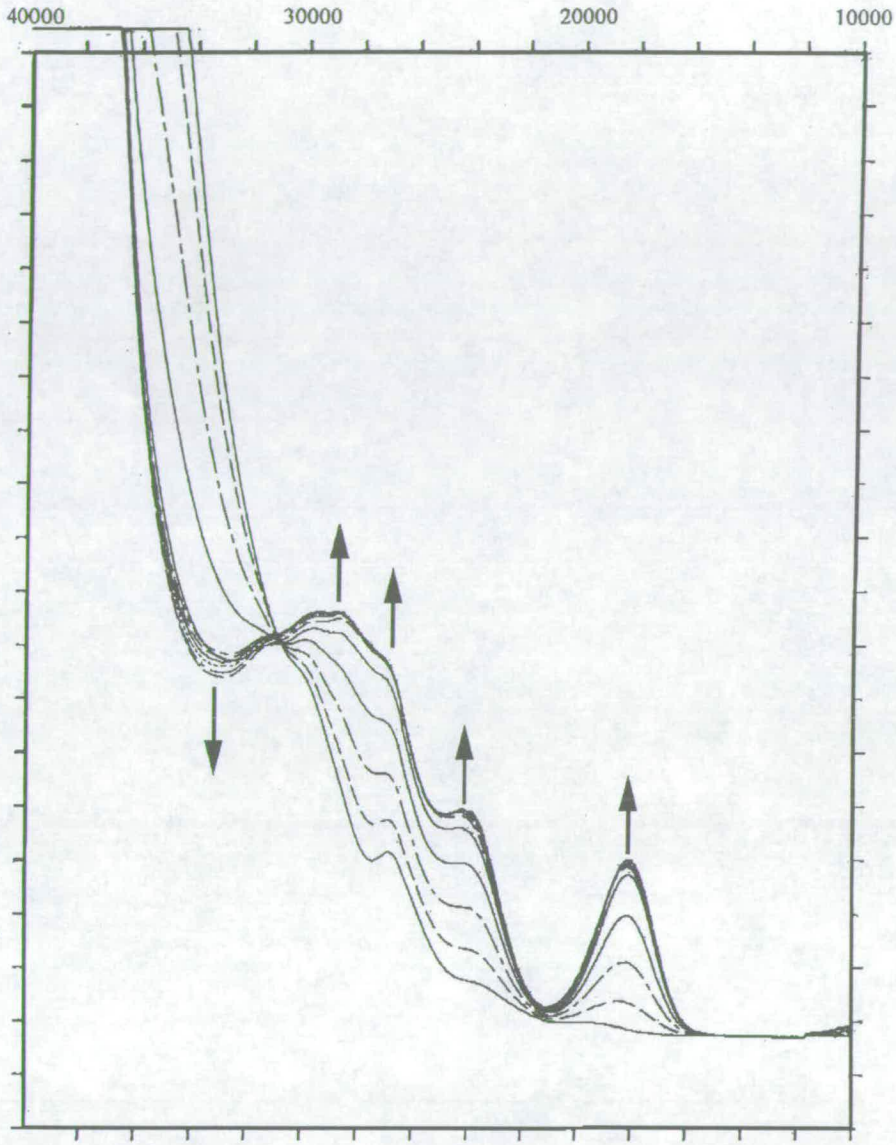

Figure 1.9 - Spectral Changes Accompanying the Oxidation of *trans*-$[Os(II)Cl_2(PMe_2Ph)_3(MeCN)]$ to *trans*-$[Os(III)Cl_2(PMe_2Ph)_3(MeCN)]^+$ in MeCN/0.1M [TBA][BF_4] at RT in an O.T.E. Cell

On oxidation back to Os(III), Figure 1.9, the spectrum shows the growth of the LMCT bands in the visible region of the spectrum. The reduction process has yielded a new product *trans*-$[OsCl_2(PMe_2Ph)_3(MeCN)]^+$ and hence the $Cl \rightarrow t_{2g}(Os)$ and $P \rightarrow t_{2g}(Os)$ charge transfer bands are at different energies than in the parent complex

mer-$[OsCl_3(PMe_2Ph)_3]$. The spectra also show an isobestic point at 31500cm^{-1}, proving that there is no transition state involved during the loss of the electron.

The O.T.E. technique was also applied to the reversible oxidation couple of the parent complex *mer*-$[OsCl_3(PMe_2Ph)_3]$. Figure 1.10 shows the spectra recorded for the oxidation of *mer*-$[OsCl_3(PMe_2Ph)_3]$ to *mer*-$[OsCl_3(PMe_2Ph)_3]^+$.

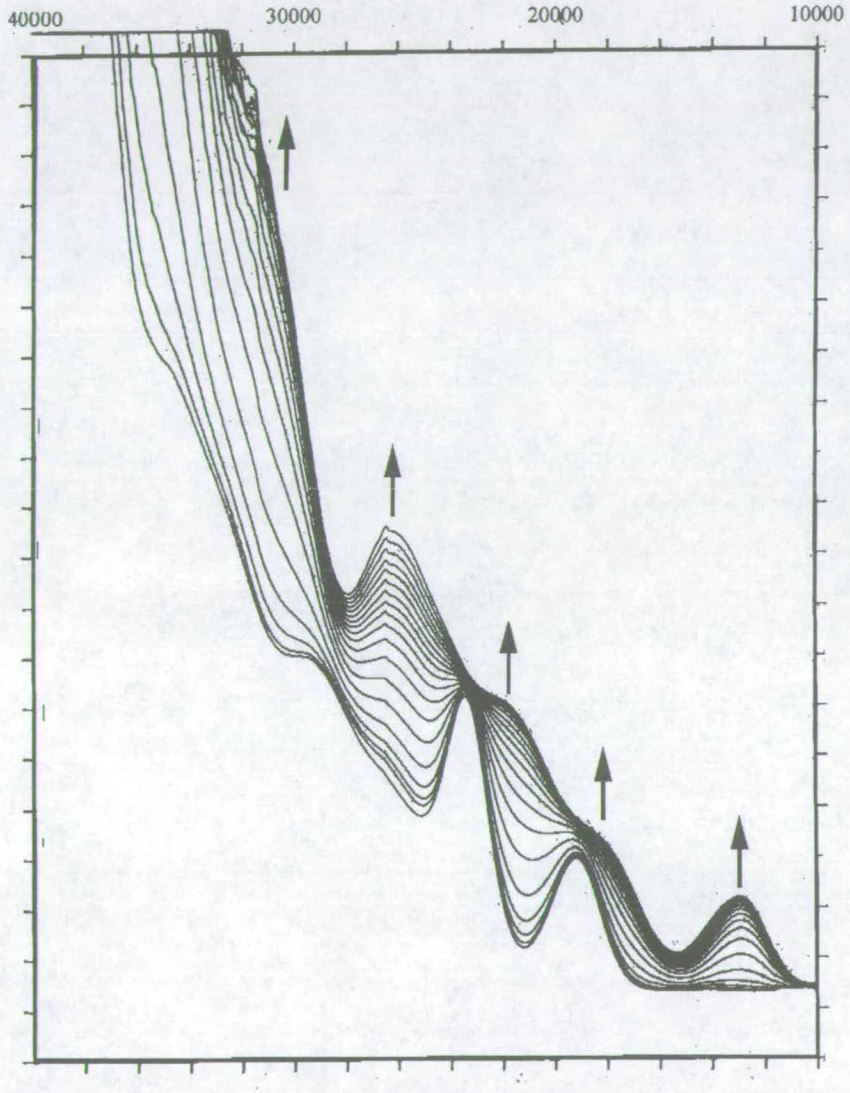

Figure 1.10 - Spectral Changes Accompanying the Oxidation of *mer*-$[OsCl_3(PMe_2Ph)_3]$ to *mer*-$[OsCl_3(PMe_2Ph)_3]^+$ in CH_2Cl_2/0.5M [TBA][BF_4] at RT using an O.T.E. Cell[††]

[††] Units are in Wavemumbers (cm^{-1})

The assignments for the Os(IV) complex follow straight forwardly from the Os(III) complex. The major bands are all shifted to lower energy by 3,000-6,000cm^{-1}.

This remainder of this Thesis details the kinetic and mechanistic studies of electron transfer reactions of monomeric osmium coordination complexes with mixed halide, tertiary phosphine and tertiary arsine ligands. Isomeric forms of the complex have been prepared and characterised and will be described in detail. Firstly, the dependence of the electrochemical response of the metal, on the tertiary phosphine and arsine ligands will be examined.

1.3 References

(1) F. P. Dwyer, R. S. Nyholm and B. T. Tyson. *J. Proc. Roy. Soc. N.S.W.*, 1948, **81**, 272.

(2) R. S. Nyholm and G. T. Sutton, *J. Chem. Soc.*, 1958, 572.

(3) L. Vaska, *Chem. Ind. (London)*, 1961, 1402.

(4) A. Araneo and C. Bianchi, *Gazz. Chim. Ital.*, 1967, **97**, 885.

(5) J. Chatt and R. G. Hayter, *J. Chem. Soc.*, 1961, 896.

(6) R.J.Sorbie, Ph.D. Thesis, University Of Edinburgh, 1989.

(7) J. Chatt, G. J. Leigh, D. M. P. Mingos and R. J. Paske, *J. Chem. Soc. (A).*, 1968, 2636.

(8) J. Chatt, G. J. Leigh and D. M. P. Mingos, *J. Chem. Soc. (A)*, 1969, 1674.

(9) A. Hudson and M. J. Kennedy, *J. Chem. Soc. (A)*, 1969, 1116.

(10) N. J. Hill, *J. Chem. Soc., Faraday Trans.*, 1972, **68**, 427.

(11) G. J. Leigh and W. Bremser, *J. Chem. Soc., Dalton Trans.*, 1972, 1217.

(12) L. Aslanov, R. Manson, A. G. Wheeler and P. O. Wimp, *J. Chem. Soc., Chem. Comm.*, 1970, 30.

(13) G. J. Leigh and D. M. P. Mingos, *J. Chem. Soc. (A)*, 1970, 587.

(14) H. P. Gunz and G. J. Leigh, *J. Chem. Soc. (A)*, 1971, 2228.

(15) J. Chatt and R. A. Rowe, *J. Chem. Soc.*, 1962, 4019.

(16) D. J. Salmon and R. A. Walton, *Inorg. Chem.*, 1978, **17**, 2379.

(17) J. E. Armstrong and R. A. Walton, *Inorg. Chem.*, 1983, **22**, 1545.

(18) P.R.Hoffman and K.G.Caulton, *J. Am. Chem. Soc.*, 1975, **97**, 4221.

(19) A. R. Chakravarty, F. A. Cotton and D. A. Tocher, *Acta Cryst.*, 1985, **C41**, 698.

(20) S. J. La Placa and J. A. Ibers, *Inorg. Chem.*, 1965, **4**, 778.

(21) M. Brookhart and M. L. H. Gran, *J. Organomet. Chem.*, 1983, **250**, 395.

(22) D. S. Moore and P. D. Robinson, *Inorg. Chem.*, 1979, **18**, 2307.

(23) C. C. Hinckley, M. Matusz and P. D. Robinson, *Acta Cryst.*, 1987, **C43**, 1880.

(24) P. G. Douglas and B. L. Shaw, *J. Chem. Soc. (A)*, 1970, 334.

(25) J. Chatt, A. E. Field and B. L. Shaw, *J. Chem. Soc.*, 1963, 3371.

(26) P. R. Brooks and B. L. Shaw, *J. Chem. Soc., Chem. Comm.*, 1968, 919.

(27) Yu. G. Borodko, V. S. Bukreer, M. L. Khidekel, G. J. Kozub and A. E. Shilov, *Zur. Strukt. Khim.*, 1967, **8**, 542.

(28) J. Chatt, G. J. Leigh and R. J. Paske, *J. Chem. Soc. (A)*, 1969, 854.

(29) J. Chatt, G. J. Leigh and P. L. Richards, *J. Chem. Soc. (A)*, 1970, 2243.

(30) J. Chatt, D. P. Melville and P. L. Richards, *J. Chem. Soc. (A)*, 1971, 1169.

(31) K. G. Srinivasamurthy, N. M. Nanje Gowda, E. G. Leelamani and G. K. N. Reddy, *Proc. Indian. Acad. Sci. (Chem. Sci.)*, 1980, **89**, 101.

(32) P. D. Robinson, C. C. Hinckley and A. Ikuo, *Acta Cryst.*, 1988, **C44**, 1491.

(33) M. M. Taqui Khan, S. Shareef Ahamed and R.A. Levenson, *J. Inorg. Nucl. Chem.*,1976, **38**, 1135.

(34) A. S. Alves, D. S. Moore, R. A Andersen and G. Wilkinson, *Polyhedron*, 1982, **1**, 83.

(35) H. Werner and J. Gotzig, *J. Organomet. Chem.*, 1985, **284**, 73.

(36) J. Gotzig, R. Werner, H. Werner, *J. Organomet. Chem.*, 1985, **285**, 99.

(37) P. E. Fanwick, I. F. Fraser, S. M. Tetrick and R. A. Walton, *Inorg. Chem.*, 1987, **26**, 3786.

(38) C. C. Hinckley, M. Matusz and P. D. Robinson, *Acta Cryst.*, 1988, **C44**, 1829.

(39) C. C. Hinckley, M. Matusz and P. D. Robinson, *Acta Cryst.*, 1988, **C44**, 371.

(40) R. A. Cipriano, W. Levason, R. A. S. Mould, D. Pletcher and M. Webster, *J. Chem. Soc., Dalton Trans.*, 1990, 339.

(41) R. A. Cipriano, W. Levason, R. A. S. Mould, D. Pletcher and M. Webster, *J. Chem. Soc., Dalton Trans.*, 1990, 2609.

(42) N. A. Champness, W. Levason, R. A. S. Mould, D. Pletcher and M. Webster, *J. Chem. Soc., Dalton Trans.*, 1991, 2777.

(43) V. T. Coombe, Ph.D. Thesis, University Of Edinburgh, 1985.

(44) V. T. Coombe, G. A. Heath, T. A. Stephenson, J. D. Whitelock and L. J. Yellowlees, *J. Chem. Soc., Dalton Trans.*, 1985, 947.

(45) A. J. McCaffery and M. D. Rowe, *J. Chem. Soc., Faraday Trans.*, 1973, 1767.

Chapter 2

Introduction - Review of Electronic and Steric Parameters of Tertiary Phosphines

Electrochemistry, Spectroelectrochemistry and Electronic Spectroscopy of *mer*-$[OsX_3L_3]$, where X is Cl or Br and L is a tertiary phosphine or arsine.

2.1 Introduction

It has long been recognised that changing the substituents on phosphorus ligands can cause marked changes in the behaviour of the free ligands and of their transition metal complexes. Originally this was rationalised in terms of their electronic effects.

The standard text book description of the transition metal - phosphine bond is based on the proposal by J. Chatt [1] that the lone pair on the phosphorus is donated to an empty metal d-orbital (σ bond) and the empty phosphorus 3d orbitals accept electron density from filled metal d-orbitals of suitable symmetry ("π backbonding") the bonding being mutually reinforcing (synergic). This is represented schematically in Figure 2.1.

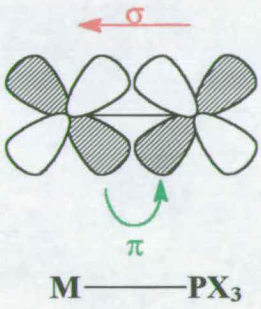

Figure 2.1 - Metal - Phosphine Bonding

This explanation of transition metal - phosphorus bonding has been a subject of much controversy since Chatt's description was published. The question being whether π backbonding is involved and if so are the phosphorus d orbitals involved.

It was widely accepted that the π - bonding effect varied from ligand to ligand. Many groups have been involved in trying to determine the extent of π-acceptance in tertiary phosphine ligands by measuring the ν(CO) stretching frequency in complexes such as $Mo(CO)_3L_3$ [2] and $Co(CO)_2(NO)L$ [3] where L is a tertiary phosphine. The ν(CO) setting frequency can be used as a measure of π-acceptance, as the bonding of CO can be described as similar to phosphine ligands (See Figure 2.1), but with the electron density back bonded to the π^* orbital, causing the frequency to be lowered. Therefore when the two ligands are bonded to the same metal centre they are in competition with each other over the electron density to be backbonded from the filled metal orbitals. These studies lead to a spectrochemical series shown below:

$NO > CO > PF_3 > SbCl_3 > AsCl_3 > PCl_3 > PCl_2(OBu) > PCl_2(OEt) > PCl_2Ph > PBr_2Me > As(OMe)_3 > PCl(OBu)_2 > As(OEt)_3 > P(OPh)_3 > PClPh_2 > P(OMe)_3 > AsPh_3 > PPh_3 > SEt_3 > AsEt_3 > PMe_3 > PEt_3 > o\text{-}C_6H_4(PEt_2)_2 > P(NC_5H_{10})_3$.

Cotton[4] later published a report stating that measuring the differences in ν(CO) stretching vibration was not a good method of measuring the π-effect, as force constants were not accounted for. Following the development of the Cotton-Kraihanzel[5] force technique, they reviewed the above results giving a slightly different order of π-acidity, most importantly that PF_3 was found to be a better π-acceptor than CO. A result later reinforced by the photoelectron spectroscopic studies of $Ni(CO)_4$[6] and $Ni(PF_3)_4$,[7] showing the PF_3 to be the better electron withdrawer.

Bigorgne opposed the idea that the phosphorus(III) ligands could be involved in any type of π-backbonding. He argued that the force constants of Ni-P bonds were not large enough to suggest substantial double bonding.[8] He also measured the B_1 ν(CO) stretching vibration for a series of $[Ni(CO)_3L]$ and $[Ni(CO)_2L_2]$ complexes[9] where L = PMe_3, PEt_3, PPh_3, $P(C{\equiv}CPh)_3$, $P(CF_3)_3$ and PF_6 and plotted them as a function of Tafts inductive constant,[10] σ, obtaining a straight line correlation.

Angelici[11] studied the complexes of the series *cis*-$[Mn(CO)_3L_2]$ where L is a tertiary phosphine or amine. A linear relationship between pK_a[12] and the ν(CO) stretching frequency for all the phosphorus ligands was observed. Essentially the pK_a parameter is a measure of the σ-donicity of the ligand, thus it was concluded that the all the phosphorus ligands showed no π-effects. Graham[13] and then Treichel[14] used force constants to separate σ- and π- effects. Their results however were debatable as they showed PBu^n_3 to be as good an acceptor as $P(OPh)_3$. On the whole these earlier studies were unsatisfactory but more recent studies have proved more successful (See Later).

In 1970 Tolman[15] repeated the work of Bigorgne[9] with a set of 70 different phosphine ligands studying the A_1 ν(CO) stretching vibration of $Ni(CO)_3L$ as a measure of the electronic effect. He believed that the description of the bonding between a transition metal and a phosphorus ligand cannot be obtained by the study of a single frequency. Therefore he used the more empirical term "electron donor acceptor property" rather than π-acceptor strength. Tolman found that it was possible to assign a contribution to the ν(CO) stretching vibration for each substituent

on a phosphorus ligand. Each substituent was given a contribution designated as a value χ_i, with a magnitude in cm^{-1}. Of all phosphorus ligands studied the lowest frequency found was that of PBu^t_3 at $2056.1cm^{-1}$, this then was taken as the origin, i.e. χ_i for Bu^t is 0 cm^{-1}. Therefore for any complex of the type $[Ni(CO)_3PX_1X_2X_3]$ the A_1 ν(CO) can be calculated using the equation:

$$\nu(CO) = 2056.1 + \sum_{i=1}^{3} \chi_i \qquad (1)$$

Later Bodner *et al*[16] determined electronic parameters for a number of tertiary phosphorus ligands using ^{13}C N.M.R. chemical shifts, these were found to be in good agreement to those of Tolman. Table 2.1 shows the calculated χ_i for various substituent groups calculated by Tolman, it will be these values that are used in this study.

Since these early attempts at isolating the σ and π components of the transition metal-phosphine bond, many groups have tried to study and isolate these components using a vast range of techniques including IR,[17] NMR,[18] UV/Vis,[19] Photoelectron[20] and Mössbauer spectroscopy[21] as well as theoretical[22] and electrochemical[23] methods and X-ray crystallography.[24] On the whole these early attempts at separating the components were unsuccessful, more recent studies by Golovin *et al*[25] have proved to be more successful and will be discussed later.

Table 2.1 - Tolman's Electronic Parameter for Substituents On Phosphorus Ligands From Reference (26)

Substituent X_i	χ_i (cm^{-1})	Substituent X_i	χ_i (cm^{-1})
-Bu^t	0.0	-OBu	6.5
-Cy	0.1	-OEt	6.8
-*o*-C_6H_4OMe	0.9	-CH_2CH_2CN	7.3
-Pr^i	1.0	-OMe, -$OCH_2CH{=}CH_2$, -$OCH_2CH_2OCH_3$	7.7
-Bu	1.4	-H	8.3
-Et	1.8	-O-2,4-$C_6H_3Me_2$	9.0
-NMe_2	1.9	-OCH_2CH_2Cl, -O-*o*-Tol, -O-*p*-Tol, -O-*p*-C_6H_4OMe	9.3
-piperidyl	2.0	-O-*o*- C_6H_4-Pr^i	9.5
-Me	2.6	-O-*o*- C_6H_4-Bu^i	9.6
-2,4,6-$C_6H_2Me_3$	2.7	-OPh	9.7
-*p*-C_6H_4OMe	3.4	-O-*o*- C_6H_4-Bu^t	10.0
-*o*-Tol, -*p*-Tol, -CH_2Ph	3.5	-OCH_2CH_2CN	10.5
-*m*-Tol	3.7	-O-*o*-Tol-*p*-Cl	10.7
-Ph	4.3	-O-*p*-C_6H_4Cl	11.1
-$CH{=}CH_2$	4.5	-C_6F_5	11.2
-*p*- C_6H_4F	5.0	-O-*o*- C_6H_4Cl	11.4
-*p*- C_6H_4Cl	5.6	-OCH_2CCl_3	11.9
-*m*- C_6H_4F	6.0	-O-*p*- C_6H_4CN	12.2
-CH_2CH_2Cl	6.1	-Cl	14.8
-O-Pr^i	6.3	-F	18.2
		-CF_3	19.6

Subsequent to 1970, the properties of phosphine ligands were rationalised in terms of the electronic effects, although there were scattered references to steric effects. Steric effects are the result of non-bonding forces between different parts of a molecule either by repulsive interactions or by structural constraints. Electronic effects are transmitted along a chemical bond and may be altered by changing the electronegativity of the substituents on a ligand.[26,27] This can be represented as follows:[26]

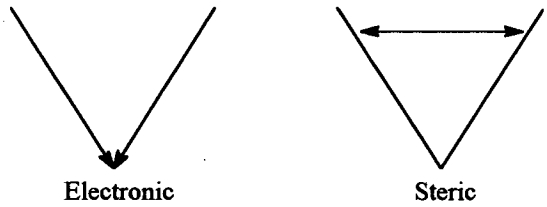

For example,[27]

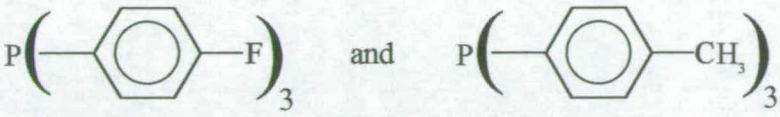

have different electronic effects, but are sterically similar, whereas the opposite holds for the following:

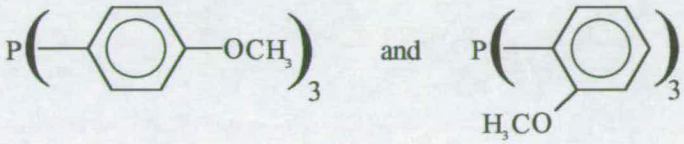

These effects are often difficult to separate, Tolman however quantified both steric[26,28] and electronic (See Earlier) parameters for a wide range of phosphorus ligands.

Steric effects were quantified by the definition of the ligand cone angle, θ, "The angle of the cone with the apex at the metal which just encloses the Van der Waals surface of all the substituent atoms on the phosphorus ligands, assuming the bond length TM-P = 2.28Å."[26] Represented schematically as:

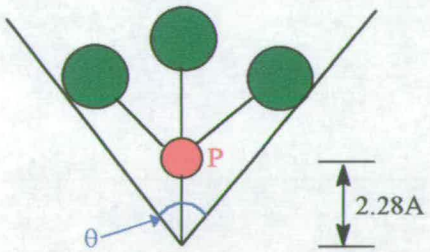

For unsymmetrical ligands Tolman introduced the concept of half cone angles, θ/2.[29] These are defined as the angles between the metal-phosphorus bond and the vector that just touches the van der Waals radii of the out most atoms.

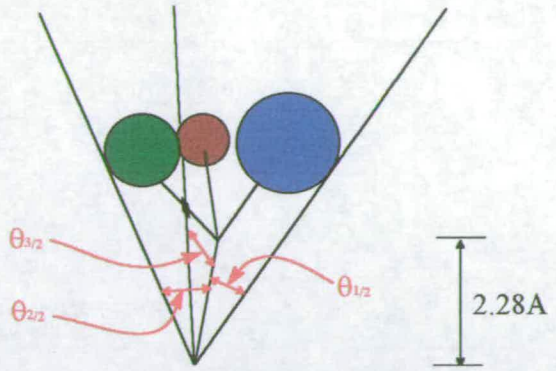

$$\theta = \sum_{i=1}^{3} \frac{\theta_i}{2}$$

Tolman defined θ as 2 times the average of the maximum θ/2 values for the three phosphorus substituents. Using CPK models as the source of data, he chose a single conformer for each ligand which minimised θ.

For bulky ligands Alyea *et al*[30] introduced the use of ligand profiles, which are plots of θ/2 versus ϕ, the angle of rotation about the metal-phosphorus vector. This aids visualisation of the ligand size. It was observed that the cone angle concept provides some measure of the bulkiness of the ligand, but it does not bring out the fact that the ligands are not solid cones.

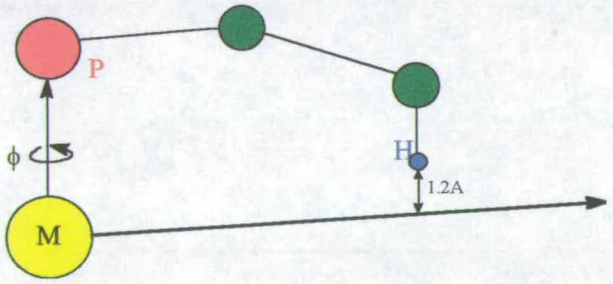

DeSanto *et al*[31] used MINDO/3 semiempirical molecular orbital calculations to examine the effects of substituent conformation on the cone angle. Tolman however recorded a much larger range of ligands, so these are the most commonly used. It will be these values that will be used in this study. Table 2.2 gives values of Tolman's cone angles, for various phosphorus ligands.

Table 2.2 - Tolman's Cone Angles for Phosphorus Ligands From Reference (26)

Phosphine Ligand	θ, deg	Phosphine Ligand	θ, deg
$P(NCH_2CH_2)_3$	108	$PEtPh_2$	140
$P(OEt)_3$	109	P(O-*o*-Tol)$_3$	141
$P(OCH_2CH_2Cl)_3$	110	$Cy_2PCH_2CH_2PCy_2$	142
$P(CH_2O)_3CR'$	114	PBu^i_3	143
$P(OCH_2CCl_2)_3$, $Et_2PCH_2CH_2PEt_2$, $P(OMe)_2Ph$, $P(OMe)_2Et$	115	PPh_3, P(*p*-Tol)$_3$, P(*m*-C_6H_4F)$_3$	145
$P(OEt)_2Ph$	116	P(O-*o*-$C_6H_4Pr^i$)$_3$	148
PMe_3	118	PPh_2Pr^i	150
$Ph_2PCH_2PPh_2$	121	P(O-*o*-C_6H_4Ph)$_3$	152
PMe_2Ph	122	$P(NMe_2)_3$, PPh_2Bu^t	157
PCl_3, PMe_2CF_3	124	$PPh_2C_6F_5$	158
$Ph_2PCH_2CH_2PPh_2$	125	$P(Pr^i)_3$, P(sec-Bu)$_3$	160
$Ph_2P(CH_2)_3PPh_2$	127	PBz_3	165
P(OPh)$_3$, P(O-*p*-Tol)$_3$, $PHPh_2$	128	PCy_3, $PPh_2(Bu^t)$	170
$P(OPr^i)_3$	130	$P(OBu^t)_3$	172
PBr_3	131	P(O-*o*-$C_6H_4Bu^t$)$_3$	175
PEt_3, PBu_3, PPr_3, $P(CH_2CH_2CN)_3$, $POMePh_2$	132	PBu^t_3	182
$POEtPh_2$	133	$P(C_6F_5)_3$	184
$PMePh_2$, PEt_2Ph	136	P(O-2,6-$C_6H_3Me_2$)$_3$	190
$P(CF_3)_3$	137	P(*o*-Tol)$_3$	194

There are many examples of cases where the behaviour of a particular series of transition metal-phosphine complexes can be related to the electronic or steric effects of the phosphorus ligand.

A. Steric

Steric effects dominate in many cases. There are examples in the literature where steric effects have been related to N.M.R. chemical shifts and coupling constants, infrared frequencies and intensities, electronic spectra, dipole moments, electrochemistry, ionisation potentials, rates of reactions, equilibrium constants and the structure of molecules.[26]

The reaction of $[OsX_6]^{2-}$ with tertiary phosphines form the series of complexes *mer*-$[OsX_3L_3]$, where X is Cl or Br and L is a tertiary phosphine.[32] The identical reaction but with the larger ligand PPh_3 gives a product mixture of $[OsO_2Cl_2(PPh_3)_2]$ and *trans*-$[OsCl_4(PPh_3)_2]$ as mentioned earlier in Chapter 1.[33]

The UV/Vis spectra of the square planar series *trans*-NiX_2L_2 (X is Cl or Br and L is a tertiary phosphine), show a marked red shift when PPr^n_3 is replaced by PPr^i_3.[34] The

frequencies of the monitored bands decrease by an amount dependent on the ligand X, the shift being greater for larger X. Therefore the shifts were attributed to lengthening of the Ni-X bonds. For the tetrahedral series $NiBr_2L_2$ it has been observed that as the size of the tertiary phosphine increases the lowest frequency transition in the electronic spectra shifts to lower energy, i.e. 11,680cm^{-1} for $PMePh_2$ (θ=136°), 11,360cm^{-1} for $PEtPh_2$ (θ=140°) and 10,800cm^{-1} for PBu^tPh_2 (θ=157°).[35] The effect was attributed to the lengthening of the Ni-P bonds. Most likely both of these effects contribute.

Electrochemical effects have also been explained using steric effects. The complexes $[Co(salen)L_2]^+$ and $[Co(DH)_2L_2]^+$, where salen is N,N'-ethylenebissalicylidene, DH is dimethylgloximato and L is a tertiary phosphine, both undergo a one electron reduction which shifts negatively as the size of the phosphine ligand increases.[36]

B. Electronic

As already mentioned there has been a considerable interest regarding the electronic parameters of phosphines.[17-24] It was not until the mid 1980's the σ and π components of the transition metal - phosphorus bond were successfully separated in a simple manner.

Studying the series of compounds $[Mn(CO)_2(\eta\text{-MeCp})L]$, where L was a tertiary phosphorus ligand, Giering *et al*[25] showed a linear relationship between the oxidation potentials[37] of the complexes and Tolman's electronic potentials of the phosphine ligands. They classified the phosphorus ligands into 3 classes.

Class I	σ-donor/π-donor
	PEt_3, PBu_3, PCy_3
Class II	σ-donor
	PMe_3, PMe_2Ph, PEt_2Ph, PBu_2Ph, $PMePh_2$, $PEtPh_2$, $P(p\text{-OPhMe})_3$, $P(p\text{-PhMe})_3$, PPh_3.
Class III	σ-donor/π-acceptor
	$P(p\text{-PhCl})_3$, $P(OMe)Ph_2$, $P(OPr^i{}_3)$, $P(OEt)_3$, $P(OMe)_3$, $P(OPh)_3$.

This classification was drawn up on the basis that σ-donor only phosphines show a correlation with pK_a i.e. Class II phosphine showed a linear relationship with pK_a. Class I and Class III phosphines would lie to the left and right of this line respectively.

For Class II compounds the ease of oxidation must be dependent on the σ-donicity of the ligand only. For Members of Class I the oxidation was easier than inferred by the pK_a, due to the enhanced electron richness of the metal centre. Class III compounds were harder to reduce then expected due to the removal of electron density from the metal, by the π-acceptor abilities of the ligands. However, pK_a values may not be appropriate because they are dependent on the interactions between phosphorus and a hard acid, H^+, rather than a soft acid such as a low valent metal centre.

Further work by the same group was centred on separating the σ and π effects of metal-phosphorus bonds without relying on pK_a values.[38]

They studied the complexes of type [Fe(η-Cp)(CO)L(COMe)], [Fe(η-Cp')(CO)L(COMe)] and [Fe(η-Cp)(CO)L(Me)], (Cp' is $C_5H_5Me^-$ and L is tertiary phosphine), where both ν(CO) and the reduction potential, E°, could be measured for the same phosphorus ligand. The σ_d (σ-donor) and π_a (π-acceptor) parameters are used in a formal sense to express the relationship between ligand properties and the properties of the complex. Therefore the linear relationships between the properties of the complexes and ν(CO) and E° can be expressed as Equations (2) and (3) for σ-donor only complexes and (4) and (5) for σ-donor/π-acceptor complexes.

<u>σ-Donor Ligands</u>

$$\nu(CO) = a\sigma_d + c \quad (2)$$

$$E^\circ = a'\sigma_d + c \quad (3)$$

<u>π-Acceptor/σ-Donor</u>

$$\nu(CO) = A\sigma_d + B\pi_a + C \quad (4)$$

$$E^\circ = A'\sigma_d + B'\pi_a + C' \quad (5)$$

By elimination of σ_d from the equations (2) to (5), equations (6) and (7) could be written relating one measured property, ν(CO), to the other (E°).

$$\nu(CO) = (a/a')E^\circ + c - ac'/a \quad (6)$$

$$\nu(CO) = (A/A')E^\circ + (B - AB'/A')\pi_a + C - AC'/A' \quad (7)$$

Equation (6) predicts that for those complexes containing pure σ-donor ligands, a plot of E° versus ν(CO) would give a straight line with only a small scatter due to experimental error. On the other hand from equation (7) ν(CO) is dependent on two variables, E° and π_a, therefore a plot of ν(CO) versus E° would show considerable scatter. Thus by plotting ν(CO) against E° it would be possible to distinguish between σ-donor and π-acceptor ligands without prior knowledge or either σ_d or π_a.

We set out to explore the effects of varying the halide and tertiary Group 15 ligands on a series of compounds of type *mer*-$[OsX_3(PR)_3]$ first made by Chatt *et al* in the 1960's.[32]

2.2 Results and Discussion

2.2.1 Introduction

A series of compounds of type *mer*-$[OsX_3(L)_3]$ were prepared using the literature preparation described by Chatt *et al*[33] where X = Cl or Br, L = PMe_3, PEt_3, PMe_2Ph, PEt_2Ph, $PMePh_2$, $PEtPh_2$, PPr^n_3, $AsPr^n_3$, $AsMe_2Ph$ and $AsEt_2Ph$.*

The solid state structure of the complexes are all very similar to that of *mer*-$[OsCl_3(PMe_2Ph)_3]$ discussed in Chapter 1. Figure 2.2 shows the slightly distorted octahedral structure of the bromide complex *mer*-$[OsBr_3(PPr^n_3)_3]$, (Table 2.3 shows the notable bond distance and angles). Note the Os-Br(2) bond distance is again longer than the other two Os-Br bonds due to the *trans* influence of the tertiary phosphine ligand.

Figure 2.3 shows the structure of one of the arsine analogues namely *mer*-$[OsCl_3(AsMe_2Ph)_3]$, Table 2.4 lists the selected bond distance and angles. The arsines are almost identical to the phosphine complexes with the exception that the Os-As distance is greater in length by ~0.1Å.

* See Chapter 6 for more details of synthesis.

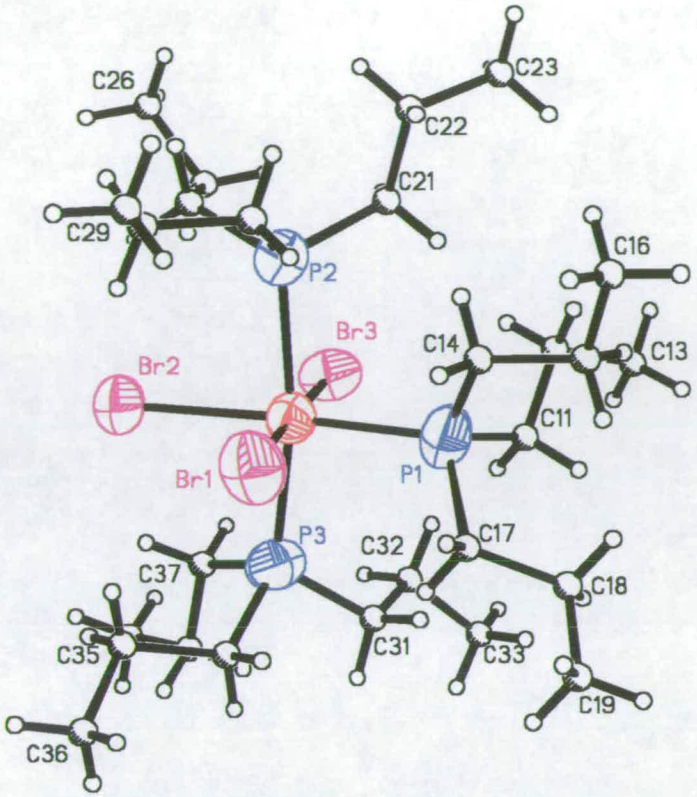

Figure 2.2 - Structure of *mer*-[$OsBr_3(PPr^n_3)_3$]

Table 2.3 - Selected Bond Distances (Å) and Angles (°) of *mer*-[$OsBr_3(PPr^n_3)_3$][†]

Os-P(1)	2.374(5)	Os-P(2)	2.435(7)	Os-Br(1)	2.511(3)
Os-P(3)	2.427(7)	Os-Br(3)	2.498(3)	Os-Br(2)	2.574(2)
P(1)-Os-P(3)	95.3(2)	P(2)-Os-Br(3)	85.8(2)	P(1)-Os-Br(2)	171.1(2)
P(1)-Os-P(2)	95.9(2)	P(1)-Os-Br(1)	82.7(2)	P(3)-Os-Br(2)	85.7(2)
P(3)-Os-P(2)	167.0(2)	P(3)-Os-Br(1)	93.4(2)	P(2)-Os-Br(2)	84.2(2)
P(1)-Os-Br(3)	95.3(2)	P(2)-Os-Br(1)	94.4(2)	Br(3)-Os-Br(2)	93.57(9)
P(3)-Os-Br(3)	86.8(2)	Br(3)-Os-Br(1)	178.02(10)	Br(1)-Os-Br(2)	88.41(9)

[†] For full crystallographic details see Appendix

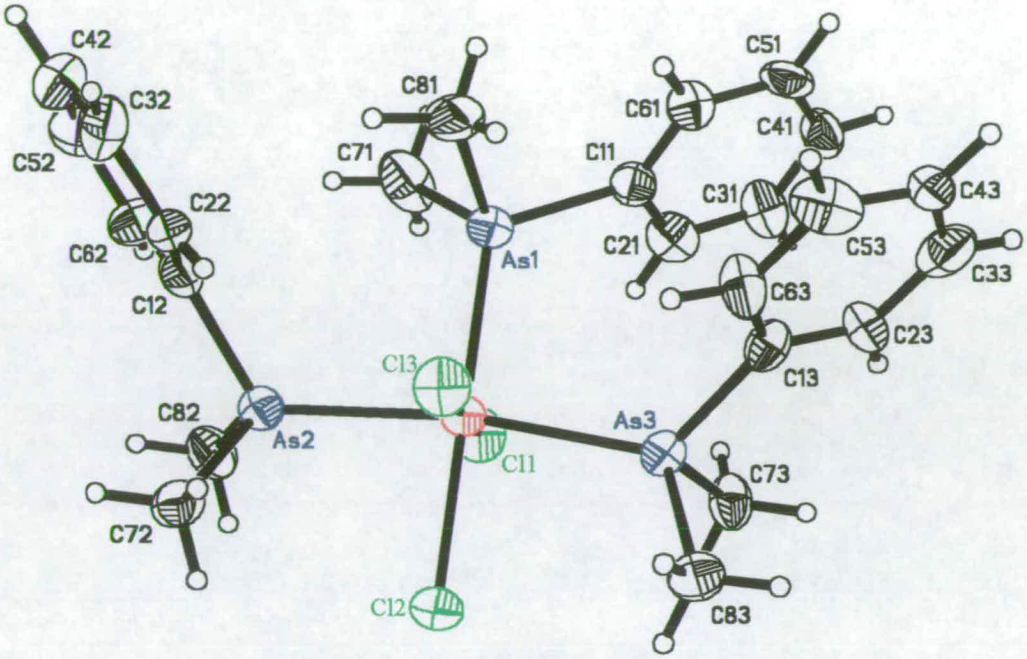

Figure 2.3 - Structure Of *mer*-[$OsCl_3(AsMe_2Ph)_3$]

Table 2.4 - Selected Bond Distances (Å) and Angles (°) of *mer*-[$OsCl_3(AsMe_2Ph)_3$]

Os(1)-Cl(3)	2.353(3)	Os(1)-Cl(2)	2.419(3)	Os(1)-As(3)	2.4715(14)
Os(1)-Cl(1)	2.377(3)	Os(1)-As(1)	2.4459(14)	Os(1)-As(2)	2.4739(13)

Cl(3)-Os(1)-Cl(1)	177.81(12)	Cl(2)-Os(1)-As(1)	175.99(9)	Cl(3)-Os(1)-As(2)	87.34(9)
Cl(3)-Os(1)-Cl(2)	92.27(12)	Cl(3)-Os(1)-As(3)	88.89(9)	Cl(1)-Os(1)-As(2)	91.68(9)
Cl(1)-Os(1)-Cl(2)	89.60(12)	Cl(1)-Os(1)-As(3)	92.39(9)	Cl(2)-Os(1)-As(2)	84.95(9)
Cl(3)-Os(1)-As(1)	91.72(9)	Cl(2)-Os(1)-As(3)	86.06(9)	As(1)-Os(1)-As(2)	94.80(5)
Cl(1)-Os(1)-As(1)	86.41(10)	As(1)-Os(1)-As(3)	94.46(5)	As(3)-Os(1)-As(2)	170.10(5)

2.2.2 Electrochemistry

We have studied the effect of variation of the ligands on the electrochemical response of the osmium metal centre. Electrochemical studies were all carried out in methylene chloride/0.5M $[TBA][BF_4]$.‡

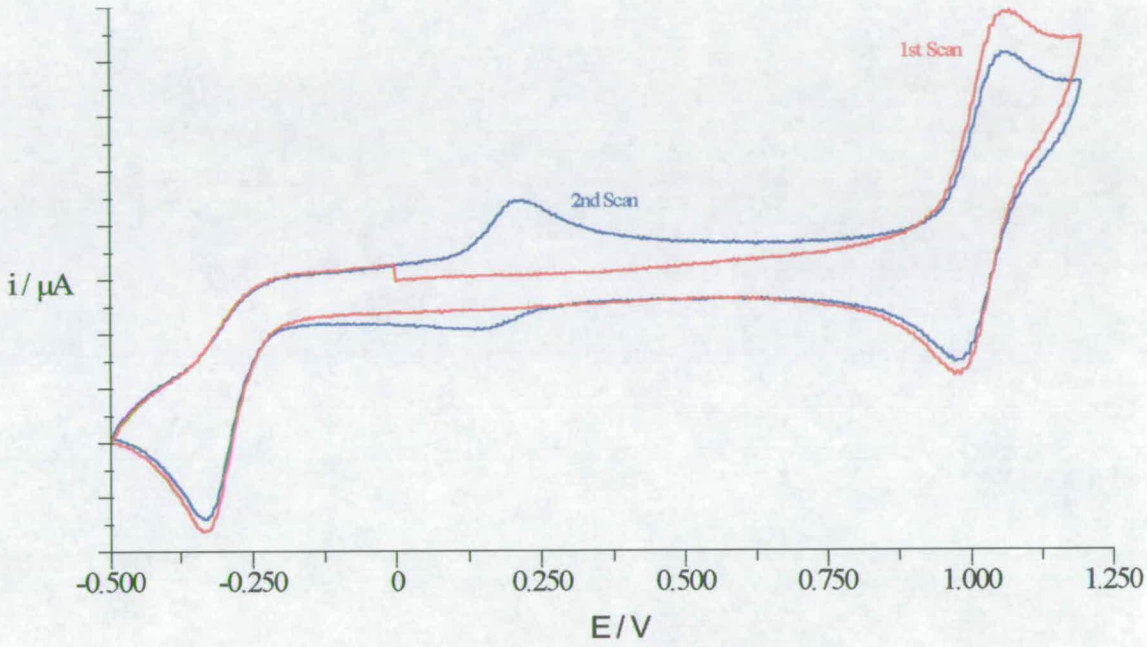

Figure 2.4 - Cyclic Voltammogram Of *mer*-$[OsCl_3(PEt_2Ph)_3]$ at RT (Scan Rate 100mVs^{-1})

Figure 2.4 shows a typical cyclic voltammetric response for one of the phosphine complexes, namely *mer*-$[OsCl_3(PEt_2Ph)_3]$, illustrating the one electron reversible oxidation and irreversible reduction processes at room temperature. The reversible oxidation is assigned as the Os(III) $\rightarrow$ Os(IV) + e^- process and the irreversible reduction as Os(III) + $e^- \rightarrow$ Os(II), followed by a rapid chemical reaction, (ec process), forming an electroactive product, $[OsX_2L_3Y]$ where X is Cl or Br, L is a tertiary phosphine and arsine and Y is a neutral coordinating ligand.§ The electrochemical response of the daughter product $[OsX_2L_3Y]$ can be observed in the second scan trace at +0.2V in Figure 2.4 above.

‡ For equipment used see Chapter 6.
§ See Chapter 1 for more details.

The arsine complexes show similar electrochemistry to that of the phosphine analogues, except that the better electron withdrawing properties of the arsine have the effect of stabilising the Os(II) complex over the time scale of the experiment. Therefore the reduction process is seen to be reversible in the cyclic voltammetic response, Figure 2.5.

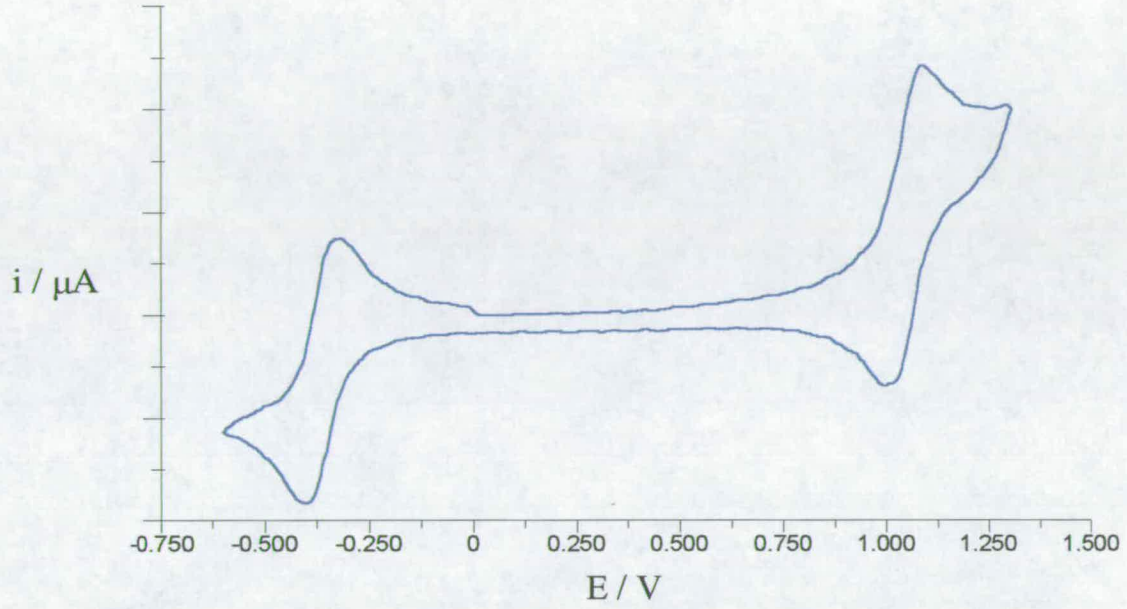

Figure 2.5 - Cyclic Voltammogram Of *mer*-$[OsCl_3(AsMe_2Ph)_3]$ at RT (Scan Rate $100mVs^{-1}$)

The oxidation and reduction potentials of the above processes at room temperature, of the chloride and bromide complexes are given in Tables 2.5 and 2.6 respectively. The redox potential is given, as is the anodic-cathodic peak difference for the oxidation and reduction couples where possible. Only the anodic peak potential is given, for the reduction of the phosphine complexes, as most of the couples were found to be chemically irreversible at room temperature.

Table 2.5 - Oxidation and Reduction Potentials for the Series *mer*-$[OsCl_3(L)_3]$, in CH_2Cl_2/0.5M [TBA]BF_4] at Room Temperature[a]

Group 15 Ligand	Reduction	Oxidation[b]
PMe_3	-0.32V	1.02V (73mV)
PMe_2Ph	-0.25V	1.08V (69mV)
$PMePh_2$	-0.18V	1.13V (73mV)
PEt_3	-0.40V	0.95V (64mV)
PEt_2Ph	-0.34V	1.03V (67mV)
$PEtPh_2$	-0.23V	1.06V (65mV)
PPr^n_3	-0.46V	0.93V (64mV)
$AsMe_2Ph$	-0.33V (72mV)	1.05V (65mV)
$AsEt_2Ph$	-0.46V (72mV)	0.96V (68mV)
$AsPr^n_3$	-0.61V (68mV)	0.89V (74mV)

a Potentials are recorded against Ag/AgCl Reference Electrode.
b Peak difference is given in parenthesis.

Table 2.6 - Oxidation and Reduction Potentials for the Series *mer*-$[OsBr_3(L)_3]$, in CH_2Cl_2/0.5M [TBA]BF_4] at Room Temperature[a]

Group 15 Ligand	Reduction	Oxidation[b]
PMe_3	-0.22V	1.03V (63mV)
PMe_2Ph	-0.12V	1.09V (70mV)
$PMePh_2$	-0.04V	1.11V (73mV)
PEt_3	-0.25V	0.98V (74mV)
PEt_2Ph	-0.21V	1.03V (74mV)
$PEtPh_2$	-0.11V	1.05V (72mV)
PPr^n_3	-0.34V	0.95V (74mV)
$AsMe_2Ph$	-0.37V (70mV)	1.05V (68mV)
$AsEt_2Ph$	-0.45V (71mV)	0.98V (68mV)
$AsPr^n_3$	-0.49V (69mV)	0.89V (72mV)

a Potentials are recorded against Ag/AgCl Reference Electrode.
b Peak difference is given in parenthesis

It is immediately obvious that varying the Group 15 ligand has a marked effect on the observed metal based oxidation and reduction potentials. For example the potential of the oxidation can be shifted 200mV more positive by replacing PPr^n_3 with $PMePh_2$.

The potentials of the tertiary arsine ligands also show considerable difference from their phosphorus analogues, e.g. oxidation of $[OsCl_3(AsEt_2Ph)_3]$ is measured at 0.96V whilst that of $[OsCl_3(PEt_2Ph)_3]$ is at 1.03V. Both the reduction and oxidation of the

arsine complexes exhibit potentials at more negative values, this is expected as arsine is widely recognised as a better electron withdrawing group than phosphine.

The potentials show no obvious dependence with Tolman's Cone Angles,[24,29] for both the reduction (Figure 2.6) and oxidation potentials (Figure 2.7). A linear relationship was obtained with Tolman's Electronic parameters,[15,26] calculated from the ν(CO) stretching frequency of the substituted $Ni(CO)_3L$ complex (See Earlier). Figures 2.8 and 2.9 show the relationship obtained for the reduction and oxidation potentials for both the chloride and bromide series.

This relationship suggests that the redox chemistry is chiefly dependent on the electronic properties of the tertiary phosphine ligands. The scatter of points away from linearity is probably due to the minimal steric effect of the ligands. The deviation is most pronounced with the larger ligands, for example the $PEtPh_2$ complexes, which has the biggest ligand cone angle of all ligands used, at 140°. Comparing the two redox processes, the oxidation step is more susceptible to these steric effect, as the loss of a electron would cause a reduction in the size of the metal electron sphere, in turn creating a smaller and more sterically hindered complex.

Figures 2.10 and 2.11 show the relationships obtained by plotting pK_a[37a,39] versus the observed reduction and oxidation potentials for the series under study. On the basis of studies by Giering *et al*[25] discussed previously we would expect the complexes with PMe_3, PMe_2Ph, $PMePh_2$, PEt_2Ph and $PEtPh_2$ to show a straight line correlation between pKa and the observed oxidation and reduction potentials, pK_a being a measure of σ-donicity as discussed earlier. The complexes with PEt_3 and PPr^n_3, would be expected to lie off the line, due to the π-character in their bonding.

In fact a single straight line correlation is not obtained in any of the plots. Two points can be made about Figures 2.10 and 2.11.

1. Each series of phosphines, i.e. methyl and ethyl exhibit a relationship with pK_a. The difference between the series is explained by their varying π-bonding character.

2. Comparing the ethyl and methyl series, the latter shows a better linear relationship than the former. This is in agreement with Giering *et al* as PEt_3 is expected to show greater π-character in bonding.

The use of pK_a values as a measure of σ-donicity is however, suspect as discussed earlier. We believe that Tolman's Electronic Parameters should be used preferentially.

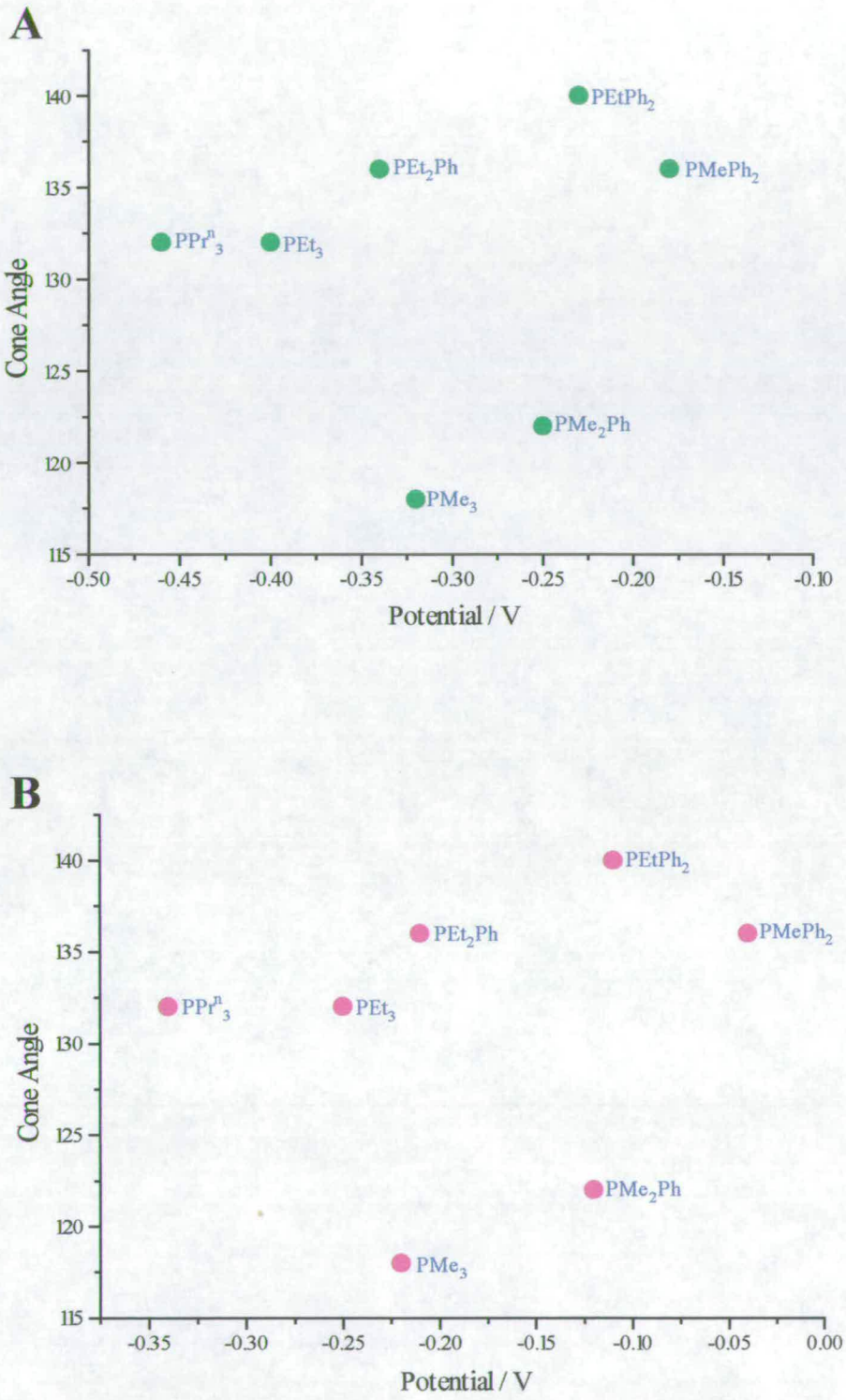

Figure 2.6 - Cone Angles Vs. Reduction Potentials for (A) *mer*-$[OsCl_3(L)_3]$ and (B) *mer*-$[OsBr_3(L)_3]$

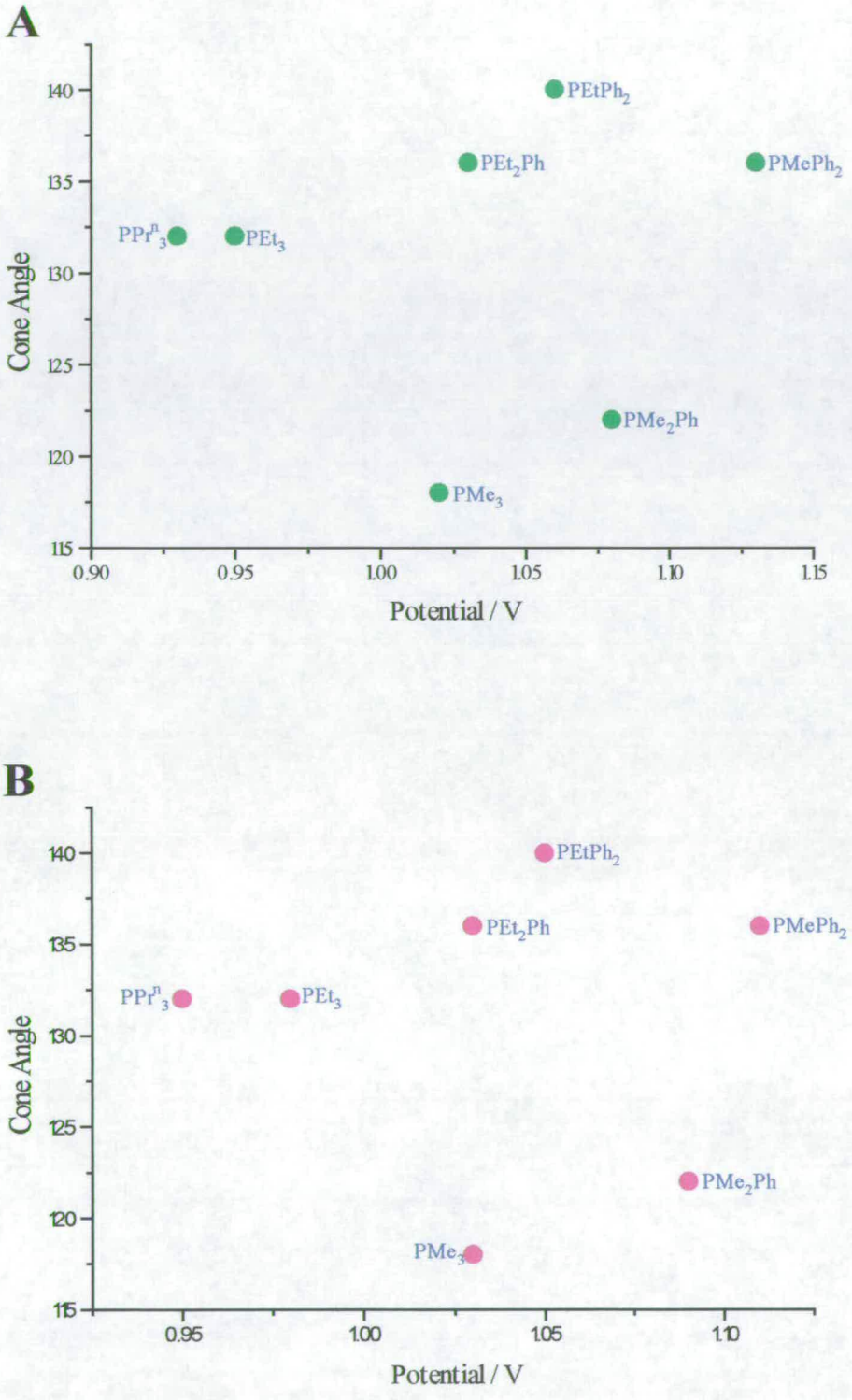

Figure 2.7 - Cone Angles Vs. Oxidation Potentials for (A) *mer*-$[OsCl_3(L)_3]$ and (B) *mer*-$[OsBr_3(L)_3]$

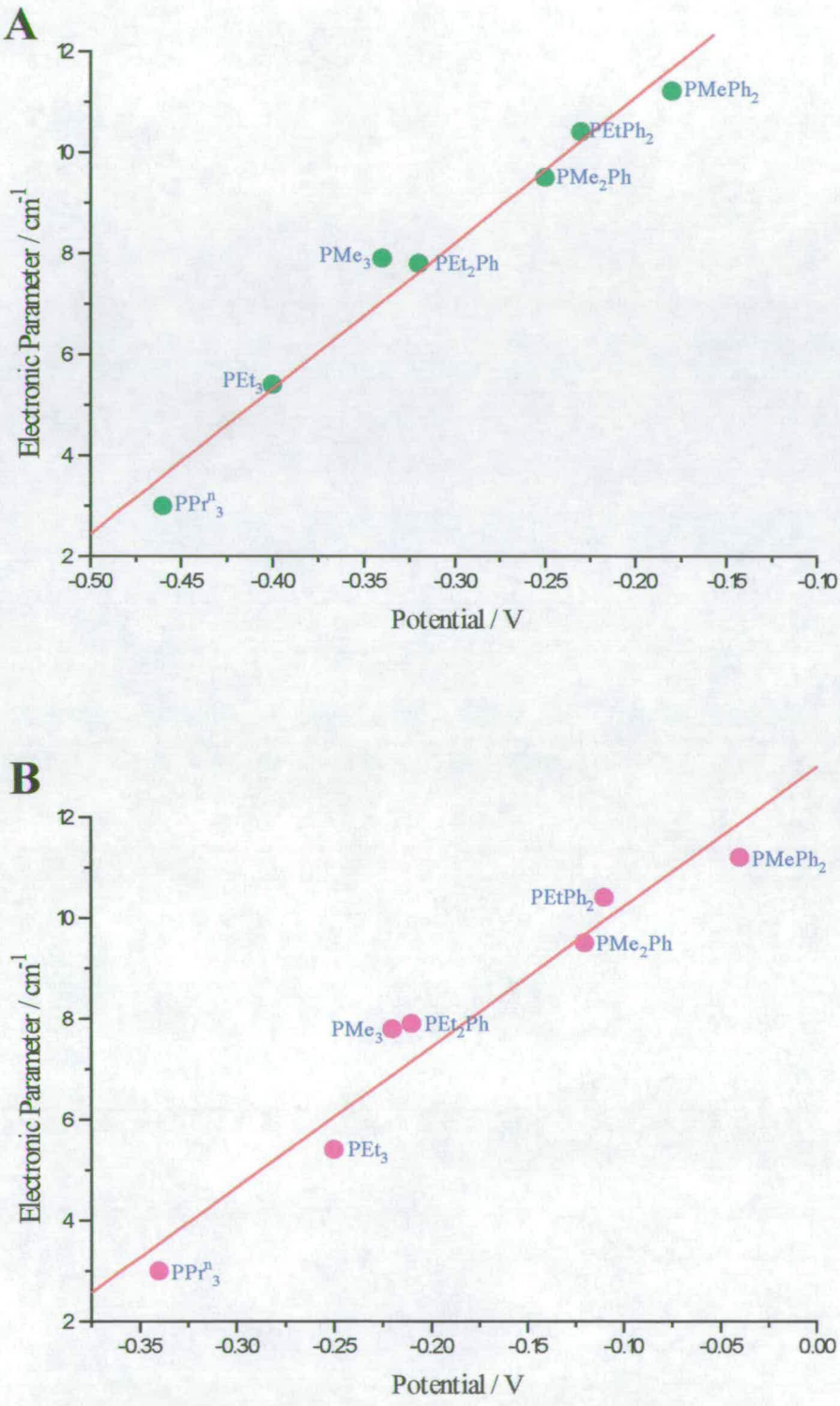

Figure 2.8 - Electronic Parameters Vs. Reduction Potentials for (A) *mer*-$[OsCl_3(L)_3]$ and (B) *mer*-$[OsBr_3(L)_3]$

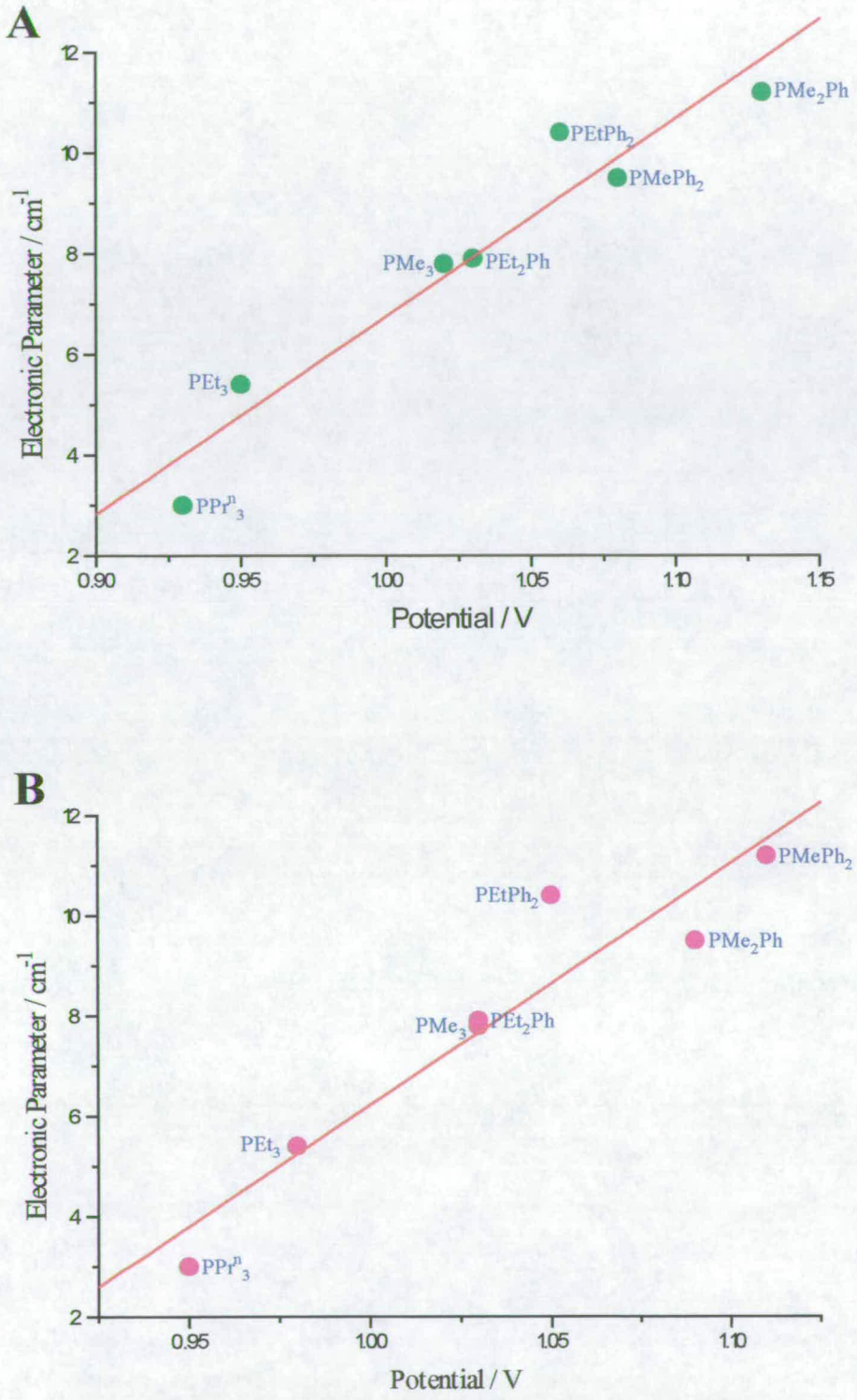

Figure 2.9 - Electronic Parameters Vs. Oxidation Potentials for (A) *mer*-$[OsCl_3(L)_3]$ and (B) *mer*-$[OsBr_3(L)_3]$

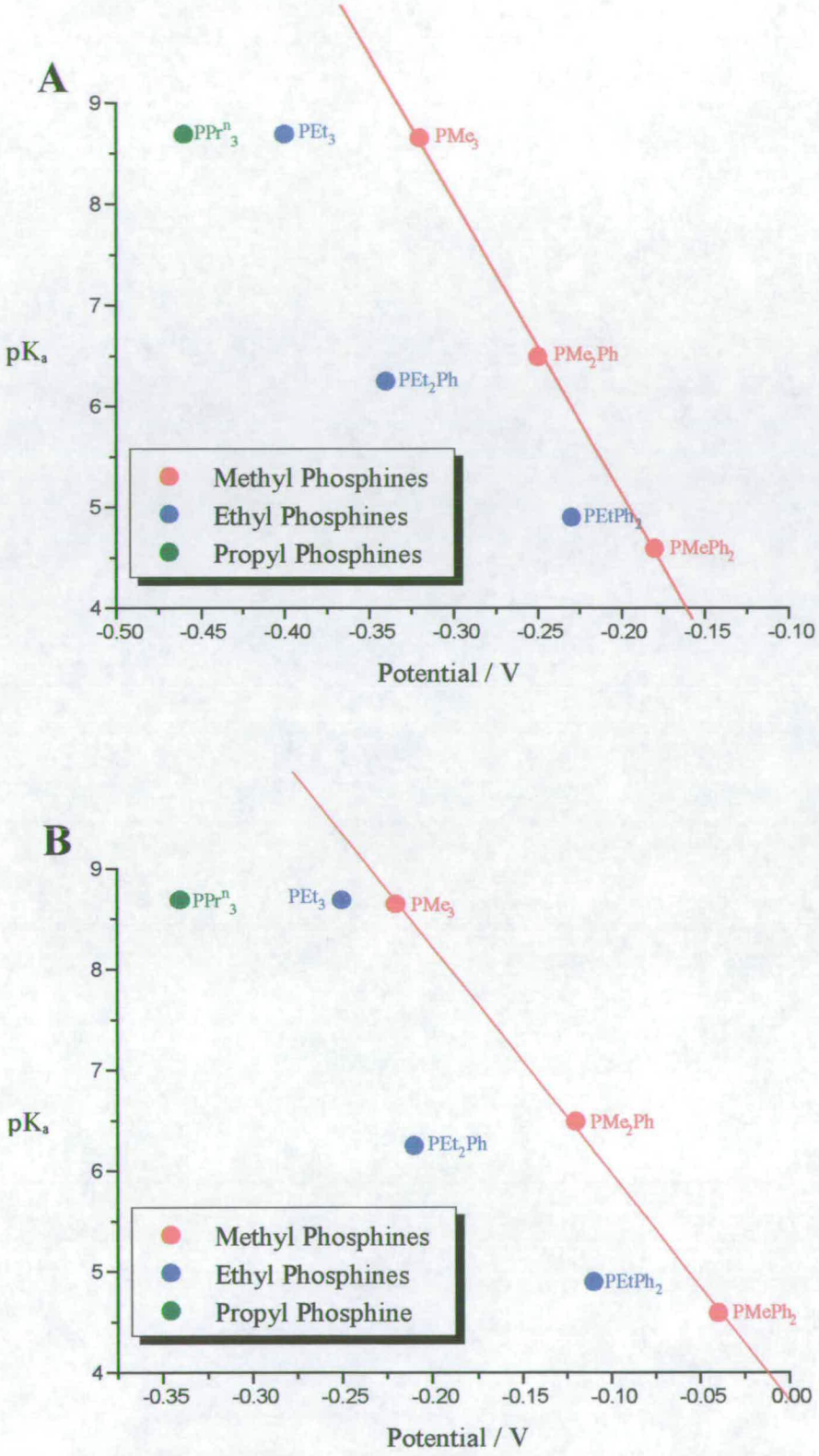

Figure 2.10 - pKa Vs. Reduction Potentials for (A) *mer*-$[OsCl_3(L)_3]$ and (B) *mer*-$[OsBr_3(L)_3]$

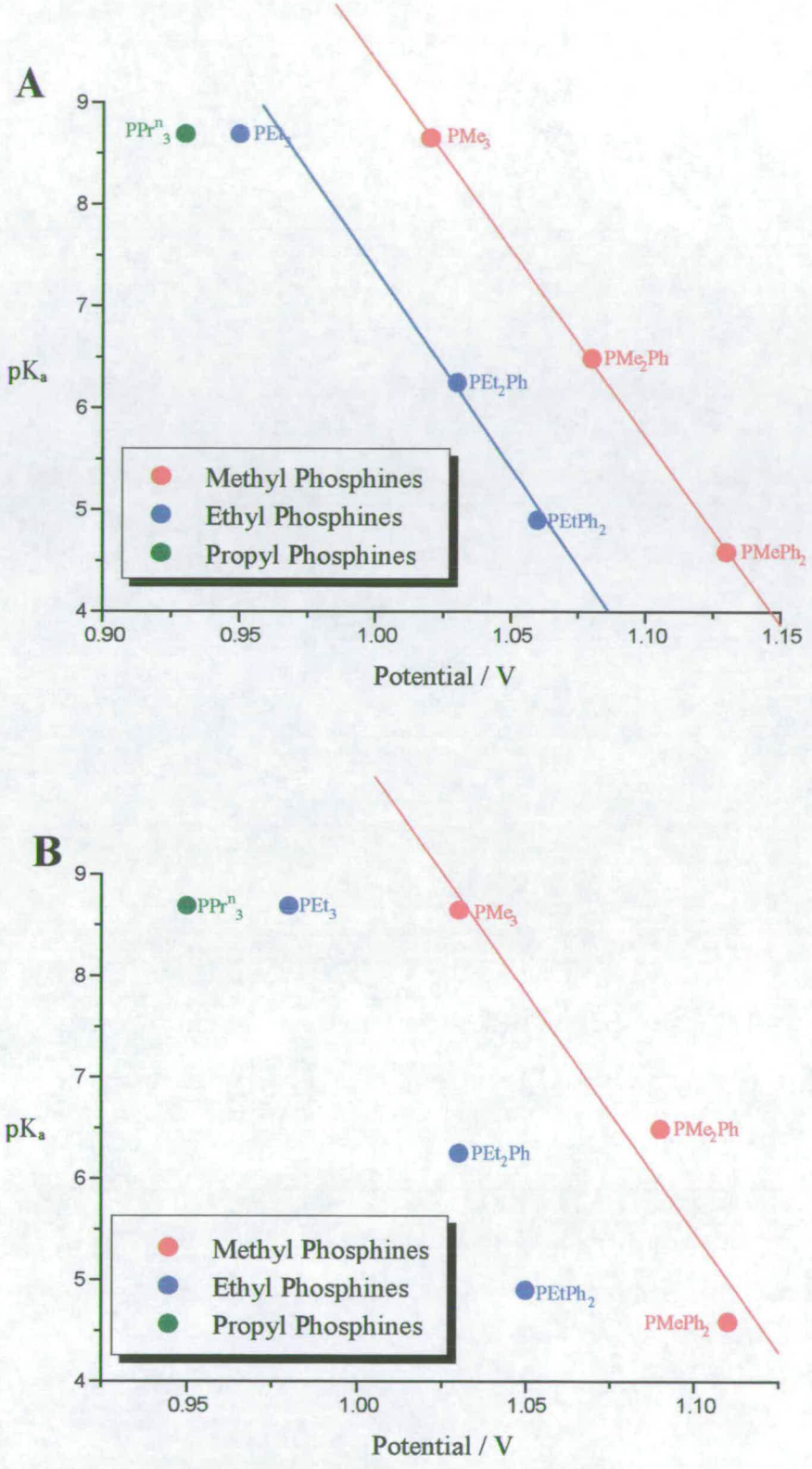

Figure 2.11 - pKa Vs. Oxidation Potentials for (A) *mer*-$[OsCl_3(L)_3]$ and (B) *mer*-$[OsBr_3(L)_3]$

2.2.3 Electronic Spectra

The UV/Vis spectra of the complexes were recorded in methylene chloride. As with mer-$[OsCl_3(PMe_2Ph)_3]$, the spectra are mostly dominated by charge transfer transitions from the full ligand based orbitals to the vacancy in the t_{2g} level. Figure 2.12 shows a typical electronic spectrum of a chloride complex, that of *mer*-$[OsCl_3(Me_3)_3]$ and Figure 2.13 shows the analogous bromide complex.

The assignment of the observed bands to electronic transitions of the chloride spectra was accomplished with the aid of Extended Hückel Molecular Orbital (EHMO) calculations undertaken on *mer*-$[OsCl_3(PMe_2Ph)_3]$ (described in Chapter 1) and *mer*-$[OsCl_3(AsMe_2Ph)_3]$ described earlier in this Chapter. The lowest energy peak which varies with L is assigned to a $\sigma(L) \rightarrow t_{2g}(Os)$ charge transition, the next to the orbital mixed $\sigma(L) + \sigma(Cl) \rightarrow t_{2g}(Os)$ transition with the transitions $\pi(Cl) \rightarrow t_{2g}(Os)$ associated with the remaining higher energy features. Visible on some spectra were also high energy and high intensity bands associated with the intraligand $\pi \rightarrow \pi^*$ transitions. Table 2.7 list the absorption peaks and assignments made for the series *mer*-$[OsCl_3L_3]$, where L is a tertiary phosphine or arsine.

The UV/Vis spectra of the bromide series were assigned via the EHMO calculation performed on *mer*-$[OsBr_3(PPr^n_3)_3]$.** Like the chloride spectra the bromide spectra can be split into three major regions. The bromide based molecular orbitals (MO) were calculated to be at higher energy than the MO's based on the phosphine or arsine ligands. Hence the lowest energy transition in the bromide spectra are assigned as $\sigma(Br) \rightarrow t_{2g}(Os)$. Similar to the chloride spectra the second region of the spectra is assigned to the mixed transitions $\sigma(Br) + \sigma(L) \rightarrow t_{2g}(Os)$ and the 3rd region as $\pi(Br) \rightarrow t_{2g}(Os)$ transitions. At high energy some complexes show high intensity bands, these are again assigned as $\pi \rightarrow \pi^*$ intraligand bands. Table 2.8 lists the absorption peaks and their assignments for the series *mer*-$[OsBr_3L_3]$ where L is a tertiary phosphine or arsine.

** See Chapter 6 for details on EHMO calculation

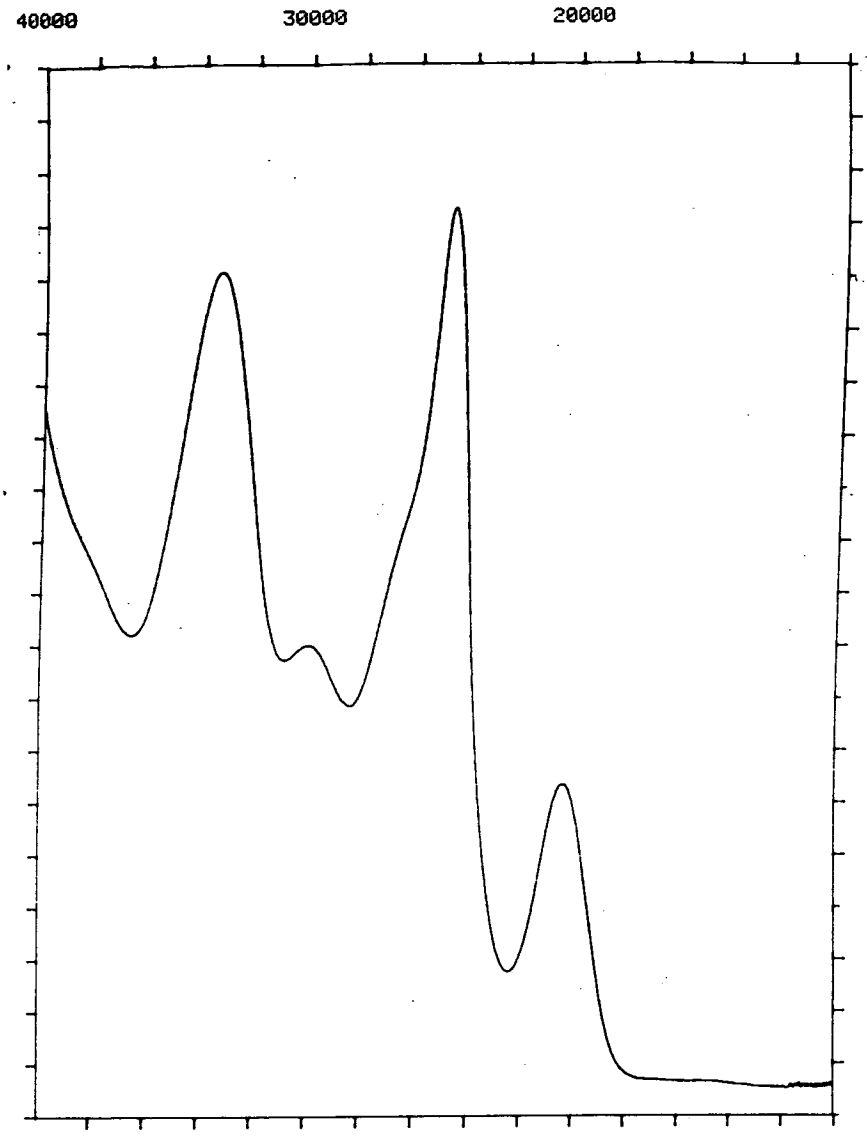

Figure 2.12 -UV/Vis Spectrum of *mer*-$[OsCl_3(Me_3)_3]$[††]

[††] Units are Wavenumbers (cm^{-1}), For Molar Extinction Coefficients See Table 2.7

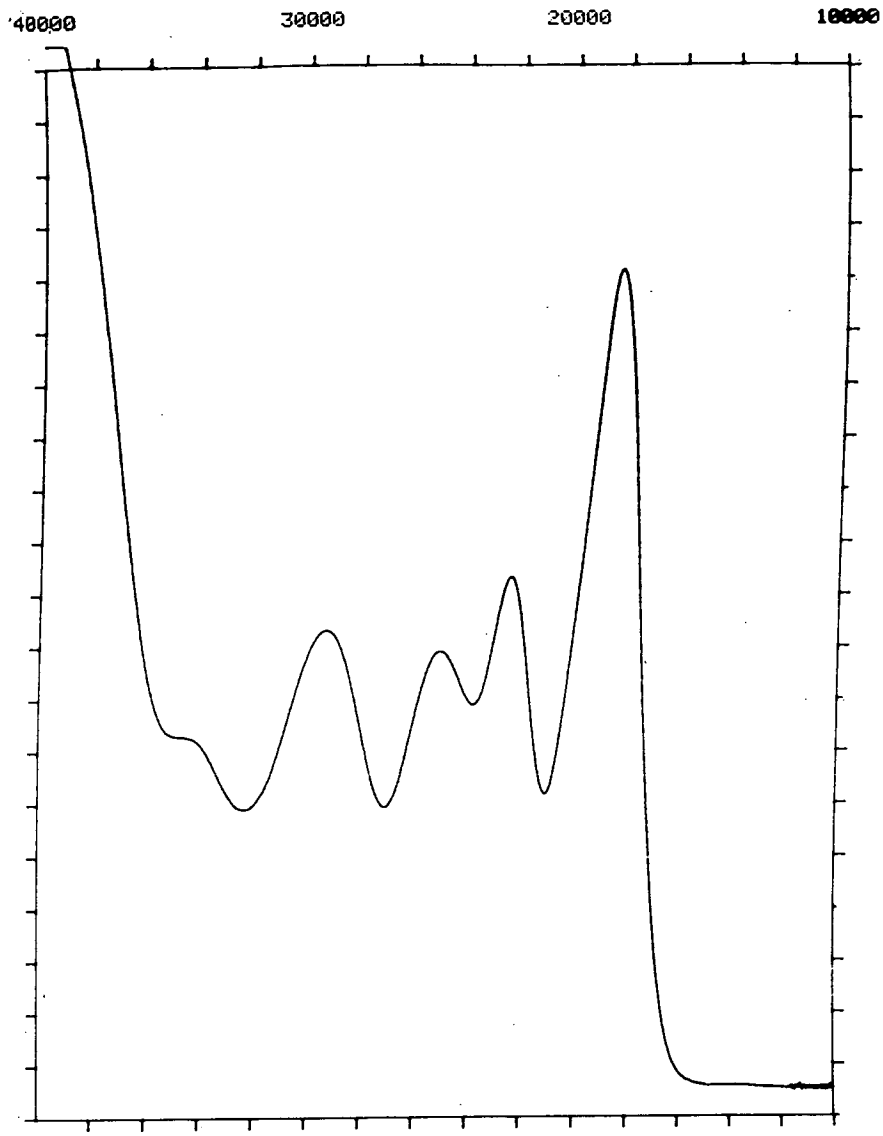

Figure 2.13 -UV/Vis Spectrum of *mer*-$[OsBr_3(Me_3)_3]$[‡‡]

‡‡ Units are Wavenumbers (cm^{-1}), For Molar Extinction Coefficients See Table 2.8

Table 2.7 - UV/Vis Spectroscopic Data for *mer*-$[OsCl_3L_3)_3]$ in CH_2Cl_2[#]

L	Colour	$\sigma(L)\rightarrow t_{2g}(Os)$	$\sigma(L)+\sigma(Cl)\rightarrow t_{2g}(Os)$	$\pi(Cl)\rightarrow t_{2g}(Os)$	Intraligand $\pi\rightarrow\pi^*$
PMe_3	Red/Brown	20300(2040)	24800(5530)	26500sh(3270), 29700(2740), 33423(5230)	
PMe_2Ph	Red/Orange	19200(660)	23500(1440)	27000sh(1210), 29400(1880)	
$PMePh_2$	Red/Brown	18900(2820)	24600(4070)	27900sh(4170), 32301(9600)	39200(52200)
PEt_3	Red	19400(740)	24200(1540)	26300(1280), 33600(2240)	
PEt_2Ph	Dark Red	18700(530)	23100(1060)	29000sh(1160)	39700(22600)
$PEtPh_2$	Orange/Red	18800(250)	22600(1510)	27000(2220)	37900(36970)
PPr^n_3	Red	19300(250)	24200(810)	26100(2200), 32900(2500)	
$AsMe_2Ph$	Dark Red/Brown	20100(1460)	24000(2730)	27000sh(1600), 31000sh,(2880) 33100sh(3400)	
$AsEt_2Ph$	Red	19400(650)	23500(1450)	27000(1070)	39100(28400)
$AsPr^n_3$	Orange/Brown	19700(970)	24300(2500)	26900(1200), 33200(2600)	41200(24100)

[#] *Units are* cm^{-1}. *Values in Parenthesis are Molar Extinction Coefficients* $\varepsilon/ M^{-1}cm^{-1}$

Table 2.8 - UV/Vis Spectroscopic Data for *mer*-$[OsBr_3L_3)_3]$ in CH_2Cl_2[#]

L	Colour	$\sigma(Br) \rightarrow t_{2g}(Os)$	$\sigma(L)+\sigma(Br) \rightarrow t_{2g}(Os)$	$\pi(Br) \rightarrow t_{2g}(Os)$	Intraligand $\pi \rightarrow \pi^*$
PMe_3	Purple	18500(3200)	22400(2120)	25000(1860), 29300(1940), 35100sh(1830)	
PMe_2Ph	Purple	17600(1670)	21400(1200)	25000(1360), 28000sh(1200)	
$PMePh_2$	Purple	17800(2720)	20500(2610)	25800(1450), 29500(2320)	
PEt_3	Purple	17400(3670)	20000(2690)	22200(2690), 25000(2630), 29600(2810)	
PEt_2Ph	Purple	17300(1500)	20900(1330)	24700(1410), 28000sh(1420)	38500sh(29950)
$PEtPh_2$	Purple	17800(1330)	20900(1330)	26000sh(1340), 29000sh(1850)	37500(21800)
PPr^n_3	Purple	17400(1870)	20000(1410)	22200(1410), 24900(1440), 29400(1540)	
$AsMe_2Ph$	Dark Purple	19600(1210)	22500(1590)	25000sh(1260), 30000(1620)	
$AsEt_2Ph$	Red/Purple	17900(1140)	19800(1110)	21400(1170), 24000(1180), 29941(1660)	38500(29743)
$AsPr^n_3$	Purple	17800(1670)	20700(1610)	22500(1230), 25800(1260), 29800(1680)	

[#] *Units are* cm^{-1}. *Values in Parenthesis are Molar Extinction Coefficients* ε/ $M^{-1}cm^{-1}$

There are two points to note about the spectra for the series *mer*-$[OsX_3L_3]$.

1. Comparing the molar extinction coefficients of the first transition for the two series of complexes, the coefficients of the bromide are considerably larger than of the chloride. This is in agreement with our assignment that the first transition of the bromide complexes is from MO's associated with Br, rather than MO's based on ligand L.

2. The lowest energy transition in the series *mer*-$[OsCl_3L_3]$, $\sigma(L) \rightarrow t_{2g}(Os)$, shows a deviation across the series ranging from 18700cm^{-1} to 20300cm^{-1} as L is altered. If the position of the band is plotted against the electronic parameter (χ_i) of the tertiary phosphine no direct correlation was observed, as shown in Figure 2.14. If however the positions were plotted as a function of the cone angle (θ), a straight line correlation is obtained for the chloride series, as shown in Figure 2.15A. Similar effects have been reported in the literature.

Bennett *et al*[40] during the study of *trans*-$[CrL_2(NCS)_4]^{2-}$ where L is a tertiary phosphine observed a red shift in the lowest energy band with increasing the steric bulk of the phosphine ligands: PMe_3(19950cm^{-1}), PEt_3(19500cm^{-1}) and PEt_2Ph(19050cm^{-1}). The electronic transitions of *trans*-$[NiX_2L_2]$ where X = NCS, Cl or Br and L = tertiary phosphine, also show a red shift due to the increased size of the phosphine ligands. The bands at ~25000cm^{-1} and ~19000cm^{-1} decreased by an amount dependent on X, the shift being greater the larger X.[41]

Unlike the chloride no linear correlation is obvious for the bromide series with plots against either χ_i or θ. Figure 2.14B shows the plot of band frequency against χ_i and Figure 2.15B shows the plot against θ series. Again the result agrees with our assignment of the bromide MO's being higher in energy than the MO's based on the Group 15 ligands.

It is interesting to note that the redox potentials vary with ligand L electronic parameter whereas the cone angle (steric) parameters of L is more useful for predicting the lowest energy band maximum for X = Cl.

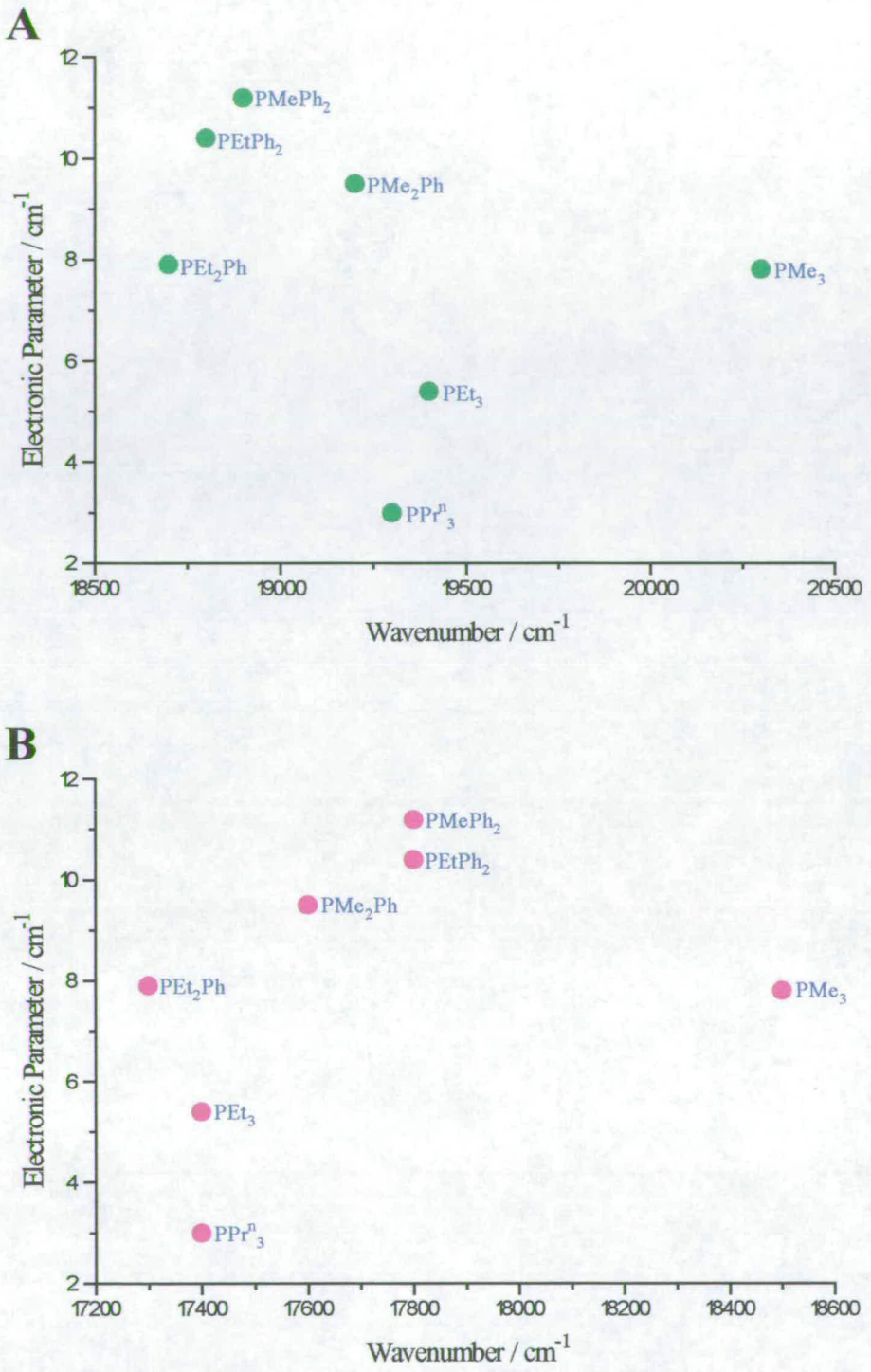

Figure 2.14 - Plot of the Energy of $\sigma(L) \rightarrow t_{2g}(Os)$ Transition versus Electronic Parameter (χ_i) of Tertiary Phosphine for (A) *mer*-$[OsCl_3L_3]$ and (B) *mer*-$[OsBr_3L_3]$

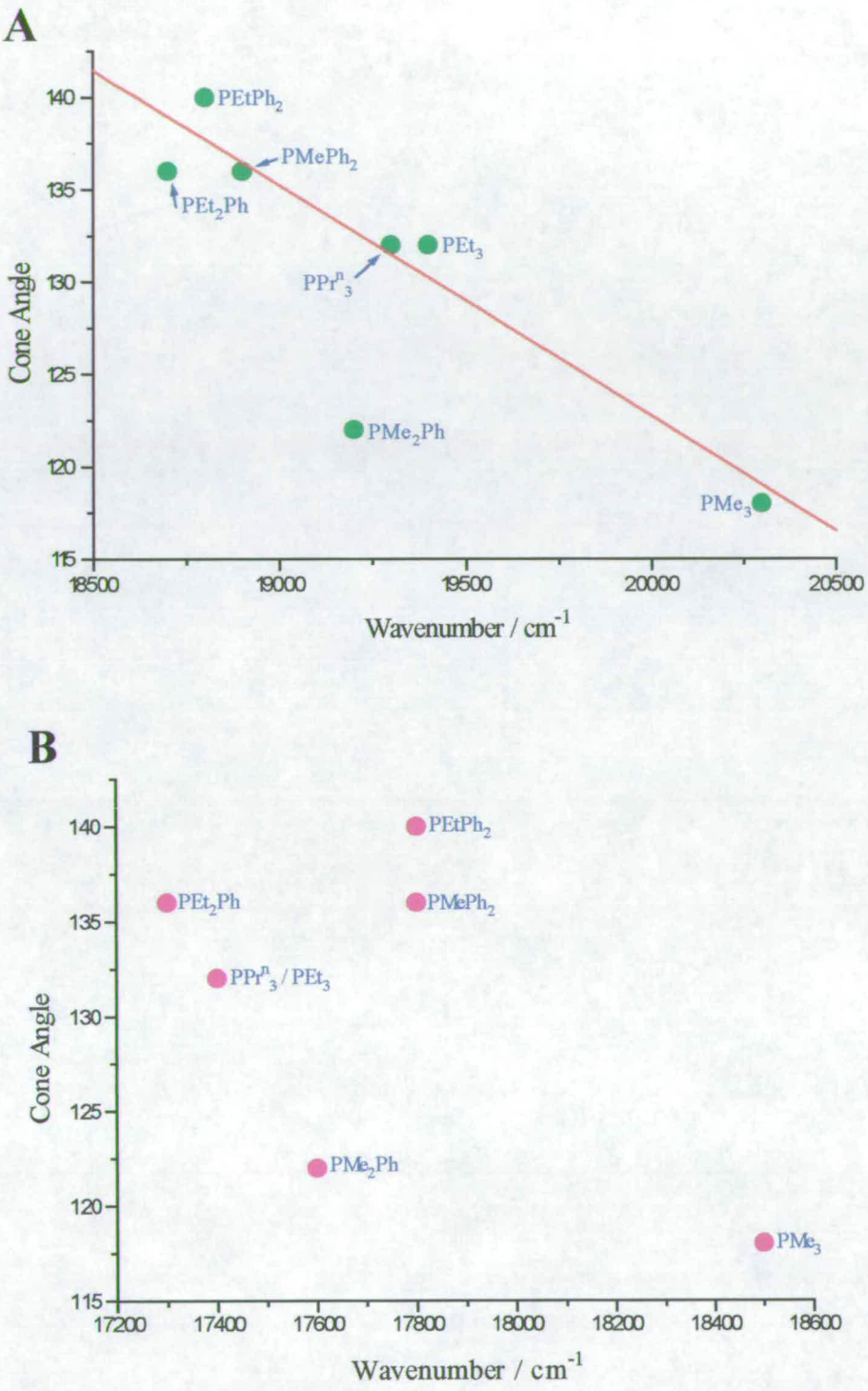

Figure 2.15 - Plot of the Energy of $\sigma(L) \rightarrow t_{2g}(Os)$ Transition versus Cone Angle (θ) of Tertiary Phosphine for (A) *mer*-$[OsCl_3L_3]$ and (B) *mer*-$[OsBr_3L_3]$

2.2.4 Spectroelectrochemistry

The ec process which all complexes in the series undergo, can be followed *in situ* by UV/Vis spectroscopy, as with *mer*-$[OsCl_3(PMe_2Ph)_3]$. Figure 2.16 shows the spectral changes which accompany the conversion of *mer*-$[OsCl_3(AsPr^n_3)_3]$ to *trans*-$[OsCl_2(AsPr^n_3)_3(MeCN)]$ as measured in an O.T.E. cell. As before the reduction results in the collapse of the LMCT bands and growth of the high energy shoulder assigned as an intraligand transition. On reoxidation to *trans*-$[OsCl_2(AsPr^n_3)_3(MeCN)]^+$ LMCT bands emerge in the visible region of the spectrum at different energies from those of the parent complex, (Figure 2.17). Again an isobestic point is observed at 32200cm^{-1} proving no transition state is involved in the oxidation.

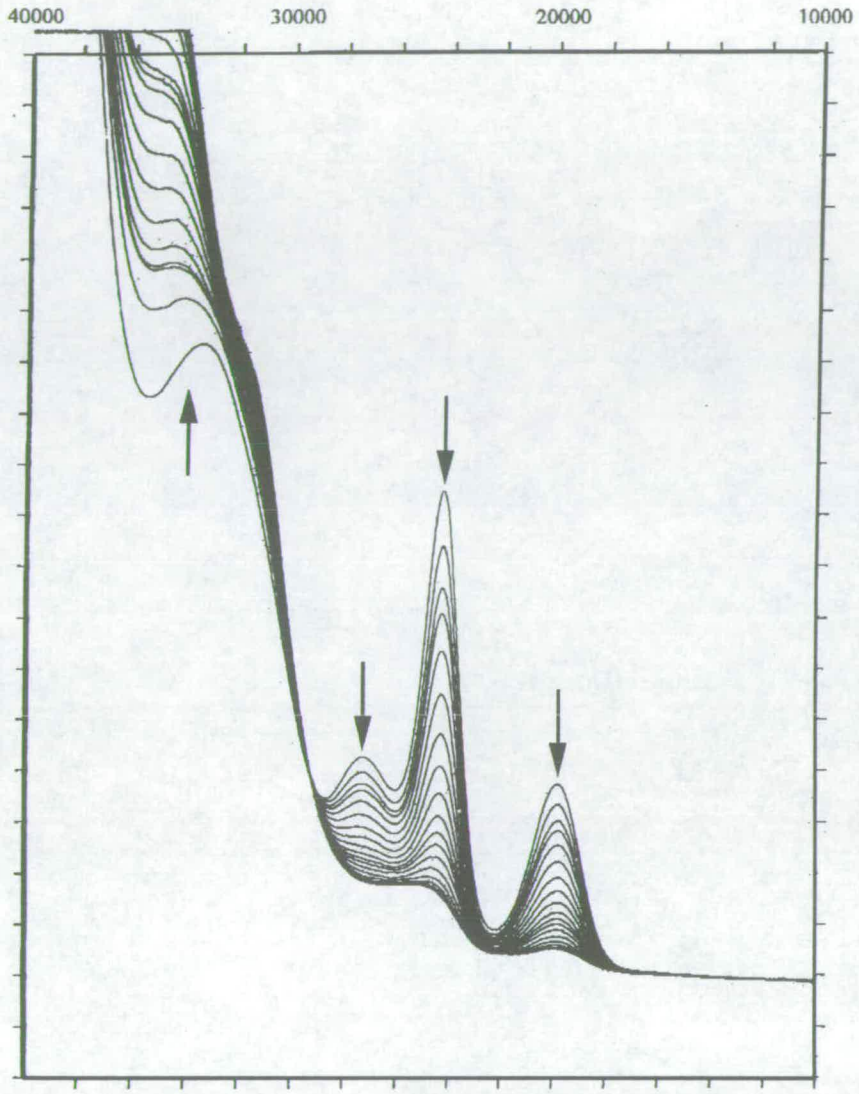

Figure 2.16 - Spectral Changes Accompanying the Reduction of *mer*-$[OsCl_3(AsPr^n_3)_3]$ to *trans*-$[OsCl_2(AsPr^n_3)_3(MeCN)]$ in MeCN/0.1M [TBA][BF_4] at RT using an O.T.E. Cell[§§]

[§§] Units are Wavenumbers (cm^{-1})

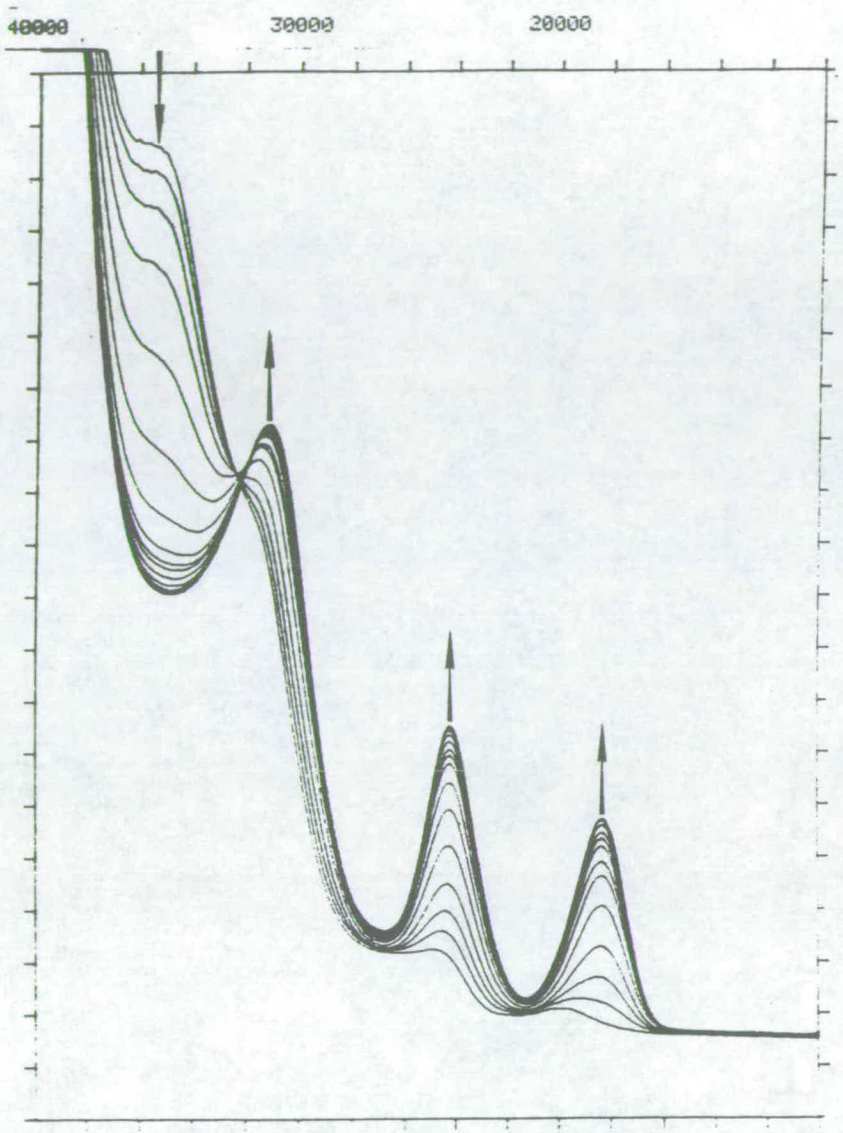

Figure 2.17 - Spectral Changes Accompanying the Oxidation of to *trans*-$[OsCl_2(AsPr^n_3)_3(MeCN)]$ to *trans*-$[OsCl_2(AsPr^n_3)_3(MeCN)]^+$ in MeCN/0.1M $[TBA][BF_4]$ at RT using an O.T.E. Cell[***]

[***] Units are Wavenumbers (cm^{-1})

2.2.5 Conclusion

The redox behaviour of the metal centre is dependent on the electronic properties of the tertiary phosphine/arsine ligands. Good correlation was achieved between the oxidation/reduction potentials and χ_i. Thus by varying L and X we can fine tune the electrochemical behaviour of the complex.

The electronic spectra of the complexes have been recorded and assigned and a good correlation was found between θ and the lowest energy transition for the chloride complexes. The lack of correlation for the bromide series agrees with our assignment that the halide based MO's are higher in energy on bromide than on chloride.

In Chapter 3 we will expand the study of these complexes by applying Lever's Additivity Model to the series and also examine the chemistry of complexes of the type *mer*-$[OsCl_3L_2L']$, where L and L' are different tertiary phosphines and/or arsines.

2.3 References

(1) J.Chatt, *Nature*, 1950, 637.

(2) E. W. Abel, M. A. Bennett and G. Wilkinson, *J.Chem. Soc.*, 1959,2323.

(3) W. D. Horrocks and R. C. Taylor, *Inorg. Chem.*, 1963, **2**, 723.

(4) F. A. Cotton, *Inorg. Chem.*, 1964, **5**, 702.

(5) F. A. Cotton and C. S. Kraihanzel, *J. Am. Chem. Soc.*, 1962, **84**, 4432.

(6) D. R. Lloyd and E. W. Schlag, *Inorg. Chem.*, 1969, **8**, 2544.

(7) J. C. Green, D. I. King and J. H. D. Eland, *J. Chem. Soc. Chem. Comm.*, 1970, 1121

(8) M. Bigorgne, *C. R. Acad. Sci. Paris*, 1960, **250**, 3484.

(9) M. Bigorgne, *J. Inorg. Nucl. Chem.*, 1964, **26**, 107.

(10) R. W. Taft, In M. S. Newman, "Steric Effects In Organic Chemistry" John Wiley and Sons, Inc., 1956, 619.

(11) R. J. Angelici, *J. Inorg. Nucl. Chem.*, 1966, **28**,2627.

(12) C. A. Streuli, *Anal. Chem.*, 1960, **32**, 985.

(13) W. A. G. Graham, *Inorg. Chem.*, 1968, **7**, 315.

(14) P. M. Treichel, *Inorg. Chem.*, 1968, **7**, 1942.

(15) C. A. Tolman, *J. Am. Chem. Soc.*, 1970, **92**, 2953.

(16) G. M. Bodner, C. Gogan and, D. N. Whittern, *J. Organomet. Chem.*, 1983, **243**, 305.

(17) **(a)** B. E. Mann, C. Masters and, B. L. Shaw, *J. Chem. Soc.*, 1971, 1104. **(b)** P. S. Braterman, D. W. Milne, E. W. Randall and, E. J. Reosenburg, *J. Chem. Soc., Dalton Trans.*, 1973, 1027. **(c)** O. Stelzer and, E. Unger, *Chem. Ber.*, 1975, **108**, 1246. **(d)** C. Barbeau and, J. Turcotte, *Can. J. Chem.*, 1976, **54**, 1603. **(e)** J. O. Albright, F. A. Tanzella and, J. G. Verkade, *J. Coord. Chem.*, 1976, **6**, 225. **(f)** R. Uson, V. Riera, J. Gimeno, M. Laguna and, M. P. Gamasa, *J. Chem. Soc., Dalton Trans.*, 1979, 996. **(g)** J. A. Timney, *J.Inorg. Chem.*, 1979, **18**, 2505. **(h)** S. Vastag, B. Heil and, L. Marko, *J. Mol Catal.*, 1979, **5**, 189. **(i)** R. G. Goel, W. P. Henry and, R. C. Srivastava, *Inorg. Chem.*, 1981, **20**, 1727. **(j)** A. Kececi and, D. Rehder, *Naturforsch.*,

B: Anorg. Chem., Org. Chem., 1981, **36B**, 20. **(k)** G. M. Gray and C. S. Kraihanzel, *J. Organomet. Chem.*, 1983, **241**, 201. **(l)** T Bartik, T. Himmler, H. G. Schulte and, K. J. Seevogel. *J. Organomet. Chem.*, 1984, **272**, 29. **(m)** K. Ihmels and, D. Redher, *Organometallics*, 1985, **4**, 1334.

(18) **(a)** G. M. Bodner, *Inorg. Chem.*, 1974, **13**, 1951. **(b)** G. M. Bodner and, L. J. Todd, *Inorg. Chem.*, 1974, **13**, 1335. **(c)** G. M. Bodner, *Inorg. Chem.*, 1975, **14**, 1932. **(d)** G. M. Bodner, *Inorg. Chem.*, 1975, **14**, 2694. **(e)** W. C. Trogler and, L.G.Marzilli, *Inorg. Chem.*, 1975, **14**, 2942. **(f)** R. W. Balk, D. J. Stufkens and, A. Oskam, *Inorg. Chim. Acta*, 1978, **28**, 133. **(g)** S. O. Grim and, R. M. Singer, *J. Coord. Chem.*, 1978, **8**, 121. **(h)** G. M. Bodner, M. P. May and, L. E. McKinney, *Inorg. Chem.*, 1980, **19**, 1951. **(i)** T. T. Derencsenyi, *Inorg. Chem.*, 1981, **20**, 665. **(j)** E. C. Alyea, R. E. Lenkinski, and, A. Somogyvari, *Polyhedron*, 1982, **1**, 130. **(k)** G. M. Bodner, C. Gagnon and, D. N. Whittern, *J. Organomet. Chem.*, 1983, **243**, 305. **(l)** A. F. Masters, G. E. Bossard, T. A. George, R. T. C. Brownlee, M. J. O'Connor, and, A. G. Wedd, *Inorg. Chem.*, 1983, **22**, 908. **(m)** R. J. Blau and, J. H. Espenson, *Inorg. Chem.*, 1986, **25**, 878. **(n)** R. V. Honeychuck and, W. H. Hersh, *Inorg. Chem.*, 1987, **26**, 1826.

(19) F. A. Cotton, W. T. Edwards, F. C. Rauch, M. A. Graham, R. N. Perutz and, J. J. Turner, *J. Coord. Chem.*, 1973, **2**, 247.

(20) **(a)** J. W. Yarbourgh and, M. B. Hall, *Inorg. Chem.*, 1978, **17**, 2269. **(b)** S. Ikuta, P. Kebarle, G. M. Bancroft, T.Chan and R. J. Puddlephatt, *J. Am. Chem. Soc.*, 1982, **104**, 5899. **(c)** B. E. Bursten, D. J. Darensbourg, G. E. Kellog and, D. L. Lichtenberger, *Inorg. Chem.*, 1984, **23**, 4361. **(d)** R. J. Puddephatt, L. Dignard-Bailey and G. M. Bancroft, *Inorg. Chim. Acta*, 1985, **96**, L91.

(21) **(a)** W. E. Carroll, F. A. Deeney, F. A. Delaney and F. J. Lalor, *J. Chem. Soc., Dalton Trans.*, 1973, 718. **(b)** H. Inoue, M. Sasagawa and, E. Fluck, *Z. Naturforsch., B: Anorg. Chem., Org. Chem.*, 1985, **40B**, 22. **(c)** B. V. Johnson, A. L. Steinmetz and, P. J. Ouseph, *J. Coord. Chem.*, 1985, **14**, 103.

(22) **(a)** M. H. Whangbo and, K. R. Steward, *Inorg. Chem.*, 1982, **21**, 1720. **(b)** S. Xiaxi, W. C. Trogler, D. E. Ellis and, Z. Berkovitch-Yellin, *J. Am. Chem. Soc.*, 1983, **105**, 7033. **(c)** D. S. Marynick, *J. Am. Chem. Soc.*, 1984, **106**, 4064.

(23) (a) C. W. Smith, G. W. Vanloon and, G. W. Baird, *J. Coord. Chem.*, 1976, **6**, 89. (b) N. G. Connelly and, M. D. Kitchen, *J. Chem. Soc., Dalton Trans.*, 1977, 931. (c) A. M. Bond, S. W. Carr, R. Colton and, D. P. Kelly, *Inorg. Chem.*, 1983, **22**, 989. (d) J. W. Hershberger and, J. K. Kochi, *Polyhedron*, 1983, **2**, 929. (e) D. J. Kuchynka, C. Amatore and, J. K. Kochi, *Inorg. Chem.*, 1986, **25**, 4087.

(24) (a) F. A. Cotton, D. J. Darensbourg and, W. H. Ilsley, *Inorg. Chem.*, 1981, **20**, 578. (b) F. A. Cotton, D. J. Darensbourg and, B. W. S. Kolthammer, *Inorg. Chem.*, 1981, **20**, 4440. (c) F. A. Cotton, D. J. Darensbourg, S. Klein, and, B. W. S. Kolthammer, *Inorg. Chem.*, 1982, **21**, 294. (d) E. C. Alyea, G. Ferguson and, A. Somogyvari, *Inorg. Chem.*, 1982, **21**, 1369. (e) F. A. Cotton, D. J. Darensbourg, S. Klein and, B. W. S. Kolthammer, *Inorg. Chem.*, 1982, **21**, 2661. (f) N. Bresciani-Pahor, M. Forcolin, L. G. Marzilli, L. Randaccio, M. F. Summers and, P. J. Toscano, *Coord. Chem. Rev.*, 1985, **63**, 1. (g) M. J. Wovkulich, J. L. Atwood, L. Canada and, J. D. Atwood, *Organometallics*, 1985, **4**, 867. (h) A. G. Orpen and, N. G. Connelly, *J. Chem. Soc., Chem. Comm.*, 1985, 1310.

(25) M. N. Golovin, M. M. Rahman, J. E. Belmonte and W. P. Giering, *Organometallics*, 1985, **4**, 1981.

(26) C. A. Tolman, *Chem. Rev.*, 1977, **77**, 313.

(27) C. A. Tolman, *Fundamen. Res. Organomet. Chem. Proc. (China-Jpn.-U.S.)*, 1982, 483.

(28) C. A. Tolman, *J. Am. Chem. Soc.*, 1970, **92**, 2956.

(29) C. A. Tolman, W. C. Seidel and, L. W. Gosser, *J. Am. Chem. Soc.*, 1974, **96**, 2329.

(30) E. C. Alyea, S. A. Dias, G. Fergusson and, R. J. Restivo, *Inorg. Chem.*, 1977, **16**, 2329.

(31) J. T. DeSanto, J. A. Mosbo, B. N. Starnoff, P. C. Bock and, R. E. Bloss, *Inorg. Chem.*, 1980, **19**, 3086.

(32) J.Chatt, G. J. Leigh, D. M. P. Mingos and R. J. Paske, *J. Chem. Soc, (A)*, 1968, 2636.

(33) D. J. Solmon and R. A. Walton, *Inorg. Chem.*, 1978, **17**, 2379

(34) G. Giacometti and, A. Turco, *J. Inorg. Nucl. Chem.*, 1960, **15**, 242.

(35) L.Que Jr., L. H. Pignolet, *Inorg. Chem.*, 1973, **12**, 156.

(36) C. W. Smith, G. W. Vanloon and M. C. Baird, *J. Coord. Chem.*, 1976, **6**, 89.

(37) **(a)** J. W. Herschberger, R. J. Klinger and, J. K. Kochi, *J. Am. Chem. Soc.*, 1983, **105**, 61. **(b)** P. M. Zizelamn, C. Amatore and, J. K. Kochi, *J. Am. Chem. Soc.*, 1984, **106**, 3771.

(38) M. M. Rahman, H-Y. Liu, K.Eriks, A.Prock and, W. P. Giering, *Organometallics*, 1989, **8**, 1.

(39) W. A. Henderson and C. A. Streuli, *J. Am. Chem. Soc.*, 1960, **82**, 5791.

(40) M. A. Bennett, R. J. H. Clark and A. D. J. Goodwin, *Inorg. Chem.*, 1967, **6**, 1625.

(41) G. Giacometti and A. Turco, *J. Inorg. Nucl. Chem.*, 1960, **15**, 242.

Chapter 3

Review Of Ligand Additivity Theory

Electrochemistry and Molecular Orbital Theory Calculations Of Mixed Phosphine/Phosphine and Phosphine/Arsine Osmium Complexes

3.1 Review of Ligand Additivity Theory

Ligand additivity theory is an attempt to quantify the electronic effects of the bound set of ligands on a metal centre. A review article has recently been published on the subject.[1] In order to classify ligands according to their electron donor-acceptor properties several techniques have been employed including I.R., N.M.R., U.V./Vis./N.I.R., Mössbauer and core and valence photoelectron spectroscopy. Theories have also been developed relating electrochemistry to ligand additivity and it is those that are reviewed here.

Consider a chemical species in solution, the potential at which oxidative or reductive current flows can be related to the standard potential E° for the chemical species in solution. Several studies have shown that these standard potentials can be related to the energy required to add or remove an electron from the system, which in turn can be related to the energies of the lowest unoccupied molecular orbital (L.U.M.O.) and highest occupied molecular orbital (H.O.M.O.).

Studies on aromatic hydrocarbons have demonstrated a linear relationship between the oxidation/reduction potentials and the calculated energy of the H.O.M.O.'s or the L.U.M.O.'s.[2,3] Similar correlations exist for inorganic systems. Treichel *et al*[4] studied the series of related manganese compounds $[Mn(CO)_{6-n}(CNMe)_n]^+$ (n = 2, 3 or 4). A linear relationship between, the number of isocyanide ligands and the experimentally determined oxidation potential was obtained. Each sequential replacement of CNMe by CO raised the oxidation potential by 0.5V per isocyanide This was rationalised by considering the ligand donor and acceptor properties. Further agreement was achieved by the correlation of the H.O.M.O. energies, as calculated by the non-emperical Fenske-Hall method and the oxidation potentials.[5]

Parallel work by Pickett and Pletcher[6] also studied the series of compounds discussed above, as well as other metal carbonyl complexes. They proposed for the series of electrochemical couples of $[M(CO)_{6-n}L_n]^{y+/(y+1)+}$ compounds where n = 0,1, *trans*-2, *mer*-3, *cis*-4 and 5, the following tenets could be expected:

1. For a series of related complexes, if the oxidation potentials are measured in the same inert solvent with the same reference system, then they should be able to measure the relative H.O.M.O. energies for the series, provided that the change

in free energies of solvation are approximately constant throughout the series and that the M.O.'s are not drastically altered by the oxidation process.

2. the change in the oxidation potential induced by the replacement of CO by L is independent of n and is a function of the ligand only.

3. the effect of altering the charge of a series, for a given L, is to add a constant, proportional to the charge, to the oxidation potential.

Hence the following relationship was proposed:

$$E^\circ = A + n\left(\frac{\delta E^\circ}{\delta n}\right)_L + Qy \qquad (1)$$

where A is a constant which depends upon the solvent and reference potential, $(\delta E^\circ/\delta n)_L$ is a parameter characteristic of the ligand L, which defines the shift in E° caused by the replacement of one CO by one molecule of L and Qy is a charge parameter. This latter parameter was defined by comparing E° values for an isoelectronic and isostructural series that only differ in overall charge such as $[V(CO)_6]^-$, $[Cr(CO)_6]$ and $[Mn(CO)_6]^+$. The examples studied yielded an average value of 1.48 for Qy. Using equation (1) the "Ligand Inductive Parameters", $(\delta E^\circ/\delta n)_L$, were calculated for several ligands.

The main disadvantage with the above relationship was that it did not permit a distinction to be made between isomeric pairs of complexes, such as *cis*- and *trans*-$[ML_4L'_2]$ or *mer*- and *fac*-$[ML_3L'_3]$. For example, the *cis* and *trans*-$[Mn(CO)_2(CNMe)_4]^+$ complexes have oxidation potentials of 1.44V and 1.28V (vs. S.C.E.) respectively and the *mer* and *fac*-$[Mn(CO)_3(CNMe)_3]^+$ display oxidations at 1.73V and 1.90V (vs. S.C.E.).[7] Equation (1) predicts that the isomeric pairs would have identical oxidation potentials.

The differences between the electrochemical response of isomers were first discussed by Bond *et al* using a quantitative bonding scheme.[8] They proposed that the H.O.M.O. of the *cis* isomer of $[Mn(CO)_2(CNMe)_4]^+$ will be involved in both of the π-backbonding interactions with one of the CO ligands, whereas the *trans* isomer would have no such interactions (Figure 3.1).

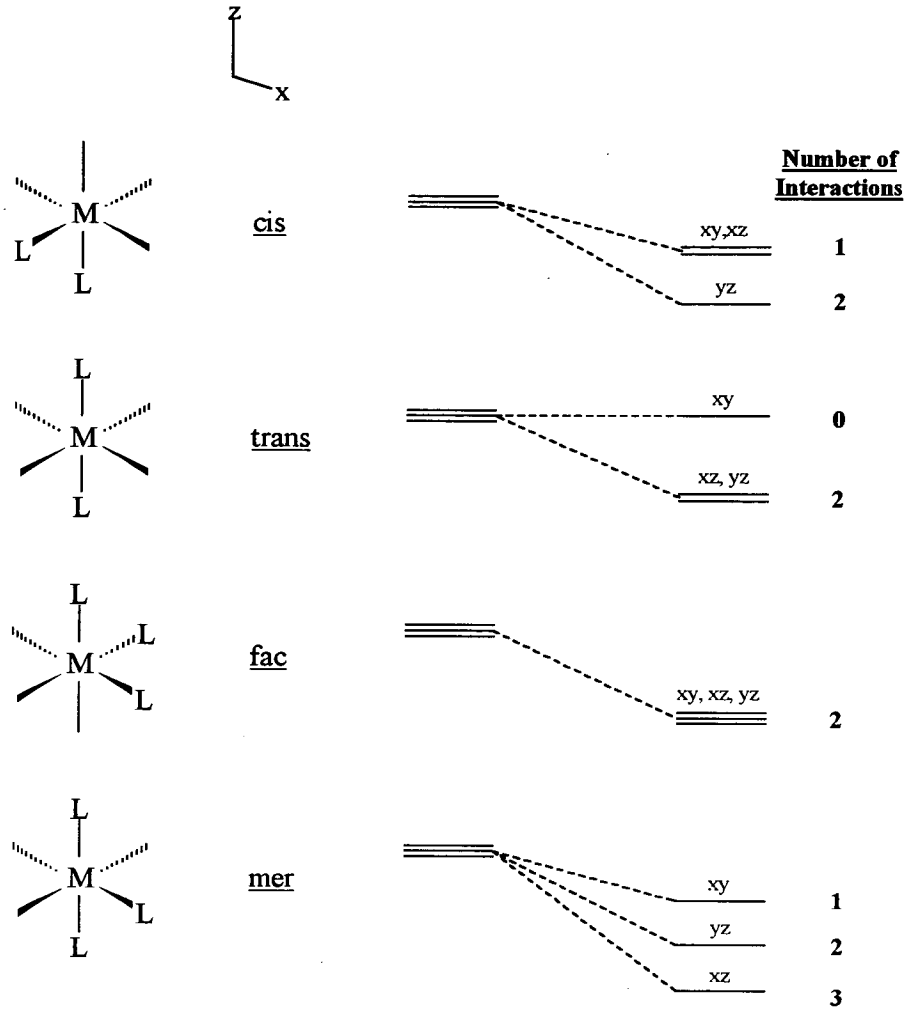

Figure 3.1 - Qualitative Diagram Showing the Energy Levels of the d_π Orbitals for Isomers of $[MnL_nL'_{(6-n)}]^+$ (n = 2, 3), where L is a better π-acceptor than L'

Likewise the H.O.M.O. of the *fac* isomer will be involved in π-backbonding interactions to two CO ligands whereas the *mer* isomer will only be involved in an interaction with one CO ligand (Figure 3.1). As CO is a better π-acceptor than CNMe the more interactions the H.O.M.O. has with CO the more it is stabilised, therefore the harder it will be to oxidise.

Treichel *et al* proposed that the effects of the ligands upon the energetics of the principal 3d molecular orbitals obeyed a simple additive relationship:[9]

$$\varepsilon_i = a + bn + cx_i \qquad (2)$$

where ε_i is the orbital energy of the ith M.O.; n is the number of carbonyl ligands in the complex; x_i is the number of carbonyl ligands that may interact with a given d orbital and a, b and c are empirically determined parameters.

These observations led Bursten to propose his ligand additivity model generalised for low spin d^6 systems of the type $[ML_nL'_{(6-n)}]$, where L and L' are ligands such as CO and CNMe respectively.[10] The model has since been extended to include d^1 complexes.[11]

The basis of the ligand additivity model for d^6 complexes was to consider the main contributing orbitals to the H.O.M.O., namely the d_π orbitals of the metal atom (d_{xy}, d_{xz} and d_{yz} in the octahedral coordinate system). Bursten assumed that the d_π orbitals interact with the ligands predominantly via empty π^* orbitals and that each ligand has an orthogonal pair of π^* orbitals.

It was postulated that the energetic contribution by the ligands upon the d_π orbitals was only dependent on:

1. The number of each type of ligand present in the complex.
2. The number of each type of ligand with which the d_π orbital can interact.

Furthermore, both these dependencies are linear, so that:

$$\varepsilon_i = a_M^0 + nb_M^L + (6-n)b_M^{L'} + x_i c_M^L + (4-x_i)c_M^{L'} \qquad (3)$$

where a_M^0 is a characteristic constant of the metal atom in its particular oxidation state; b_M^L and $b_M^{L'}$ are constants dependent on the energetic effect of the metal binding to L and L' and c_M^L and $c_M^{L'}$ are constants describing the energetic effect of the interaction between the metal orbital and L and L' respectively.

Equations (2) and (3) form the basis of the ligand additivity model; they imply the following about the energetic effects of a $[ML_nL'_{(6-n)}]$ system:

1. The gross ligand effects upon the metal atom must be independent of isomer, i.e. the average orbital energy depends only on n.
2. The gross effect on the metal of replacing a ligand is independent of n.

3. The d_π orbitals do not rehybridise upon ligand replacement even though they may be allowed to do so by symmetry.

4. The effect of allowing one of the d orbitals to interact with L instead of L' is independent of L.

5. The orbital energy of any d_π M.O. is dependent only on the number of each type of ligand available for bonding and is independent of the stereochemistry of the ligands about the orbital.

To apply the model to electrochemical data a linear correspondence between the energy of the H.O.M.O. and the oxidation potential was assumed:

$$E_{1/2} = k_1(-\varepsilon_{HOMO}) + k_2 \qquad (4)$$

where k_1 and k_2 are empirically derived parameters. Therefore from this relationship and equations (2) and (4) the following equation was described:

$$E_{1/2} = A_M^0 + nB_M^L + (6-n)B_M^{L'} + x_{HOMO}C_M^L + (4-x_{HOMO})C_M^{L'} \qquad (5)$$

where $A_M{}^0 = k_1a_M{}^0 + k_2$; $B_M{}^L = -k_1b_M{}^L$; $C_M{}^L = -k_1c_M{}^L$, etc. x_{HOMO} is the number of ligands L that interact with the H.O.M.O. of the complex. Equation (4) reduces to:

$$E_{1/2} = A + Bn + Cx_{HOMO} \qquad (6)$$

where A, B, and C are empirically derived parameters which can be related to a, b, and c by equation (5). The $E_{½}$ values predicted are dependent on the precise electronic configuration at the metal centre. Table 3.1 details these precise predictions.

Table 3.1 - $E_{½}$ values for d^n configurations, (n = 1-6), of $[ML_nL'_{(6-n)}]$ where L' is a poorer π acceptor than L. Low Spin state of M*

		d^3, d^4, d^5, d^6		d^1		d^2	
Compound	n	x_{HOMO}	$E_{½}$	x_{HOMO}	$E_{½}$	x_{HOMO}	$E_{½}$
ML'_6	0	0	A	0	A	0	A
MLL'_5	1	0	A+B	1	A+B+C	1	A+B+C
trans-$ML_2L'_4$	2	0	A+2B	2	A+2B+2C	2	A+2B+2C
cis-$ML_2L'_4$	2	1	A+2B+C	2	A+2B+2C	1	A+2B+C
mer-$ML_3L'_3$	3	1	A+3B+C	3	A+3B+3C	2	A+3B+2C
fac-$ML_3L'_3$	3	2	A+3B+2C	2	A+3B+2C	2	A+3B+2C
trans-$ML_4L'_2$	4	2	A+4B+2C	4	A+4B+4C	2	A+4B+2C
cis-$ML_4L'_2$	4	2	A+4B+2C	3	A+4B+3C	3	A+4B+3C
ML_5L'	6	3	A+5B+3C	4	A+5B+4C	3	A+5B+3C
ML_6	6	4	A+6B+4C	4	A+6B+4C	4	A+6B+4C

Bursten's model fits to a large number of complexes. The following complexes fit the observed electrochemical data:

$[Mn(CO)_n(CNMe)_{6-n}]^{1+/2+}$ where n = 0, 1, *trans*-2, *cis*-2, *mer*-3, *fac*-3 in CH_2Cl_2
$[Mn(CO)_n(CNMe)_{6-n}]^{1+/2+}$ where n = 0, 1, *trans*-2, *mer*-3, *cis*-4, 5 in MeCN
$[Mn(CO)_n(CNPh)_{6-n}]^{1+/2+}$ where n = 0,1, *trans*-2, *cis*-2, *mer*-3, *fac*-3, *cis-4* in CH_2Cl_2
$[Cr(CO)_n(CNMe)_{6-n}]^{0/1+}$ where n = *fac*-3, *cis*-4, 5 in CH_2Cl_2
$[Cr(CO)_n(CNPh)_{6-n}]^{0/1+}$ where n = 0, 1, *cis*-2, *fac*-3, *cis*-4, 5, 6 in CH_2Cl_2
$[Nb(CNMe)_nCl)_{6-n}]^{(-2+n)/(-1+n)}$ where n = 0, 1, *cis*-2 in MeCN
$[Ta(CNMe)_nCl)_{6-n}]^{(-2+n)/(-1+n)}$ where n = 0, 1, *cis*-2 in MeCN

The biggest disadvantage of Bursten's method was that in order to calculate an $E_{½}$ potential the values of A, B and C must be known. In order to obtain these constants $E_{½}$ values for three members of a substitution series have to be measured. The model itself has only been applied to low spin d^6/d^5 and d^1/d^0 couples Neither of these complexes is likely to involve rehybridisation of the orbitals on oxidation and hence should fit the model. Some other couples, a d^5/d^4 oxidation for example, probably would involve such a reorganisation. This would result in a deviation away from the linear correlation between oxidation potential and the energy of the H.O.M.O.

Since Bursten reported his additivity theory several other workers have attempted to define methods which will predict $E_{½}$ values for a given complex. In 1980 Chatt *et al*

proposed their "Ligand Parameter" method,[12] followed more recently in 1990 by Lever and his "Electrochemical Parametrisation" method.[13]

Chatt *et al*[12] utilised ligand parameters which were defined as:

$$P_L = E^{ox}_{1/2}[Cr(CO)_5L] - E^{ox}_{1/2}[Cr(CO)_6] \quad (7)$$

In other words P_L is the ligand induced change in the oxidative $E_{½}$ potential as compared to $[Cr(CO)_6]$. Table 3.2 quotes the experimentally derived ligand constants, P_L, found by Chatt.

Table 3.2 - Table of Ligand Constants P_L.(From Ref. (12))

Ligand	P_L	Ligand	P_L	Ligand	P_L
N^+	1.46	CNMe	-0.43	I^-	-1.15
NO^+	1.40	NCMe	-0.58	NCO^-	-1.16
CO	0.00	py	-0.59	Br^-	-1.17
N_2	-0.07	NH_3	-0.77	Cl^-	-1.19
$P(OPh)_3$	-0.18	CF_3COO^-	-0.78	H^-	-1.22
PPh_3	-0.35	NCS^-	-0.88	N_3^-	-1.26
CNPh	-0.38	CN^-	-1.00	OH^-	-1.55
NCPh	-0.40				

The authors examined the relationship between P_L and the oxidation potentials of several series of compounds, *trans*-$[MLY(dppe)_2]$, where dppe is $Ph_2PCH_2CH_2PPh_2$; when M = Mo, Y = NO^+, CO, N_2, NCPh or N_3^-, M = Fe, Y = H, and M = Re, Y = N_2. The plots were linear but all had varying slopes. The authors proposed the relationship:

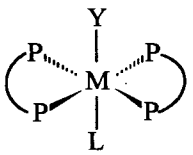

$$E^{ox}_{1/2} = E_s + \beta P_L \quad (8)$$

where E_s is the value of $E_{½}$ for $[MLY(dppe)_2]$, when L is the standard ligand CO, (P_L = 0) and is a measure of a sites electron richness. β is dimensionless and corresponds to the gradient of the plots of $E_{½}$ vs. P_L. β is a measure of the site polarisability.

Datta analysed the Ru(II)/Ru(III) couple of the series [Ru(bipy)$_2$LL'], (where bipy = 2,2'-bipyridyl; L/L' = Cl/Cl, py/Cl, PPh_3/Cl, py/py, MeCN/MeCN, PPh_3/PPh_3, en, bipy and papy) and [Ru(papy)$_2$LL'], (where papy = 2-phenylazopyridine; L/L' = OH/OH, Cl/Cl, py/py, py/MeCN, en, bipy and papy).[14] Variation of the ligands L and L' gave a satisfactory correlation between the observed potentials and that calculated by the summation $P_L+P_{L'}$. This observation gave weight to the theory that the ligand constants are additive. Values of P_L were obtained for the bidentate ligands en (ethylenediamine), bipy and papy of -1.57V, -1.14V. and -0.76V respectively. Interestingly $P_{en} \approx 2P_{NH3}$ and $P_{bipy} \approx 2P_{py}$, although P_{en} is more negative than $2P_{NH3}$, and P_{bipy} is more positive than $2P_{py}$. This is in order as the alkyl groups in en are expected to donate more electron density and the conjugation in bipy is expected to promote its π-accepting ability.

In the same paper Datta proposed the idea of combining both Bursten's model of ligand additivity and Chatt's ligand parameters. Thus application of Chatt's Equation (7) to Bursten's model compound [Cr(CO)$_5$L] gives values of P_L which can be evaluated using the following relationships: $(B^L_{Cr} - B^{CO}_{Cr} + C^L_{Cr} - C^{CO}_{Cr})$ or $(B^L_{Cr} - B^{CO}_{Cr} - C^{CO}_{Cr})$ depending on the availability of proper π-accepting orbitals on L. This relationship holds for all ligands considered except N^+ and NO^+. The P_L values of N^+ and NO^+ represent their electrostatic interaction compared to CO *i.e.* $(B^L_{Cr} - B^{CO}_{Cr})$.

For carbonyl complexes like [Cr(CO)$_4$LL'], when L and L' are poorer electron acceptors than CO, the potential of the Cr^0/Cr^1 couple can be written as:

$$E^{ox}_{1/2} = A^0_{Cr} + B^{CO}_{Cr} + 4C^{CO}_{Cr} + (P_L + P_{L'}) \qquad (9)$$

A plot of $E^0_{1/2}$ vs. $(P_L+P_{L'})$ should result in a slope of unity and an intercept of the half wave potential for the Cr^0/Cr^1 couple of [Cr(CO)$_6$]. For *cis*-[Cr(CO)$_4$LL'], where L/L' = MeCN/MeCN, Py/Py, MeNC/MeNC, PPh_3/PPh_3, CO/py, CO/MeCN, CO/MeNC and CO/PPh_3, a slope of 0.96 and an intercept of +1.34V was calculated which compares very favourably with the predicted slope of unity and the experimentally determined Cr^0/Cr^1 couple of [Cr(CO)$_6$] at +1.36V.

Transferability of P_L values to other metal d^6 carbonyl complexes does not follow immediately from Bursten's model. The potential of a d^6/d^5 oxidation couple of a

complex of type $[M(CO)_4LL']$, (L and L' are poorer π-acceptors than CO) can be expressed as:

$$E_M^{ox} = A_M^0 + 6B_M^{CO} + 4C_M^{CO} + (\pi_L + \pi_{L'}) \qquad (10)$$

where π_L or $\pi_{L'} = E_M^0[M(CO)_5(L \text{ or } L')] - E_M^0[M(CO)_6]$. The linear relationship of E_M^0 with $(P_L+P_{L'})$ means that $(P_L+P_{L'}) \propto (\pi_L+\pi_{L'})$ and the proportionality constant could be calculated from the appropriate $(P_L+P_{L'})$ versus $(\pi_L+\pi_{L'})$ plot.

Even with the linking of Chatt's ligand parameters to Bursten's Ligand additivity model there has not been widespread use of this approach since P_L values are known for relatively few ligands. Its lack of use may also be because it was seen to be of value to organometallic chemistry rather than to coordination chemistry.

However, the common basis that electrochemical parameters are additive with respect to ligand substitution was used by Lever in his "Electrochemical Parametization" model of 1990.[13] He calculated his ligand parameters E_L using the Ru(III)/Ru(II) couple, obtained from a vast range of complexes with a general formula $[Ru(bipy)_nL_{(6-2n)}]^{y+}$.

In order to obtain these ligand parameters, Lever first considered the cation $[Ru(bipy)_3]^{2+}$ whose Ru(III)/Ru(II) couple occurs at +1.53V vs. N.H.E. in acetonitrile. Since the complex contains six identical Ru-N bonds the E_L contribution for 2,2'-bipyridine was first defined as 1.53/6 = 0.255V. He went on to study the $E_{½}$ potentials of the Ru(III)/Ru(II) couples for the series of compounds $[Ru(bipy)_nL_{(6-2n)}]^{y+}$ where n =0, 1, 2, or 3. The E_L value for ligand L, $E_L(L)$, was derived from the following equation:

$$E_{obs}(Ru(III)/Ru(II)) = 2n \times 0.255 + (6-2n)E_L(L) \qquad (11)$$

$E_L(L)$ was calculated from three types of compound $[Ru(bipy)_2L_2]^{y+}$, $[Ru(bipy)L_4]^{y+}$ (by equation (11)) and from $[RuL_6]^{y+}$ by a straight division calculation. In this way $E_L(L)$ values for over 100 ligands were initially defined. These values were subsequently used to redefine the best (least squares) average value for E_L(2,2'-bipyridine) by using a data base of 94 ruthenium bipy complexes. The final average value of E_L(2,2'-bipy) found was 0.259V. The E_L values were all recalculated using

this new value of E_L(2,2'-bipy). E_L(L) values for all Ru(III) complexes not containing bipy were then calculated.

Thus we can now predict the expected $E_{½}$ values for any octahedral complex of the type $[RuX_xY_yZ_z]$, by utilising equation (12).

$$E_{calc} = xE_L(X) + yE_L(Y) + zE_L(Z) \qquad (12a)$$

or $$E_{calc} = \sum_{o}^{i} a_i E_L(L_i) = \sum E_L \qquad (12b)$$

A plot of the calculated $E_{½}$ values, E_{calc}, were plotted against the observed potentials, E_{obs} and the equation of the best fit line was found to be:

$$E_{obs} = 0.97\left(\sum E_L\right) + 0.04 \qquad (13)$$

A line passing through the origin with a gradient of 1 would mean that the calculated data matched the observed data exactly. Thus the above correlation is an extremely good match of calculated and experimentally determined data.

Lever also showed a linear correlation between his E_L values and Chatt's P_L ligand parameters. The equation of the best fit for a plot of P_L vs. E_L is:

$$P_L = 1.17E_L - 0.86 \qquad (14)$$

This relationship was used by Lever where the P_L value of a complex was known but there were no appropriate ruthenium complex from which to derive E_L.

To allow for E_L(L) parameters to be of use in the prediction of $E_{½}$ potentials of other metal ions in a range of oxidation states Lever suggested a least squares plot similar to that above. Therefore for a general species $[MX_xY_yZ_z]$ he proposed a plot of the observed potentials for any M(n)/M(n-1) couple against those calculated by equation (12). Least squares analysis to fit calculated to the observed data yields the equation:

$$E_{obs} = S_M\left(\sum_{0}^{i} a_i E_L(L_i)\right) + I_M \qquad (15a)$$

$$\text{or } E_{obs} = S_M\left(\sum E_L\right) + I_M \qquad (15b)$$

All complexes of given stereochemistry and spin state would fall on the same line therefore a unique S_M and I_M for a specific couple M(n)/M(n-1) can be calculated. Lever calculated S_M and I_M in his original paper for various metals and oxidation states. Table 3.3 shows the values he calculated for 6 coordinate complexes in organic solvents plus others which have since been published.

Table 3.3 - Electrochemical Parameters For Oxidation-Reduction Couples of Octahedral Metal Complexes in Organic Solvents

Couple	S_M[a]	I_M[a]
Chromium		
Cr(III)/Cr(II) L.S.[b]	1.18(0.06)	-1.72(0.15)
Cr(III)/Cr(II) H.S.[b]	0.84(0.05)	-1.18(0.09)
Cr(I)/Cr(0)[b]	0.52(0.02)	-1.75(0.12)
Iron		
Fe(III)/Fe(II) L.S.[b]	1.10(0.05)	-0.43(0.12)
Fe(III)/Fe(II) H.S.[b]	0.89(0.04)	-0.25(0.04)
Manganese		
Mn(II)/Mn(I)[b]	0.81(0.02)	-1.76(0.08)
Molybdenum		
Mo(I)/Mo(0)[b]	0.74(0.03)	-2.25(0.10)
Niobium		
Nb(V)/Nd(IV)[b]	0.76(0.02)	1.24(0.02)
Nb(IV)/Nb(III)[b]	0.75(0.01)	-0.12(0.01)
Osmium		
Os(V)/Os(IV)[c]	1.00(0.02)	2.905(0.02)
Os(IV)/Os(III)[e]	1.05(0.02)	1.095(0.02)
Os(III)/Os(II)[b]	1.01(0.02)	-0.40(0.11)
Rhenium		
Re(IV)/Re(III)[d]	0.86(0.04)	0.51(0.13)
Re(III)/Re(II)[d]	1.17(0.06)	-0.88(0.17)
Re(II)/Re(I) Lower[d]	0.27(0.07)	-1.43(0.11)
Re(II)/Re(I) Upper[d]	0.76(0.03)	-0.95(0.13)
Tantalum		
Ta(V)/Ta(IV)[b]	0.79(0.08)	0.66(0.07)
Technetium		
Tc(IV)/Tc(III)[c]	1.00(0.10)	0.64(0.09)
Tc(III)/Tc(II)[c]	1.29(0.08)	-0.91(0.11)
Tc(II)/Tc(I)[c]	1.39(0.12)	-2.07(0.10)

a Standard deviations of slope and intercept are given in parentheses in volts.
b From reference (13). *c* From reference (14). *d* From Reference (15).
e From Reference (16). H.S. High Spin. L.S. Low Spin

3.2 Results and Discussion

3.2.1 Application Of Lever's Additivity Model to *mer*-[OsX_3L_3]

In Chapter 2 we demonstrated for the series *mer*-[OsX_3L_3], the linear relationship between the observed oxidation and reduction potentials and the electronic parameters of the tertiary phosphine ligands. Employing Lever's Ligand Additivity Theory the potentials of the complexes could be predicted by the equation:

$$E_{calc} = S_M\left[\sum(E_L)\right] + I_M + C_{ref} \qquad (16)$$

where S_M and I_M are constants for a specific redox couple (See Table 3.3), $\Sigma(E_L)$ the sum of the specific electronic contributions of all ligands and C_{ref} relates the potentials, from the Standard Hydrogen Reference Electrode (S.H.E.) used in collection of the E_L values, to Ag/AgCl Reference Electrode used in this study.[18]

Lever calculated E_L values for tertiary Group 15 ligands some of which were employed in this study, Table 3.4.

Table 3.4 - E_L Values for Tertiary Group 15 Ligands Calculated by Lever[13]

Group 15 Ligand	E_L
PMe_3	0.33
PMe_2Ph	0.34
PEt_3	0.34
PPr^n_3	0.34
PBu^n_3	0.29
PPh_3	0.39
$AsPh_3$	0.38
PPh_3	0.38

Hence by equation (16) and the values of E_L for Cl and Br (-0.24 and -0.22 respectively) we can predict the oxidation and reduction potentials for the series *mer*-[OsX_3L_3] where X = Cl or Br and L = PMe_3, PMe_2Ph, PEt_3 or PPr^n_3. Tables 3.5 and 3.6 compares the results of the calculations versus the observed values of the metal based couples.

Table 3.5 - Calculated Oxidation and Reduction Potentials for the series *mer*-$[OsCl_3L_3]$ (vs. Ag/AgCl)

	Oxidation		Reduction	
	Calc.	Obs.	Calc.	Obs.
PMe_3	1.18V	1.02V	-0.32V	-0.32V
PMe_2Ph	1.22V	1.08V	-0.29V	-0.25V
PEt_3	1.22V	0.95V	-0.29V	-0.40V
PPr^n_3	1.22V	0.93V	-0.29V	-0.48V

Table 3.6 - Calculated Oxidation and Reduction Potentials for the series *mer*-$[OsBr_3L_3]$ (vs. Ag/AgCl)

	Oxidation		Reduction	
	Calc.	Obs.	Calc.	Obs.
PMe_3	1.24V	1.03V	-0.26V	-0.22V
PMe_2Ph	1.27V	1.09V	-0.23V	-0.12V
PEt_3	1.27V	0.98V	-0.23V	-0.25V
PPr^n_3	1.27V	0.95V	-0.23V	-0.34V

The calculation gives a poor approximation to the observed value. The calculated values are found to be ~0.2V and ~0.1V in error compared to the observed oxidation and reduction potentials respectively. This constant error in the calculated value is possibly due because both processes form a charged species which is not accounted for in Lever's Additivity Model.

3.2.2 Complexes of Type *mer*-$[OsCl_3L_2L']$

A number of complexes of type *mer*-$[OsCl_3L_2L']$ were prepared from the reaction of *trans*-$[OsCl_4L_2]$ with excess L' in benzene, where L and L' are different tertiary phosphines or arsines.*

3.2.2.1 Structure of Complexes of type *mer*-$[OsCl_3L_2L']$

Crystallographic studies were undertaken on three of the complexes prepared. Figures 3.2, 3.3 and 3.4 shows the structures of *mer*-$[OsCl_3(PPr^n_3)_2(PEtPh_2)]$, *mer*-

* For synthetic details see Chapter 6.

$[OsCl_3(PPr^n_3)_2(AsPr^n_3)]$ and *mer*-$[OsCl_3(P(OMe)_2Ph)_2(AsPr^n_3)]$ respectively, likewise Tables 3.7, 3.8 and 3.9 list the selected bond distances and angles for each structure. As before the complexes are all slightly distorted octahedra with the steric bulk of the Group 15 ligands forcing the structure away from ideality. Note again that the *trans* influence of the phosphine/arsine ligands lengthens the *trans* Os-Cl distance by ~0.1Å compared to mutually *trans* Cl ligands as discussed earlier. For all complexes no structure scrambling was observed in solution from that measured in solid state.

In the solid state structure of *mer*-$[OsCl_3(PPr^n_3)_2(AsPr^n_3)]$ (Figure 3.3) there was some degree of disorder involving scrambling between the *trans* P(1) and As ligands the components were fixed as having the same positions with occupancy 60%/40%. There was no ambiguity about the identity of the ligand *trans* to the unique chloride.

The complexes *mer*-$[OsCl_3(PPr^n_3)_2(AsPr^n_3)]$ and *mer*-$[OsCl_3(PPr^n_3)_2(PEtPh_2)]$ were prepared from the reaction of *trans*-$[OsCl_4(PPr^n_3)_2]$ with excess $AsPr^n_3$ and $PEtPh_2$ respectively i.e. the substitution of a halide for a Group 15 ligand:

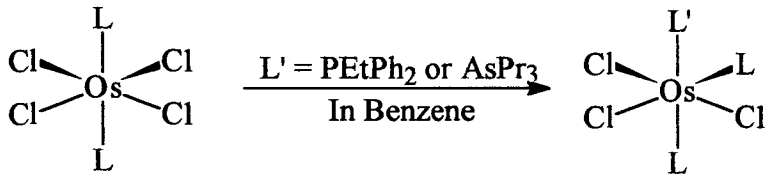

The same reaction but in the presence of the phosphonite $P(OMe)_2Ph$ resulted in the substitution of a halide plus a PPr^n_3 ligand forming the complex *mer*-$[OsCl_3(P(OMe)_2Ph)_2(AsPr^n_3)]$ with the $P(OMe)_2Ph$ ligands *trans* to each other:

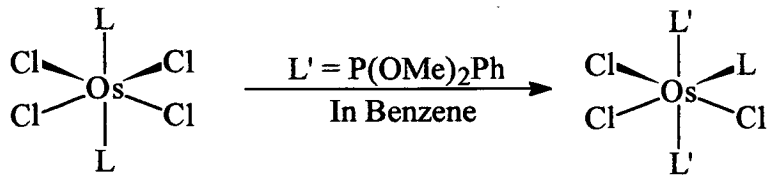

Phosphonite ligands are known to be strong σ donors hence they have a large *trans* influence. Therefore the stable conformation of the complex is where the two greatest σ-donors are *trans* to one another therefore negating this *trans* influence. Strong σ-donors also form stable bonds as is observed in the structure of *mer*-$[OsCl_3(P(OMe)_2Ph)_2(AsPr^n_3)]$, Figure 3.4 and Table 3.9. This structure shows a

reduction in the *trans* Os-P bond distances compared to similar complexes i.e. average *trans* Os-P bond distance 2.364Å and 2.408Å in *mer*-$[OsCl_3(P(OMe)_2Ph)_2(AsPr^n_3)]$ and *mer*-$[OsCl_3(PPr^n_3)_2(PEtPh_2)]$ respectively.

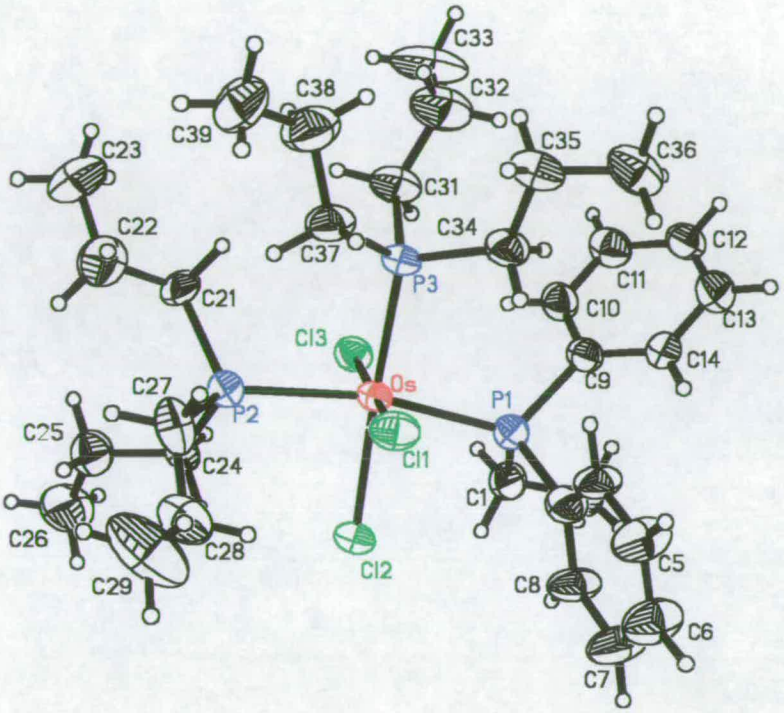

Figure 3.2 - Structure of *mer*-$[OsCl_3(PPr^n_3)_2(PEtPh_2)]$

Table 3.7 - Selected Bond Distance and Angles for *mer*-$[OsCl_3(PPr^n_3)_2(PEtPh_2)]$[†]

Os-Cl(1)	2.348(2)	Os-P(3)	2.377(2)	Os-P(1)	2.421(2)
Os-Cl(3)	2.364(2)	Os-P(2)	2.395(2)	Os-Cl(2)	2.436(2)
Cl(1)-Os-Cl(3)	174.94(7)	P(3)-Os-P(2)	95.77(8)	Cl(1)-Os-Cl(2)	89.85(8)
Cl(1)-Os-P(3)	82.09(8)	Cl(1)-Os-P(1)	94.10(8)	Cl(3)-Os-Cl(2)	94.85(8)
Cl(3)-Os-P(3)	93.26(8)	Cl(3)-Os-P(1)	88.56(8)	P(3)-Os-Cl(2)	171.79(8)
Cl(1)-Os-P(2)	92.89(9)	P(3)-Os-P(1)	98.54(8)	P(2)-Os-Cl(2)	86.14(8)
Cl(3)-Os-P(2)	85.56(8)	P(2)-Os-P(1)	164.81(8)	P(1)-Os-Cl(2)	80.41(7)

[†] For Full Crystallographic Details see Appendix

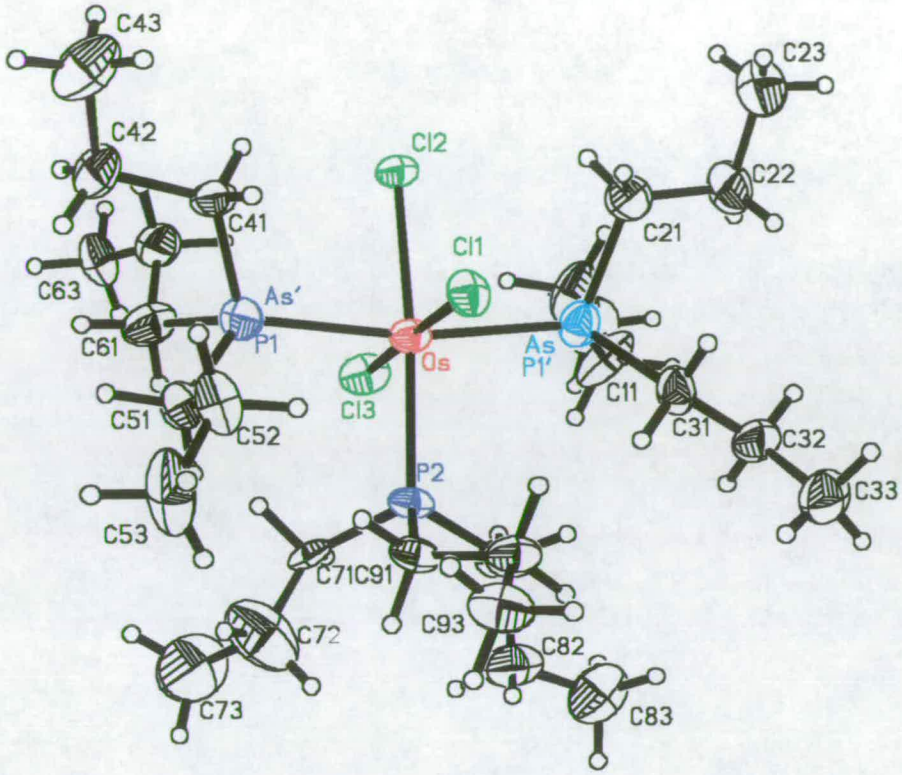

Figure 3.3 - Structure of *mer*-[$OsCl_3(PPr^n_3)_2(AsPr^n_3)$]

Table 3.8 - Selected Bond Distance and Angles for *mer*-[$OsCl_3(PPr^n_3)_2(AsPr^n_3)$][‡]

Os-P(2)	2.348(4)	Os-Cl(1)	2.361(4)	Os-As'	2.410(4)	Os-As	2.440(2)
Os-Cl(3)	2.349(4)	Os-P(1)	2.410(4)	Os-Cl(2)	2.431(3)	Os-P(1')	2.440(2)

P(2)-Os-Cl(3)	83.8(2)	P(2)-Os-Cl(2)	171.7(2)	As'-Os-As	170.02(11)
P(2)-Os-Cl(1)	96.1(2)	Cl(3)-Os-Cl(2)	88.1(2)	Cl(2)-Os-As	86.37(13)
Cl(3)-Os-Cl(1)	177.6(2)	Cl(1)-Os-Cl(2)	92.1(2)	P(2)-Os-P(1')	95.7(2)
P(2)-Os-P(1)	93.20(14)	P(1)-Os-Cl(2)	85.45(13)	Cl(3)-Os-P(1')	92.00(14)
Cl(3)-Os-P(1)	93.43(14)	As'-Os-Cl(2)	85.45(13)	Cl(1)-Os-P(1')	85.62(11)
Cl(1)-Os-P(1)	88.98(14)	P(2)-Os-As	95.7(2)	P(1)-Os-P(1')	170.02(11)
P(2)-Os-As'	93.20(14)	Cl(3)-Os-As	92.00(14)	As'-Os-P(1')	170.02(11)
Cl(3)-Os-As'	93.43(14)	Cl(1)-Os-As	85.62(11)	Cl(2)-Os-P(1')	86.37(13)
Cl(1)-Os-As'	88.98(14)	P(1)-Os-As	170.02(11)		

‡ See Appendix for Full Crystallographic Details

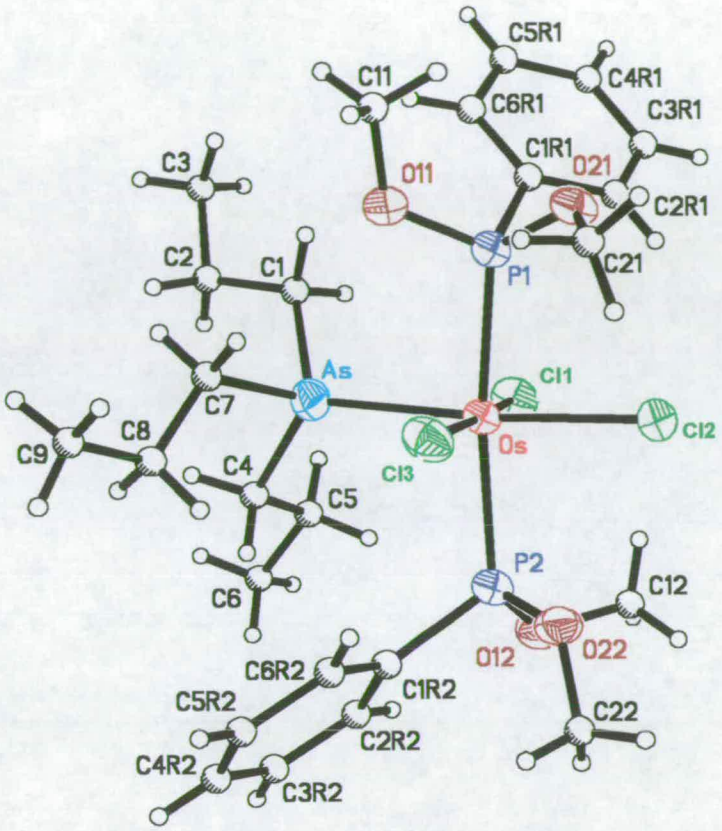

Figure 3.4 - Structure of *mer*-$[OsCl_3(P(OMe)_2Ph)_2(AsPr^n_3)]$

Table 3.9 - Selected Bond Distance and Angles for *mer*-$[OsCl_3(P(OMe)_2Ph)_2(AsPr^n_3)]$[§]

Os-As	2.4839(11)	Os-P(2)	2.382(2)	Os-Cl(1)	2.366(2)
Os-P(1)	2.347(2)	Os-Cl(2)	2.401(2)	Os-Cl(3)	2.357(2)

As-Os-P(1)	90.26(6)	P(1)-Os-P(2)	170.10(8)	P(2)-Os-Cl(1)	92.85(8)
As-Os-P(2)	98.13(6)	P(1)-Os-Cl(2)	85.96(8)	P(2)-Os-Cl(3)	87.00(8)
As-Os-Cl(2)	172.66(6)	P(1)-Os-Cl(1)	93.18(8)	Cl(2)-Os-Cl(1)	89.54(8)
As-Os-Cl(1)	84.38(7)	P(1)-Os-Cl(3)	87.76(8)	Cl(2)-Os-Cl(3)	96.08(8)
As-Os-Cl(3)	90.05(7)	P(2)-Os-Cl(2)	86.25(8)	Cl(1)-Os-Cl(3)	174.36(8)

[§] For Full Crystallographic Details see Appendix

3.2.2.2 Electrochemistry of *mer*-[$OsCl_3L_2L'$]

The electrochemical response of complexes of type *mer*-[$OsCl_3L_2L'$] is very similar to that described in Chapter 2. All the complexes show two metal based one electron couples, Figure 3.5. The reversible oxidation is assigned to a Os(III)/Os(IV) process and the reduction to a Os(III)/Os(II) process.

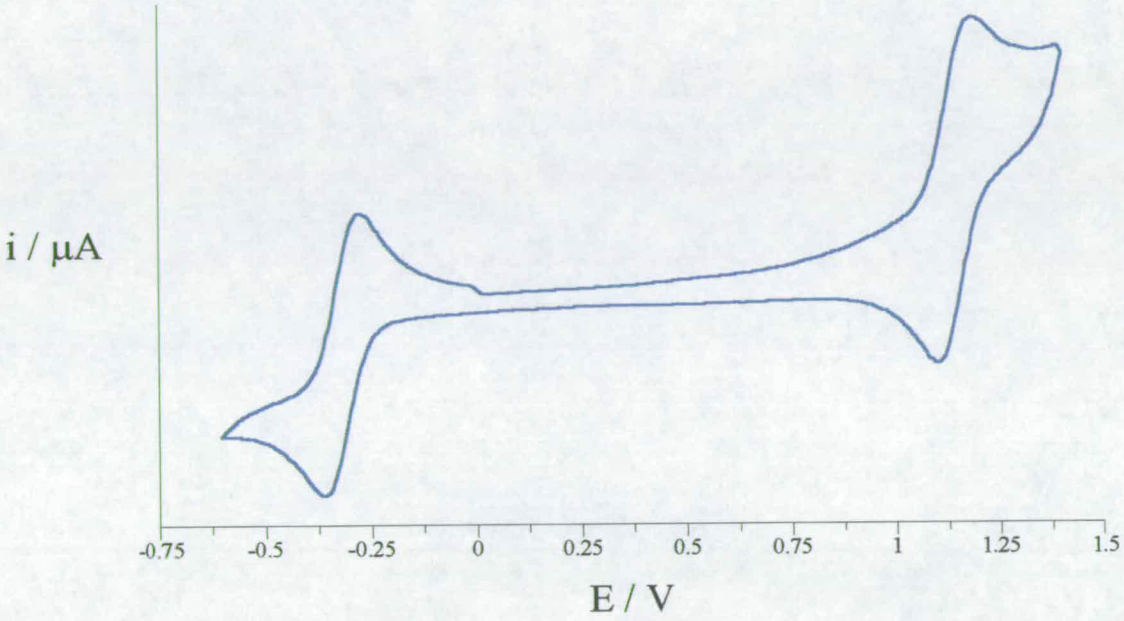

Figure 3.5 - Cyclic Voltammogram Of *mer*-[$OsCl_3(P(OMe)_2Ph)_2(AsPr^n_3)$] in CH_2Cl_2/0.5M [TBA][BF_4] at RT

In the study of the series *mer*-[OsX_3L_3] where X = Cl or Br and L = a tertiary phosphine or arsine (Chapter 2) the greater acceptor properties of the arsine ligands were found to stabilise the Os(II) complex over the time scale of the electrochemical experiment. Here a similar effect is observed: for the complexes with an $AsPr^n_3$ ligand in the position *trans* to a halide i.e. *mer*-[$OsCl_3(P(OMe)_2Ph)_2(AsPr^n_3)$] and *mer*-[$OsCl_3(PMePh_2)_2(AsPr^n_3)$] (See Later) a reversible couple was observed. The complexes with a phosphine ligand *trans* to the halide i.e. *mer*-[$OsCl_3(PPr^n_3)_2(AsPr^n_3)$] and *mer*-[$OsCl_3(PPr^n_3)_2(PEtPh_2)$] show an irreversible couple at room temperature, but the Os(II) complex can be stabilised by cooling the solution to -40°C.

For mixed phosphine or mixed phosphine/arsine complexes we would expect by Lever's Model that the potential of the observed metal based couples could be predicted by the summation of the ligand effects of all ligands. For complexes of type *mer*-[$OsCl_3L_2L'$] we would predict the potentials to lie between the potentials of

the parent complexes *mer*-$[OsCl_3L_3]$ and *mer*-$[OsCl_3L'_3]$. Hence the potentials could be calculated from the equation;

$$E = \frac{2E_L + E_{L'}}{3} \qquad (17)$$

where E_L and $E_{L'}$ are the measured potentials for the complexes *mer*-$[OsCl_3L_3]$ and *mer*-$[OsCl_3L'_3]$ respectively. So for the complex *mer*-$[OsCl_3(PPr^n_3)_2(AsPr^n_3)]$ the reduction potential would be expected to lie between -0.46V (the reduction of *mer*-$[OsCl_3(PPr^n_3)_3]$) and -0.70V (the reduction of *mer*-$[OsCl_3(AsPr^n_3)_3]$), likewise for the oxidation. Table 3.10 shows the recorded potentials for the mixed phosphine, phosphine/arsine complexes prepared, with the potentials expected in parenthesis plus the redox potentials of the parent complexes.

Table 3.10 - Electrochemical Potentials for Complexes of type *mer*-$[OsCl_3L_2L']$ (calculated values in parenthesis) plus the Redox Potentials of the Parent Complexes of type *mer*-$[OsCl_3L_3]$ in CH_2Cl_2/ 0.5M [TBA][BF_4] at RT (vs. Ag/AgCl)

Complex	Oxidation	Reduction
mer-$[OsCl_3(PPr^n_3)_2(AsPr^n_3)]$	0.94V (0.91V)	-0.45V (-0.54V)
mer-$[OsCl_3(PPr^n_3)_2(PEtPh_2)]$	0.95V (0.97V)	-0.43V (-0.17V)
mer-$[OsCl_3(P(OMe)_2Ph)_2(AsPr^n_3)]$	1.13V (1.20V)	-0.43V (-0.38V)
mer-$[OsCl_3(PMePh_2)_2(AsPr^n_3)]$	0.88V (1.05V)	-0.58V (-0.35V)
mer-$[OsCl_3(PMePh_2)_3]$	1.13V	-0.18V
mer-$[OsCl_3(PEtPh_2)_3]$	1.06V	-0.23V
mer-$[OsCl_3(PPr^n_3)_3]$	0.93V	-0.46V
mer-$[OsCl_3(AsPr^n_3)_3]$	0.89V	-0.70V
mer-$[OsCl_3(P(OMe)_2Ph)_3]$	*~(1.33V)*	*~(0.1V)*

All attempts to synthesise complexes of type *mer*-$[OsX_3L_3]$ where L was a phosphonite ligand failed. The couples for the parent complex *mer*-$[OsCl_3(P(OMe)_2Ph)_3]$ were estimated by employing the linear relationship found between χ_i and $E_{½}$ described in Chapter 2. The ligand $P(OMe)_2Ph$ has a χ_i of 19.7cm^{-1}, therefore the reduction and oxidation potentials were predicted as ~0.1V and ~1.33V respectively (See Figure 3.6).

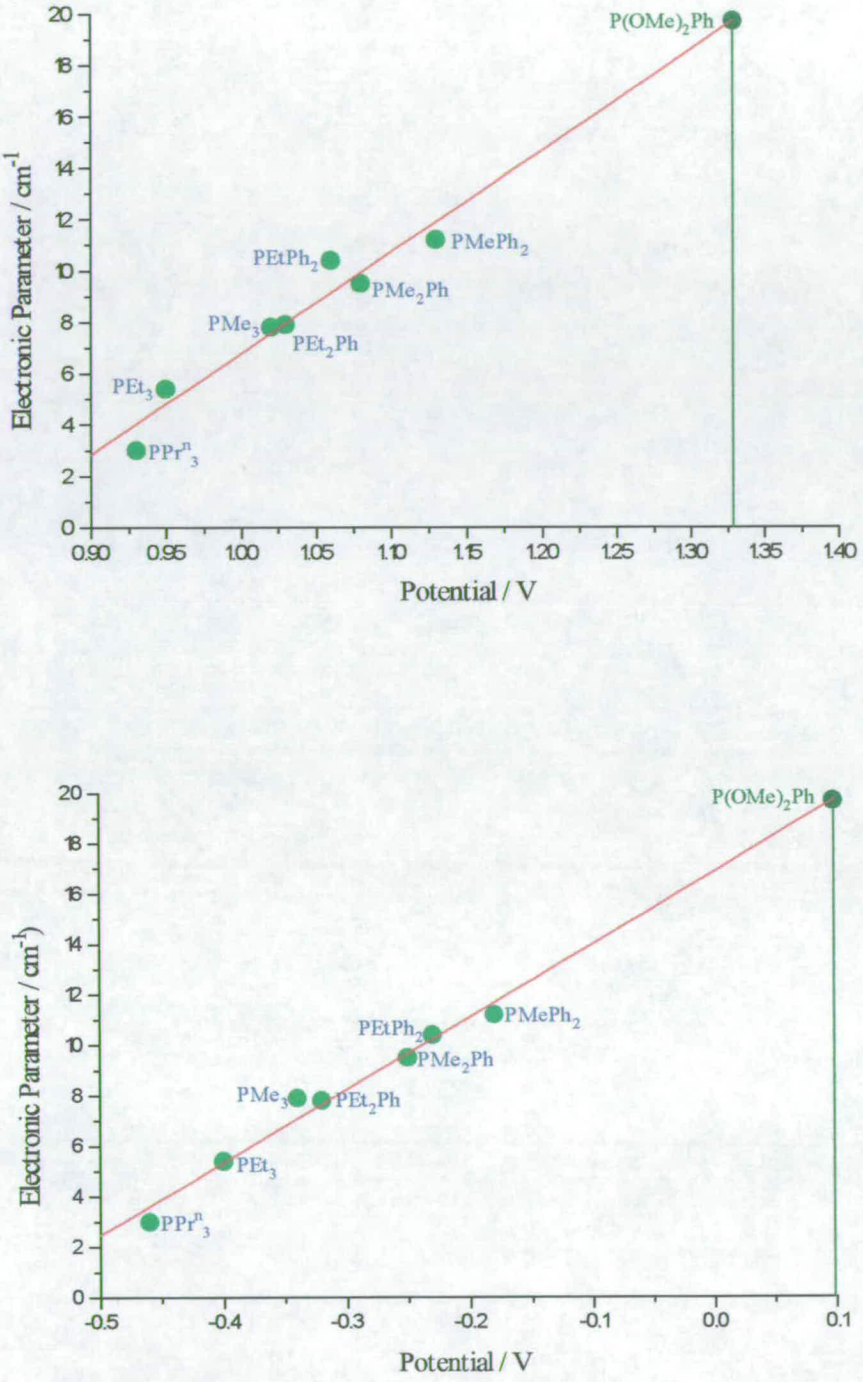

Figure 3.6 - Estimation of Reduction and Oxidation Couples for *mer*-$[OsCl_3(P(OMe)_2Ph)_3]$

The mixed ligand complexes are not in as close agreement with those predicted using Lever's Theory as expected. Rather the oxidation and reduction potentials of the mixed ligand complexes are found to be displaced from the predicted value towards the potential of one of the parent compounds.

The potentials for;

mer-$[OsCl_3(PPr^n_3)_2(AsPr^n_3)]$ are closer to *mer*-$[OsCl_3(PPr^n_3)_3]$ than predicted.
mer-$[OsCl_3(PPr^n_3)_2(PEtPh_2)]$ are closer to *mer*-$[OsCl_3(PPr^n_3)_3]$ than predicted.
mer-$[OsCl_3(P(OMe)_2Ph)_2(AsPr^n_3)]$ are closer to *mer*-$[OsCl_3(AsPr^n_3)_3]$ than predicted.
mer-$[OsCl_3(PMePh_2)_2(AsPr^n_3)]$ are closer to *mer*-$[OsCl_3(AsPr^n_3)_3]$ than predicted.

For complexes *mer*-$[OsCl_3(PPr^n_3)_2(AsPr^n_3)]$, *mer*-$[OsCl_3(PPr^n_3)_2(PEtPh_2)]$ and *mer*-$[OsCl_3(P(OMe)_2Ph)_2(AsPr^n_3)]$ we observe that the metal based redox potentials are shifted towards that of the tertiary phosphine or arsine which is <u>*trans*</u> to a chloride ligand, see Figures 3.2, 3.3 and 3.4. We therefore predict that complex *mer*-$[OsCl_3(PMePh_2)_2(AsPr^n_3)]$ will have the structure shown below:

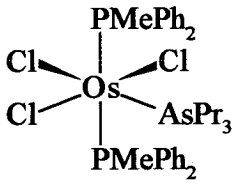

In order to gain further insight into why the phosphine/arsine *trans* to a chloride ligand appears to have a stronger influence on the redox potentials than the mutually *trans* phosphine/arsines we decided to examine the results of Extended Hückel Molecular Orbital Calculations on these mixed compounds.

3.2.2.3 EHMO Calculations on Complexes Of Type *mer*-[$OsCl_3L_2L'$]

Extended Hückel Molecular Orbital Calculations were undertaken on the complexes *mer*-[$OsCl_3(PPr^n_3)_2(AsPr^n_3)$], *mer*-[$OsCl_3(P(OMe)_2Ph)_2(AsPr^n_3)$] and *mer*-[$OsCl_3(PPr^n_3)_2(PEtPh_2)$].** The computations were carried out on atomic positions obtained from the X-ray diffraction crystal structures (See Above).

As the complexes under study all contain low spin Os(III) metal centres in an octahedral configuration, we will only consider here the metal t_{2g} set of molecular orbitals. Five electrons equates to two full orbitals and one half filled orbital. The half (or semi-) filled orbital (SOMO) will be the highest occupied molecular orbital.

Figure 3.7A, B and C shows the results of the EHMO calculation for *mer*-[$OsCl_3(PPr^n_3)_2(AsPr^n_3)$] and details the significant molecular contributions to the SOMO (Figure 3.7C) and the two closest energy molecular orbitals SOMO-1 (Figure 3.7B) and SOMO-2 (Figure 3.7A). Unsurprisingly the three orbitals are clearly recognisable as the d orbitals that make up the t_{2g} sub set of metal-based orbitals Likewise Figure 3.8A, B, C and 3.9A, B, C present the plots for *mer*-[$OsCl_3(P(OMe)_2Ph)_2(AsPr^n_3)$] and *mer*-[$OsCl_3(PPr^n_3)_2(PEtPh_2)$] respectively. We shall discuss the results of *mer*-[$OsCl_3(PPr^n_3)_2(AsPr^n_3)$] but the arguments hold for any of the complexes.

Figure 3.7A shows the molecular orbital calculated to be two levels below the SOMO (SOMO-2). This orbital is clearly the d_{xz} orbital. The orbital can π-interact with one halide, the two phosphorus atoms and the arsenic atom (See Figure 3.10).

** For details see Chapter 6.

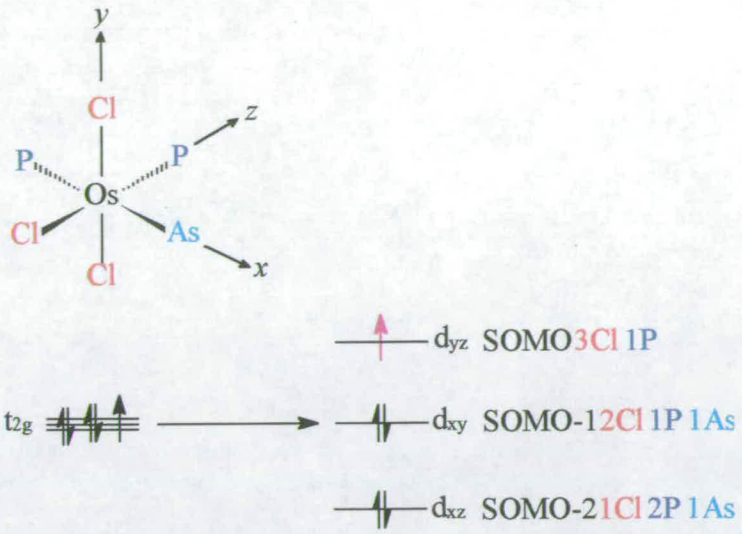

Figure 3.10 -Splitting of the metal t_{2g} level for level for *mer*-[$OsCl_3L_2L'$]

The SOMO-1 level (Figure 3.7B) involves the d_{xy} level, π-interacting with two halides, the arsenic atom and a phosphorus atom. The SOMO (Figure 3.7C) itself involves the d_{yz} orbital which is involved with π-interactions to all three halides and the phosphorus atom *trans* to the chloride.

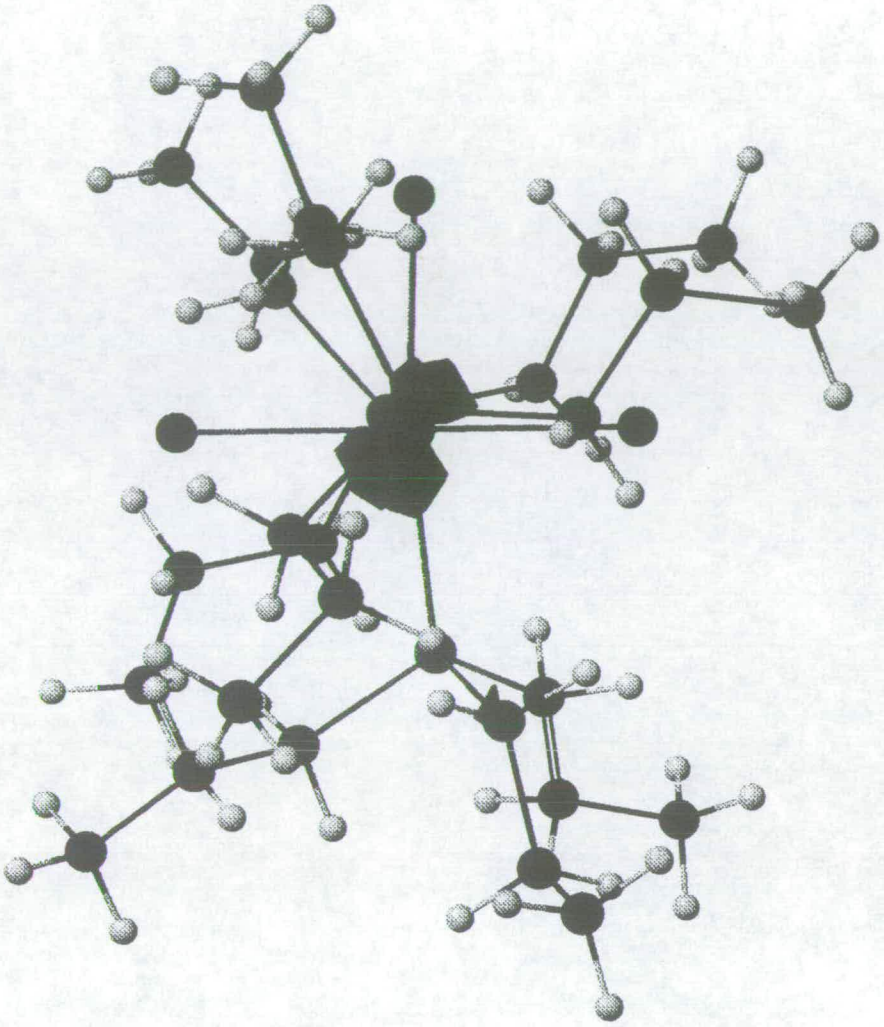

Figure 3.7A - Plot of *mer*-[$OsCl_3(PPr^n_3)_2(AsPr^n_3)$] showing the d_{xz} orbital (SOMO-2) at -11.212eV

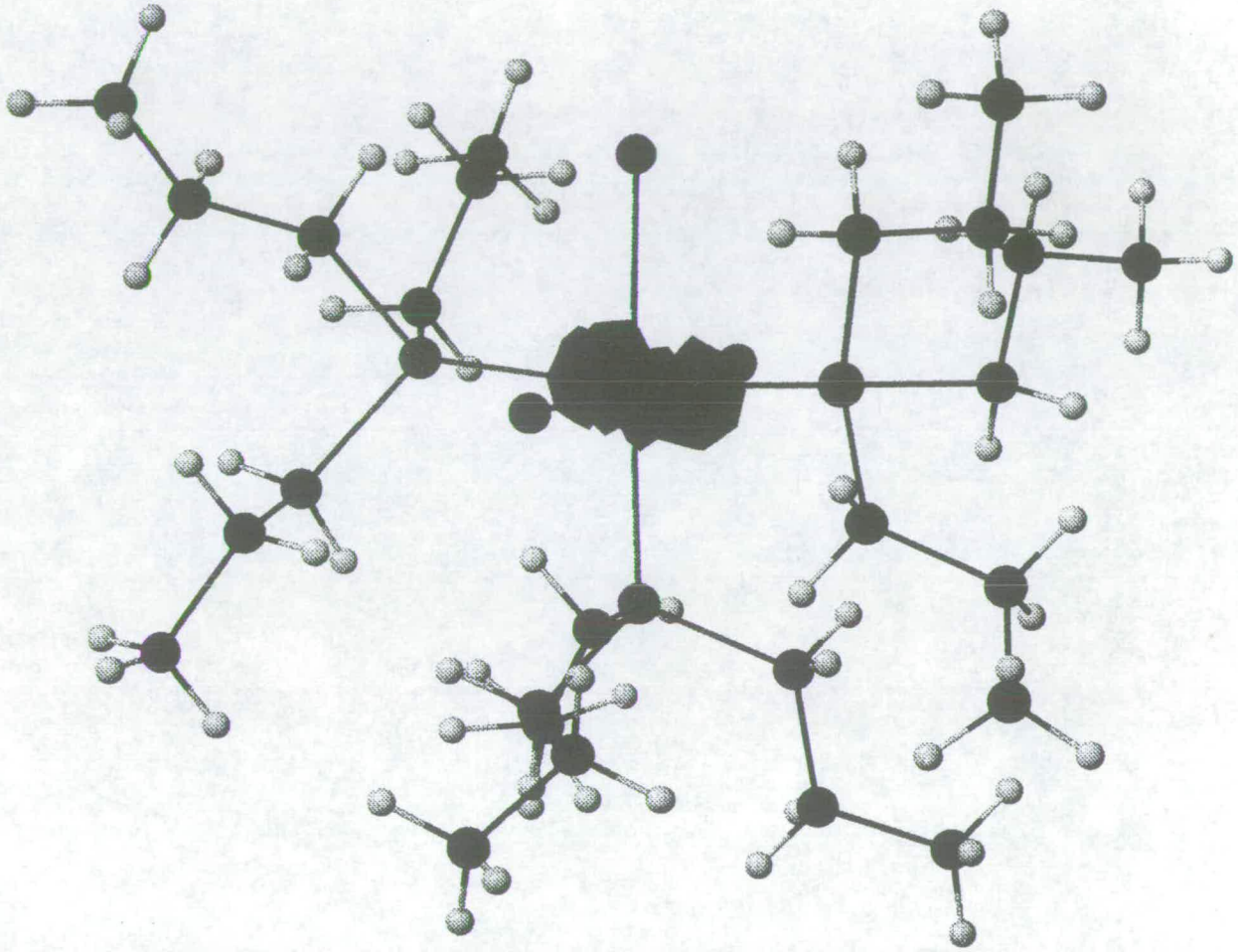

Figure 3.7B - Plot of *mer*-[$OsCl_3(PPr^n_3)_2(AsPr^n_3)$] showing the d_{xy} orbital (SOMO-1) at -10.991eV

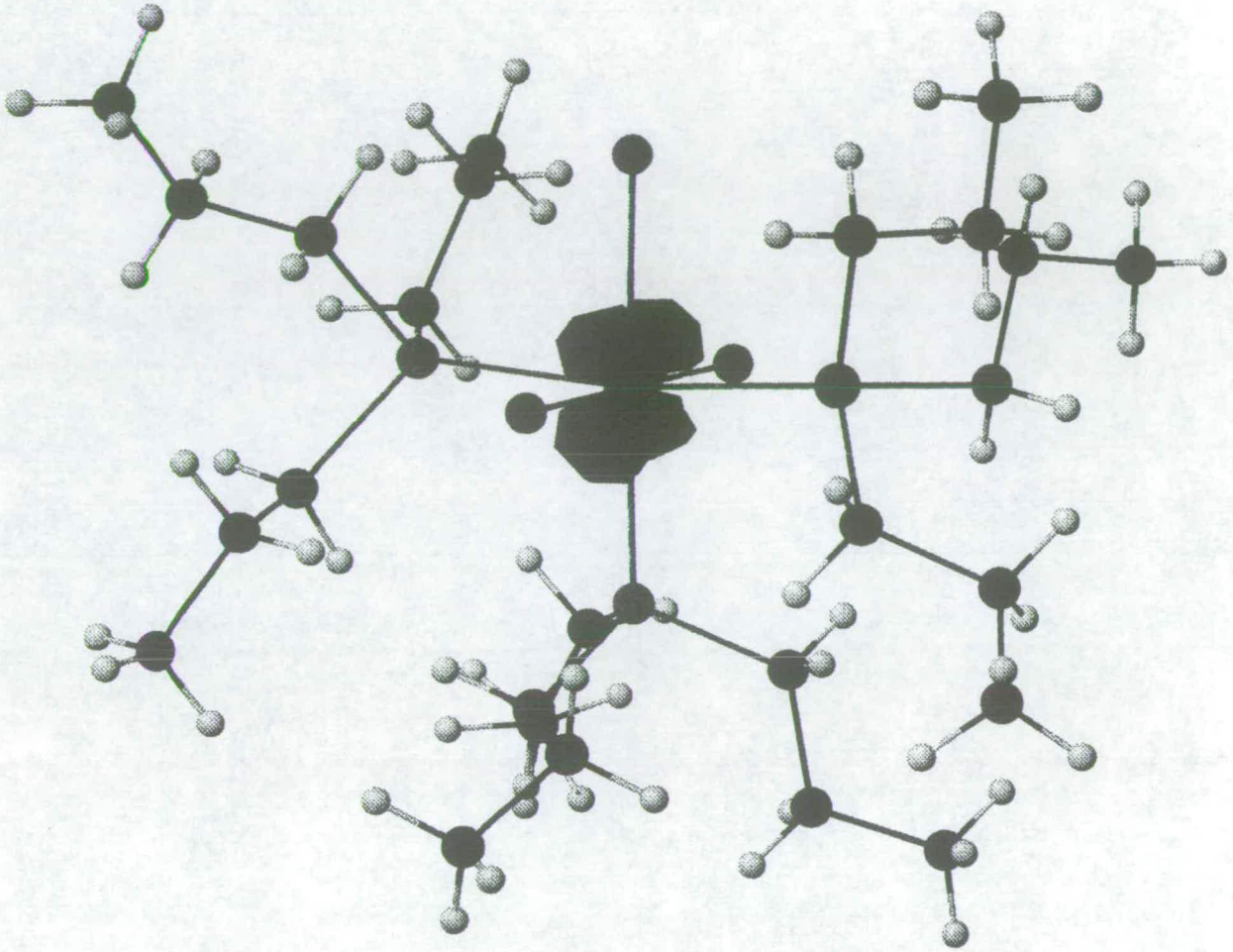

Figure 3.7C - Plot of *mer*-[$OsCl_3(PPr^n_3)_2(AsPr^n_3)$] showing the d_{yz} orbital (SOMO) at -10.906eV

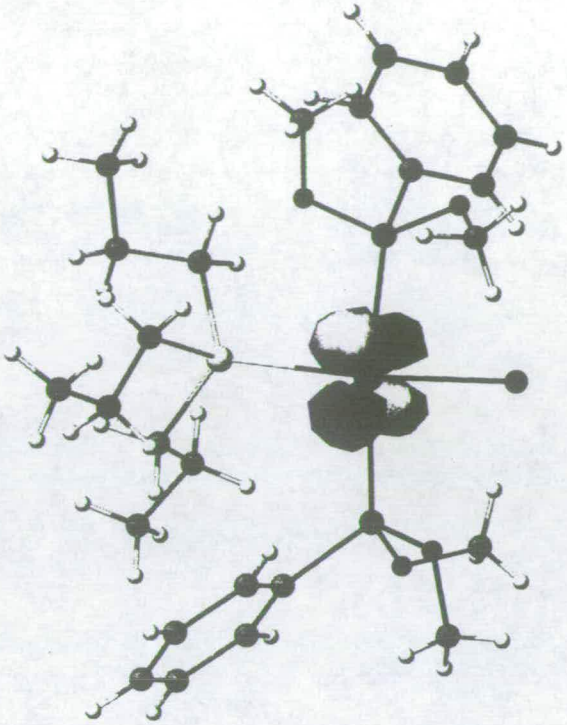

Figure 3.8A - Plot of *mer*-[$OsCl_3(P(OMe)_2Ph)_2(AsPr^n_3)$] showing the SOMO-2 Level at -9.456eV

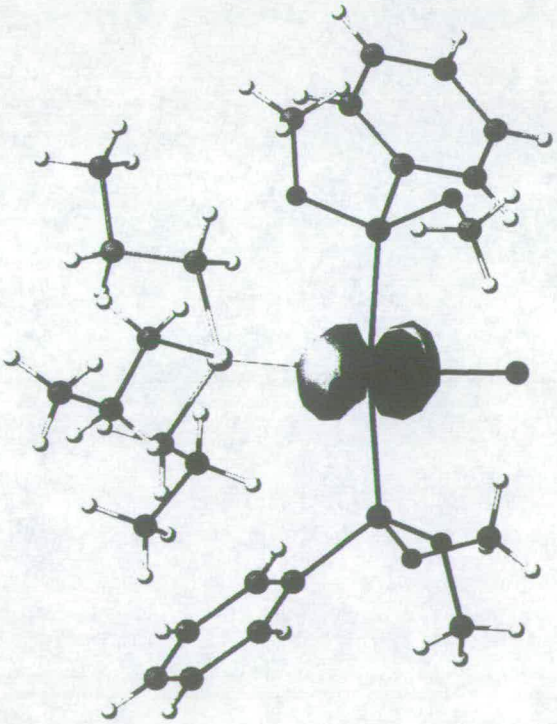

Figure 3.8B - Plot of *mer*-[$OsCl_3(P(OMe)_2Ph)_2(AsPr^n_3)$] showing the SOMO-1 Level at -9.337eV

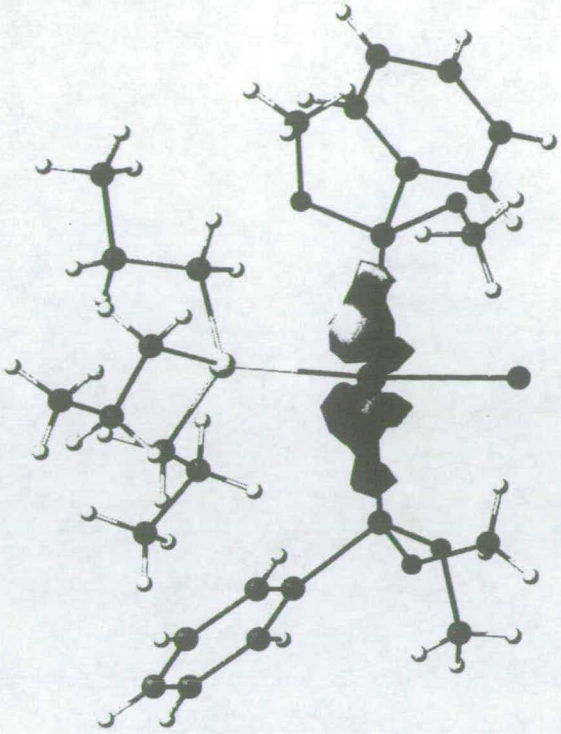

Figure 3.8C - Plot of *mer*-[$OsCl_3(P(OMe)_2Ph)_2(AsPr^n_3)$] showing the SOMO Level at -9.292eV

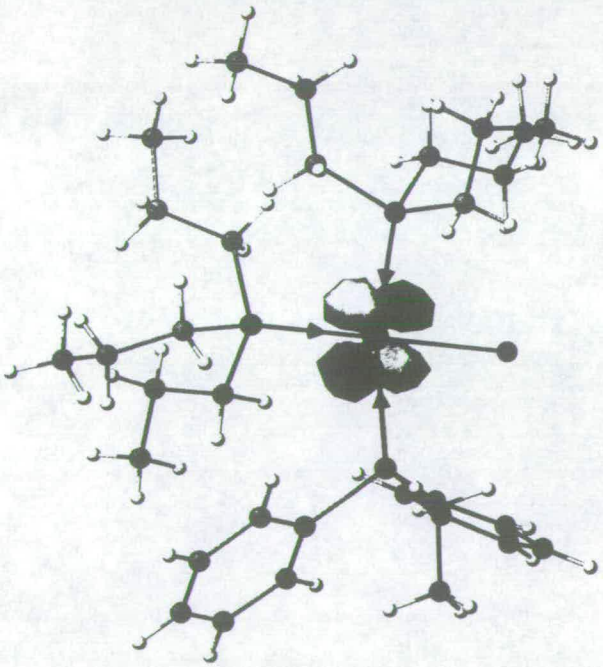

Figure 3.9A - Plot of *mer*-[$OsCl_3(PPr^n_3)_2(PEtPh_2)$] showing the SOMO-2 Level at -9.418eV

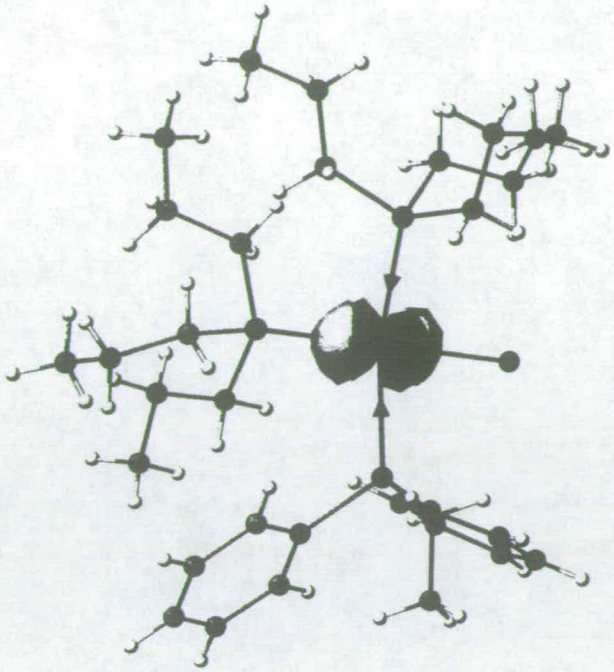

Figure 3.9B - Plot of *mer*-[$OsCl_3(PPr^n_3)_2(PEtPh_2)$] showing the SOMO-1 Level at -9.338eV

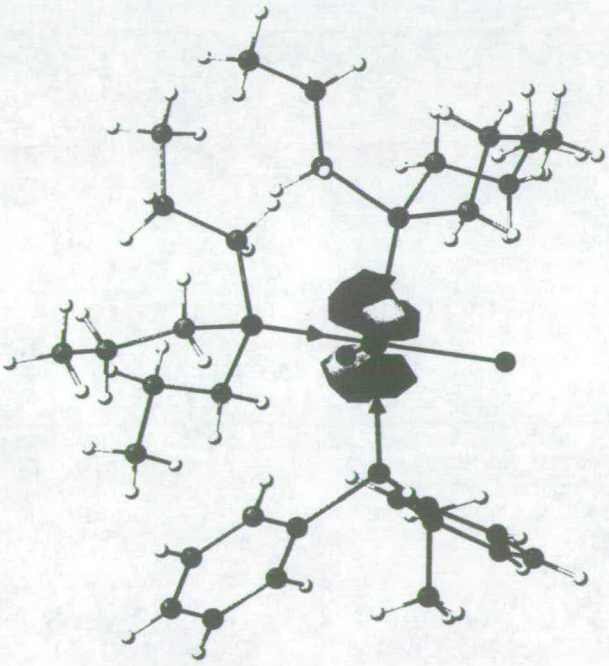

Figure 3.9C - Plot of *mer*-[$OsCl_3(PPr^n_3)_2(PEtPh_2)$] showing the SOMO Level at -9.303eV

The oxidation and reduction processes for the complexes of type *mer*-[$OsCl_3L_2L'$] involve only one electron. Both processes will involve addition or removal of a electron to/from the SOMO orbital. The SOMO itself interacts with all three halides plus the Group 15 ligand *trans* to a halide.

Therefore, this phosphine/arsine appears to have a greater influence on the electrochemical response of the complex than the Group 15 ligands at other sites within the compound which do not interact directly with the SOMO. This accordingly accounts for the observation that the complexes of type *mer*-[$OsCl_3L_2L'$] show potentials closer to one parent than predicted by Lever's Additivity Model.

3.2.3 Conclusion

Lever's Ligand Additivity Model has been applied to the complexes under study. A fair correlation was found between the observed potentials and those predicted for the complex *mer*-[OsX_3L_3].

Detailed Extended Hückel Molecular Calculations were undertaken on complexes of type *mer*-[$OsCl_3L_2L'$]. The SOMO was found to interact with three halides and one tertiary phosphine/arsine. We conclude that the Group 15 ligand *trans* to the halide has the greater effect on the electrochemical response of the complex than the other Group 15 ligands.

3.3 References

(1) B. E. Bursten and M. R. Green, *Prog. Inorg. Chem.*, 1988, **36**, 474.

(2) G. J. Hoijtink, *Rec. Trav. Chim. Pays-Bas*, 1955, **74**, 1525.

(3) G. J. Hoijtink, *Rec. Trav. Chim. Pays-Bas*, 1958, **77**, 555.

(4) **(a)** P. M. Treichel, G. E. Dirreen and H. J. Mueh, *J. Organomet. Chem.*, 1972, **44**, 339. **(b)** P. M. Treichel, H. J. Mueh and B. E. Bursten, *J. Organomet. Chem.*, 1972, **44**, 339.

(5) A. C. Sarapu and R. F. Fenske, *Inorg. Chem.*, 1975, **14**, 247.

(6) C. J. Pickett and D. Pletcher, *J. Organomet. Chem.*, 1975, **102**, 327.

(7) P. M. Treichel, H. J. Mueh and B. E. Bursten, *J. Organomet. Chem.*, 1976, **110**, C49.

(8) F. L. Wimmer, M. R. Snow and A. M. Bond, *Inorg. Chem.*, 1974, **13**, 1617.

(9) P. M. Treichel, H. J. Mueh and B. E. Bursten, *Isr. J. Chem.*, 1977, **15**, 253.

(10) B. E. Bursten, *J. Am. Chem. Soc.*, 1982, **104**, 1299.

(11) B. E. Bursten, M. R. Green, V. Katovic, J. R. Kirk and D. Lightner Jr., *Inorg. Chem.*, 1986, **25**, 831.

(12) **(a)** J. Chatt, C. T. Kan, G. J. Leigh, C. J. Pickett and D. R. Stanley, *J. Chem. Soc., Dalton. Trans.*, 1980, 2032. **(b)** J.Chatt, *Coord. Chem. Rev.*, 1982, **43**, 337.

(13) A. B. P. Lever, *Inorg. Chem.*, 1990, **29**, 1271.

(14) D. Datta, *J.Chem. Soc., Dalton Trans.*, 1986, 1907.

(15) J. Lu, A. Yamano and M. J. Clarke, *Inorg. Chem.*, 1990, **29**, 3483.

(16) A. B. P. Lever, *Inorg. Chem.*, 1991, **30**, 1980.

(17) K. J. Taylor, Ph. D. Thesis, University Of Edinburgh, 1990.

(18) A. J. Bard and L. R. Faulkner, *Electrochemical Methods Fundamentals and Applications*, Wiley, New York, 1980.

Chapter 4

Kinetic Study of the Series *mer*-[OsX_3L_3]

4.1 Introduction - Kinetic Methods Employed in Cyclic Voltammetry

In the literature several techniques have been proposed to study the kinetic properties of an ec (electrochemical followed by chemical) reaction of type,

$$O + ne^- \rightleftharpoons R \xrightarrow{k_f} Z$$

by electrochemical means. Here we will describe three of these techniques, and apply them to the study of the series *mer*-$[OsX_3L_3]$. Before discussion of the kinetic methods it is necessary to briefly describe the mechanism involved in cyclic voltammetry.

4.1.1 Cyclic Voltammetry

Cyclic Voltammetry is carried out on a quiet (unstirred) solution. The vast concentration of inert electrolyte in solution means that mass transport is limited by diffusion: migration and convection can be ignored.

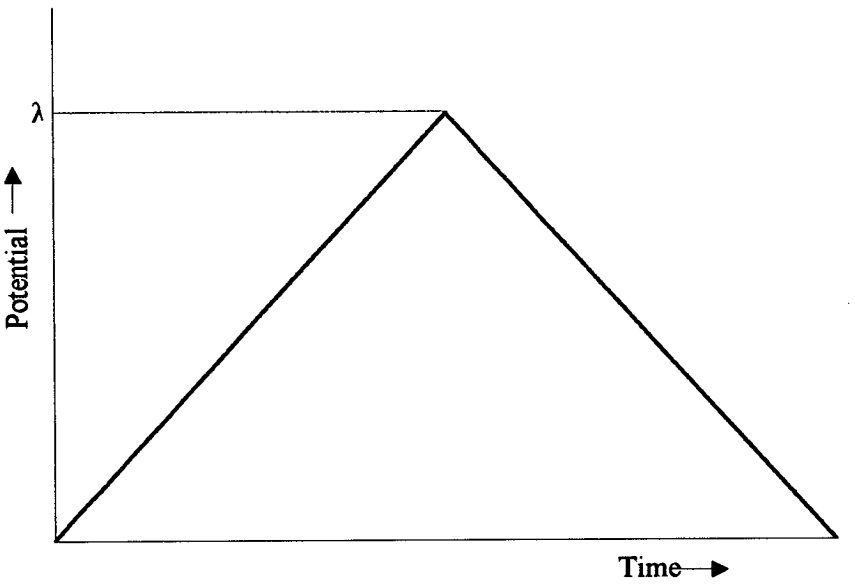

Figure 4.1 - Triangular Waveform of Cyclic Voltammetry

The potential of the electrode is varied linearly with time, and is swept out to a certain potential, E_λ, the switching potential, See Figure 4.1. After this point the potential is ramped back to the starting point usually at the same rate as the forward scan.

The rate at which the potential is changed is defined as the scan rate, ν, usually measured as mVs^{-1} or Vs^{-1}. The current, i, is measured as a function of the potential, E. A typical cyclic voltammogram for a reversible process is shown in Figure 4.2.

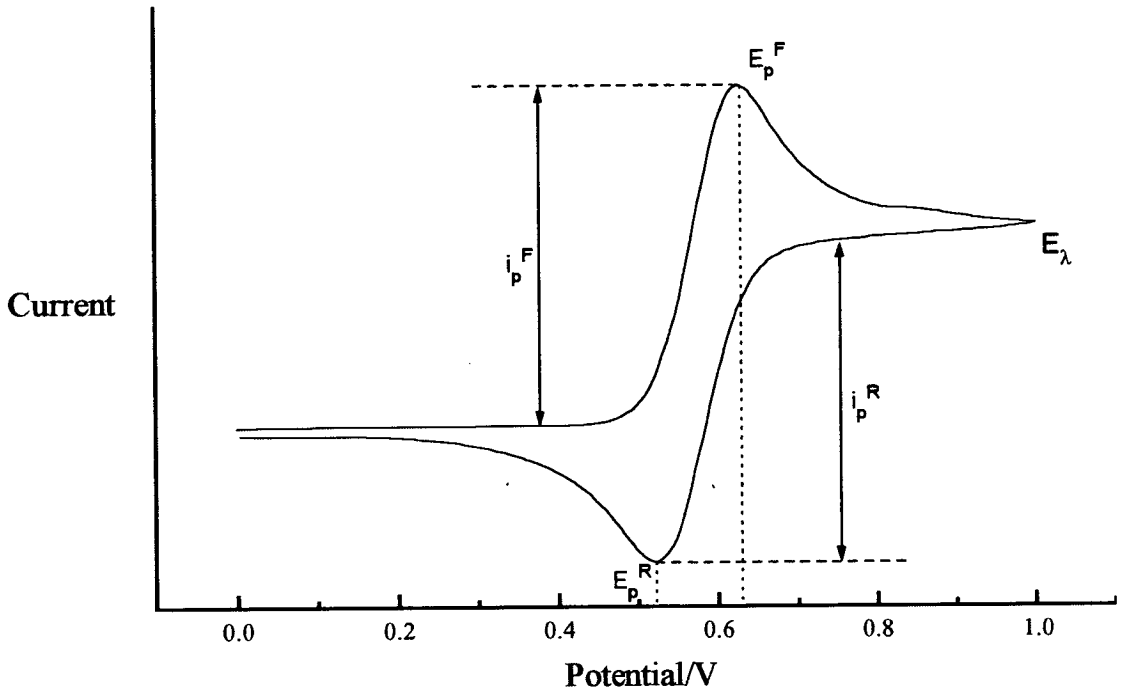

Figure 4.2 - A typical Voltammetric Response for a Reversible Process

The current response is an asymmetric peaked form, the current increasing as the potential of the electrode is scanned into the range were the reactant begins to be oxidised (or reduced) at the electrode. The rate of the reaction increases rapidly as the potential increases leading to most of the reactant near to the surface of the electrode being consumed. The current therefore is limited by the diffusion rate that additional reactant can reach the surface of the electrode from the bulk solution. The current maximum is obtained when the increase in current due to the increasingly favourable potentials is equal to the rate of new reactant diffusing to the electrode. After this point the latter effect is limiting and the current falls.

Beyond this point the potential ramp is reversed at the switching potential. Then the oxidised (or reduced) reactant at the electrode is re-reduced (re-oxidised) and a return

peak is observed at a more negative (positive) potential than the forward peak. The shape of this return peak is governed by the similar electron transfer and diffusion rate factors as the forward.

The parameters obtained from a cyclic voltammetric experiment can be used to determine the nature of a particular charge transfer reaction this can be in one of four classes.

A. Reversible	Electron transfer is more rapid than diffusion of the test species to the electrode.
B. Quasi-Reversible	Rate of electron transfer and diffusion similar.
C. Irreversible	Rate of electron transfer is slower than diffusion to the electrode surface.
D. Partially-Reversible	Irreversible chemical reaction follows a reversible or quasi-reversible electron transfer.

The parameters most important in determining the type of charge transfer reaction under study are the forward and reverse peak currents and potentials, respectively: i_p^F, i_p^R, E_p^F and E_p^R. The average between E_p^F and E_p^R is the $E_{½}$ for the redox process being examined. Table 4.1 lists the criteria for each type of electron transfer reaction. Note that before application of the criteria noted overleaf it is imperative that the iR drop across the solution has been properly compensated for.

Table 4.1 - Criteria for Electron Transfer from Cyclic Voltammetry

Reversible	E_p is independent of ν.
	$E_p^F - E_p^R = 59/n$ mV at 25°C.
	$\frac{1}{2}[E_p^F + E_p^R] = E_{\frac{1}{2}}$, independent of concentration.
	$i_p/\nu^{\frac{1}{2}}$ (current function) is independent of ν.
	$i_p^R/i_p^F = 1$ and is independent of ν.
Quasi - reversible	E_p shifts with ν.
	$E_p^F - E_p^R$ increases as ν increases.
	$i_p/\nu^{\frac{1}{2}}$ is independent of ν.
	i_p^R/i_p^F generally = 1.
Partially -reversible	E_p increases by 30/n mV for a ten fold increase of ν, at low ν.
	$i_p/\nu^{\frac{1}{2}}$ is independent of ν.
	i_p^R/i_p^F tends to 1 as ν increases.
Irreversible	E_p shifts with ν.
	$i_p/\nu^{\frac{1}{2}}$ is independent of ν.
	There is no peak i_p^R.

4.1.2 Kinetic Methods

4.1.2.1 Nicholson and Shain

Nicholson and Shain[1] calculated a large number of single cycle voltammetric theoretical curves, varying both k_f/a, where k_f is the rate constant and $a = nFv/RT$ and E_λ the switching potential. For a constant value of the parameter $k_f\tau$ where τ is the time in seconds from $E_{1/2}$ to E_λ, the ratios of anodic to cathodic peak currents were found to be constant. Thus they calculated a working curve for the ratio of peaks currents, i_a/i_c, as a function of $k_f\tau$, Table 4.2.

Table 4.2-Ratio Of Anodic to Cathodic Peak Currents (Reference 1)

$k_f\tau$	i_a/i_c
0.004	1.00
0.023	0.986
0.035	0.967
0.066	0.937
0.105	0.900
0.195	0.828
0.350	0.727
0.525	0.641
0.550	0.628
0.778	0.551
1.050	0.486
1.168	0.466
1.557	0.415

Therefore if $E_{1/2}$ is known a rate constant could be calculated from a single cyclic voltammetric curve.

In 1966 Nicholson[2] published a simple method of calculating the anodic:cathodic peak current ratio using the equation:

$$\frac{i_{sp}}{i_{cp}} = \frac{(i_{ap})_o}{(i_{cp})_o} + \frac{0.485(i_{sp})_o}{(i_{cp})_o} + 0.086 \qquad (1)$$

Where Figure 4.3 shows the definitions of all symbols used in (1).

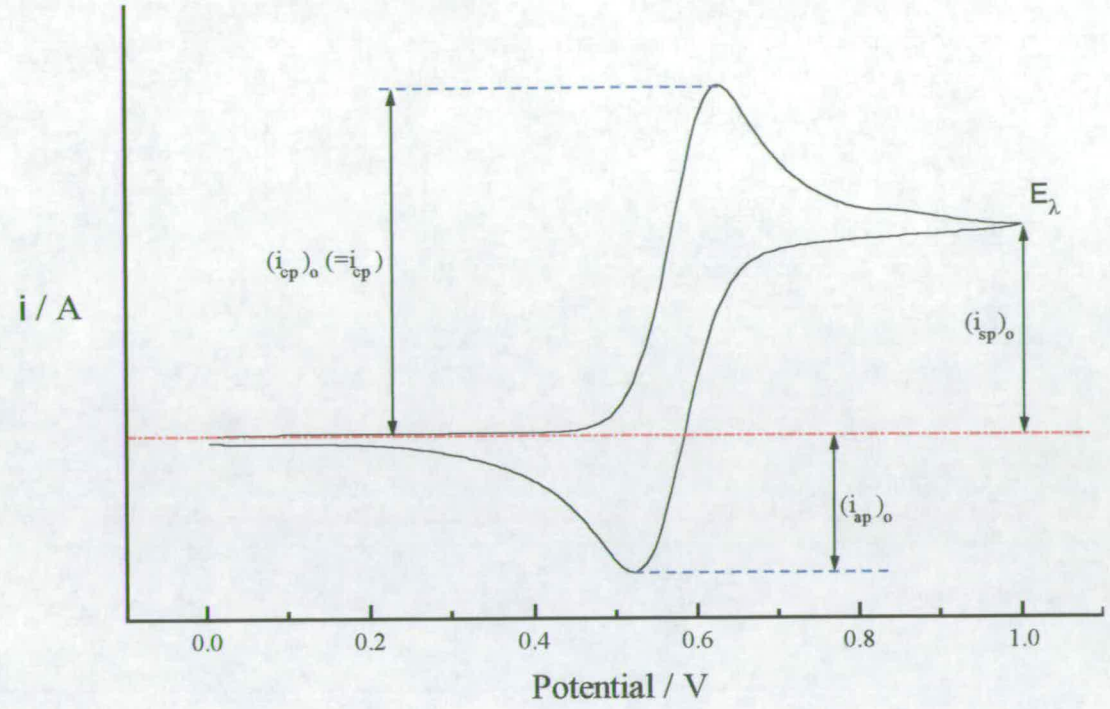

Figure 4.3 - Cyclic Voltammetric Response Showing Values for Nicholson and Shain Kinetic Method

Therefore it was possible to calculate a rate constant from one cyclic voltammogram using only three points on the curve.

4.1.2.2 Convolution Technique

By treatment of the linear potential sweep data the voltammetric i vs. E curves can be transformed into forms resembling steady state voltammetric curves. This transformation makes use of the convolution principle and has been facilitated by the development and availability of computers for the processing and acquisition of data. The technique delivers quantities directly related to the concentration of the electroactive species at the electrode surface rather than the flux of the compound as recorded in the original technique.

Consider an electrode reaction that generates a species where there originally was none. Diffusion then occurs away from the electrode by diffusion rate D if the reaction involved n electrons and the current density is i(t)/A then the surface concentration of the electrogenerated species can be shown to be in the form;[3]

$$c^s(t) = \frac{i(t)*g(t)}{nAFD^{1/2}} \tag{2}$$

For a species consumed at the electrode Equation (2) is replaced by;

$$c^s(t) = c^b - \frac{i(t)*g(t)}{nFAD^{1/2}} \tag{3}$$

Where c^b is the initially uniform concentration of the electroactive species, F is Faraday's constant. The asterisk indicates the operation of convolution defined by the integral;

$$i(t)*g(t) = \int_0^t i(\tau)g(t-\tau)d\tau = \int_0^t i(t-\tau)g(\tau)d\tau \tag{4}$$

g(t) is a "convolution function" , having dimensions of time$^{-½}$. Its form is dependent on the geometry of the region into which the electrogenerated species diffuses and on whether or not that species is involved in a homogeneous chemical reaction.[4] In the simplest case of planar semi-infinite geometry g(t) becomes $\pi^{-½}t^{-½}$. The convolution then reduces to the simpler operation of semi-integration:[5]

$$i(t)*g(t) = \frac{1}{\pi^{1/2}}\int_0^t \frac{i(\tau)d\tau}{(t-\tau)^{1/2}} = \frac{d^{-1/2}i}{dt^{-1/2}} \tag{5}$$

The convolution of a voltammogram results in an S-shaped curve where voltammetric curves are replaced by waves. In the case of a fast and uncomplicated electron transfer, the wave can be described using the equation;

$$E = E_{1/2} + \left(\frac{RT}{nF}\right)\ln\left[\frac{m_d - m}{m}\right] \tag{6}$$

where m denotes the current convolution. The height of the plateau is given by the formula:

$$m_d = nFAD^{1/2}C \tag{7}$$

When the semi-infinite diffusion geometry has spherical, rather than planar symmetry, the g(t) function must be modified to allow for the more rapid diffusion possible from a convex sphere.[6] If the diffusing species undergoes an irreversible first-order (or pseudo-first-order) reaction, e.g.

$$O + ne \rightleftharpoons R \xrightarrow{k_f} Z$$

then the convoluting function has to be modified, by the multiplication of e^{-kt}. Therefore the kinetic convolution integral becomes;[7,8]

$$i(t)*i(g) = \Pi^{-1/2} \int_0^t \left[(t-\tau)^{-1/2} i e^{-k_f(t-\tau)}\right] d\tau \qquad (8)$$

A numerical evaluation of i(t)*g(t) cannot be obtained directly from equation (8), because of the point of singularity in the kernel at $t = \tau$ however this can be overcome by an integration in parts;

$$i(t)*i(g) = 2\Pi^{-1/2} t^{1/2} i(\tau = 0) e^{-k_f t} + 2\Pi^{-1/2} \int_0^t [(t-\tau)^{1/2} \left(k_f i + \frac{di}{d\tau}\right) e^{-k_f(t-\tau)}] d\tau \quad (9)$$

The $di/d\tau$ term can be obtained from the cyclic voltammogram data by using the least squares differentiation procedure described by Savitzky and Golay.[9] Then the integral can be evaluated using the trapezoidal rule. By choosing a starting point for the cyclic voltammogram, where the concentration of R is 0 (usually 200mV away from $E_{½}$) the homogenous rate constant can be determined by systematically varying k until a value is found which gives i(t)*g(t) = 0 at the starting point.

The calculations were carried out by the programmes described in the experimental section. As an example Figure 4.4B shows the convolution integral (with the correct k value chosen) applied to the cyclic voltammetric response shown in Figure 4.4A.

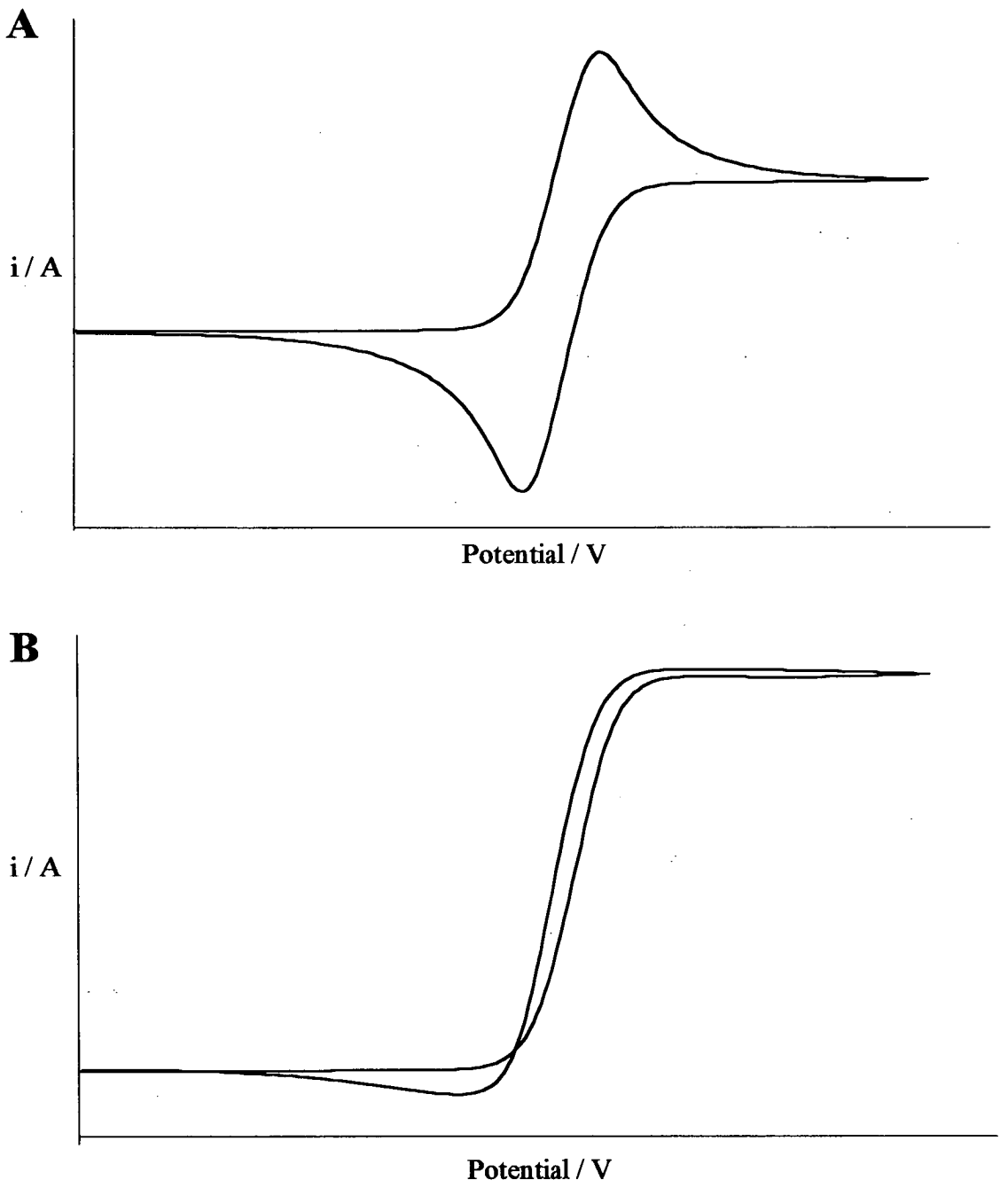

Figure 4.4 - Example of Convolution Integral (Figure 4.3B) Applied to CV shown in Figure 4.3A

4.1.2.3 Double Potential Step Chronoamperometry

For the reaction,

$$O + ne \rightleftharpoons R \xrightarrow{k_f} Z$$

the Differential Pulse technique involves producing the product R under diffusion controlled conditions for a set time interval and then measuring its loss. To undertake the measurement a waveform of type shown in Figure 4.5 is applied to the working electrode.

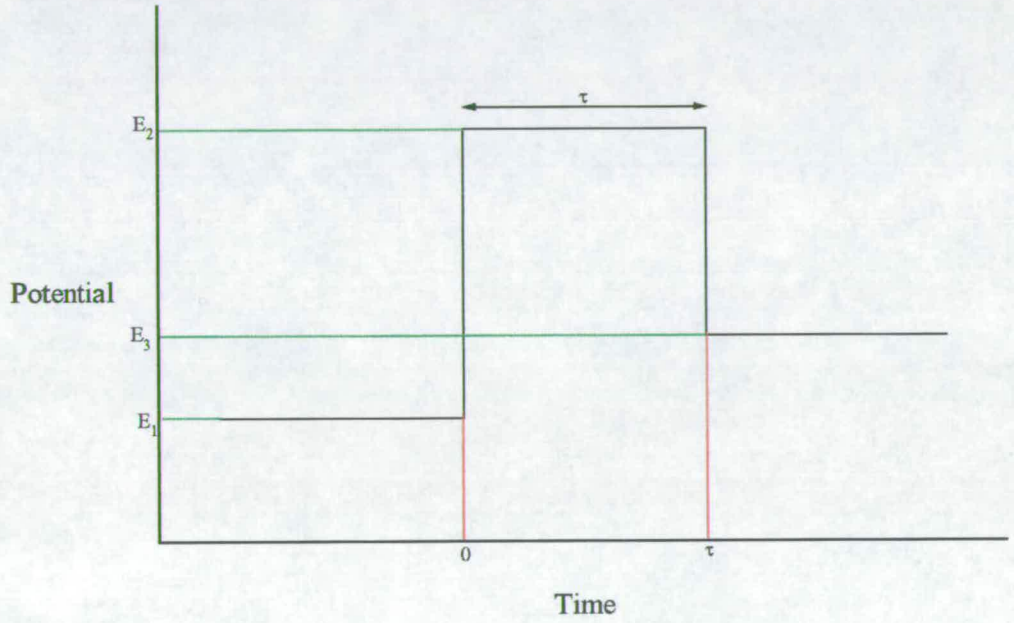

Figure 4.5 - Waveform Applied for Double Potential Step Studies

The potential E_1 is selected so that no reaction occurs (current = 0). Then at time t = 0 a pulse to potential E_2, where the reduction of O is diffusion controlled. After time τ the potential is stepped back to E_3 where O is produced again at a diffusion controlled rate.

Thus the current from the last pulse is used to measure the amount of R present at the electrode. The higher the rate k_f the less R present therefore the lower the current measured. Figure 4.6 shows the current response observed during the time period of the experiment.

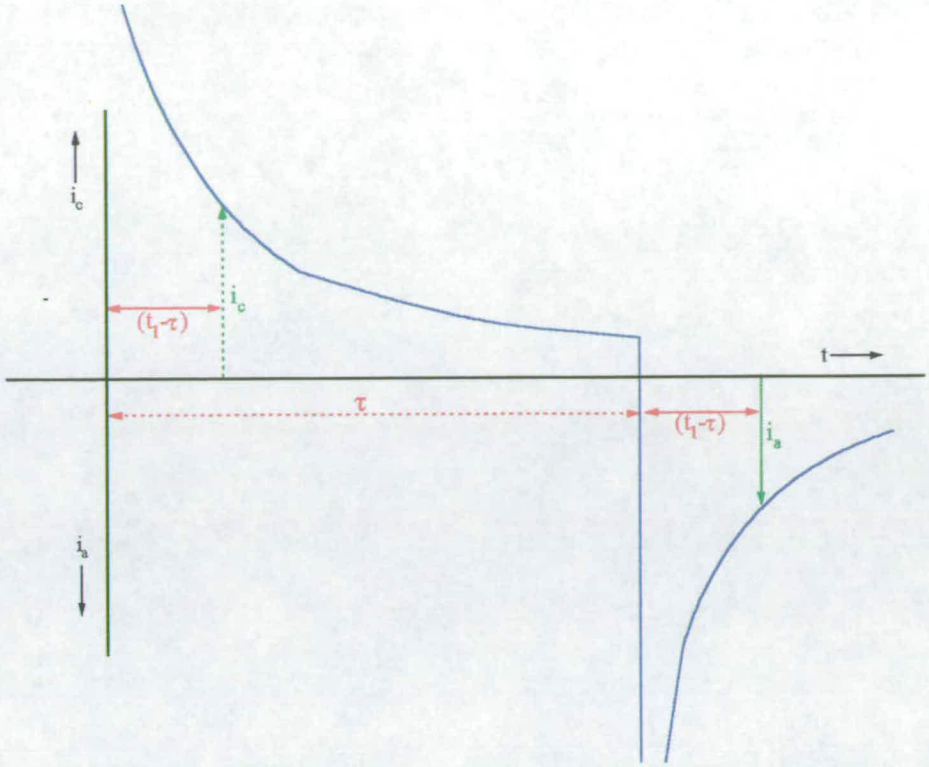

Figure 4.6 - Typical Cathodic-Anodic Current-Time Curves Resulting from a Double Potential Step Experiment

The current time response curve is best analysed by taking the ratio of the forward and reverse currents at set time periods. This negates any dependence on electrode area, solution concentration and diffusion coefficients. It can be shown that $-i_a/i_c$ is related to k_f, t and τ by the complex equation;[10]

$$-\frac{i_a}{i_c} = \phi\left[k_f\tau, \frac{(t-\tau)}{\tau}\right] - \sqrt{\frac{(t-\tau)/\tau}{1+(t-\tau)/\tau}} \qquad (10)$$

where $\phi = e^{-\frac{k_f\tau}{2}} I_0\left(k_f\tau/2\right) + 2e^{-\frac{k_f\tau}{2}} e^{-k_f(t-\tau)} \times \sum_{n=1}^{\infty} I_n\left(k_f\tau/2\right) \frac{\int_0^{k\,(t-\tau)} \cdots \int_0^{\lambda_2} \lambda_1^n e^{\lambda_1} d\lambda_1 \ldots d\lambda_n}{[k_f(t-\tau)]^n}$

However it is a simple matter to obtain values of k_f, by comparison of experimentally determined values of $-i_a/i_c$ with theoretical values of the reduced time $(t-\tau)/\tau$,[10] see Figure 4.6. A wide range of values of the reduced time are investigated to ensure reliable values of k_f are obtained.

4.1.2.4 Summary

All the described techniques were employed during the course of this study. The Nicholson and Shain method was found to be inaccurate due to only 3 points being used to describe a cyclic voltammetric experiment.

Convolution was an improvement over Nicholson and Shain as all points from a CV were used in the calculation. However, a dependence of the calculated rate was found with variation in the scan rate which not expected from the theory. Complications were also found if the electroactive product gave a couple at similar potentials to the original couple.

Double Potential Step Chronoamperometry was found give the most reproducible results and the ability to calculate the kinetic values many times from a single experiment help to minimise any errors found in a single calculation. Therefore, it is results from the differential pulse experiments that are presented in the following section.

4.2 Results and Discussion

4.2.1 Introduction

In Chapters 1 and 2 we showed that the complexes of the series *mer*-$[OsX_3L_3]$, where X is Cl or Br and L is a tertiary phosphine or arsine, when reduced to Os(II) undergo an ec type reaction forming the product $[OsX_2L_3Y]$ (where Y is a neutral coordinating ligand). The mechanism is shown below:

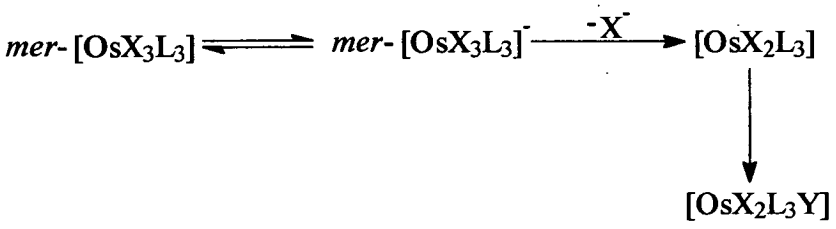

A series of kinetic measurements have been undertaken. Preliminary results using the method of Nicholson and Shain and the convolution method have led us to believe the rate determining step (RDS) for the ec reaction is the loss of the halide forming the 5-coordinate intermediate.

Here we will report values obtained using Double Potential Step Chrono-amperometry. We will also discuss the trends observed when employing the other methods which time did not allow to be repeated using the more accurate technique. The results are arranged so as to illustrate the dependence of the rate of reaction on variation of one factor, such as substituting the halide, Group 15 ligand or the solvent.

4.2.2 Results

4.2.2.1 Dependence on Halide

The kinetics of the complexes *mer*-$[OsCl_3(PMe_2Ph)_3]$ and *mer*-$[OsBr_3(PMe_2Ph)_3]$ were studied in dmf / 0.1M $[TBA][BF_4]$ at various temperatures. At 298 ± 1K the rate of reaction was measured as $8.2s^{-1}$ and $25.7s^{-1}$ for *mer*-$[OsCl_3(PMe_2Ph)_3]$ and *mer*-$[OsBr_3(PMe_2Ph)_3]$ respectively. It is widely known that Br^- is a better leaving group than Cl^-. The bromide ion is better solvated then the smaller chloride ion and thus is stabilised. The above experimental results were therefore in agreement with expectation.

Figure 4.7 and 4.8 show the Arrhenius plot of ln k_f vs. 1/T for the chloride and bromide complexes. The gradient of the determined straight lines give activation energies of 21.0 ± 3 $kJmol^{-1}$ and 62.4 ± 3 $kJmol^{-1}$ for the chloride and bromide complexes respectively. Hence the energy to initiate the reaction is greater in the bromide complex than the chloride.

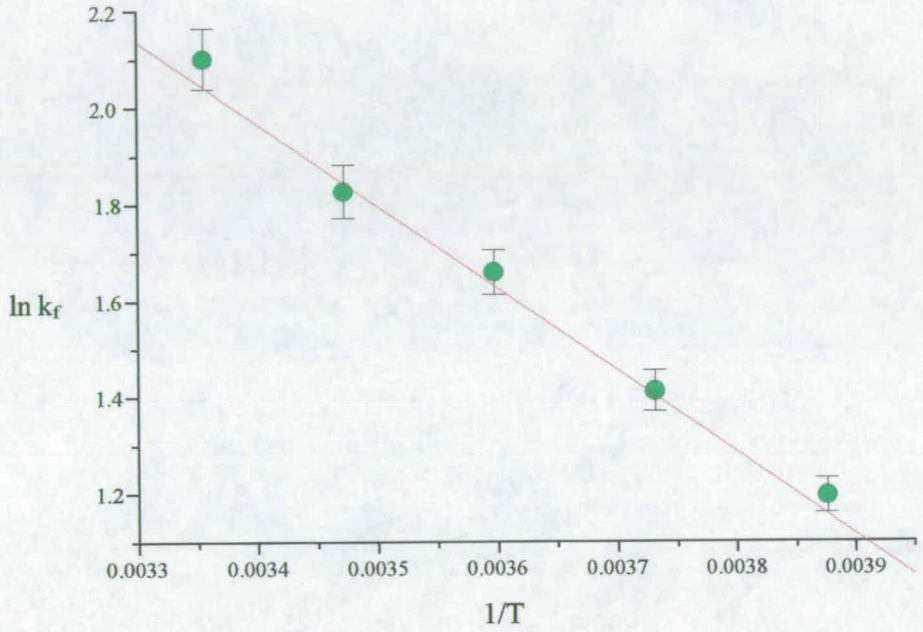

Figure 4.7 - Arrhenius Plot for *mer*-$[OsCl_3(PMe_2Ph)_3]$ in dmf / 0.1M $[TBA][BF_4]$

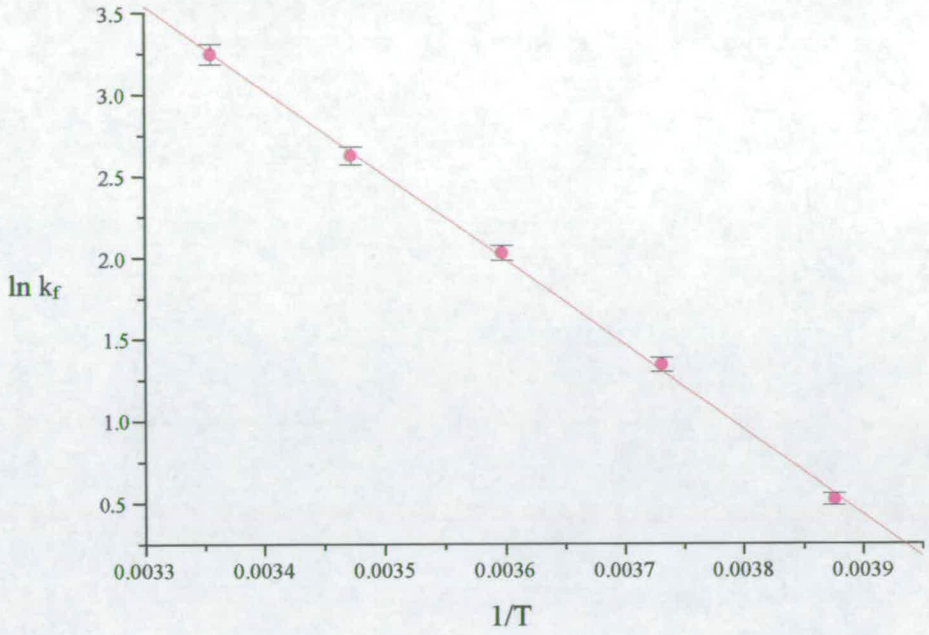

Figure 4.8 - Arrhenius Plot for *mer*-[$OsBr_3(PMe_2Ph)_3$] in dmf / 0.1M [TBA][BF_4]

4.2.2.2 Variation of the Group 15 Ligand

The rate of reaction of *mer*-[$OsCl_3(PMePh_2)_3$] was measured in dmf / 0.1M [TBA][BF_4] at various temperatures. At 298K the rate was measured to be $16.6s^{-1}$ compared with $8.2s^{-1}$ for *mer*-[$OsCl_3(PMe_2Ph)_3$]. In Chapter 2 we reported by the way of pK_a values and Tolman's Electronic Parameters that $PMePh_2$ has greater σ-donor properties than PMe_2Ph. Hence the *trans* effect of $PMePh_2$ is greater and the breaking of the Os-Cl bond is easier and faster to accomplish then for PMe_2Ph.

Figure 4.9 shows the Arrhenius plot for *mer*-[$OsCl_3(PMePh_2)_3$]. The slope of the graph gives a activation energy of 21.4 ± 3kJmol^{-1} identical to that of 21.0 ± 3 kJmol^{-1} for *mer*-[$OsCl_3(PMe_2Ph)_3$]. Hence the activation energy for the chloride complexes studied does not depend on the nature of the phosphine ligands. Further tertiary phosphine complexes should be studied to test the generality of the above observation.

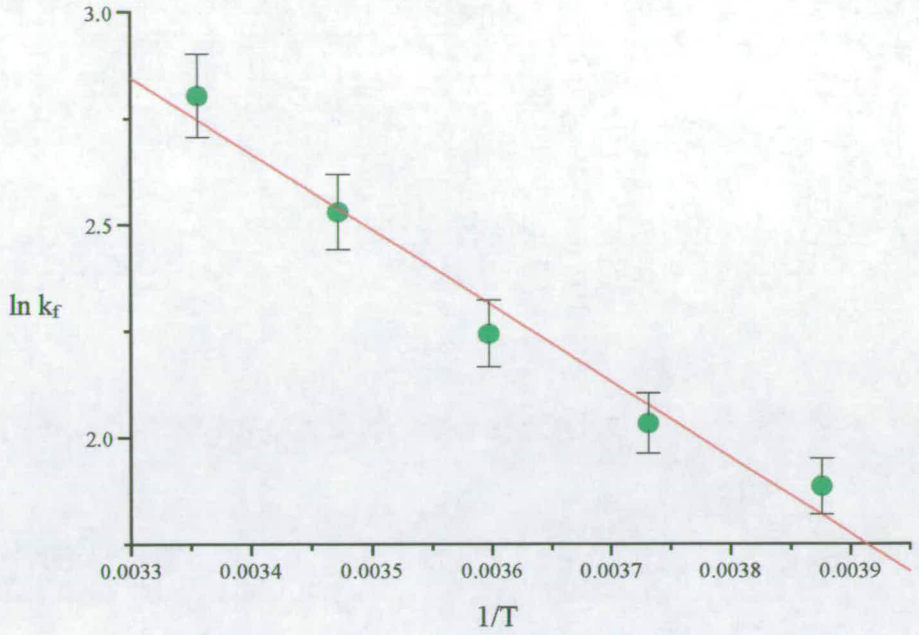

Figure 4.9 - Arrhenius Plot for *mer*-[$OsCl_3(PMePh_2)_3$] in dmf / 0.1M [TBA][BF_4]

Studies of arsine ligand complexes have found that the π-accepting ability of the ligand stabilises the Os(II) state so that the chemical reaction only occurs at temperatures greater than 323K. Therefore although the rate of halide loss is much slower for arsine containing complexes.

4.2.2.3 Variation of Solvent

Preliminary studies employing the convolution technique on *mer*-[$OsCl_3(PMe_2Ph)_3$] in CH_2Cl_2 / 0.5M [TBA][BF_4] and MeCN / 0.1M [TBA][BF_4] have shown the reaction to be consistently faster in the latter case. CH_2Cl_2 is known to be a poor solvating agent towards Cl^- ions. In addition MeCN is a better coordinating ligand then CH_2Cl_2 so the product of the reaction is a relatively stable six coordinate complex compared to a 5 coordinate complex for the non-coordinating CH_2Cl_2.

4.2.3 Conclusion

The results described above all support the theory that the Rate Determining step for the reaction;

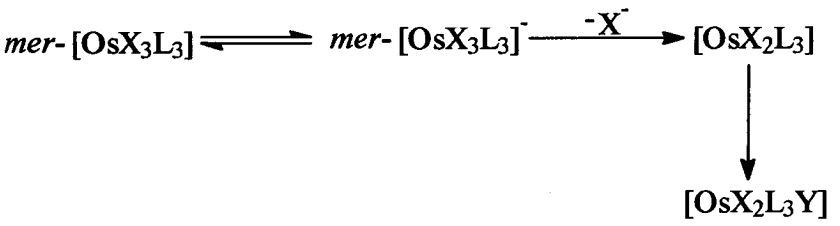

is the loss of halide forming the 5 coordinate intermediate i.e.

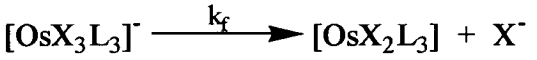

4.3 References

(1) R. S. Nicholson and I. Shain, *Anal. Chem.*, 1964, **36**, 1964.

(2) R. S. Nicholson, *Anal. Chem.*, 1966, **36**, 1407.

(3) A. J. Bard and L. R. Faulkner, *Electrochemical Methods, Fundamentals and Applications*, John Wiley and Sons, New York, 1980.

(4) K. B. Oldham, *Anal. Chem.*, 1986, **58**, 2296.

(5) K. B. Oldham and J. Spanier, *J. Electroanal. Chem.* 1970, **26**, 331.

(6) J. C. Myland, K. B. Oldham and C. G. Zoski, *J. Electroanal. Chem.*, 1985, **193**, 3.

(7) F.E. Woodward, R. D Goodin and P. J. Kinlen, *Anal. Chem.*, 1984, **56**, 1920.

(8) A. Blagg, S. W. Carr, G. R. Cooper, I. D. Dobson, J. B. Gill, D. X. Goodall, B. L. Shaw, N. Taylor and T. Boddington, *J. Chem. Soc., Dalton Trans.*, 1985, 1213.

(9) A. Savitzky and M. J. E. Golay, *Anal. Chem.*, 1964, **36**, 1627.

(10) W. M. Schwarz and I. Shain, *J. Phys. Chem.*, 1965, **69**, 30.

Chapter 5

Electrochemical and Spectroelectrochemical Study of the Series *fac*-$[OsCl_3L_3]$

5.1 Introduction

In the previous Chapters we have undertaken a detailed study of the series *mer*-$[OsX_3L_3]$ where X = Cl or Br and L is a tertiary phosphine or arsine. In this chapter we continue the study with that of the isomeric series *fac*-$[OsCl_3L_3]$.

The facial isomers were prepared by the method of Douglas and Shaw:[1] by the reaction of the *mer*-$[OsCl_3L_3]$ where L is PMe_2Ph, PEt_2Ph, $AsMe_2Ph$ or $AsEt_2Ph$ with $NaBH_4$ forming the hydride $[OsH_4L_3]$, which when reacted with HCl gas in methanol formed the insoluble facial isomer.*

5.2 Results and Discussion

5.2.1 Structure

Levason *et. al.*[2] reported the structure of *fac*-$[OsCl_3(PEt_2Ph)_3]$ in 1990. Figure 5.1 shows the structure of the complex, with Table 5.1 listing the selected bond distances and angles. For example note that the Cl-Os-Cl angles are all less than 90° whereas the related phosphine angles are considerably greater. This is presumably a direct consequence of the steric bulk of the phosphine ligands.

For comparison the X-ray diffraction structure of *mer*-$[OsCl_3(PEt_2Ph)_3]$ was measured and solved as part of this study. Figure 5.2 shows the structure obtained from the measurement while Table 5.2 list the selected bond distance and angles. As before the *mer* isomer structure shows the trans influence of the phosphine on the Os-Cl(2) bond distance, lengthening it by ~0.1Å with respect to the other Os-Cl bonds. The *fac* isomer shows this lengthening to all its metal halide bonds as expected as each Cl is trans to a tertiary phosphine ligand.

* For full details, preparation and characterisation see Chapter 6.

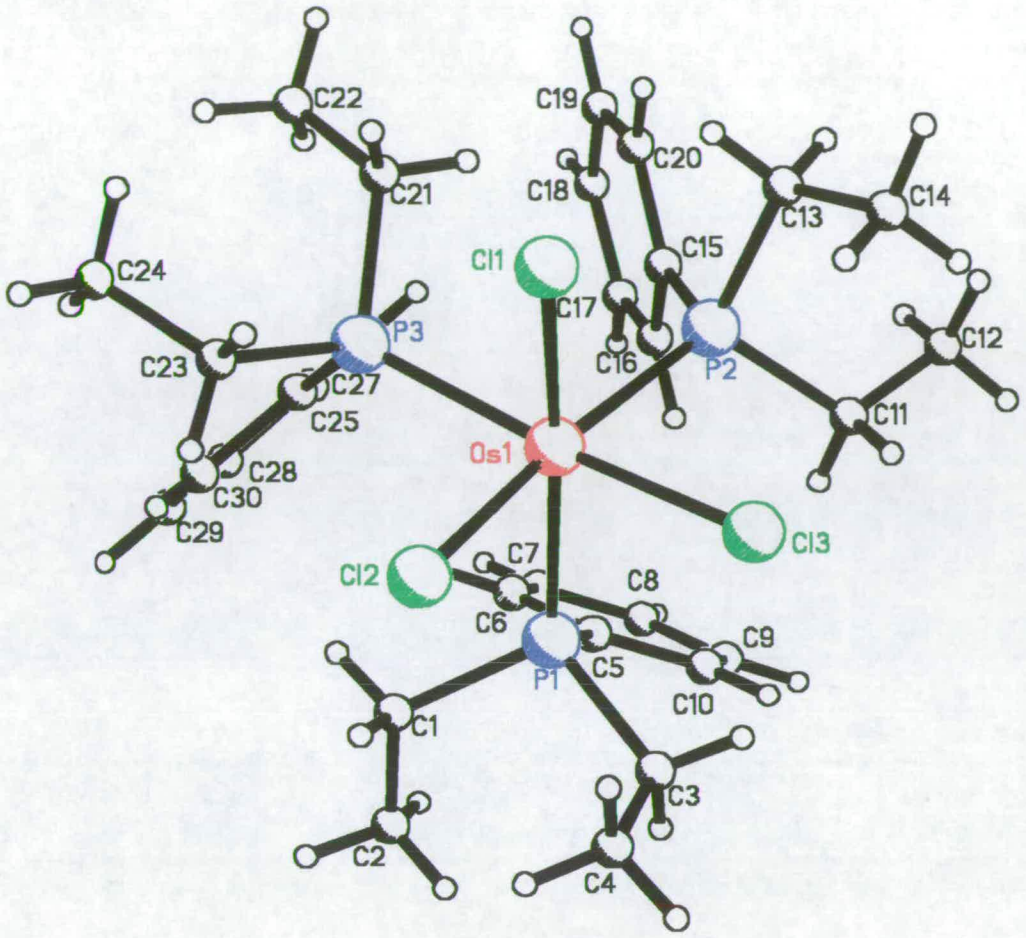

Figure 5.1 - Structure of *fac*-[$OsCl_3(PMe_2Ph)_3$] (Ref. (2))

Table 5.1 - Selected Bond Distances and Angles for *fac*-[$OsCl_3(PMe_2Ph)_3$] (Ref. (2))

Os-Cl(1)	2.442(3)	Os-Cl(3)	2.449(2)	Os-P(2)	2.380(2)
Os-Cl(2)	2.447(2)	Os-P(1)	2.380(2)	Os-P(3)	2.375(2)

Cl(1)-Os-Cl(2)	84.4(1)	P(1)-Os-Cl(2)	81.7(1)
Cl(1)-Os-Cl(3)	85.8(1)	P(1)-Os-Cl(3)	87.3(1)
Cl(2)-Os-Cl(3)	84.5(1)	P(2)-Os-Cl(1)	88.6(1)
P(1)-Os-P(2)	103.9(1)	P(2)-Os-Cl(3)	83.6(1)
P(1)-Os-P(3)	104.6(1)	P(3)-Os-Cl(1)	80.6(1)
P(2)-Os-P(3)	101.5(1)	P(3)-Os-Cl(2)	88.6(1)

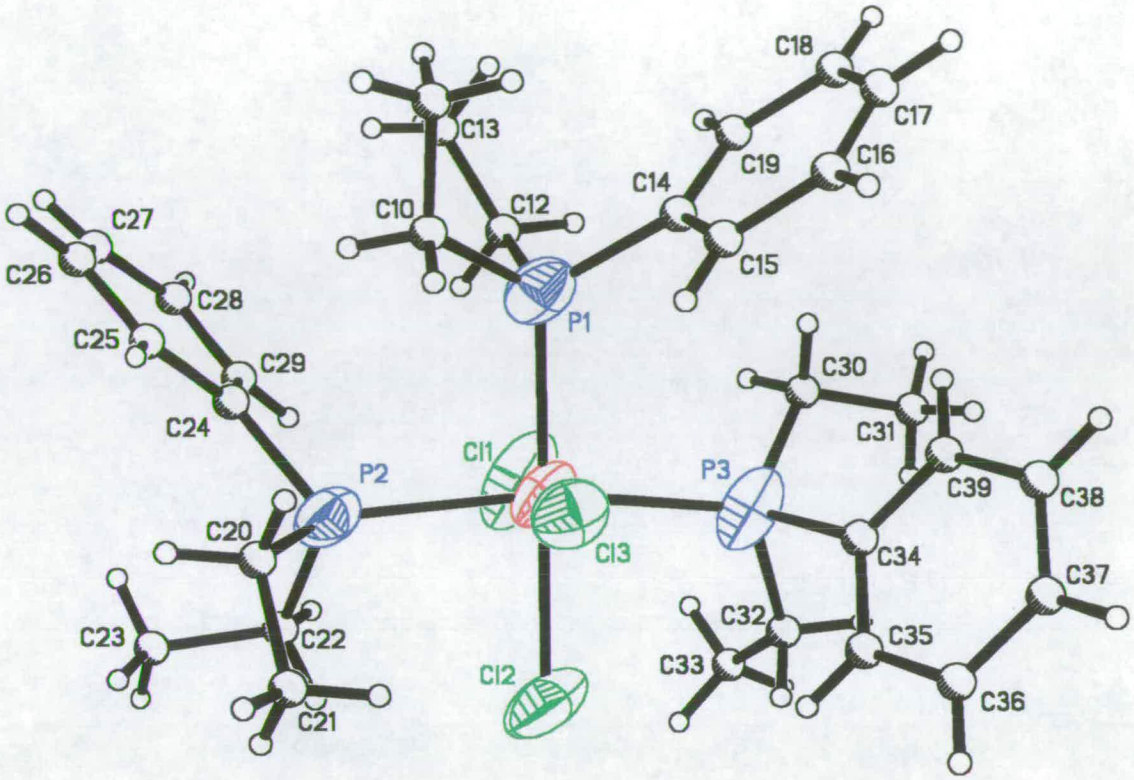

Figure 5.2 - Structure of *mer*-[$OsCl_3(PEt_2Ph)_3$]

Table 5.2 - Selected Bond Distance (Å) and Angles (°) for *mer*-[$OsCl_3(PEt_2Ph)_3$]

Os(1)-Cl(1)	2.350(4)	Os(1)-Cl(3)	2.344(3)	Os(1)-P(2)	2.440(4)
Os(1)-Cl(2)	2.436(4)	Os(1)-P(1)	2.373(4)	Os(1)-P(3)	2.413(4)

Cl(3)-Os(1)-Cl(1)	179.0(2)	P(1)-Os(1)-Cl(2)	174.6(2)
Cl(3)-Os(1)-P(1)	87.46(13)	P(3)-Os(1)-Cl(2)	85.0(2)
Cl(1)-Os(1)-P(1)	93.4(2)	Cl(3)-Os(1)-P(2)	91.73(14)
Cl(3)-Os(1)-P(3)	93.52(13)	Cl(1)-Os(1)-P(2)	87.8(2)
Cl(1)-Os(1)-P(3)	86.82(14)	P(1)-Os(1)-P(2)	94.58(14)
P(1)-Os(1)-P(3)	96.3(2)	P(3)-Os(1)-P(2)	168.1(2)
Cl(3)-Os(1)-Cl(2)	87.2(2)	Cl(2)-Os(1)-P(2)	84.60(14)
Cl(1)-Os(1)-Cl(2)	91.9(2)		

5.2.2 Electrochemistry

The series of compounds was studied electrochemically in CH_2Cl_2/0.5M [TBA][BF_4]. The electrochemical response of *fac*-[$OsCl_3(PMe_2Ph)_3$] at room temperature is shown in Figure 5.3.

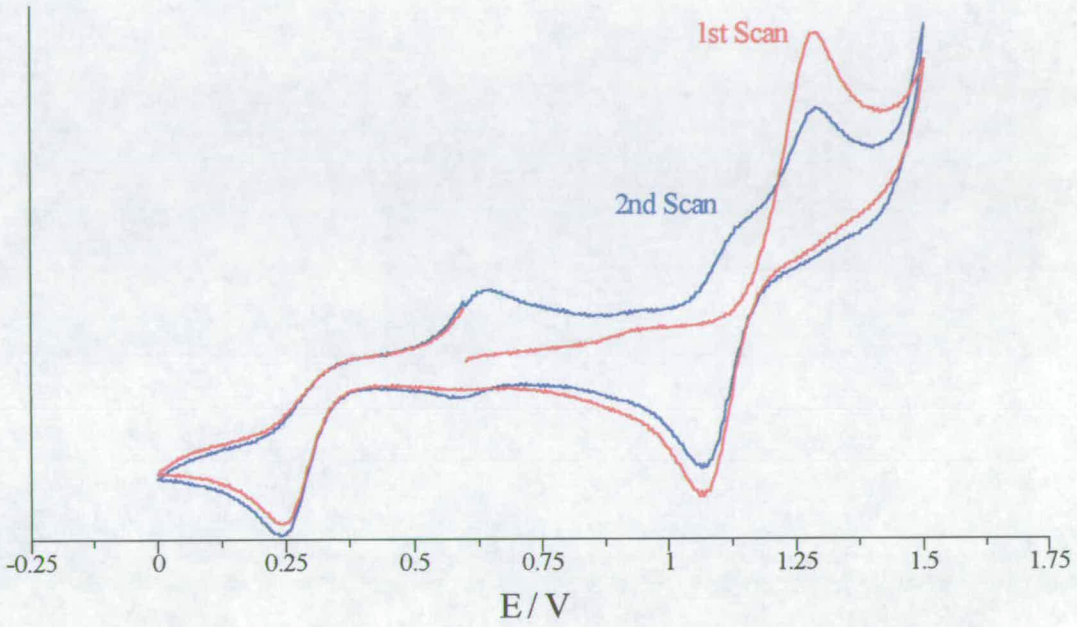

Figure 5.3 - Cyclic Voltammogram of *fac*-[$OsCl_3(PMe_2Ph)_3$] in CH_2Cl_2/0.5M [TBA][BF_4] at RT, Scan Rate 100mVs^{-1}

As with the analogous mer compounds the *fac* isomers show two one electron metal based couples; a reduction and an oxidation. Unlike the *mer* isomers both couples are irreversible and produce electroactive daughter products at different potentials.

Table 5.3 lists the recorded electrochemical potentials for the series of compounds prepared in this study, as well as the daughter product potentials for both couples.

Table 5.3 - Electrochemical Response of the Series *fac*-$[OsCl_3L_3]$ in CH_2Cl_2/0.5M [TBA][BF_4] at RT (vs. Ag/AgCl)

	Oxidation		Reduction	
L	Parent Couple	Daughter Product	Parent Couple	Daughter Product
PMe_2Ph	1.20V	1.06V	0.24V	0.64V
$AsMe_2Ph$	1.21V	1.04V	-0.02V	0.62V
$AsEt_2Ph$	1.22V	0.98V	-0.11V	0.46v

The potential for the forward couple is reported

The complex *fac*-$[OsCl_3(PEt_2Ph)_3]$ was found to decompose when dissolved in solution therefore the couples could not be recorded for this species.

The ec mechanism involved in the reductive process is believed to be similar to that of the *mer* complexes with the loss of a halide ligand and the gain of a neutral coordinating ligand (See Chapters 1 and 2). Bulk electroreduction of the complex has shown the presence of free chloride in solution to support this mechanism.

We expect the complex to form one of the thermodynamically stable complexes either *cis* or *trans*-$[OsCl_2L_3Y]$ (where Y is a neutral coordinating ligand) as found for the *mer* complexes (See Chapters 1 and 2). Such a product would involve rearrangement of the complex (See Figure 5.4). The initial product formed has not been confirmed as the partial solubility of the complexes make the isolation of the product difficult. However the potential of the initially formed daughter product indicates that it is not that formed from halide loss of the *mer* species.

Preliminary kinetic studies have shown that the reaction rate is considerably faster than that of the related *mer* complex (See Chapter 4). This is expected as the *fac* isomer has three Os-Cl bonds weakened by the *trans* influence of the Group 15 ligands whereas the *mer* isomer has only one (See Crystal Structures).

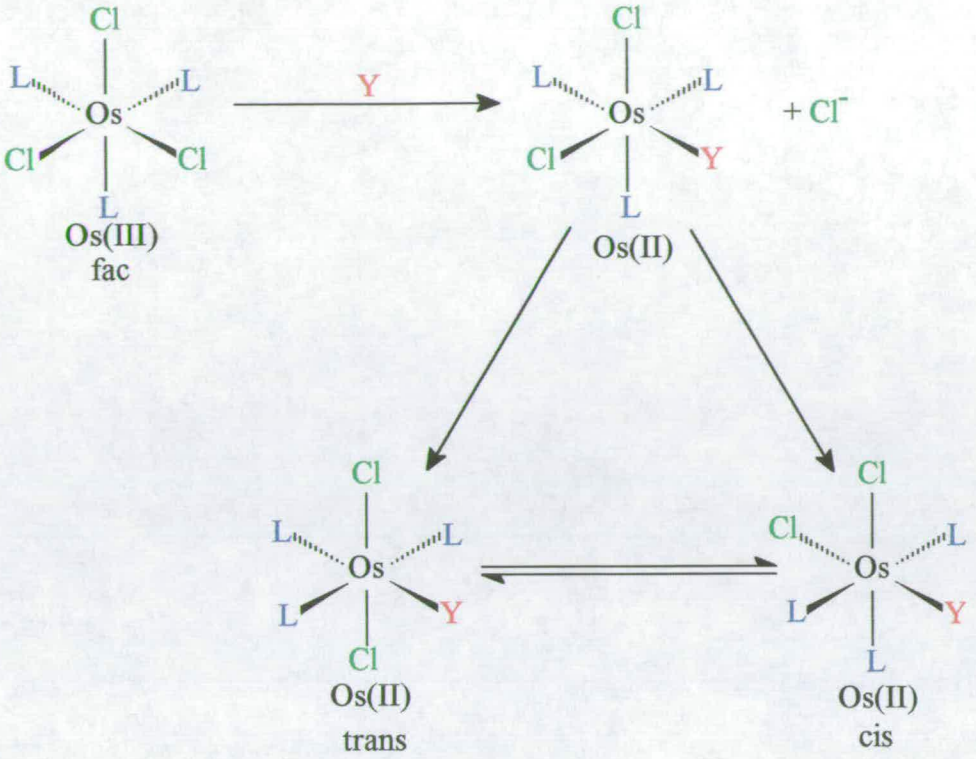

Figure 5.4 - Possible Mechanisms for Reduction of *fac*-$[OsCl_3L_3]$

The irreversible oxidation of the parent complex is also worth some discussion. The couple produces a daughter product at ~1V which can be assigned as the *mer* isomer.

The *mer* isomer has be isolated from the *fac* isomer electrochemically by bulk electroxidation and chemically by oxidation with $NOBF_4$ in CH_2Cl_2 under inert atmosphere. Mass Spectra and electrochemistry have been used to confirm that isomerisation has been oxidatively induced. Figure 5.5 shows that the isomerisation reaction can be partially frozen out by studying the solution at fast scan rates using an ultra micro working electrode.

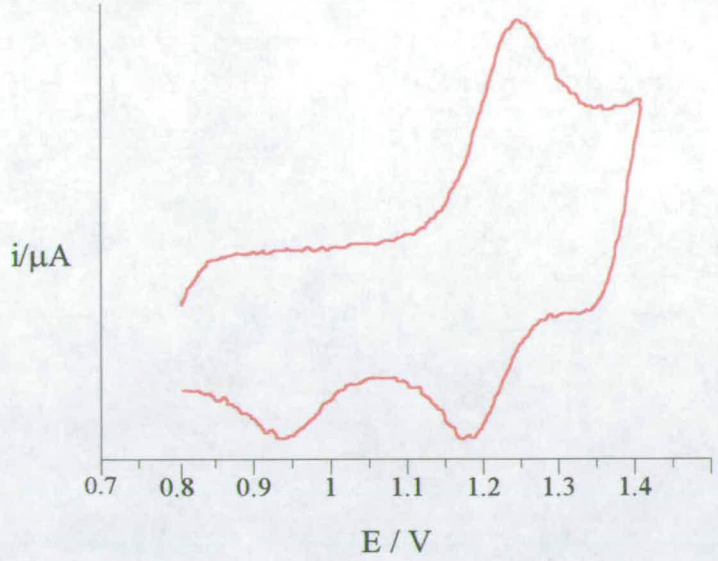

Figure 5.5 - Cyclic Voltammogram of Os(II)/Os(III) couple of *fac*-$[OsCl_3(PMe_2Ph)_3]$ in CH_2Cl_2 / 0.5M [TBA][BF_4] at RT. Scan Rate $1000Vs^{-1}$

The reaction can also be followed by *in situ* UV/Vis spectroscopy. Figure 5.5 shows the conversion of *fac*-$[OsCl_3(PMe_2Ph)_3]$ to *mer*-$[OsCl_3(PMe_2Ph)_3]^+$.

The absorption bands in the UV/Vis Spectra of the *fac* isomers were assigned to electronic transitions using an Extended Hückel Molecular Orbital Calculation carried out on the structure of *fac*-$[OsCl_3(PEt_2Ph)_3]$ described earlier[†]. The lower energy bands of the *fac* isomer are assigned as $\sigma Cl + \sigma L \rightarrow t_{2g}Os(III)$ whilst at higher energy the bands are $\pi Cl \rightarrow t_{2g}Os(III)$ charge transfer transitions.

[†] See Chapter 6 for Details of EHMO Calculations

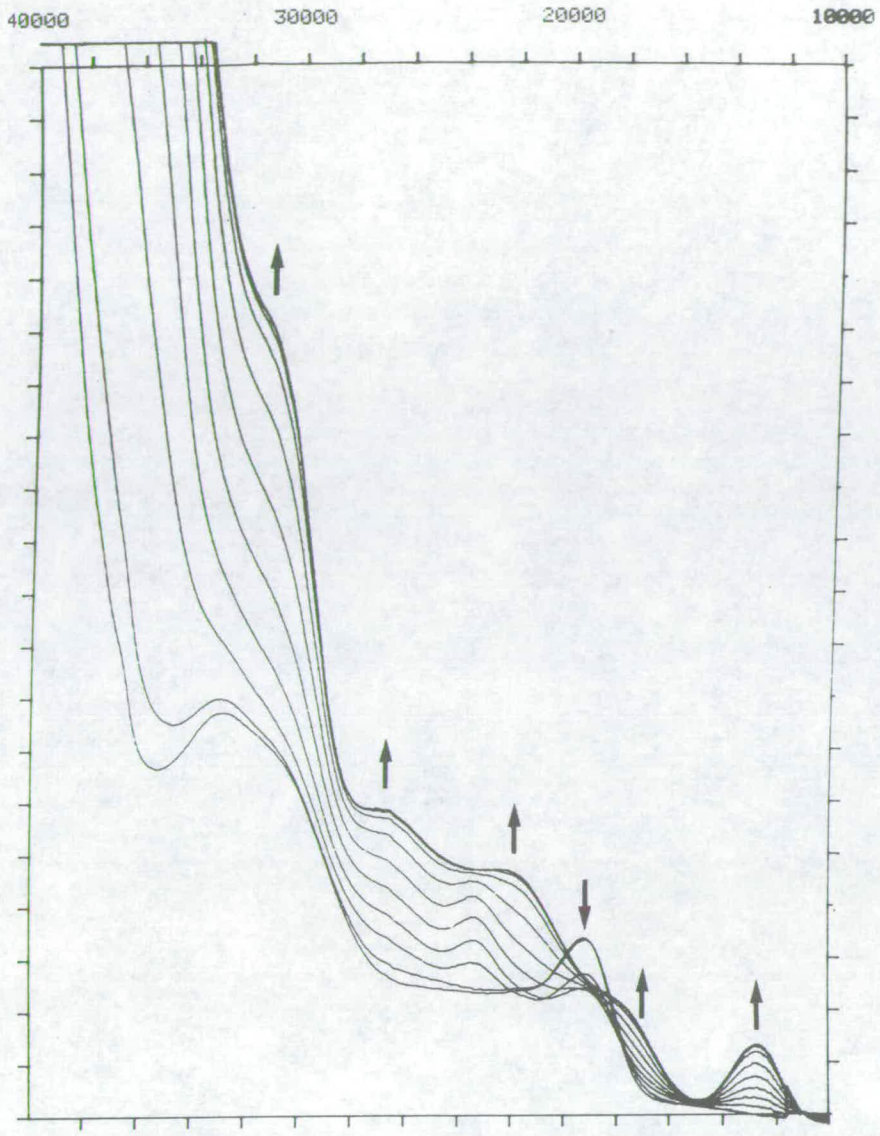

Figure 5.6 - Spectral Changes for the Conversion of *fac*-$[OsCl_3(PMe_2Ph)_3]$ to *mer*-$[OsCl_3(PMe_2Ph)_3]^+$ in CH_2Cl_2/0.5M [TBA][BF_4][‡]

The collapse of these bands can be seen in Figure 5.6, as can the growth of the bands associated with the charge transfer transitions to the Os(IV) *mer* complex. On reduction the growth of the bands associated with *mer*-$[Os(III)Cl_3(PMe_2Ph)_3]$ (as described in Chapter 2) are visible in Figure 5.7.

‡ Units are in Wavenumbers (cm^{-1})

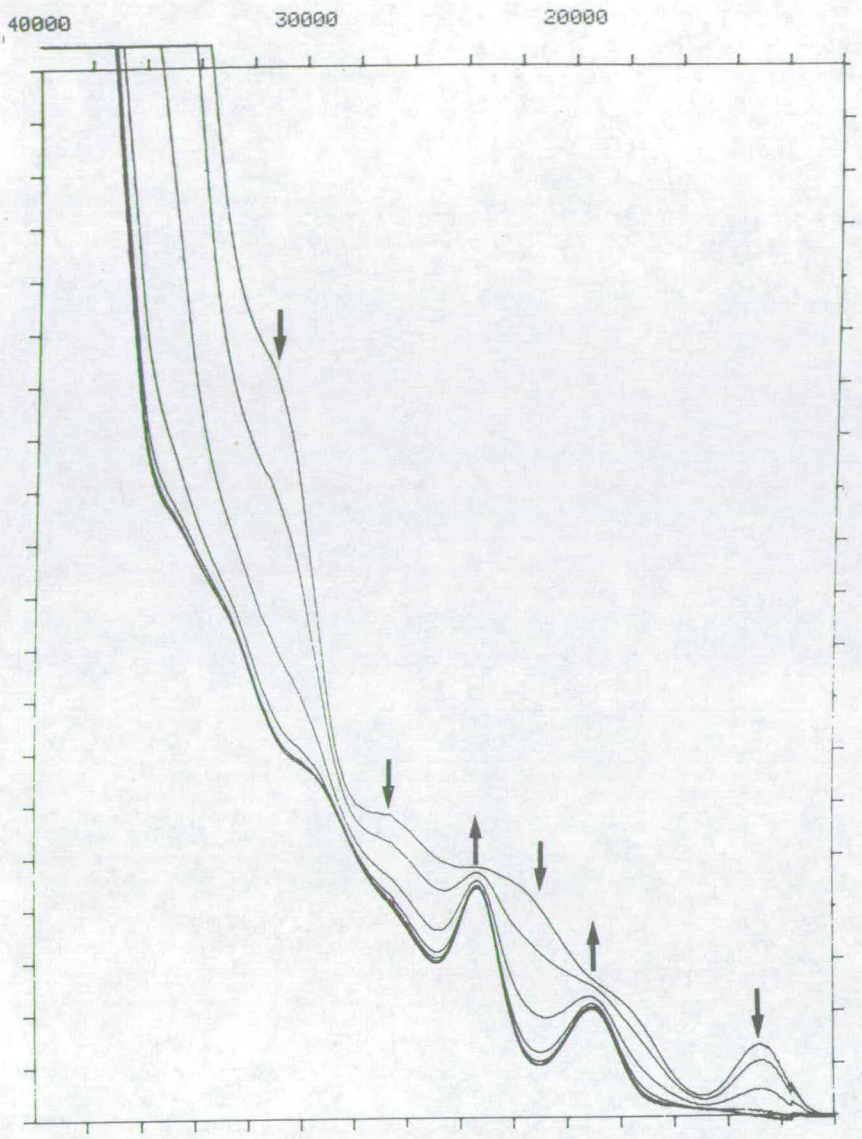

Figure 5.7 - Spectral Changes for the Conversion of *mer*-$[OsCl_3(PMe_2Ph)_3]^+$ to *mer*-$[OsCl_3(PMe_2Ph)_3]$ in CH_2Cl_2/0.5M [TBA][BF_4][‡]

The cause of the isomerisation is due to the electronic configuration of each isomer. Figure 5.8 shows the configuration of the metal t_{2g} orbitals for each isomer. The removal of the 5th electron as occurs on oxidation means that the *mer* form is the stable form for Os(IV) hence the isomerisation is favoured.

‡ Units are in Wavenumbers (cm^{-1})

Figure 5.8 would also suggest that the *fac* structure should be favoured for Os(II) oxidation state. However, this prediction cannot be experimentally tested on these compounds due to the chemical instability of the Os(II) *fac* species.

The mechanism of isomerisation of octahedral complexes has been the centre of much interest in recent years. There are two possible mechanisms: a dissociative mechanism, or an intramolecular rearrangement mechanism.

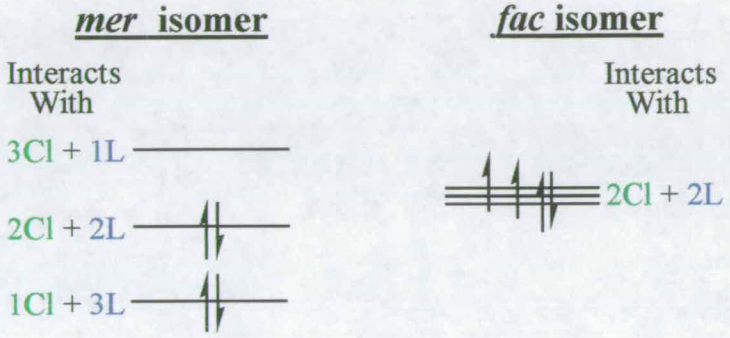

Figure 5.8 - Electronic Configuration of the Os t_{2g} Orbitals in *mer* and *fac*-$[OsX_3L_3]$

Many groups have shown that *cis-trans/fac-mer* isomerisation must follow an intramolecular, non dissociative course. Complexes studied include $[M(CO)_4(ER_3)_2]$ (where M = Re, Ru or Os and E = Si, Ge, Sn or Pb),[3,4] $[Cr(CO)_4(C(OMe)Me)(PR_3)]$ (where R = Et or Cy),[5] $[Mo(CO)_4(PR_3)_2]$ (where R = Me, Et or Bu)[6-8] and $[Mn(CO)_4Ph(P(OPh)_3)]$.[9]

Bailar proposed a mechanism for this intramolecular rearrangement now called the "Bailar Twist".[10] The mechanism involves the twist of one face of an octahedral complex by 120° via a trigonal prism transition state, see Figure 5.9. Hence converting a *trans* isomer to *cis* and *fac* to *mer*.

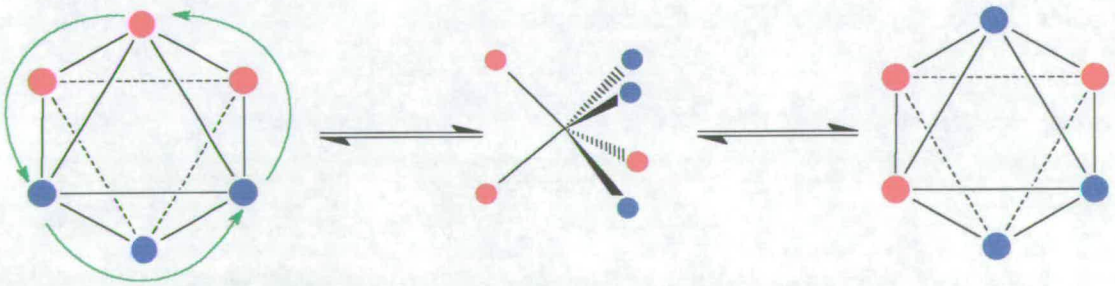

Figure 5.9 - Mechanism for the "Bailar Twist"

In the study of $[Cr(CO)_3(P(OMe)_3)_3]$ Bond *et. al.* studied the rate of reaction for the *fac-mer* isomerisation via electrochemical methods.[11] They reported an activation energy of 15.9 ± 0.7 $kJmol^{-1}$ for the isomerisation. This was in agreement with the same group's earlier studies on $[M(CO)_2(P\text{-}P)_2]$ (where M = Cr, Mo or W and P-P = bis(diphenyl-phosphino)methane in which they proved the intramolecular rearrangement and calculated the activation of the twist.[11]

Kinetic measurement carried out on the isomerisation of *fac*-$[OsCl_3(PMe_2Ph)_3]$ to *mer*-$[OsCl_3(PMe_2Ph)_3]$ in CH_2Cl_2 / 0.5M $[TBA][BF_4]$[§] by the double potential step chronoamperometry described in Chapter 4, gave an Arrhenius plot shown in Figure 5.10. Analysis of the slope of the graph gave an activation energy of 26 ± 4 $kJmol^{-1}$ which is in agreement with the values obtained by Bond *et al.*

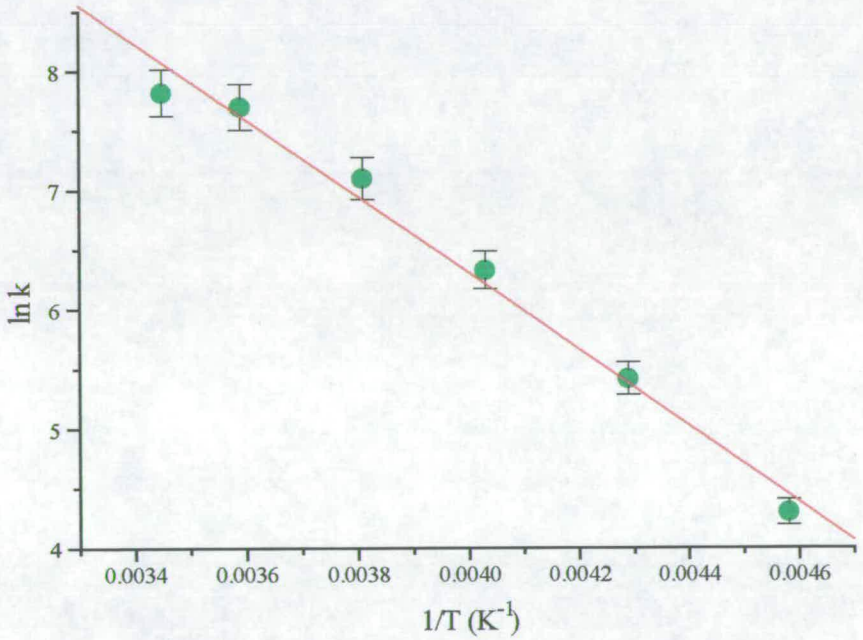

Figure 5.10 - Arrhenius Plot of the Isomerisation of *fac*-$[OsCl_3(PMe_2Ph)_3]$ to *mer*-$[OsCl_3(PMe_2Ph)_3]^+$ in CH_2Cl_2/0.5M $[TBA][BF_4]$

The barrier of the Bailar twist mechanism is the steric hindrance in the intermediate trigonal prism. Analysis of the crystal structure of both the *fac* and *mer* isomers have

---

§ The experiment was carried out by Dr. Alan Brown.

shown that the structure is possible with only a small distortion of the methyl or ethyl groups away from their ideal.

The activation energy recorded for the *fac-mer* isomerisation is similar to the values recorded for the substitution reaction in Chapter 4. Therefore it is still not clear which mechanism is employed here. Further study is needed to clarify, although this will be difficult due to the low solubility of the *fac* isomer.

5.2.3 Conclusion

We have reported the electrochemistry of a series of *fac* isomers of the type $[OsCl_3L_3]$, showing two metal based irreversible couples, an oxidation and reduction. Preliminary studies into the reduction has shown that the process involves loss of a halide and prediction of the products has been made.

Detailed studies of the oxidation process show the complex to undergo isomerisation to the more stable *mer* isomer. Kinetic studies have failed to prove the mechanism for the rearrangement.

5.3 - References

(1) P. G. Douglas and B. L. Shaw, *J. Chem. Soc.*, 1970, 334.

(2) R. A. Cipriano, W. Levason, R. A. S. Mould, D. Pletcher and M. Webster, *J. Chem. Soc., Dalton Trans.*, 1990, 2609.

(3) W. A. G. Graham, R. K. Pomeroy and L.Vancea, *J. Am. Chem. Soc.*, 1976, **98**, 1407.

(4) H. P. Calhoun, W. A. G. Graham, R. K. Pomeroy and L.Vancea, *Inorg. Chem.*, 1977, **16**, 1508.

(5) H. Fischer, E. O. Fischer, H. Werner, *J. Organomet. Chem.*, 1974, **73**, 331.

(6) D. J. Darensbourg and R. L. Kump, *Inorg. Chem.*, 1978, **17**, 2680.

(7) D. J. Darensbourg, *Inorg. Chem.*, 1979, **18**, 14.

(8) F. A. Cotton, D. J. Darensbourg, S. Klein and B. W. S. Kolthammer, *Inorg. Chem.*, 1982, **21**, 2661.

(9) R. P. Stewart Jr., *Inorg. Chem.*, 1979, **18**, 2083.

(10) J. C. Bailar Jr., *J. Inorg. Nucl. Chem.*,1958, **8**, 165.

(11) A. M. Bond, R. Colton and J. E. Kevehordes, *Inorg. Chem.*, 1986, **25**, 749.

(12) A. M. Bond, B. S. Grabaric and J. J. Jockowski, *Inorg. Chem.*, 1978, **17**, 2153.

Chapter 6

Experimental

Preparation and Characterisation of Complexes

Equipment

Description of EHMO Calculations

6.1 Preparation and Characterisation

All preparations were carried out under an inert atmosphere in pre-purged solutions unless otherwise stated. Osmium tetroxide was obtained from Johnson Matthey. Most phosphines were available from commercial suppliers those that were not were synthesised by literature methods. All solvents were HPLC grade and used as supplied without further purification, except dichloromethane which was stored over KOH pellets for one week and heated to reflux over P_2O_5.

Tetra-n-butylammonium tetrafluoroborate, [TBA][BF_4], was prepared by the dropwise addition of tetrabutylammonium hydroxide to tertafluoroboric acid (100cm^3), stirring and diluting as required. The pH of the solution was monitored and once neutral the white precipitate was filtered and washed with distilled water (4 × 100cm^3). The product was recrystallised by dissolving in a hot water/methanol mixture. The resulting white crystals were filtered, washed with distilled water (4 × 100cm^3) and dried *in vacuo* at 75°C for 1 week.

6.1.1 Preparation and Characterisation of the series *mer*-[OsX_3L_3]

Complexes of type *mer*-[$OsCl_3L_3$], where L is PMe_3, PMe_2Ph, $PMePh_2$, PEt_3, PEt_2Ph, $PEtPh_2$, PPr^n_3, $AsPr^n_3$, $AsMe_2Ph$ and $AsEt_2Ph$, were made by the method of Chatt *et al*[1] OsO_4 (0.25g, 0.98 mmol) was reacted with concentrated HCl (2 cm^3) in ethanol (50 cm^3) forming $H_2[OsCl_6]$. After addition of excess phosphine or arsine (4 mmol), the solution was refluxed under nitrogen. The time the solution was heated differed for the various phosphine and arsine ligands. On cooling to 0°C the red/orange product dropped out of solution as a micro crystalline solid which was isolated and washed with diethyl ether and dried *in vacuo*. Table 6.1 shows the yields obtained and the results from the microanalysis.

The analogous bromine complexes were either obtained by the same route as the chloro compound using hydrobromic acid or by the halide exchange reaction of the chloride complex. The chloride complex (0.2g, 0.2 mmol) was refluxed with LiBr (2 mmol) in nitrogen purged ethanol (30cm^3) for one hour. On cooling to 0°C the purple bromide complexes precipitated out of solution, the product was isolated and washed with diethyl ether. Table 6.2 shows the yields and CHN data for the compounds.

Table 6.1- Yields and CHN data for the series *mer*-[$OsCl_3L_3$]

L	Yield	Formula	CHN Results#	
PMe_3	38%	$C_9H_{27}Cl_3OsP_3$	21.08(20.60)%C)	5.37(5.19)%H
PMe_2Ph	41%	$C_{24}H_{33}Cl_3OsP_3$	40.50(40.50)%C	4.69(4.67)%H
$PMePh_2$	78%	$C_{39}H_{39}Cl_3OsP_3$	50.85(52.21)%C	4.38(4.38)%H
PEt_3	45%	$C_{18}H_{45}Cl_3OsP_3$	34.06(33.21)%C	6.82(6.97)%H
PEt_2Ph	68%	$C_{30}H_{45}Cl_3OsP_3$	43.97(45.31)%C	6.22(5.70)%H
$PEtPh_2$	81%	$C_{42}H_{45}Cl_3OsP_3$	53.87(53.70)%C	4.73(4.83)%H
PPr^n_3	43%	$C_{27}H_{63}Cl_3OsP_3$	41.08(41.72)%C	7.80(8.17)%H
$AsPr^n_3$	52%	$C_{27}H_{63}Cl_3OsAs_3$	36.52(35.67)%C	7.17(6.98)%H
$AsMe_2Ph$	63%	$C_{24}H_{33}Cl_3OsAs_3$	34.03(34.20)%C	3.87(3.95)%H
$AsEt_2Ph$	40%	$C_{30}H_{45}Cl_3OsP_3$	38.88(38.87)%C	4.59(4.89)%H

 # Calculated Values are given in Parenthesis

Table 6.2- Yields and CHN data for the series *mer*-[$OsBr_3L_3$]

Ligand	Yield	Formula	CHN Results#	
PMe_3[b]	61%	$C_9H_{27}Br_3OsP_3$	16.39(16.42)%C	4.16(4.13)%H
PMe_2Ph[b]	76%	$C_{24}H_{33}Br_3OsP_3$	34.60(34.10)%C	3.79(3.94)%H
$PMePh_2$[b]	60%	$C_{39}H_{39}Br_3OsP_3$	44.86(45.95)%C	3.58(3.81)%H
PEt_3[b]	59%	$C_{18}H_{45}Br_3OsP_3$	27.89(27.56)%C	5.92(5.78)%H
PEt_2Ph[a]	89%	$C_{30}H_{45}Br_3OsP_3$	45.04(45.31)%C	5.68(5.70)%H
$PEtPh_2$[a]	68%	$C_{42}H_{45}Br_3OsP_3$	44.74(47.03)%C	4.22(4.23)%H
PPr^n_3[a]	70%	$C_{27}H_{63}Br_3OsP_3$	35.95(35.62)%C	6.69(6.98)%H
$AsPr^n_3$[a]	71%	$C_{27}H_{63}Br_3OsAs_3$	30.50(31.11)%C	5.87(6.09)%H
$AsMe_2Ph$[a]	67%	$C_{24}H_{33}Br_3OsAs_3$	30.95(29.38)%C	3.76(3.41)%H
$AsEt_2Ph$[a]	52%	$C_{30}H_{45}Br_3OsAs_3$	34.44(33.98)%C	4.74(4.28)%H

 # Calculated Values are given in Parenthesis
a Prepared via chloride analogue b Prepared direct from OsO_4.

The complexes were also analysed by F.A.B. Mass spectrometry, Tables 6.3 and 6.4 shows the details of this study.

Table 6.3 - Mass Spectral Data for Complexes of Type *mer*-$[OsCl_3L_3]$

Complex	Mass Number of Peak (m/z)	Probable Ion
$[OsCl_3(PMe_3)_3]^b$	523*	$[OsCl_3(PMe_3)_3]^+$
	485	$[OsCl_2(PMe_3)_3]^+$
	449	$[OsCl_3(PMe_3)_2]^+$
	413	$[OsCl_2(PMe_3)_2]^+$
$[OsCl_3(PMe_2Ph)_3]^c$	711	$[OsCl_3(PMe_2Ph)_3]^+$
	676	$[OsCl_2(PMe_2Ph)_3]^+$
	573	$[OsCl_3(PMe_2Ph)_2]^+$
	538*	$[OsCl_2(PMe_2Ph)_2]^+$
$[OsCl_3(PMePh_2)_3]^b$	897	$[OsCl_3(PMePh_2)_3]^+$
	862	$[OsCl_2(PMePh_2)_3]^+$
	697	$[OsCl_3(PMePh_2)_2]^+$
	662*	$[OsCl_2(PMePh_2)_2]^+$
$[OsCl_3(PEt_3)_3]^b$	652	$[OsCl_3(PEt_3)_3]^+$
	616	$[OsCl_2(PEt_3)_3]^+$
	580	$[OsCl(PEt_3)_3]^+$
	533	$[OsCl_3(PEt_3)_2]^+$
	496*	$[OsCl_2(PEt_3)_2]^+$
	459	$[OsCl(PEt_3)_2]^+$
$[OsCl_3(PEt_2Ph)_3]^d$	796	$[OsCl_3(PEt_2Ph)_3]^+$
	761	$[OsCl_2(PEt_2Ph)_3]^+$
	629	$[OsCl_3(PEt_2Ph)_2]^+$
	594*	$[OsCl_2(PEt_2Ph)_2]^+$
$[OsCl_3(PEtPh_2)_3]^b$	940	$[OsCl_3(PEtPh_2)_3]^+$
	903	$[OsCl_2(PEtPh_2)_3]^+$
	869	$[OsCl(PEtPh_2)_3]^+$
	723	$[OsCl_3(PEtPh_2)_2]^+$
	690*	$[OsCl_2(PEtPh_2)_2]^+$
	654	$[OsCl(PEtPh_2)_2]^+$

Table 6.3 - Mass Spectral Data for Complexes of Type *mer*-$[OsCl_3L_3]$ (cont.)

$[OsCl_3(PPr^n{}_3)_3]^b$	777	$[OsCl_3(PPr^n{}_3)_3]^+$
	744*	$[OsCl_2(PPr^n{}_3)_3]^+$
	616	$[OsCl_3(PPr^n{}_3)_2]^+$
	581	$[OsCl_2(PPr^n{}_3)_2]^+$
	546	$[OsCl(PPr^n{}_3)_2]^+$
$[OsCl_3(AsPr^n{}_3)_3]^a$	910	$[OsCl_3(AsPr^n{}_3)_3]^+$
	875	$[OsCl_2(AsPr^n{}_3)_3]^+$
	705*	$[OsCl_3(AsPr^n{}_3)_2]^+$
	670	$[OsCl_2(AsPr^n{}_3)_3]^+$
$[OsCl_3(AsMe_2Ph)_3]^b$	844*	$[OsCl_3(AsMe_2Ph)_3]^+$
	809	$[OsCl_2(AsMe_2Ph)_3]^+$
	660	$[OsCl_3(AsMe_2Ph)_2]^+$
	624	$[OsCl_2(AsMe_2Ph)_2]^+$
	478	$[OsCl_3(AsMe_2Ph)]^+$
	443	$[OsCl_2(AsMe_2Ph)]^+$
$[OsCl_3(AsEt_2Ph)_3]^b$	926	$[OsCl_3(AsEt_2Ph)_3]^+$
	892	$[OsCl_2(AsEt_2Ph)_3]^+$
	716*	$[OsCl_3(AsEt_2Ph)_2]^+$
	681	$[OsCl_2(AsEt_2Ph)_3]^+$
	509	$[OsCl_3(AsEt_2Ph)]^+$

The spectra all showed complex isotopic distribution.
** denotes 100% peak,* ***a*** *- spectrum were recorded using 3-nitro-benzyl alcohol.*
b - 3-NOBA/CH_3CN *mixture.* ***c*** - 3-NOBA/CH_2Cl_2 *mixture.*
d - 3-NOBA/CH_2Cl_2/MeCN *mixture.*

Table 6.4 - Mass spectral data for complexes of type *mer*-$[OsBr_3L_3]$

Complex	Mass Number of Peak (m/z)	Probable Ion
$[OsBr_3(PMe_3)_3]^b$	658	$[OsBr_3(PMe_3)_3]^+$
	579	$[OsBr_2(PMe_3)_3]^+$
	504*	$[OsBr_3(PMe_3)_2]^+$
$[OsBr_3(PMe_2Ph)_3]^b$	844	$[OsBr_3(PMe_2Ph)_3]^+$
	763*	$[OsBr_2(PMe_2Ph)_3]^+$
	708	$[OsBr_3(PMe_2Ph)_2]^+$
	685	$[OsBr(PMe_2Ph)_3]^+$
	625	$[OsBr_2(PMe_2Ph)_2]^+$
	545	$[OsBr(PMe_2Ph)_2]^+$
$[OsBr_3(PMePh_2)_3]^b$	1030	$[OsBr_3(PMePh_2)_3]^+$
	952	$[OsBr_2(PMePh_2)_3]^+$
	871	$[OsBr(PMePh_2)_3]^+$
	830	$[OsBr_3(PMePh_2)_2]^+$
	752*	$[OsBr_2(PMePh_2)_2]^+$
	670	$[OsBr(PMePh_2)_2]^+$
	591	$[Os(PMePh_2)_2]^+$
$[OsBr_3(PEt_3)_3]^b$	787	$[OsBr_3(PEt_3)_3]^+$
	707	$[OsBr_2(PEt_3)_3]^+$
	665	$[OsBr_3(PEt_3)_2]^+$
	585*	$[OsBr_2(PEt_3)_2]^+$
$[OsBr_3(PEt_2Ph)_3]^c$	929	$[OsBr_3(PEt_2Ph)_3]^+$
	848	$[OsBr_2(PEt_2Ph)_3]^+$
	763	$[OsBr_3(PEt_2Ph)_2]^+$
	682*	$[OsBr_2(PEt_2Ph)_2]^+$
$[OsBr_3(PEtPh_2)_3]^b$	993	$[OsBr_2(PEtPh_2)_3]^+$
	912*	$[OsBr(PEtPh_2)_3]^+$
	858	$[OsBr_3(PEtPh_2)_2]^+$
	778	$[OsBr_2(PEtPh_2)_2]^+$

Table 6.4 - Mass spectral data for complexes of type *mer*-$[OsBr_3L_3]$ (cont.)

$[OsBr_3(PPr^n_3)_3]^b$	911	$[OsBr_3(PPr^n_3)_3]^+$
	832	$[OsBr_2(PPr^n_3)_3]^+$
	751	$[OsBr_3(PPr^n_3)_2]^+$
	671*	$[OsBr_2(PPr^n_3)_2]^+$
$[OsBr_3(AsPr^n_3)_3]^a$	1043	$[OsBr_3(AsPr^n_3)_3]^+$
	962*	$[OsBr_2(AsPr^n_3)_3]^+$
	839	$[OsBr_3(AsPr^n_3)_2]^+$
	758	$[OsBr_2(AsPr^n_3)_2]^+$
$[OsBr_3(AsMe_2Ph)_3]^b$	977	$[OsBr_3(AsMe_2Ph)_3]^+$
	898*	$[OsBr_2(AsMe_2Ph)_3]^+$
	794	$[OsBr_3(AsMe_2Ph)_2]^+$
$[OsBr_3(AsEt_2Ph)_3]^b$	1061	$[OsBr_3(AsEt_2Ph)_3]^+$
	980	$[OsBr_2(AsEt_2Ph)_3]^+$
	850	$[OsBr_3(AsEt_2Ph)_2]^+$
	769*	$[OsBr_2(AsEt_2Ph)_3]^+$

The spectra all showed complex isotopic distribution.
** denotes 100% peak,* ***a*** *- spectrum were recorded using 3-nitro-benzyl alcohol.*
b - 3-NOBA/CH_3CN *mixture.* ***c*** - 3-NOBA/CH_2Cl_2 *mixture.*
d - 3-NOBA/CH_2Cl_2/MeCN *mixture.*

6.1.2 Preparation and Characterisation of the series *mer*-[$OsCl_3L_2L'$]

The mixed ligand complexes, $[OsCl_3(PPr^n_3)_2(AsPr^n_3)]$ and $[OsCl_3(PPr^n_3)_2(PEtPh_2)]$, were synthesised via *trans*-$[OsCl_4(PPr^n_3)_2]$. An ethanol ($50cm^3$) solution of osmium tetroxide (0.25g, .98 mmol) and concentrated HCl ($2cm^3$) was refluxed for 1 hour with excess PPr^n_3 (4 mmol). On cooling the product was isolated as a brown powder identified as *trans*-$[OsCl_4(PPr^n_3)_2]$ (Yield 56%).

Trans-$[OsCl_4(PPr^n_3)_2]$ (0.1g, 0.17 mmol) was dissolved in benzene ($10cm^3$) and refluxed for 30mins in the presence of excess $PEtPh_2/AsPr^n_3$ (2.5 mmol). The reaction mixture was reduced to dryness under low pressure then redissolved in ethanol. On standing at low temperatures crystals of *mer*-$[OsCl_3(PPr^n_3)_2(AsPr^n_3)_3]$ and *mer*-$[OsCl_3(PPr^n_3)_2(PEtPh_2)]$ developed suitable for X-ray diffraction studies. Likewise the complexes *mer*-$[OsCl_3(P(OMe)_2Ph)_2(AsPr^n_3)]$ and *mer*-$[OsCl_3(PMePh_2)_2(AsPr^n_3)]$ were synthesised from *trans*-$[OsCl_4(AsPr^n_3)_2]$refluxed with excess $P(OMe)_2Ph$ and $PMePh_2$ respectively. Tables 6.5 and 6.6 show the yields and analysis of the compounds.

Table 6.5- Yields and CHN Data for the Series *mer*-[$OsCl_3L_2L'$]

Complex	Yield	C (Found)	C (Required)	H (Found)	H (Required)
$[OsCl_3(PPr^n_3)_2(AsPr^n_3)]$	74%	39.05%	39.49%	7.02%	7.73%
$[OsCl_3(PPr^n_3)_2(PEtPh_2)]$	69%	46.01%	46.24%	7.03%	6.91%
$[OsCl_3(P(OMe)_2Ph)_2(AsPr^n_3)]$	75%	36.71%	35.68%	5.43%	6.10%
$[OsCl_3(PMePh_2)_2(AsPr^n_3)]$	72%	47.09%	46.64%	5.20%	5.26%

Table 6.6 - Mass Spectra Data for Complexes of Type *mer*-$[OsCl_3L_2L']$

Complex	Mass Number of Peak (m/z)	Probable Ion
$[OsCl_3(PPr^n_3)_2(AsPr^n_3)]^b$	821	$[OsCl_3(PPr^n_3)_2(AsPr^n_3)]^+$
	661	$[OsCl_3(PPr^n_3)(AsPr^n_3)]^+$
	617	$[OsCl_3(PPr^n_3)_2]^+$
	588*	$[OsCl(PPr^n_3)(AsPr^n_3)]^+$
$[OsCl_3(PPr^n_3)_2(PEtPh_2)]^a$	831	$[OsCl_3(PPr^n_3)_2(PEtPh_2)]^+$
	797	$[OsCl_2(PPr^n_3)_2(PEtPh_2)]^+$
	672	$[OsCl_3(PPr^n_3)(PEtPh_2)]^+$
	636	$[OsCl_2(PPr^n_3)_2(PEtPh_2)]^+$
	618	$[OsCl_3(PPr^n_3)_2]^+$
	583*	$[OsCl_2(PPr^n_3)_2]^+$
$[OsCl_3(P(OMe)_2Ph)_2(AsPr^n_3)]^a$	841	$[OsCl_3(AsPr^n_3)(P(OMe)_2Ph)_2]^+$
	807*	$[OsCl_2(AsPr^n_3)(P(OMe)_2Ph)_2]^+$
	772	$[OsCl(AsPr^n_3)(P(OMe)_2Ph)_2]^+$
	671	$[OsCl_3(AsPr^n_3)(P(OMe)_2Ph)]^+$
	636	$[OsCl_2(AsPr^n_3)(P(OMe)_2Ph)]^+$/ $[OsCl_3(P(OMe)_2Ph)_2]^+$
	600	$[OsCl(AsPr^n_3)(P(OMe)_2Ph)]^+$/ $[OsCl_2(P(OMe)_2Ph)_2]^+$
$[OsCl_3(PMePh_2)_2(AsPr^n_3)]^a$	901	$[OsCl_3(PMePh_2)_2(AsPr^n_3)]^+$
	866	$[OsCl_2(PMePh_2)_2(AsPr^n_3)]^+$
	697	$[OsCl_3(PMePh_2)_2]^+$
	662*	$[OsCl_2(PMePh_2)_2]^+$
	625	$[OsCl(PMePh_2)_2]^+$
	591	$[Os(PMePh_2)_2]^+$
	499	$[OsCl_3(PMePh_2)]^+$
	461	$[OsCl_2(PMePh_2)]^+$
	425	$[OsCl(PMePh_2)]^+$

*The spectra all showed complex isotopic distribution. * denotes 100% peak,*
a - 3-NOBA/CH_3CN *mixture.* ***b*** - 3-NOBA/CH_2Cl_2 *mixture.*

6.1.3 Preparation and Characterisation of the series *fac*-[$OsCl_3L_3$]

The *fac* isomers [$OsCl_3L_3$], where L is PMe_2Ph, PEt_2Ph, $AsMe_2Ph$ or $AsEt_2Ph$ were prepared from the corresponding *mer* isomers *via* the tetrahydrides intermediates, [OsH_4L_3], according to the method of Douglas and Shaw.[2] The tetrahydrides were generated *in situ* by the reflux of *mer*-[$OsCl_3L_3$] (0.4g, 0.56 mmol), where L is PMe_2Ph, PEt_2Ph, $AsMe_2Ph$ or $AsEt_2Ph$ with $NaBH_4$ (2 mmol) in ethanol ($30cm^3$) for 1 hour. The reaction mixture was reduced to dryness under reduced pressure and the tetrahydride complex [OsH_4L_3] isolated with benzene ($4 \times 30cm^3$). Evaporation of benzene gave a yellow oil which was dissolved in methanol. The yellow solution was bubbled with HCl gas which resulted in the precipitation of the *fac* isomer as a red/pink powder, which was filtered and washed with hexane and diethyl ether. Tables 6.7 and 6.8 show the yields analytical results obtained.

Table 6.7 - Yields and CHN Data for the *fac* isomers

Complex	Yield	C (Found)	C (Required)	H (Found)	H (Required)
fac-[$OsCl_3(PMe_2Ph)_3$]	66%	40.30%	40.50%	4.63%	4.67%
fac-[$OsCl_3(PEt_2Ph)_3$]	62%	45.28%	45.31%	5.89%	5.70%
fac-[$OsCl_3(AsMe_2Ph)_3$]	60%	34.09%	34.20%	3.92%	3.95%
fac-[$OsCl_3(AsEt_2Ph)_3$]	29%	38.79%	38.87%	4.81%	4.89%

Table 6.8 - Mass Spectral Data for the *fac* Isomers

Complex	Mass Number of Peak (m/z)	Probable Ion
fac-$[OsCl_3(PMe_2Ph)_3]^a$	712	$[OsCl_3(PMe_2Ph)_3]^+$
	677	$[OsCl_2(PMe_2Ph)_3]^+$
	641*	$[OsCl(PMe_2Ph)_3]^+$
fac-$[OsCl_3(PEt_2Ph)_3]^a$	763*	$[OsCl_2(PEt_2Ph)_3]^+$
	724	$[OsCl(PEt_2Ph)_3]^+$
	690	$[Os(PEt_2Ph)_3]^+$
	595	$[OsCl_2(PEt_2Ph)_3]^+$
	556	$[OsCl(PEt_2Ph)_3]^+$
fac-$[OsCl_3(AsMe_2Ph)_3]^b$	843	$[OsCl_3(AsMe_2Ph)_3]^+$
	808	$[OsCl_2(AsMe_2Ph)_3]^+$
	771	$[OsCl(AsMe_2Ph)_3]^+$
	661	$[OsCl_3(AsMe_2Ph)_2]^+$
	626*	$[OsCl_2(AsMe_2Ph)_2]^+$
	589	$[OsCl(AsMe_2Ph)_2]^+$
fac-$[OsCl_3(AsEt_2Ph)_3]^b$	927	$[OsCl_3(AsEt_2Ph)_3]^+$
	893*	$[OsCl_2(AsEt_2Ph)_3]^+$
	856	$[OsCl(AsEt_2Ph)_3]^+$
	717	$[OsCl_3(AsEt_2Ph)_2]^+$
	680	$[OsCl_2(AsEt_2Ph)_2]^+$

The spectra all showed complex isotopic distribution.
** denotes 100% peak,* ***a*** *-* 3-NOBA/CH_3CN *mixture.* ***b*** *- 3-NOBA matrix*

6.2 Equipment

Microanalyses was carried out on a Perkin Elmer 2400 CHN Elemental Analyser. Mass Spectrum analysis was undertaken using the Fast Atom Bombardment (FAB) Technique on a Kratos MS50TC. Crystallographic studies employed a Stoë-Stadi 4 circle diffractometer. All the above were run by the Chemistry Department Service.

All electrochemical measurements were carried out using Eco Chemie B.V. AUTOLAB® systems fitted with either PSTAT10 or PGSTAT20 potentiostats. General Purpose Electrochemical System (GPES) software (version 3.1, 3.3, 4.0, 4.2 and 4.3) was used in conjunction with this hardware. Fast scan measurements were undertaken employing a ADC750 fast scan generator, coupled to the PGSTAT20 potentiostat. All solutions were purged by inert gas either N_2 or argon before the experiment.

A standard three electrode cell (Figure 6.1) was employed for all electrochemical measurements. The reference electrode used for all measurements was Ag/AgCl (Ferrocene/ferrocinium = 0.55V).[3] The counter electrode was a strip of platinum metal and the working electrode was a micro platinum electrode (normally of diameter 0.5mm/1mm, ultra microelectrodes diameter 25μm were employed for fast scan experiments). Low temperature studies were undertaken in a jacketed cell cooled by a Haake F3Q refrigerated circulation unit.

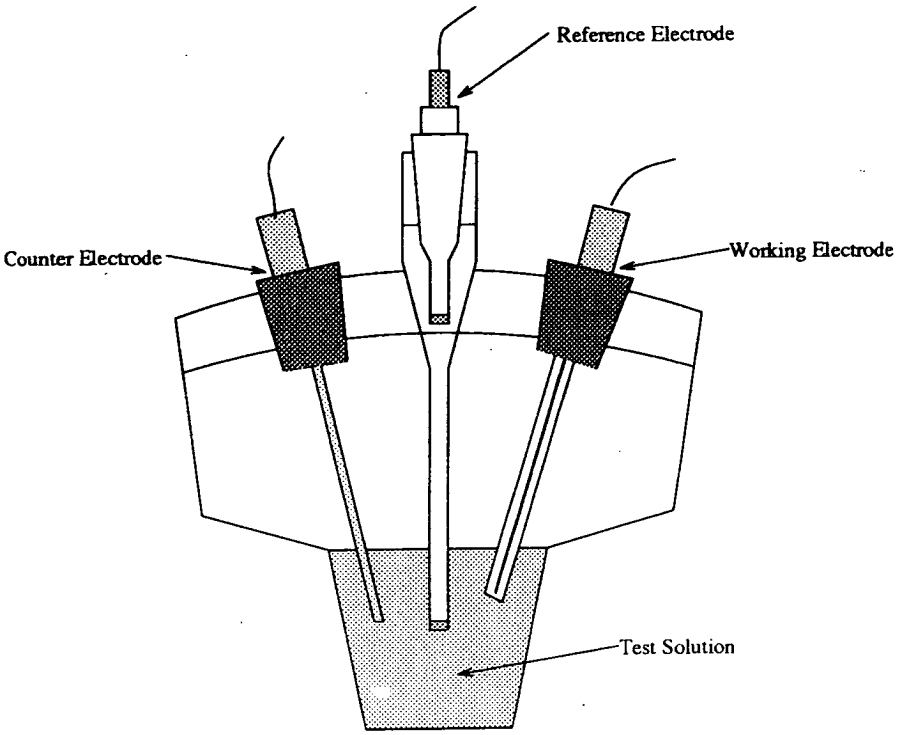

Figure 6.1 - Standard 3 Electrode Cell

Coulometric experiments were carried out in a three compartment (H-type) cell with a Pt gauze working electrode separated from the Pt counter electrode by a double glass frit, see Figure 6.2 for the cell design.

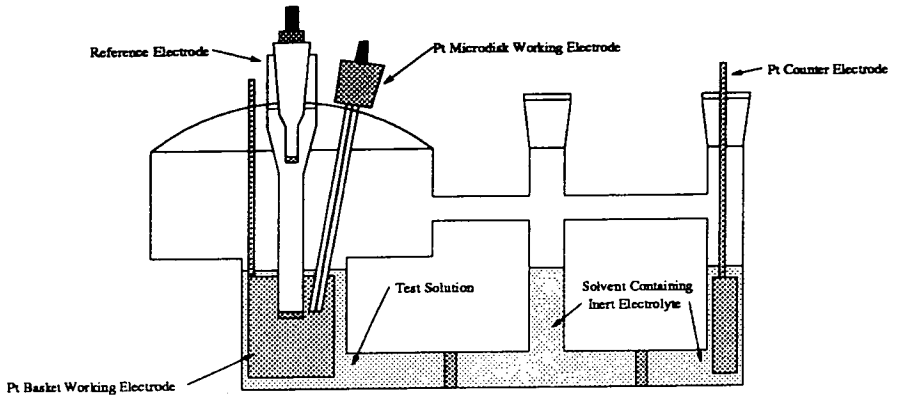

Figure 6.2 - Schematic of 3 Compartment H-Type Cell used for Coulometry

Spectroelectrochemical studies were carried out using an Optically Transparent Electrode (O.T.E.) system. Figure 6.3 shows the design of the optical cell that was then placed in a PTFE block (Figure 6.4) and flushed with temperature controlled nitrogen gas. The O.T.E. cell was connected to a Metröhm Herisau E506 Polarecord potentiostat, and used in conjunction with the λ9 UV/Vis spectrometer described below.

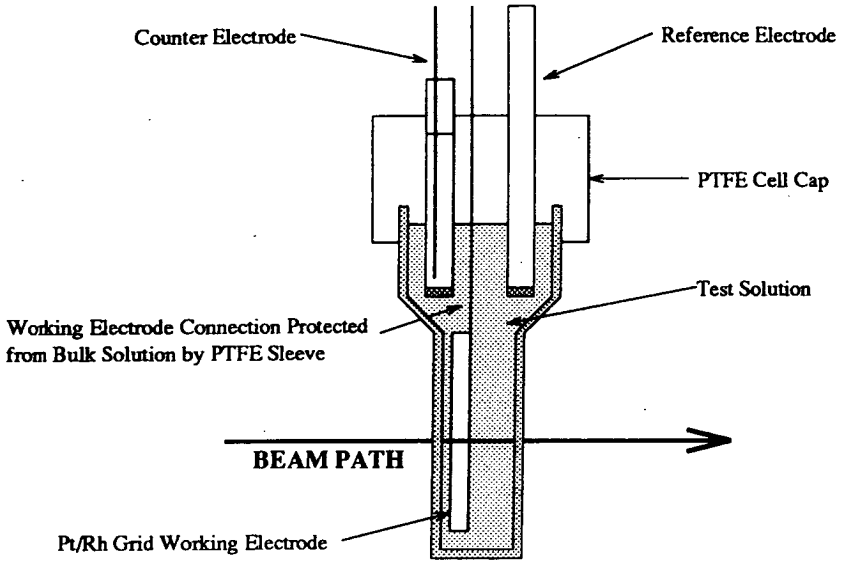

Figure 6.3 - Design of Optically Transparent Electrode Cell

Electronic spectra were recorded on a Perkin Elmer Lambda 9 UV/VIS/NIR Spectrophotometer, connected to a Perkin Elmer PP-1 Plotter Printer.

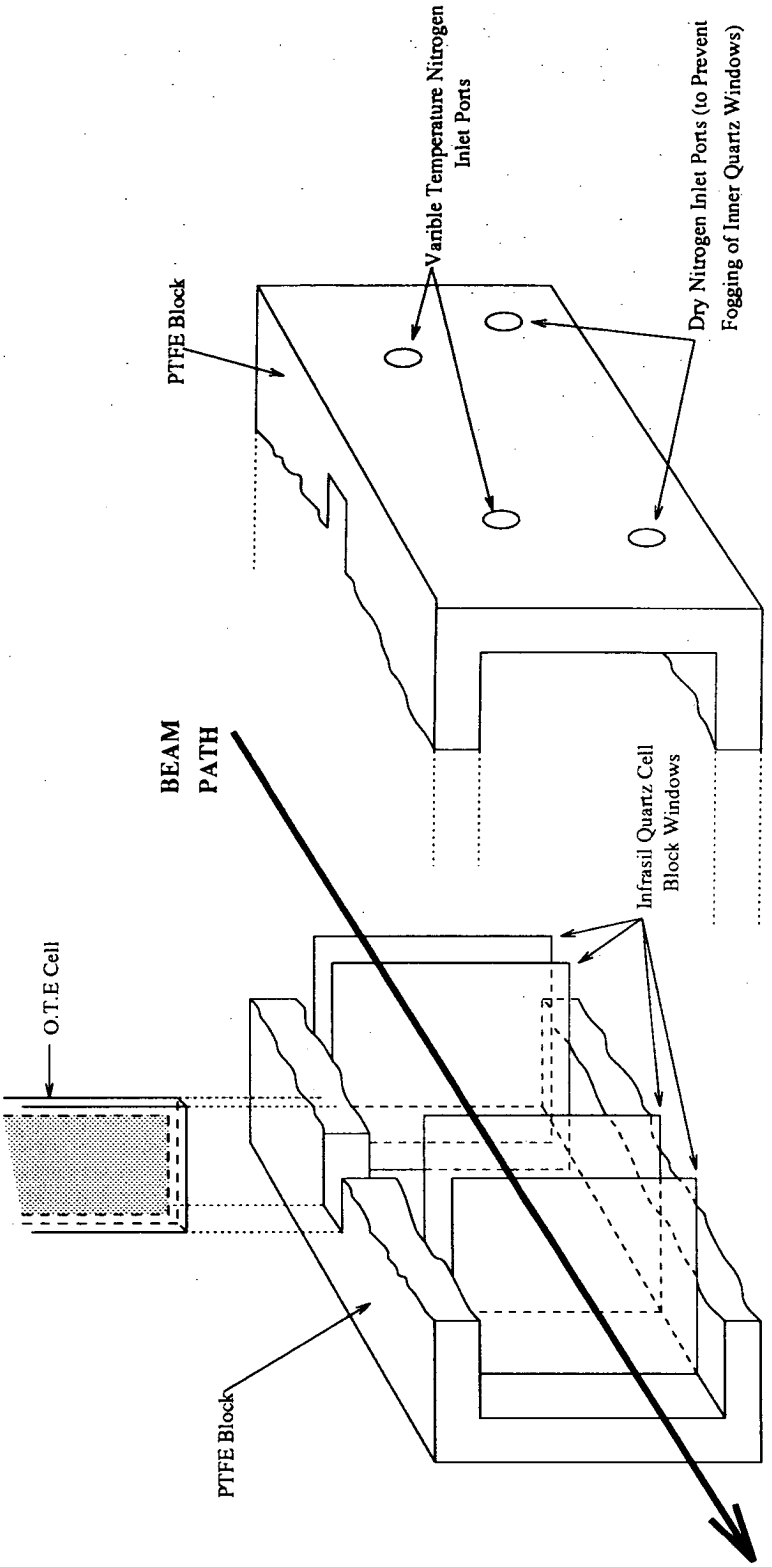

Figure 6.4 - Design of P.T.F.E Block employed with O.T.E. Cell

6.3 Extended Hückel Molecular Orbital Calculations

Extended Hückel Molecular Orbital Calculations were carried out at Heriot Watt University, Edinburgh using the CAChe[5] package of programs version 3.8 using the ICON8 EHMO program.[6]

6.3.1 General Methodology

To run an EHMO calculation a model or the structure of a molecule must be known, and a basis set of atomic orbital (AO) parameters chosen for all the elements in the structure.

Molecular orbitals are derived by the Linear Combination of Atomic Orbitals (LCAO) approach. In the simplest (diatomic) case Ψ (a MO), is calculated from the corresponding A.O's, ϕ_i and ϕ_j by the equation;

$$\Psi = c_i\phi_i + c_j\phi_j \qquad (1)$$

where c_i and c_j are coefficients. The AO wavefunctions are represented by normalised Slater-type orbitals (STO's) which have the form;

$$\Psi = R(r).Y(\theta,\phi) \qquad (2)$$

The radial wavefunction (R) is controlled by the Slater exponent that defines the diffuseness of the STO's in physical terms. The basis set employed in each case was STO-3G, inlaid in the CAChe software.

In order to calculate orbital energies, a secular determinant is set up from a series of equations of type below, using evaluated Hamiltonian operators (H_{ii} and H_{ij}) and overlap integrals (S_{ij});

$$\sum c_{ij}\left(H_{ij} - S_{ij}E\right) = 0 \qquad (3)$$

where $H_{ij} = \int \Psi_i H \Psi_j$ and $S_{ij} = \int \Psi_i \Psi_j$

The values of H_{ii} used were the valence shell ionisation potentials (VSIPs). The values of H_{ij} were calculated using the modified Wolfsberg-Helmholtz formula,[7] with $K = 1.75$.

Using the approximations and formulae described, the energies of MO's and the contributions of each AO may be determined from VSIPOs and Slater exponents of atomic orbitals. Total energy can be calculated from the sum of all one electron energies. Bond overlap populations for all bonds and electron density (and hence the atomic charge) for all atoms in the model may also be calculated.

6.4 References

(1) J. Chatt, G. J. Leigh, D. M. P. Mingos and R. J. Paske, *J. Chem. Soc., (A)*, 1968, 2636.

(2) P. G. Douglas and B. L. Shaw, *J. Chem. Soc. (A)*, 1970, 334.

(3) A. J. Bard and L. R. Faulkner, *Electrochemical Methods, Fundamentals and Applications*, John Wiley and Sons, New York, 1980.

(4) J. Crosier and A. M. Glazer, *J. Appl. Crystallogr.*, 1986, **19**, 105.

(5) CAChe : *Computer Aided Chemistry*, Oxford Molecular Group, 1995.

(6) ICON8, J. Howell, A. Rossi, D. Wallace, K. Haraki and R. Hoffmann, Quantum Chemistry Program Exchange, University Of Indiana, 1977, No. 344.

(7) J. H. Ammeter, H.-B. Burgi, J. C. Thibault and R. Hoffman, *J. Am. Chem. Soc.*, 1978, **100**, 3686.

Appendix

Crystallographic Details

All data were collected on equipment already mentioned in the Experimental section. All structures were solved and refined using SHELX programmes,[1-3] unless otherwise stated. All diagrams were prepared using the program SHELXTL/PC.[3]

*A*1.1 Structure of *mer*-[$OsCl_3(PMe_2Ph)_3$]

Suitable crystals for X-ray analysis were grown by recrystallisation from a ethanol/conc. HCl solution. Table *A*1.1 shows the details of the crystal data and structural refinement.

Table *A*1.1 - Crystal Data and Structure Refinement for *mer*-[$OsCl_3(PMe_2Ph)_3$]

Empirical formula	$C_{24}H_{33}Cl_3OsP_3$
Formula weight	710.96
Temperature	150(2)K
Wavelength	0.71073 Å
Crystal system	Monoclinic
Space group	P21/n
Unit cell dimensions	a = 10.765(2)Å, α = 90°
	b = 38.914(8)Å, β = 107.26(3)°
	c = 13.591(3)Å, γ = 90°
Volume	5437(2)Å^3
Z	8
Density (calculated)	1.737 Mg m^{-3}
Absorption coefficient	5.174 mm^{-1}
F(000)	2792
Crystal colour and shape	Deep red tablet
Crystal size	0.39 x 0.39 x 0.14 mm
Theta range for data collection	2.53° to 22.54°
Index ranges	$-11 \le h \le 11, 0 \le k \le 41, 0 \le l \le 14$
Reflections collected	9723
Independent reflections	7126 [R_{int} = 0.0242]
Refinement method	Full-matrix least-squares on F^2
Data / restraints / parameters	7125 / 0 / 560
Goodness-of-fit on F^2	1.005
Final R indices [I>2sigma(I)]	R1 = 0.0389, wR2 = 0.0865
R indices (all data)	R1 = 0.0581, wR2 = 0.0945
Extinction coefficient	0.00130(6)
Largest diff. peak and hole	1.325 and -1.277 eÅ^{-3}

The structure was solved by Direct Methods. All non hydrogen atoms were refined anisotropically and the positions of the hydrogen atoms were calculated and allowed to ride on their attached atom. A single (isotropic) thermal parameter for all H atoms was refined. Table *A*1.2 lists the atomic coordinates for *mer*-[$OsCl_3(PMe_2Ph)_3$] a view of the two molecules in the asymmetric unit is given in Fig *A*1.1. The

interatomic distances and interatomic angles are given in Table *A*1.3A and *A*1.3B respectively.

Table *A*1.2 - Fractional Atomic coordinates ($\times 10^4$) and Equivalent Isotropic Displacement Parameters ($Å^2 \times 10^3$) for *mer*-$[OsCl_3(PMe_2Ph)_3]$

	x	y	z	U(eq)
Os(1)	8140(1)	101(1)	7151(1)	15(1)
Os(2)	7456(1)	-2046(1)	7436(1)	16(1)
Cl(1)	8430(2)	87(1)	8934(1)	23(1)
Cl(2)	6378(2)	-313(1)	6882(2)	28(1)
Cl(3)	7873(2)	87(1)	5370(2)	27(1)
Cl(4)	8821(2)	-1561(1)	7719(2)	22(1)
Cl(5)	6126(2)	-2540(1)	7120(2)	29(1)
Cl(6)	9268(2)	-2430(1)	8217(2)	29(1)
P(1)	9842(2)	496(1)	7316(2)	19(1)
P(2)	9422(2)	-418(1)	7371(2)	19(1)
P(3)	6507(2)	533(1)	7001(2)	21(1)
P(4)	5571(2)	-1727(1)	6653(2)	19(1)
P(5)	8067(2)	-2144(1)	5892(2)	20(1)
P(6)	7332(2)	-1985(1)	9157(2)	21(1)
C(11)	9466(8)	926(2)	6749(6)	23(2)
C(12)	9891(9)	1227(3)	7288(7)	27(2)
C(13)	9661(9)	1544(3)	6815(8)	34(2)
C(14)	8986(10)	1563(3)	5784(9)	37(3)
C(15)	8576(10)	1273(3)	5222(8)	35(3)
C(16)	8796(9)	949(3)	5695(7)	29(2)
C(17)	10809(9)	578(3)	8624(6)	29(2)
C(18)	11077(9)	373(2)	6708(7)	29(2)
C(21)	11197(8)	-409(2)	7705(6)	18(2)
C(22)	11914(8)	-325(2)	8686(6)	21(2)
C(23)	13272(10)	-301(3)	8955(7)	33(3)
C(24)	13880(10)	-373(3)	8230(8)	36(3)
C(25)	13190(9)	-457(3)	7239(7)	31(2)
C(26)	11854(9)	-479(2)	6972(6)	25(2)
C(27)	8932(9)	-697(2)	6249(7)	31(2)
C(28)	9201(9)	-685(2)	8386(7)	27(2)
C(31)	6989(8)	953(2)	7615(6)	19(2)

	x	y	z	U(eq)
C(32)	6643(9)	1263(3)	7109(7)	28(2)
C(33)	7050(9)	1569(3)	7601(8)	33(3)
C(34)	7807(9)	1574(3)	8627(9)	38(3)
C(35)	8105(9)	1264(3)	9144(8)	33(3)
C(36)	7713(8)	957(2)	8653(7)	24(2)
C(37)	5269(9)	406(3)	7595(8)	33(3)
C(38)	5532(9)	626(3)	5697(6)	31(2)
C(41)	6521(8)	-1615(3)	9525(6)	21(2)
C(42)	5583(8)	-1647(3)	10048(6)	27(2)
C(43)	5098(10)	-1349(3)	10367(7)	42(3)
C(44)	5491(10)	-1031(3)	10170(7)	40(3)
C(45)	6409(9)	-1004(3)	9645(7)	35(3)
C(46)	6917(9)	-1290(3)	9339(6)	25(2)
C(47)	8934(8)	-1939(3)	10089(6)	32(3)
C(48)	6675(10)	-2358(3)	9615(7)	37(3)
C(51)	7559(8)	-1850(2)	4794(6)	20(2)
C(52)	7956(8)	-1516(2)	4899(7)	24(2)
C(53)	7632(9)	-1290(3)	4091(7)	33(2)
C(54)	6865(9)	-1399(3)	3136(7)	29(2)
C(55)	6455(9)	-1737(3)	2997(7)	35(3)
C(56)	6783(8)	-1964(3)	3816(6)	26(2)
C(57)	7688(10)	-2565(2)	5364(6)	30(2)
C(58)	9807(9)	-2121(3)	6128(7)	32(2)
C(61)	4296(8)	-1707(2)	7307(6)	19(2)
C(62)	3881(9)	-1396(3)	7592(6)	30(3)
C(63)	2872(9)	-1387(3)	8038(7)	37(3)
C(64)	2311(10)	-1689(4)	8224(7)	44(3)
C(65)	2744(10)	-1980(4)	7948(7)	48(4)
C(66)	3729(8)	-2010(3)	7500(6)	27(2)
C(67)	4622(9)	-1891(3)	5410(6)	34(3)
C(68)	5836(9)	-1282(2)	6381(7)	24(2)

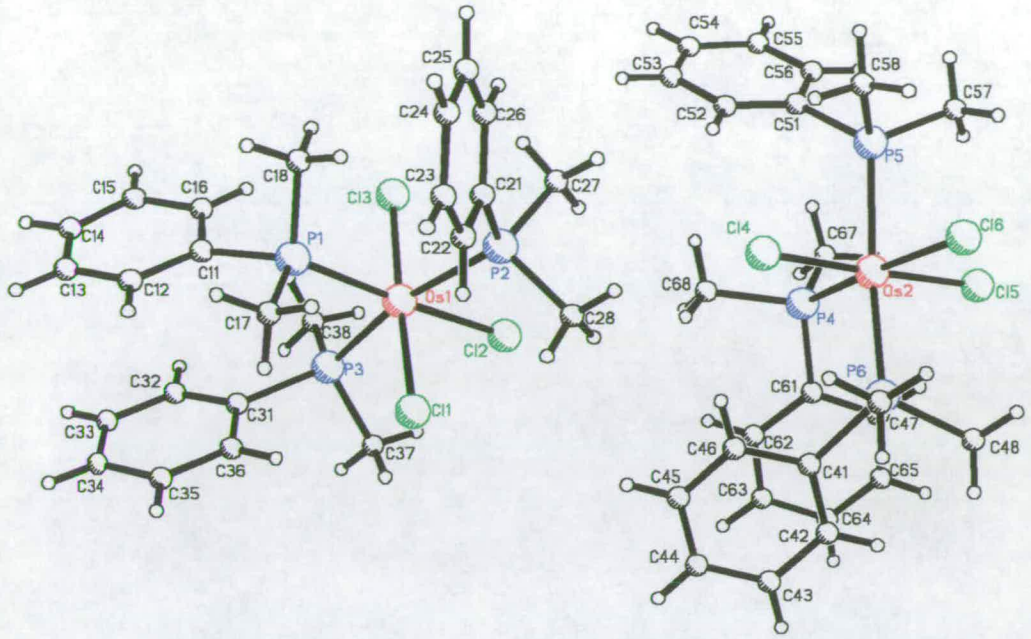

Fig *A*1.1 - Asymmetric Unit of *mer*-[$OsCl_3(PMe_2Ph)_3$]

Table *A*1.3A - Bond Lengths (Å) for *mer*-[$OsCl_3(PMe_2Ph)_3$]

Os(1)-P(1)	2.351(2)
Os(1)-Cl(1)	2.351(2)
Os(1)-Cl(3)	2.352(2)
Os(1)-P(3)	2.399(2)
Os(1)-P(2)	2.413(2)
Os(1)-Cl(2)	2.430(2)
Os(2)-P(4)	2.347(2)
Os(2)-Cl(4)	2.352(2)
Os(2)-Cl(5)	2.360(2)
Os(2)-P(6)	2.394(2)
Os(2)-P(5)	2.409(2)
Os(2)-Cl(6)	2.436(2)
P(1)-C(17)	1.802(8)
P(1)-C(18)	1.824(8)
P(1)-C(11)	1.838(10)
P(2)-C(28)	1.797(8)
P(2)-C(27)	1.817(8)
P(2)-C(21)	1.829(9)
P(3)-C(38)	1.809(8)
P(3)-C(37)	1.820(8)
P(3)-C(31)	1.837(9)
P(4)-C(68)	1.809(9)

P(4)-C(67)	1.810(9)
P(4)-C(61)	1.846(8)
P(5)-C(57)	1.787(9)
P(5)-C(58)	1.806(9)
P(5)-C(51)	1.829(9)
P(6)-C(48)	1.805(10)
P(6)-C(47)	1.820(8)
P(6)-C(41)	1.827(9)
C(11)-C(12)	1.387(13)
C(11)-C(16)	1.403(12)
C(12)-C(13)	1.379(13)
C(13)-C(14)	1.376(14)
C(14)-C(15)	1.362(14)
C(15)-C(16)	1.402(13)
C(21)-C(22)	1.367(12)
C(21)-C(26)	1.410(11)
C(22)-C(23)	1.401(12)
C(23)-C(24)	1.364(13)
C(24)-C(25)	1.371(13)
C(25)-C(26)	1.377(13)
C(31)-C(32)	1.387(12)
C(31)-C(36)	1.394(12)

C(32)-C(33)	1.372(13)
C(33)-C(34)	1.392(14)
C(34)-C(35)	1.387(14)
C(35)-C(36)	1.373(13)
C(41)-C(46)	1.382(13)
C(41)-C(42)	1.403(12)
C(42)-C(43)	1.391(14)
C(43)-C(44)	1.36(2)
C(44)-C(45)	1.384(13)
C(45)-C(46)	1.359(13)
C(51)-C(52)	1.364(12)
C(51)-C(56)	1.415(12)
C(52)-C(53)	1.369(12)
C(53)-C(54)	1.382(13)
C(54)-C(55)	1.381(14)
C(55)-C(56)	1.383(13)
C(61)-C(62)	1.385(13)
C(61)-C(66)	1.388(13)
C(62)-C(63)	1.392(13)
C(63)-C(64)	1.38(2)
C(64)-C(65)	1.32(2)
C(65)-C(66)	1.376(14)

Table *A*1.3B - Bond Angles (°) for *mer*-[$OsCl_3(PMe_2Ph)_3$]

P(1)-Os(1)-Cl(1)	93.12(8)
P(1)-Os(1)-Cl(3)	88.07(8)
Cl(1)-Os(1)-Cl(3)	177.42(8)
P(1)-Os(1)-P(3)	94.61(8)
Cl(1)-Os(1)-P(3)	88.44(8)
Cl(3)-Os(1)-P(3)	93.75(8)
P(1)-Os(1)-P(2)	97.71(8)
Cl(1)-Os(1)-P(2)	87.57(8)
Cl(3)-Os(1)-P(2)	90.00(8)
P(3)-Os(1)-P(2)	167.24(8)
P(1)-Os(1)-Cl(2)	176.84(7)
Cl(1)-Os(1)-Cl(2)	89.98(8)
Cl(3)-Os(1)-Cl(2)	88.81(8)
P(3)-Os(1)-Cl(2)	86.09(8)
P(2)-Os(1)-Cl(2)	81.80(8)
P(4)-Os(2)-Cl(4)	93.65(8)
P(4)-Os(2)-Cl(5)	87.28(9)
Cl(4)-Os(2)-Cl(5)	178.16(7)
P(4)-Os(2)-P(6)	95.68(8)
Cl(4)-Os(2)-P(6)	88.46(8)
Cl(5)-Os(2)-P(6)	93.03(8)
P(4)-Os(2)-P(5)	96.35(8)
Cl(4)-Os(2)-P(5)	87.15(8)
Cl(5)-Os(2)-P(5)	91.17(8)
P(6)-Os(2)-P(5)	167.42(8)
P(4)-Os(2)-Cl(6)	174.05(9)
Cl(4)-Os(2)-Cl(6)	92.30(8)
Cl(5)-Os(2)-Cl(6)	86.78(9)
P(6)-Os(2)-Cl(6)	84.58(8)
P(5)-Os(2)-Cl(6)	83.82(8)
C(17)-P(1)-C(18)	102.0(5)
C(17)-P(1)-C(11)	104.0(4)
C(18)-P(1)-C(11)	98.5(4)
C(17)-P(1)-Os(1)	114.6(3)
C(18)-P(1)-Os(1)	116.0(3)
C(11)-P(1)-Os(1)	119.1(3)
C(28)-P(2)-C(27)	103.2(5)
C(28)-P(2)-C(21)	100.8(4)
C(27)-P(2)-C(21)	104.0(4)
C(28)-P(2)-Os(1)	112.1(3)
C(27)-P(2)-Os(1)	112.5(3)
C(21)-P(2)-Os(1)	122.2(3)

C(38)-P(3)-C(37)	101.6(5)
C(38)-P(3)-C(31)	105.7(4)
C(37)-P(3)-C(31)	100.7(4)
C(38)-P(3)-Os(1)	114.9(3)
C(37)-P(3)-Os(1)	112.8(3)
C(31)-P(3)-Os(1)	118.9(3)
C(68)-P(4)-C(67)	103.0(5)
C(68)-P(4)-C(61)	104.1(4)
C(67)-P(4)-C(61)	99.8(4)
C(68)-P(4)-Os(2)	115.6(3)
C(67)-P(4)-Os(2)	114.2(3)
C(61)-P(4)-Os(2)	118.0(3)
C(57)-P(5)-C(58)	102.5(5)
C(57)-P(5)-C(51)	105.5(4)
C(58)-P(5)-C(51)	99.1(4)
C(57)-P(5)-Os(2)	113.9(3)
C(58)-P(5)-Os(2)	112.0(3)
C(51)-P(5)-Os(2)	121.3(3)
C(48)-P(6)-C(47)	103.0(5)
C(48)-P(6)-C(41)	105.7(5)
C(47)-P(6)-C(41)	99.4(4)
C(48)-P(6)-Os(2)	113.4(3)
C(47)-P(6)-Os(2)	111.9(3)
C(41)-P(6)-Os(2)	121.0(3)
C(12)-C(11)-C(16)	118.3(9)
C(12)-C(11)-P(1)	123.5(7)
C(16)-C(11)-P(1)	118.0(7)
C(13)-C(12)-C(11)	121.6(9)
C(14)-C(13)-C(12)	119.3(10)
C(15)-C(14)-C(13)	120.8(10)
C(14)-C(15)-C(16)	120.4(9)
C(11)-C(16)-C(15)	119.4(10)
C(22)-C(21)-C(26)	118.6(8)
C(22)-C(21)-P(2)	119.5(6)
C(26)-C(21)-P(2)	121.8(7)
C(21)-C(22)-C(23)	120.9(8)
C(24)-C(23)-C(22)	119.0(9)
C(23)-C(24)-C(25)	121.5(9)
C(24)-C(25)-C(26)	119.5(8)
C(25)-C(26)-C(21)	120.4(8)
C(32)-C(31)-C(36)	118.7(8)
C(32)-C(31)-P(3)	123.5(7)

A1.2 Structure Of *mer*-[$OsBr_3(PPr^n_3)_3$]

Crystals suitable for X-ray diffraction studies were obtained from the reaction mixture at low temperature (see Chapter 6 for details). Table *A*1.4 shows the crystal and refinement details.

Table *A*1.4 - Crystal Data and Structure Refinement for *mer*-[$OsBr_3(PPr^n_3)_3$]

Empirical formula	$C_{27}H_{63}Br_3OsP_3$
Formula weight	910.61
Temperature	293(2) K
Wavelength	0.71073 A
Crystal system	Orthorhombic
Space group	$P2_12_12_1$
Unit cell dimensions	a = 13.356(2) Å, α = 90°.
	b = 14.508(2) Å, β = 90°.
	c = 19.705(3) Å, γ = 90°.
Volume	3818.2(10) $Å^3$
Z	4
Density (calculated)	1.584 Mgm^{-3}
Absorption coefficient	6.619 mm^{-1}
F(000)	1804
Crystal size	0.24 x 0.15 x 0.11 mm
Theta range for data collection	2.50° to 27.52°.
Index ranges	$-17 \le h \le 17, -18 \le k \le 18, -25 \le l \le 25$
Reflections collected	11354
Independent reflections	4864 [R(int) = 0.1702]
Refinement method	Full-matrix least-squares on F^2
Data / restraints / parameters	4848 / 136 / 183
Goodness-of-fit on F^2	0.948
Final R indices [I>2sigma(I)]	R1 = 0.0708, wR2 = 0.1178
R indices (all data)	R1 = 0.2229, wR2 = 0.1631
Absolute structure parameter	-0.02(3)
Largest diff. peak and hole	0.885 and -0.792 $e.Å^{-3}$

The structure was solved using the Direct Methods program SIR92.[4] Due to a weak data set only the osmium, phosphines and bromine's were refined anisotropically. The propyl groups showed disorder, which where dealt with, using the following constraints.

1. Similarity distance restraints on all P-C bond lengths.

2. Geometry restraints on the propyl groups (1,2 and 1,3 C-C distances).

3. Modelling of 3 propyl groups as disordered. Two of which disordered at the C2 position (C12 and C25), the other at both the C2 and C3 positions (C18 and C19).

Figure *A*1.2 shows a schematic of the structure and Tables *A*1.5 and *A*1.6 details the crystallographic data obtained.

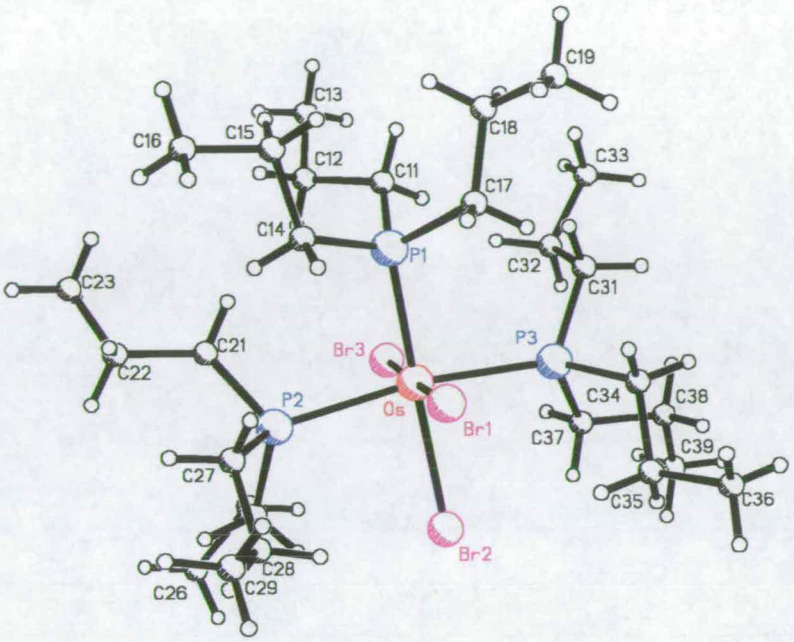

Figure *A*1.2 - Structure of *mer*-[$OsBr_3(PPr^n_3)_3$]

Table *A*1.5 - Atomic Coordinates (x 10^4) and Equivalent Isotropic Displacement Parameters ($Å^2$ x 10^3) for *mer*-[$OsBr_3(PPr^n_3)_3$]

	x	y	z	U(eq)
Os	3261(1)	9796(1)	9646(1)	61(1)
P(1)	2715(5)	10152(5)	8530(3)	80(2)
C(11)	3510(17)	9725(15)	7848(12)	170(14)
C(12)	3362(37)	8722(14)	7623(19)	157(20)
C(12')	3068(20)	9024(43)	7353(25)	157(20)
C(13)	3917(24)	8555(17)	6947(11)	173(15)
C(14)	1382(8)	9902(17)	8420(8)	87(7)
C(15)	938(12)	10036(20)	7712(9)	144(12)
C(16)	-130(13)	9649(20)	7674(11)	146(12)
C(17)	2663(23)	11399(9)	8382(10)	144(13)
C(18)	2710(59)	11727(15)	7643(12)	169(15)
C(19)	2509(51)	12771(18)	7609(21)	169(15)
C(18')	3176(56)	11758(15)	7736(22)	169(15)
C(19')	3160(52)	12817(15)	7726(24)	169(15)
P(2)	2149(5)	8485(4)	9808(3)	77(2)
C(21)	2038(13)	7776(13)	9045(8)	87(8)
C(22)	1079(16)	7217(17)	8953(10)	142(12)
C(23)	1104(21)	6678(18)	8283(12)	164(14)
C(24)	2486(18)	7713(11)	10496(8)	128(11)

	x	y	z	U(eq)
C(25)	3310(19)	7004(19)	10376(17)	104(12)
C(25')	2388(29)	6674(11)	10379(18)	104(12)
C(26)	3128(19)	6160(12)	10849(13)	145(12)
C(27)	876(10)	8765(18)	10082(8)	106(9)
C(28)	741(13)	8994(18)	10840(7)	110(10)
C(29)	-306(16)	9404(21)	10959(12)	178(15)
P(3)	4615(5)	10912(4)	9657(4)	81(2)
C(31)	5235(17)	11225(13)	8861(9)	118(10)
C(32)	5889(18)	10478(14)	8528(10)	126(11)
C(33)	6442(21)	10871(20)	7910(11)	180(15)
C(34)	4360(21)	12060(9)	10007(8)	105(9)
C(35)	4145(22)	12098(12)	10776(8)	122(11)
C(36)	4015(28)	13095(14)	11013(11)	184(16)
C(37)	5664(10)	10530(12)	10180(10)	94(8)
C(38)	6565(12)	11197(14)	10233(12)	122(10)
C(39)	7369(13)	10782(18)	10698(14)	155(13)
Br(1)	1964(2)	10971(2)	9967(1)	92(1)
Br(2)	3640(2)	9583(2)	10917(1)	83(1)
Br(3)	4536(2)	8636(2)	9285(1)	76(1)

U(eq) is defined as one third of the trace of the orthogonalized Uij tensor

Table *A*1.6A - Bond Lengths (Å) for *mer*-[$OsBr_3(PPr^n_3)_3$]

Os-P(1)	2.374(5)
Os-P(3)	2.427(7)
Os-P(2)	2.435(7)
Os-Br(3)	2.498(3)
Os-Br(1)	2.511(3)
Os-Br(2)	2.574(2)
P(1)-C(11)	1.820(10)
P(1)-C(14)	1.830(9)
P(1)-C(17)	1.834(10)
C(11)-C(12')	1.529(10)
C(11)-C(12)	1.534(10)
C(12)-C(13)	1.545(10)
C(12')-C(13)	1.546(10)

C(14)-C(15)	1.529(9)
C(15)-C(16)	1.534(10)
C(17)-C(18)	1.532(10)
C(17)-C(18')	1.536(10)
C(18)-C(19)	1.540(10)
C(18')-C(19')	1.537(10)
P(2)-C(24)	1.816(9)
P(2)-C(21)	1.828(9)
P(2)-C(27)	1.830(10)
C(21)-C(22)	1.526(9)
C(22)-C(23)	1.535(10)
C(24)-C(25)	1.525(10)
C(24)-C(25')	1.530(10)

C(25)-C(26)	1.558(10)
C(25')-C(26)	1.547(10)
C(27)-C(28)	1.542(9)
C(28)-C(29)	1.538(10)
P(3)-C(37)	1.826(9)
P(3)-C(31)	1.832(9)
P(3)-C(34)	1.834(9)
C(31)-C(32)	1.540(9)
C(32)-C(33)	1.536(10)
C(34)-C(35)	1.542(9)
C(35)-C(36)	1.529(9)
C(37)-C(38)	1.547(9)
C(38)-C(39)	1.535(9)

Table *A*1.6B - Bond Angles (°) for *mer*-[$OsBr_3(PPr^n_3)_3$]

P(1)-Os-P(3)	95.3(2)
P(1)-Os-P(2)	95.9(2)
P(3)-Os-P(2)	167.0(2)
P(1)-Os-Br(3)	95.3(2)
P(3)-Os-Br(3)	86.8(2)
P(2)-Os-Br(3)	85.8(2)
P(1)-Os-Br(1)	82.7(2)
P(3)-Os-Br(1)	93.4(2)
P(2)-Os-Br(1)	94.4(2)
Br(3)-Os-Br(1)	178.02(10)
P(1)-Os-Br(2)	171.1(2)
P(3)-Os-Br(2)	85.7(2)
P(2)-Os-Br(2)	84.2(2)
Br(3)-Os-Br(2)	93.57(9)
Br(1)-Os-Br(2)	88.41(9)
C(11)-P(1)-C(14)	114.4(10)
C(11)-P(1)-C(17)	103.9(10)
C(14)-P(1)-C(17)	98.1(14)
C(11)-P(1)-Os	115.5(11)

C(14)-P(1)-Os	111.4(5)
C(17)-P(1)-Os	111.9(8)
C(12')-C(11)-P(1)	118.1(9)
C(12)-C(11)-P(1)	117.4(9)
C(11)-C(12)-C(13)	109.6(10)
C(11)-C(12')-C(13)	109.9(10)
C(15)-C(14)-P(1)	117.4(8)
C(14)-C(15)-C(16)	110.9(9)
C(18)-C(17)-P(1)	117.1(9)
C(18')-C(17)-P(1)	116.7(9)
C(17)-C(18)-C(19)	109.9(10)
C(17)-C(18')-C(19')	110.1(10)
C(24)-P(2)-C(21)	106.7(10)
C(24)-P(2)-C(27)	98.4(11)
C(21)-P(2)-C(27)	107.0(8)
C(24)-P(2)-Os	115.4(8)
C(21)-P(2)-Os	112.4(6)
C(27)-P(2)-Os	115.6(9)
C(22)-C(21)-P(2)	117.7(9)

C(21)-C(22)-C(23)	110.8(10)
C(25)-C(24)-P(2)	118.6(9)
C(25')-C(24)-P(2)	118.3(9)
C(24)-C(25)-C(26)	108.9(9)
C(24)-C(25')-C(26)	109.2(9)
C(28)-C(27)-P(2)	116.2(8)
C(29)-C(28)-C(27)	109.7(9)
C(37)-P(3)-C(31)	102.2(10)
C(37)-P(3)-C(34)	101.9(11)
C(31)-P(3)-C(34)	100.4(9)
C(37)-P(3)-Os	112.0(5)
C(31)-P(3)-Os	119.6(9)
C(34)-P(3)-Os	118.1(9)
C(32)-C(31)-P(3)	116.6(9)
C(33)-C(32)-C(31)	110.4(9)
C(35)-C(34)-P(3)	115.8(9)
C(36)-C(35)-C(34)	110.8(9)
C(38)-C(37)-P(3)	116.4(8)
C(39)-C(38)-C(37)	109.8(9)

*A*1.3 Structure of *mer*-[$OsCl_3(AsMe_2Ph)_3$]

The complex was synthesised as described in Chapter 6, by the reaction of OsO_4 with $AsMe_2Ph$ in an ethanolic/HCl solution. Crystals were obtained from the reaction mixture left at low temperature. Table *A*1.7 presents the crystal refinement details.

Table *A*1.7 - Crystal Data and Structure Refinement for *mer*-[$OsCl_3(AsMe_2Ph)_3$]

Empirical formula	$C_{24}H_{33}As_3Cl_3Os$
Formula weight	842.81
Temperature	220(2)K
Wavelength	0.71073 Å
Crystal system	Orthorhombic
Space group	Pbca
Unit cell dimensions	a = 10.4591(8)Å, α = 90°.
	b = 16.8448(13)Å β = 90°.
	c = 31.965(4)Å γ = 90°
Volume	5631.6(9)$Å^3$
Z	8
Density (calculated)	1.988 Mgm^{-3}
Absorption coefficient	8.323 mm^{-1}
F(000)	3224
Crystal description	Red tablet
Crystal size	0.39 x 0.31 x 0.19 mm
Theta range for data collection	2.50°to 25.02°
Index ranges	$-1 \le h \le 12$, $0 \le k \le 20$, $0 \le l \le 38$
Reflections collected	8838
Independent reflections	4959 [$R_{int} = 0.0643$]
Scan type	omega
Absorption correction	Psi-scans ($T_{min} = 0.020$, $T_{max} = 0.055$
Data / restraints / parameters	4944/0/281 (Full-matrix least-squares on F^2)
Goodness of fit on F^2	1.008
Conventional R [F>4sigma(F)]	$R_1 = 0.0562$ [2834 data]
R indices (all data)	$R_1 = 0.1220$, $wR_2 = 0.1292$
Extinction coefficient	0.00028(4)
Final maximum delta/sigma	-0.001
Weighting scheme	calc $w=1/[s^{-2}(Fo^2)+(0.0565P)^2 + 0.0000P]$
	where $P=(Fo^2 + 2Fc^2)/3$
Largest diff. peak and hole	1.497 and -1.198 e.$Å^{-3}$

As before the structure was solved by direct methods, and all non-hydrogen atoms were refined anisotropically. Figure *A*1.3 shows the structure of the complex, while Table *A*1.8 lists the atomic positions and Table *A*1.9 the bond lengths and angles.

Table *A*1.8 - Atomic Coordinates ($x10^4$) and Equivalent Isotropic Displacement Parameters ($Å^2x10^3$) for *mer*-$[OsCl_3(AsMe_2Ph)_3]$

	x	y	z	U(eq)
Os(1)	-502(1)	2527(1)	1409(1)	28(1)
Cl(1)	-1068(4)	3766(2)	1744(1)	42(1)
Cl(2)	648(4)	3245(2)	891(1)	43(1)
Cl(3)	-1583(3)	1776(2)	1919(1)	40(1)
As(1)	164(1)	1328(1)	1036(1)	34(1)
C(11)	-612(13)	1126(7)	481(4)	35(3)
C(21)	-553(13)	1719(8)	184(4)	44(4)
C(31)	-1104(13)	1579(9)	-200(4)	44(4)
C(41)	-1704(14)	893(8)	-288(4)	42(4)
C(51)	-1783(13)	315(7)	22(4)	40(4)
C(61)	-1233(14)	440(8)	405(4)	43(4)
C(71)	1972(13)	1319(10)	879(5)	63(5)
C(81)	-27(17)	320(7)	1320(4)	59(5)
As(2)	1357(1)	2538(1)	1888(1)	33(1)
C(12)	2282(13)	1558(7)	2007(4)	35(3)
C(22)	1620(16)	990(7)	2251(4)	45(4)
C(32)	2245(17)	274(10)	2365(5)	61(5)
C(42)	3501(17)	165(10)	2226(5)	59(5)
C(52)	4095(16)	722(9)	1989(4)	54(4)
C(62)	3499(14)	1417(9)	1883(4)	46(4)
C(72)	907(14)	2854(8)	2449(4)	45(4)
C(82)	2708(14)	3273(8)	1747(4)	52(4)
As(3)	-2538(1)	2661(1)	1023(1)	32(1)
C(13)	-3463(12)	1746(8)	820(4)	33(3)
C(23)	-3967(13)	1732(8)	424(4)	40(4)
C(33)	-4710(15)	1077(8)	297(4)	53(4)
C(43)	-4933(14)	444(8)	566(5)	45(4)
C(53)	-4397(14)	462(8)	964(4)	49(4)
C(63)	-3670(13)	1106(8)	1095(4)	44(4)
C(73)	-2514(14)	3380(7)	555(4)	41(3)
C(83)	-3865(13)	3133(8)	1358(4)	44(4)

U(eq) is defined as one third of the trace of the orthogonalized Uij tensor

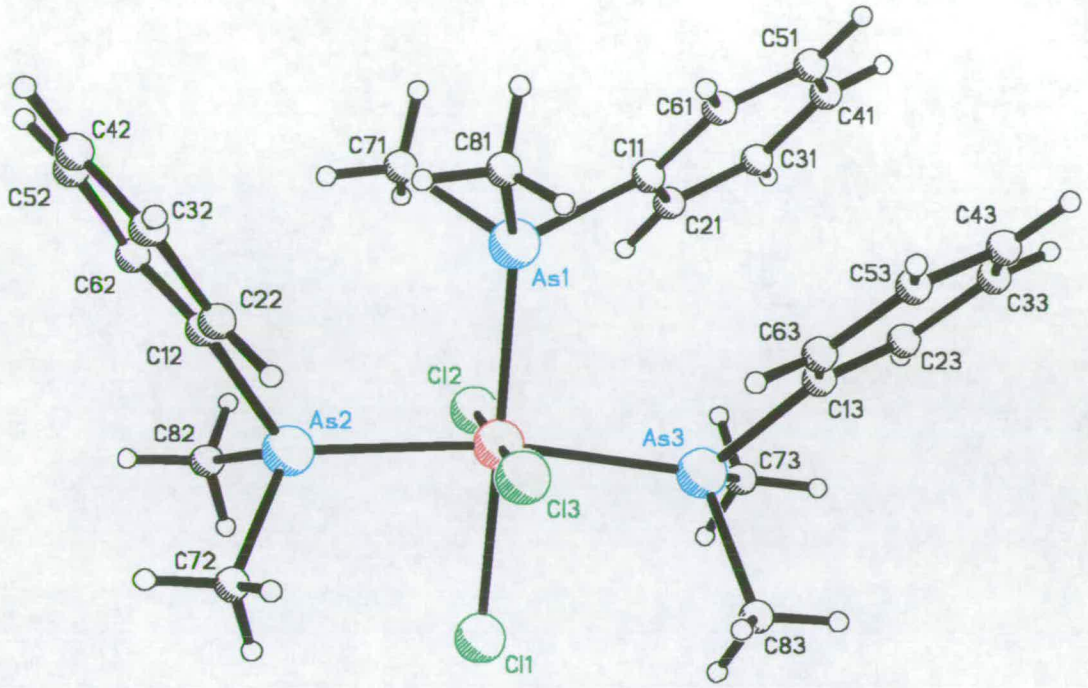

Figure *A*1.3 - Diagram of *mer*-[$OsCl_3(AsMe_2Ph)_3$]

Table *A*1.9A - Bond Lengths (Å) *mer*-[$OsCl_3(AsMe_2Ph)_3$]

Os(1)-Cl(3)	2.353(3)
Os(1)-Cl(2)	2.377(3)
Os(1)-Cl(1)	2.419(3)
Os(1)-As(1)	2.4459(14)
Os(1)-As(3)	2.4715(14)
Os(1)-As(2)	2.4739(13)
As(1)-C(81)	1.936(13)
As(1)-C(71)	1.957(13)
As(1)-C(11)	1.982(12)
C(11)-C(61)	1.35(2)
C(11)-C(21)	1.38(2)
C(21)-C(31)	1.38(2)
C(31)-C(41)	1.34(2)
C(41)-C(51)	1.39(2)
C(51)-C(61)	1.37(2)
As(2)-C(72)	1.929(12)
As(2)-C(82)	1.932(13)

As(2)-C(12)	1.952(13)
C(12)-C(62)	1.35(2)
C(12)-C(22)	1.42(2)
C(22)-C(32)	1.42(2)
C(32)-C(42)	1.40(2)
C(42)-C(52)	1.36(2)
C(52)-C(62)	1.37(2)
As(3)-C(73)	1.924(11)
As(3)-C(83)	1.926(13)
As(3)-C(13)	1.932(13)
C(13)-C(23)	1.37(2)
C(13)-C(63)	1.41(2)
C(23)-C(33)	1.41(2)
C(33)-C(43)	1.39(2)
C(43)-C(53)	1.39(2)
C(53)-C(63)	1.39(2)

Table *A* 1.9B- Bond Angles (°) for *mer*-[$OsCl_3(AsMe_2Ph)_3$]

Cl(3)-Os(1)-Cl(2)	177.81(12)
Cl(3)-Os(1)-Cl(1)	92.27(12)
Cl(2)-Os(1)-Cl(1)	89.60(12)
Cl(3)-Os(1)-As(1)	91.72(9)
Cl(2)-Os(1)-As(1)	86.41(10)
Cl(1)-Os(1)-As(1)	175.99(9)
Cl(3)-Os(1)-As(3)	88.89(9)
Cl(2)-Os(1)-As(3)	92.39(9)
Cl(1)-Os(1)-As(3)	86.06(9)
As(1)-Os(1)-As(3)	94.46(5)
Cl(3)-Os(1)-As(2)	87.34(9)
Cl(2)-Os(1)-As(2)	91.68(9)
Cl(1)-Os(1)-As(2)	84.95(9)
As(1)-Os(1)-As(2)	94.80(5)
As(3)-Os(1)-As(2)	170.10(5)
C(81)-As(1)-C(71)	102.4(7)
C(81)-As(1)-C(11)	103.1(6)
C(71)-As(1)-C(11)	99.4(6)
C(81)-As(1)-Os(1)	117.8(4)
C(71)-As(1)-Os(1)	114.0(4)
C(11)-As(1)-Os(1)	117.5(4)
C(61)-C(11)-C(21)	121.2(13)
C(61)-C(11)-As(1)	120.4(10)
C(21)-C(11)-As(1)	118.3(10)
C(31)-C(21)-C(11)	118.1(13)
C(41)-C(31)-C(21)	122.0(14)
C(31)-C(41)-C(51)	118.7(12)
C(61)-C(51)-C(41)	120.3(13)
C(11)-C(61)-C(51)	119.8(13)

C(72)-As(2)-C(82)	102.6(6)
C(72)-As(2)-C(12)	99.9(5)
C(82)-As(2)-C(12)	103.0(6)
C(72)-As(2)-Os(1)	112.7(4)
C(82)-As(2)-Os(1)	115.8(4)
C(12)-As(2)-Os(1)	120.3(4)
C(62)-C(12)-C(22)	120.2(14)
C(62)-C(12)-As(2)	123.8(11)
C(22)-C(12)-As(2)	115.9(10)
C(12)-C(22)-C(32)	119.3(15)
C(42)-C(32)-C(22)	117.6(17)
C(52)-C(42)-C(32)	121.1(16)
C(42)-C(52)-C(62)	121.4(16)
C(12)-C(62)-C(52)	120.4(16)
C(73)-As(3)-C(83)	100.4(6)
C(73)-As(3)-C(13)	104.3(5)
C(83)-As(3)-C(13)	99.0(6)
C(73)-As(3)-Os(1)	115.7(4)
C(83)-As(3)-Os(1)	112.4(4)
C(13)-As(3)-Os(1)	121.8(4)
C(23)-C(13)-C(63)	120.3(13)
C(23)-C(13)-As(3)	121.1(10)
C(63)-C(13)-As(3)	118.5(10)
C(13)-C(23)-C(33)	119.4(13)
C(43)-C(33)-C(23)	121.1(13)
C(33)-C(43)-C(53)	118.7(13)
C(63)-C(53)-C(43)	121.0(13)
C(53)-C(63)-C(13)	119.5(13)

*A*1.4 Structure Of *mer*-$[OsCl_3(PPr^n_3)_2(PEtPh_2)]$

The crystals were obtained from the reaction of *trans*-$[OsCl_4(PPr^n_3)_2]$ with excess $PEtPh_2$ in benzene (see experimental section). Table *A*1.10 shows the data for the studied crystal.

Table *A*1.10 - Crystal Data and Structure Refinement for *mer*-$[OsCl_3(PPr^n_3)_2(PEtPh_2)]$

Empirical formula	$C_{32}H_{57}Cl_3OsP_3$
Formula weight	831.24
Temperature	150(2)K
Wavelength	0.71073Å
Crystal system	Orthorhombic
Space group	Pbca
Unit cell dimensions	a = 15.799(3)Å, α = 90°.
	b = 19.644(4)Å, β = 90°.
	c = 23.934(6)Å, γ = 90°.
Volume	7428(3)Å^3
Z	8
Density (calculated)	1.487 Mg m^{-3}
Absorption coefficient	3.798 mm^{-1}
F(000)	3368
Crystal Shape and Colour	Orange wedge
Crystal size	0.51 x 0.39 x 0.31 mm
Theta range for data collection	2.58° to 25.00°.
Index ranges	$-18 \le h \le 17, 0 \le k \le 23, 0 \le l \le 28$
Reflections collected	12747
Independent reflections	6513 [R_{int} = 0.0532]
Refinement method	Full-matrix least-squares on F^2
Data / restraints / parameters	6506 / 0 / 359
Goodness-of-fit on F^2	1.034
Final R indices [I>2sigma(I)]	R1 = 0.0498, wR2 = 0.1092
R indices (all data)	R1 = 0.0774, wR2 = 0.1289
Largest diff. peak and hole	1.937 and -1.279 eÅ^{-3}

All non hydrogen atoms were refined anisotropically and the hydrogens themselves were fixed and allowed to move with their associated atoms. Figure *A*1.4 shows the structure of the complex and Tables *A*1.11, *A*1.12A and *A*1.12B show the details obtained from the structure.

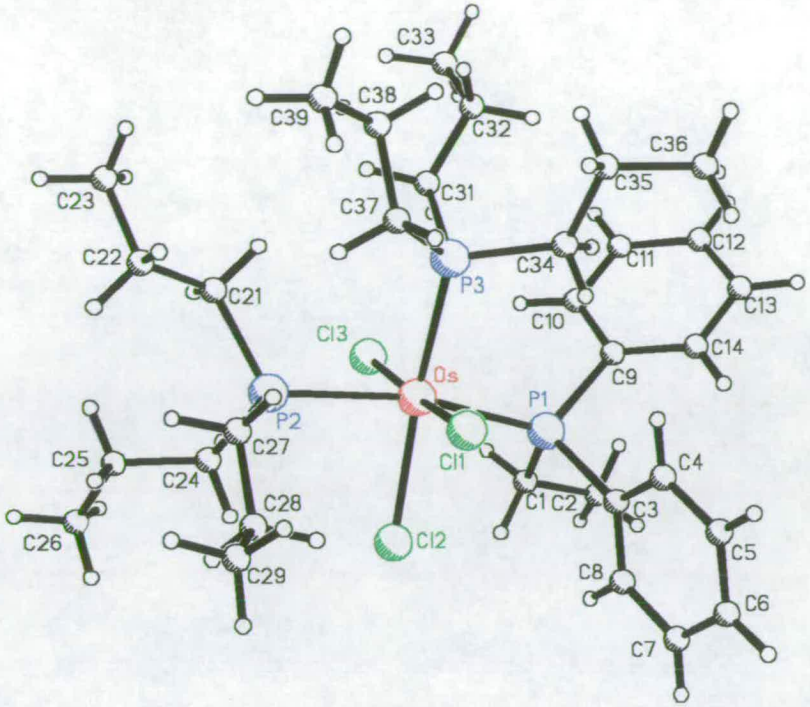

Figure *A*1.4 - Structure for *mer*-[$OsCl_3(PPr^n_3)_2(PEtPh_2)$]

Table *A*1.11 - Atomic Coordinates ($\times 10^4$) and Equivalent Isotropic Displacement Parameters ($Å^2 \times 10^3$) for *mer*-[$OsCl_3(PPr^n_3)_2(PEtPh_2)$]

	x	y	z	U(eq)
Os	1798(1)	2117(1)	1782(1)	33(1)
Cl(1)	3240(1)	2405(1)	1771(1)	46(1)
Cl(2)	1430(2)	3321(1)	1783(1)	43(1)
Cl(3)	381(1)	1732(1)	1759(1)	40(1)
P(1)	1646(2)	2297(1)	2777(1)	38(1)
P(2)	1684(2)	2180(1)	785(1)	41(1)
P(3)	2359(2)	994(1)	1806(1)	38(1)
C(1)	633(6)	2714(5)	2942(4)	46(2)
C(2)	421(6)	2777(5)	3567(4)	50(2)
C(3)	2433(6)	2860(5)	3085(4)	48(2)
C(4)	3274(6)	2651(4)	3139(4)	49(2)
C(5)	3895(7)	3065(5)	3349(5)	66(3)
C(6)	3690(7)	3703(6)	3509(5)	70(3)
C(7)	2868(7)	3951(6)	3445(5)	73(4)
C(8)	2252(6)	3519(4)	3224(5)	57(3)
C(9)	1553(6)	1574(4)	3265(3)	40(2)
C(10)	927(6)	1103(4)	3149(4)	45(2)
C(11)	788(7)	565(5)	3503(4)	50(2)
C(12)	1280(8)	478(5)	3967(4)	58(3)
C(13)	1928(7)	931(5)	4085(4)	58(3)

	x	y	z	U(eq)
C(14)	2049(7)	1484(5)	3730(4)	50(3)
C(21)	1383(8)	1367(5)	425(4)	64(3)
C(22)	1688(13)	1232(7)	-124(5)	118(7)
C(23)	1262(13)	543(7)	-335(6)	131(7)
C(24)	801(6)	2738(4)	587(3)	46(2)
C(25)	607(7)	2823(6)	-19(4)	61(3)
C(26)	-112(9)	3329(6)	-122(5)	87(4)
C(27)	2599(7)	2536(6)	415(4)	60(3)
C(28)	2755(8)	3266(6)	533(5)	70(3)
C(29)	3606(8)	3504(8)	267(7)	113(6)
C(31)	1562(7)	306(5)	1806(5)	56(3)
C(32)	1721(8)	-367(6)	2053(6)	81(4)
C(33)	942(8)	-829(5)	2032(7)	96(5)
C(34)	2983(6)	844(5)	2429(4)	47(2)
C(35)	3613(7)	257(5)	2486(5)	57(3)
C(36)	3935(6)	201(5)	3073(4)	61(3)
C(37)	3108(7)	816(5)	1236(4)	54(3)
C(38)	3209(9)	101(6)	1041(5)	79(4)
C(39)	3818(8)	44(6)	541(4)	79(4)

Table *A*1.12A - Bond Lengths (Å) for *mer*-[$OsCl_3(PPr^n_3)_2(PEtPh_2)$]

Os-Cl(1)	2.348(2)
Os-Cl(3)	2.364(2)
Os-P(3)	2.377(2)
Os-P(2)	2.395(2)
Os-P(1)	2.421(2)
Os-Cl(2)	2.436(2)
P(1)-C(3)	1.820(10)
P(1)-C(1)	1.840(9)
P(1)-C(9)	1.843(8)
P(2)-C(27)	1.834(10)
P(2)-C(24)	1.837(9)
P(2)-C(21)	1.875(10)
P(3)-C(34)	1.811(9)
P(3)-C(37)	1.838(10)

P(3)-C(31)	1.848(10)
C(1)-C(2)	1.539(12)
C(3)-C(8)	1.367(12)
C(3)-C(4)	1.397(13)
C(4)-C(5)	1.371(13)
C(5)-C(6)	1.351(14)
C(6)-C(7)	1.40(2)
C(7)-C(8)	1.395(14)
C(9)-C(14)	1.374(12)
C(9)-C(10)	1.384(13)
C(10)-C(11)	1.373(12)
C(11)-C(12)	1.365(14)
C(12)-C(13)	1.39(2)

C(13)-C(14)	1.392(13)
C(21)-C(22)	1.43(2)
C(22)-C(23)	1.59(2)
C(24)-C(25)	1.492(12)
C(25)-C(26)	1.53(2)
C(27)-C(28)	1.48(2)
C(28)-C(29)	1.56(2)
C(31)-C(32)	1.470(14)
C(32)-C(33)	1.53(2)
C(34)-C(35)	1.529(12)
C(35)-C(36)	1.499(14)
C(37)-C(38)	1.490(13)
C(38)-C(39)	1.54(2)

Table *A*1.12B - Bond Angles (°) for *mer*-[$OsCl_3(PPr^n_3)_2(PEtPh_2)$]

Cl(1)-Os-Cl(3)	174.94(7)
Cl(1)-Os-P(3)	82.09(8)
Cl(3)-Os-P(3)	93.26(8)
Cl(1)-Os-P(2)	92.89(9)
Cl(3)-Os-P(2)	85.56(8)
P(3)-Os-P(2)	95.77(8)
Cl(1)-Os-P(1)	94.10(8)
Cl(3)-Os-P(1)	88.56(8)
P(3)-Os-P(1)	98.54(8)
P(2)-Os-P(1)	164.81(8)
Cl(1)-Os-Cl(2)	89.85(8)
Cl(3)-Os-Cl(2)	94.85(8)
P(3)-Os-Cl(2)	171.79(8)
P(2)-Os-Cl(2)	86.14(8)
P(1)-Os-Cl(2)	80.41(7)
C(3)-P(1)-C(1)	103.7(4)
C(3)-P(1)-C(9)	105.4(4)
C(1)-P(1)-C(9)	98.0(4)
C(3)-P(1)-Os	114.8(3)
C(1)-P(1)-Os	111.2(3)

C(9)-P(1)-Os	121.2(3)
C(27)-P(2)-C(24)	104.2(5)
C(27)-P(2)-C(21)	107.7(5)
C(24)-P(2)-C(21)	101.4(5)
C(27)-P(2)-Os	116.2(3)
C(24)-P(2)-Os	110.2(3)
C(21)-P(2)-Os	115.6(3)
C(34)-P(3)-C(37)	103.2(5)
C(34)-P(3)-C(31)	104.5(5)
C(37)-P(3)-C(31)	107.4(5)
C(34)-P(3)-Os	112.0(3)
C(37)-P(3)-Os	113.5(3)
C(31)-P(3)-Os	115.1(3)
C(2)-C(1)-P(1)	115.7(6)
C(8)-C(3)-C(4)	117.0(9)
C(8)-C(3)-P(1)	122.1(8)
C(4)-C(3)-P(1)	120.6(7)
C(5)-C(4)-C(3)	122.7(9)
C(6)-C(5)-C(4)	118.9(10)
C(5)-C(6)-C(7)	121.0(10)
C(6)-C(7)-C(8)	118.7(10)

C(3)-C(8)-C(7)	121.5(9)
C(14)-C(9)-C(10)	119.0(8)
C(14)-C(9)-P(1)	124.6(7)
C(10)-C(9)-P(1)	116.4(7)
C(11)-C(10)-C(9)	120.4(9)
C(12)-C(11)-C(10)	120.5(10)
C(11)-C(12)-C(13)	120.4(9)
C(12)-C(13)-C(14)	118.6(9)
C(9)-C(14)-C(13)	121.1(10)
C(22)-C(21)-P(2)	119.7(10)
C(21)-C(22)-C(23)	107.8(13)
C(25)-C(24)-P(2)	118.3(7)
C(24)-C(25)-C(26)	112.5(9)
C(28)-C(27)-P(2)	114.2(8)
C(27)-C(28)-C(29)	110.9(11)
C(32)-C(31)-P(3)	122.8(8)
C(31)-C(32)-C(33)	112.5(10)
C(35)-C(34)-P(3)	123.4(7)
C(36)-C(35)-C(34)	111.1(9)
C(38)-C(37)-P(3)	118.8(8)
C(37)-C(38)-C(39)	112.3(10)

*A*1.5 Structure Of *mer*-[$OsCl_3(PPr^n_3)_2(AsPr^n_3)$]

Crystals suitable for X-ray analysis were obtained from the reaction mixture (See Experimental Section) on standing at low temperature. The data for the crystal used in analysis are shown in Table *A*1.13.

Table *A*1.13 - Crystal Data and Structure Refinement for *mer*-[$OsCl_3(PPr^n_3)_2(AsPr^n_3)$]

Empirical formula	$C_{27}H_{63}AsCl_3OsP_2$
Formula weight	821.18
Temperature	150(2)K
Wavelength	0.71073Å
Crystal system	Orthorhombic
Space group	$P2_12_12_1$
Unit cell dimensions	a = 13.232(8)Å, α = 90°
	b = 14.337(5)Å, β = 90°
	c = 18.611(11)Å, γ = 90°
Volume	3531(3)$Å^3$
Z	4
Density (calculated)	1.545 Mg m^{-3}
Absorption coefficient	.4.874 mm^{-1}
F(000)	1660
Crystal colour and shape	Red Block
Crystal size	0.35 x 0.27 x 0.23 mm
Theta range for data collection	2.61° to 25.06°.
Index ranges	$-15 \le h \le 15$, $0 \le k \le 17$, $0 \le l \le 22$.
Reflections collected	4532
Independent reflections	3594 [R_{int} = 0.0740]
Refinement method	Full-matrix least-squares on F^2
Data / restraints / parameters	3539 / 0 / 317
Goodness-of-fit on F^2	1.116
Final R indices [I>2sigma(I)]	R1 = 0.0521, wR2 = 0.1133
R indices (all data)	R1 = 0.0755, wR2 = 0.1691
Absolute structure parameter	0.10(3)
Largest diff. peak and hole	1.313 and -2.130 e.$Å^{-3}$

Direct Methods was used to solve the structure. All non hydrogen atoms were refined anisotropically, with hydrogen atoms fixed and allowed to ride on attached atoms. There were problems with scrambling between trans P(1) and As, occupancy 60%/40% and hence the components were fixed as having the same positions. Table *A*1.14 lists the atomic coordinates, and Figure *A*1.5 shows the structure of the complex.

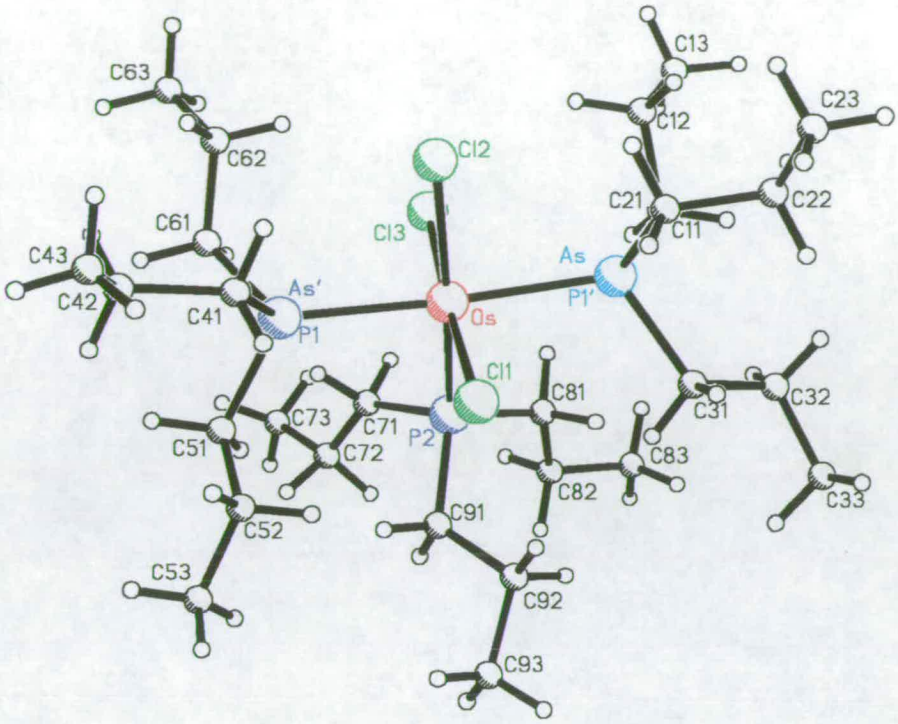

Figure *A*1.5 - Structure of *mer*-[$OsCl_3(PPr^n_3)_2(AsPr^n_3)$]

Table *A*1.14 - Atomic Coordinates ($\times 10^4$) and Equivalent isotropic Displacement Parameters ($Å^2 \times 10^3$) for *mer*-[$OsCl_3(PPr^n_3)_2(AsPr^n_3)$]

	x	y	z	U(eq)
Os	2381(1)	9070(1)	7440(1)	28(1)
As	3603(2)	10339(2)	7530(2)	38(1)
P(1)	1070(3)	7958(2)	7168(2)	37(1)
P(1')	3603(2)	10339(2)	7530(2)	38(1)
As'	1070(3)	7958(2)	7168(2)	37(1)
P(2)	2366(4)	8716(3)	8672(2)	30(1)
Cl(1)	1139(3)	10250(3)	7496(3)	34(1)
Cl(2)	2545(4)	9234(3)	6145(2)	36(1)
Cl(3)	3668(3)	7943(3)	7395(3)	40(1)
C(11)	4999(12)	10030(17)	7626(11)	55(6)
C(12)	5469(15)	9678(18)	6928(12)	58(7)
C(13)	6584(17)	9395(19)	7061(13)	69(7)
C(21)	3552(18)	11149(16)	6711(10)	49(6)
C(22)	4255(20)	11962(17)	6740(12)	66(7)
C(23)	4247(23)	12519(19)	6070(13)	74(8)
C(31)	3344(17)	11242(14)	8276(10)	41(5)
C(32)	4248(17)	11630(16)	8693(10)	51(6)
C(33)	3910(20)	12264(17)	9280(12)	59(6)

	x	y	z	U(eq)
C(41)	234(13)	8338(13)	6420(8)	34(4)
C(42)	-558(15)	7624(17)	6135(11)	51(6)
C(43)	-1201(18)	8069(20)	5555(12)	69(7)
C(51)	80(14)	7670(15)	7841(10)	45(5)
C(52)	-639(17)	8408(15)	8030(13)	55(6)
C(53)	-1336(20)	8133(19)	8650(14)	81(10)
C(61)	1505(17)	6756(15)	6897(10)	48(5)
C(62)	2093(17)	6716(14)	6190(10)	48(5)
C(63)	2514(19)	5800(12)	6047(10)	52(5)
C(71)	2377(26)	7533(14)	8839(9)	75(9)
C(72)	2049(23)	7010(18)	9379(17)	91(10)
C(73)	2397(32)	6002(17)	9443(15)	107(11)
C(81)	3439(12)	9097(18)	9134(9)	39(5)
C(82)	3596(20)	8870(16)	9942(10)	63(7)
C(83)	4479(19)	9346(19)	10247(13)	66(7)
C(91)	1338(13)	9093(15)	9184(9)	35(4)
C(92)	1231(15)	10081(15)	9400(9)	42(5)
C(93)	281(19)	10254(18)	9826(11)	56(7)

Table *A*1.15A - Bond Lengths (Å) for *mer*-[$OsCl_3(PPr^n_3)_2(AsPr^n_3)$]

Os-P(2)	2.348(4)
Os-Cl(3)	2.349(4)
Os-Cl(1)	2.361(4)
Os-P(1)	2.410(4)
Os-As'	2.410(4)
Os-Cl(2)	2.431(3)
Os-As	2.440(2)
Os-P(1')	2.440(2)
As-C(11)	1.91(2)
As-C(21)	1.92(2)
As-C(31)	1.93(2)
P(1)-C(51)	1.86(2)
P(1)-C(41)	1.86(2)
P(1)-C(61)	1.89(2)

P(1')-C(11)	1.91(2)
P(1')-C(21)	1.92(2)
P(1')-C(31)	1.93(2)
As'-C(51)	1.86(2)
As'-C(41)	1.86(2)
As'-C(61)	1.89(2)
P(2)-C(71)	1.72(2)
P(2)-C(91)	1.75(2)
P(2)-C(81)	1.75(2)
C(11)-C(12)	1.53(3)
C(12)-C(13)	1.55(3)
C(21)-C(22)	1.49(3)
C(22)-C(23)	1.48(3)
C(31)-C(32)	1.53(3)

C(32)-C(33)	1.49(3)
C(41)-C(42)	1.56(3)
C(42)-C(43)	1.51(3)
C(51)-C(52)	1.47(3)
C(52)-C(53)	1.53(3)
C(61)-C(62)	1.53(3)
C(62)-C(63)	1.45(3)
C(71)-C(72)	1.33(3)
C(72)-C(73)	1.52(3)
C(81)-C(82)	1.55(3)
C(82)-C(83)	1.47(3)
C(91)-C(92)	1.48(3)
C(92)-C(93)	1.51(3)

Table *A*1.15B - Bond Angles (°) for *mer*-[$OsCl_3(PPr^n_3)_2(AsPr^n_3)$]

P(2)-Os-Cl(3)	83.8(2)
P(2)-Os-Cl(1)	96.1(2)
Cl(3)-Os-Cl(1)	177.6(2)
P(2)-Os-P(1)	93.20(14)
Cl(3)-Os-P(1)	93.43(14)
Cl(1)-Os-P(1)	88.98(14)
P(2)-Os-As'	93.20(14)
Cl(3)-Os-As'	93.43(14)
Cl(1)-Os-As'	88.98(14)
P(1)-Os-As'	0.0(2)
P(2)-Os-Cl(2)	171.7(2)
Cl(3)-Os-Cl(2)	88.1(2)
Cl(1)-Os-Cl(2)	92.1(2)
P(1)-Os-Cl(2)	85.45(13)
As'-Os-Cl(2)	85.45(13)
P(2)-Os-As	95.7(2)
Cl(3)-Os-As	92.00(14)
Cl(1)-Os-As	85.62(11)
P(1)-Os-As	170.02(11)
As'-Os-As	170.02(11)
Cl(2)-Os-As	86.37(13)
P(2)-Os-P(1')	95.7(2)
Cl(3)-Os-P(1')	92.00(14)
Cl(1)-Os-P(1')	85.62(11)
P(1)-Os-P(1')	170.02(11)
As'-Os-P(1')	170.02(11)
Cl(2)-Os-P(1')	86.37(13)
As-Os-P(1')	0.0(2)
C(11)-As-C(21)	104.4(11)

C(11)-As-C(31)	105.1(9)
C(21)-As-C(31)	99.2(8)
C(11)-As-Os	118.3(8)
C(21)-As-Os	112.0(7)
C(31)-As-Os	115.6(6)
C(51)-P(1)-C(41)	98.7(8)
C(51)-P(1)-C(61)	101.1(10)
C(41)-P(1)-C(61)	104.4(8)
C(51)-P(1)-Os	120.9(6)
C(41)-P(1)-Os	113.0(6)
C(61)-P(1)-Os	116.1(7)
C(11)-P(1')-C(21)	104.4(11)
C(11)-P(1')-C(31)	105.1(9)
C(21)-P(1')-C(31)	99.2(8)
C(11)-P(1')-Os	118.3(8)
C(21)-P(1')-Os	112.0(7)
C(31)-P(1')-Os	115.6(6)
C(51)-As'-C(41)	98.7(8)
C(51)-As'-C(61)	101.1(10)
C(41)-As'-C(61)	104.4(8)
C(51)-As'-Os	120.9(6)
C(41)-As'-Os	113.0(6)
C(61)-As'-Os	116.1(7)
C(71)-P(2)-C(91)	102.3(13)
C(71)-P(2)-C(81)	102.2(12)
C(91)-P(2)-C(81)	105.5(7)
C(71)-P(2)-Os	112.9(6)
C(91)-P(2)-Os	118.2(6)
C(81)-P(2)-Os	114.0(7)
C(12)-C(11)-As	113.1(13)

C(12)-C(11)-P(1')	113.1(13)
As-C(11)-P(1')	0.0(3)
C(11)-C(12)-C(13)	110(2)
C(22)-C(21)-As	115(2)
C(22)-C(21)-P(1')	115(2)
As-C(21)-P(1')	0.0(2)
C(23)-C(22)-C(21)	113(2)
C(32)-C(31)-As	118(2)
C(32)-C(31)-P(1')	118(2)
As-C(31)-P(1')	0.0(2)
C(33)-C(32)-C(31)	111(2)
C(42)-C(41)-P(1)	117.6(13)
C(42)-C(41)-As'	117.6(13)
P(1)-C(41)-As'	0.0(3)
C(43)-C(42)-C(41)	110(2)
C(52)-C(51)-P(1)	117(2)
C(52)-C(51)-As'	117(2)
P(1)-C(51)-As'	0.0(3)
C(51)-C(52)-C(53)	113(2)
C(62)-C(61)-P(1)	114.9(14)
C(62)-C(61)-As'	114.9(14)
P(1)-C(61)-As'	0.0(3)
C(63)-C(62)-C(61)	113(2)
C(72)-C(71)-P(2)	134(2)
C(71)-C(72)-C(73)	120(3)
C(82)-C(81)-P(2)	121(2)
C(83)-C(82)-C(81)	113(2)
C(92)-C(91)-P(2)	121(2)
C(91)-C(92)-C(93)	112(2)

*A*1.6 Structure of *mer*-$[OsCl_3(P(OMe)_2Ph)_2(AsPr^n_3)]$

The complex was prepared by the reaction of *trans*-$[OsCl_4(AsPr^n_3)_2]$ with excess $P(OMe)_2Ph$ in benzene. Crystals suitable for diffraction were obtained from the reaction mixture in ethanol. Table *A*1.16 details the crystal and refinement parameters.

Table *A*1.16 - Crystal Data and Structure Refinement for *mer*-$[OsCl_3(P(OMe)_2Ph)_2(AsPr^n_3)]$

Empirical formula	$C_{25}H_{43}AsCl_3O_4OsP_2$ + $C_{0.8}H_{2.4}O_{0.4}$ solvate
Formula weight	859.43
Temperature	220.0(2)K
Wavelength	0.71073Å
Crystal system	Monoclinic
Space group	$P2_1/n$
Unit cell dimensions	a = 12.613(3)Å α = 90°
	b = 15.112(4)Å β= 92.74(3)°
	c = 17.930(9)Å γ = 90°
Volume	3414(2)Å^3
Z	4
Density (calculated)	1.672 Mgm^{-3}
Absorption coefficient	5.055 mm^{-1}
F(000)	1702
Crystal description	Orange lath
Crystal size	0.39 x 0.16 x 0.04 mm
Theta range for data collection	2.64° to 25.04°
Index ranges	$-15 \le h \le 14, 0 \le k \le 17, 0 \le l \le 21$
Reflections collected	7751
Independent reflections	6000 [R_{int} = 0.0673]
Scan type	Omega 2θ
Absorption correction	Psi-scans (T_{min} = 0.063, T_{max} = 0.101)
Data / restraints / parameters	5983/3/340 (Full-matrix least-squares on F^2)
Goodness-of-fit on F^2	0.979
Conventional R [F>4sigma(F)]	R1 = 0.0474 [3949 data]
R indices (all data)	R1 = 0.0928, wR2 = 0.0918
Final maximum delta/sigma	0.093
Weighting scheme	calc w=1/[s^{-2}(Fo^2)+(0.0340P)^2+0.0000P]
	where P=(Fo^2+2Fc^2^)/3
Largest diff. peak and hole	0.734 and -0.751 eÅ^{-3}

The structure was solved by direct methods and all non-hydrogen atoms were refined anisotropically. Table *A*1.17 shows the atomic positions in the structure given in Figure *A*1.6 whilst Tables *A*1.18A and B detail the bond lengths and angles.

Table *A*1.17 - Atomic Coordinates (x 10^4) and Equivalent Isotropic Displacement Parameters (Å^2 x 10^3) for *mer*-[$OsCl_3(P(OMe)_2Ph)_2(AsPr^n_3)$]

	x	y	z	U(eq)
Os	5577(1)	1647(1)	8099(1)	28(1)
Cl(1)	6559(2)	344(2)	8466(1)	37(1)
Cl(2)	5560(2)	1169(2)	6842(1)	41(1)
Cl(3)	5485(2)	2239(2)	9311(1)	39(1)
As	4688(1)	2989(1)	7570(1)	39(1)
C(1)	5453(7)	3501(7)	6749(6)	57(3)
C(2)	4967(10)	4232(8)	6318(7)	86(4)
C(3)	5748(11)	4670(11)	5825(8)	143(8)
C(4)	3238(7)	2920(7)	7130(6)	52(3)
C(5)	3089(7)	2265(7)	6519(6)	53(3)
C(6)	1949(8)	2299(7)	6166(6)	60(3)
C(7)	4624(7)	4002(6)	8226(6)	52(3)
C(8)	3683(9)	4108(8)	8649(7)	72(4)
C(9)	3697(10)	4864(8)	9208(7)	91(4)
P(1)	7236(2)	2338(2)	8033(1)	31(1)
O(11)	7145(4)	3380(4)	8176(3)	41(2)
C(11)	8047(7)	3937(6)	8402(6)	55(3)
O(21)	8182(4)	2008(4)	8602(3)	33(1)
C(21)	8092(7)	1928(7)	9385(5)	50(3)
C(1R1)	7961(6)	2206(6)	7194(5)	31(2)
C(2R1)	8217(6)	1362(6)	6977(5)	37(2)
C(3R1)	8762(7)	1223(7)	6336(6)	49(3)
C(4R1)	9059(7)	1928(7)	5902(5)	51(3)
C(5R1)	8814(8)	2775(8)	6111(6)	54(3)
C(6R1)	8236(6)	2913(6)	6753(5)	41(2)
P(2)	4027(2)	819(2)	8350(1)	34(1)
O(12)	3607(4)	67(4)	7780(3)	44(2)
C(12)	4274(7)	-635(6)	7553(6)	51(3)
O(22)	4286(4)	344(4)	9129(3)	41(2)
C(22)	3528(7)	-186(7)	9510(6)	56(3)
C(1R2)	2762(6)	1335(6)	8487(5)	37(2)
C(2R2)	1866(7)	1216(7)	8009(6)	50(3)
C(3R2)	931(8)	1641(9)	8128(8)	72(3)
C(4R2)	865(8)	2188(8)	8729(8)	76(4)
C(5R2)	1729(9)	2322(7)	9232(7)	67(4)
C(6R2)	2679(7)	1886(6)	9094(6)	48(3)
Disordered ethanol: Total occupancy = 0.8 molecules per complex molecule				
C(1E)	9615(11)	5365(7)	116(10)	108(6)
O(1E)	10293(23)	6137(12)	-66(18)	170(13)

U(eq) is defined as one third of the trace of the orthogonalized Uij tensor.

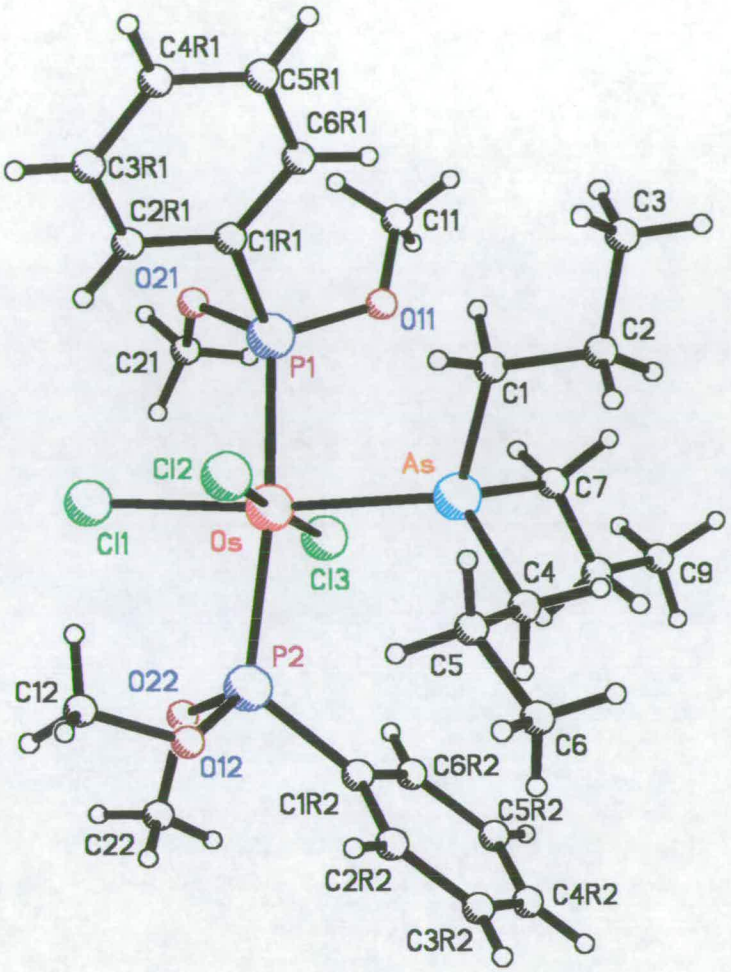

Figure *A*1.6 - Diagram of *mer*-[$OsCl_3(P(OMe)_2Ph)_2(AsPr^n_3)$]

Table *A*1.18A - Bond Lengths (Å) for *mer*-[$OsCl_3(P(OMe)_2Ph)_2(AsPr^n_3)$]

Os-As	2.4839(11)
Os-P(1)	2.347(2)
Os-P(2)	2.382(2)
Os-Cl(1)	2.401(2)
Os-Cl(2)	2.366(2)
Os-Cl(3)	2.357(2)
As-C(1)	1.958(9)
As-C(4)	1.959(9)
As-C(7)	1.935(10)
C(1)-C(2)	1.466(14)
C(2)-C(3)	1.51(2)
C(4)-C(5)	1.482(13)
C(5)-C(6)	1.544(12)

C(7)-C(8)	1.448(13)
C(8)-C(9)	1.519(14)
P(1)-O(11)	1.600(7)
P(1)-O(21)	1.611(6)
P(1)-C(1R1)	1.808(8)
O(11)-C(11)	1.456(9)
O(21)-C(21)	1.419(9)
C(1R1)-C(2R1)	1.376(12)
C(1R1)-C(6R1)	1.383(11)
C(2R1)-C(3R1)	1.383(11)
C(3R1)-C(4R1)	1.382(13)
C(4R1)-C(5R1)	1.373(13)
C(5R1)-C(6R1)	1.407(12)

P(2)-O(12)	1.602(6)
P(2)-O(22)	1.590(6)
P(2)-C(1R2)	1.804(8)
O(12)-C(12)	1.425(10)
O(22)-C(22)	1.443(10)
C(1R2)-C(6R2)	1.379(12)
C(1R2)-C(2R2)	1.397(12)
C(2R2)-C(3R2)	1.367(13)
C(3R2)-C(4R2)	1.36(2)
C(4R2)-C(5R2)	1.40(2)
C(5R2)-C(6R2)	1.400(12)
C(1E)-O(1E)	1.492(10)
C(1E)-C(1E)#1	1.540(10)

Table *A*1.18B - Bond Angles (°) for *mer*-[$OsCl_3(P(OMe)_2Ph)_2(AsPr^n_3)$]

As-Os-P(1)	90.26(6)
As-Os-P(2)	98.13(6)
As-Os-Cl(1)	172.66(6)
As-Os-Cl(2)	84.38(7)
As-Os-Cl(3)	90.05(7)
P(1)-Os-P(2)	170.10(8)
P(1)-Os-Cl(1)	85.96(8)
P(1)-Os-Cl(2)	93.18(8)
P(1)-Os-Cl(3)	87.76(8)
P(2)-Os-Cl(1)	86.25(8)
P(2)-Os-Cl(2)	92.85(8)
P(2)-Os-Cl(3)	87.00(8)
Cl(1)-Os-Cl(2)	89.54(8)
Cl(1)-Os-Cl(3)	96.08(8)
Cl(2)-Os-Cl(3)	174.36(8)
C(7)-As-C(1)	100.4(5)
C(7)-As-C(4)	102.8(4)
C(1)-As-C(4)	101.7(4)
C(7)-As-Os	116.4(3)
C(1)-As-Os	112.3(3)
C(4)-As-Os	120.4(3)
C(2)-C(1)-As	119.1(8)
C(1)-C(2)-C(3)	111.8(11)
C(5)-C(4)-As	114.6(7)
C(4)-C(5)-C(6)	111.3(8)
C(8)-C(7)-As	117.7(8)
C(7)-C(8)-C(9)	116.4(10)
O(11)-P(1)-O(21)	105.1(3)
O(11)-P(1)-C(1R1)	106.6(4)
O(21)-P(1)-C(1R1)	96.0(3)

O(11)-P(1)-Os	111.0(2)
O(21)-P(1)-Os	117.7(2)
C(1R1)-P(1)-Os	118.7(3)
C(11)-O(11)-P(1)	123.5(6)
C(21)-O(21)-P(1)	124.2(5)
C(2R1)-C(1R1)-C(6R1)	119.0(8)
C(2R1)-C(1R1)-P(1)	118.3(7)
C(6R1)-C(1R1)-P(1)	122.7(7)
C(1R1)-C(2R1)-C(3R1)	120.6(9)
C(2R1)-C(3R1)-C(4R1)	120.6(9)
C(5R1)-C(4R1)-C(3R1)	119.6(9)
C(4R1)-C(5R1)-C(6R1)	119.7(10)
C(1R1)-C(6R1)-C(5R1)	120.4(9)
O(22)-P(2)-O(12)	106.8(4)
O(22)-P(2)-C(1R2)	102.8(4)
O(12)-P(2)-C(1R2)	97.2(4)
O(22)-P(2)-Os	105.5(2)
O(12)-P(2)-Os	120.1(2)
C(1R2)-P(2)-Os	122.5(3)
C(12)-O(12)-P(2)	121.9(5)
C(22)-O(22)-P(2)	123.6(6)
C(6R2)-C(1R2)-C(2R2)	118.2(8)
C(6R2)-C(1R2)-P(2)	118.0(7)
C(2R2)-C(1R2)-P(2)	123.8(8)
C(3R2)-C(2R2)-C(1R2)	121.5(11)
C(4R2)-C(3R2)-C(2R2)	119.6(11)
C(3R2)-C(4R2)-C(5R2)	121.5(10)
C(4R2)-C(5R2)-C(6R2)	117.8(11)
C(1R2)-C(6R2)-C(5R2)	121.5(10)
O(1E)-C(1E)-C(1E)#1	97.2(13)

Symmetry transformations used to generate equivalent atoms: #1 -x+2,-y+1,-z

*A*1.7 Structure of *mer*-[$OsCl_3(PEt_2Ph)_3$]

Suitable crystals for crystallographic study were obtained from the reaction mixture at low temperature (see Chapter 6). Table *A*1.19 shows the details of the crystal and refinement.

Table *A*1.19 - Crystal Data and Structure Refinement for *mer*-[$OsCl_3(PEt_2Ph)_3$]

Empirical formula	$C_{30}H_{45}Cl_3OsP_3$
Formula weight	795.12
Temperature	296(2) K
Wavelength	0.71073Å
Crystal system	Monoclinic
Space group	$P2_1/n$
Unit cell dimensions	a = 12.380(3) Å, α = 90°
	b = 14.690(3) Å, β =& 92.01(3)°
	c: = 18.430(4) Å, γ = 90°
Volume	3349.7(12)Å^3
Z	4
Density (calculated)	1.577 Mg m^{-3}
Absorption coefficient	4.208 mm^{-1}
F(000)	1588
Crystal size	0.30 x 0.20 x 0.15 mm
θ range for data collection	2.61° to 22.50°
Limiting indices	$-14 \le h \le 14$, $0 \le k \le 17$, $0 \le l \le 21$
Reflections collected	5652
Independent reflections	4378 (R_{int} = 0.3263)
Absorption correction	None
Refinement method	Full-matrix least-squares on F^2
Data / restraints / parameters	4378 / 97 / 348
Goodness-of-fit on F^2	0.997
Final R indices [I>2σ(I)]	R1 = 0.0577, wR2 = 0.0740
R indices (all data)	R1 = 0.1413, wR2 = 0.0950
Largest diff. peak and hole	0.549 and -0.531 eÅ^{-3}

As before Direct Methods was employed to solve the structure, and all non-hydrogen atoms were refined anisotropically. C(33) was found to be disordered in the structure hence was therefore modelled over three sites. Figure *A*1.7 shows the structure whilst Table *A*1.20 lists the atomic positions and Tables *A*1.21A and B list the bond lengths and angles obtained from the structure.

Table *A*1.20 - Atomic Coordinates (x 10^4) and Equivalent Isotropic Displacement Parameters (Å^2 x 10^3) for *mer*-[$OsCl_3(PEt_2Ph)_3$]

	x	y	z	U(eq)
Os(1)	6806(1)	2017(1)	8206(1)	54(1)
Cl(1)	7067(4)	3594(2)	8097(3)	97(2)
Cl(2)	7056(3)	2082(3)	9522(2)	90(2)
Cl(3)	6564(3)	443(2)	8332(2)	59(1)
P(1)	6573(3)	1802(3)	6934(2)	60(1)
C(10)	7442(11)	920(9)	6569(7)	66(5)
C(11)	7238(13)	555(10)	5817(7)	96(6)
C(12)	6857(15)	2867(12)	6457(9)	131(8)
C(13)	7300(16)	2890(14)	5741(9)	166(9)
C(14)	5248(12)	1381(12)	6570(9)	77(5)
C(15)	4933(14)	536(13)	6806(9)	82(6)
C(16)	3992(17)	147(12)	6507(10)	109(7)
C(17)	3421(13)	618(16)	6006(10)	109(8)
C(18)	3682(18)	1458(15)	5776(11)	128(10)
C(19)	4631(16)	1844(14)	6063(11)	130(9)
P(2)	8767(3)	1848(3)	8215(2)	59(1)
C(20)	9278(12)	703(10)	8422(8)	81(5)
C(21)	9124(12)	381(12)	9188(8)	110(7)
C(22)	9432(11)	2557(10)	8906(8)	84(6)
C(23)	10644(12)	2541(12)	8948(8)	120(8)
C(24)	9534(10)	2187(9)	7421(7)	55(4)
C(25)	10126(12)	1583(9)	7017(8)	81(5)
C(26)	10717(13)	1892(12)	6439(8)	97(6)
C(27)	10729(14)	2792(11)	6299(9)	102(7)
C(28)	10136(12)	3416(10)	6647(8)	84(6)
C(29)	9570(11)	3097(9)	7239(7)	59(4)
P(3)	4940(4)	2358(3)	8426(3)	72(2)
C(30)	4245(12)	3044(14)	7697(9)	129(8)
C(31)	3179(16)	3441(16)	7881(16)	251(15)
C(32)	4755(14)	3068(12)	9260(10)	113(7)
C33a	5285(33)	3933(23)	9491(28)	82(18)
C33'b	3603(51)	3493(39)	9307(34)	115(31)
C33"c	4825(44)	4099(28)	9044(35)	38(20)
C(34)	4065(12)	1401(9)	8658(9)	63(5)
C(35)	4209(12)	975(11)	9321(9)	84(6)
C(36)	3541(16)	267(12)	9517(10)	101(7)
C(37)	2737(16)	12(14)	9059(12)	119(10)
C(38)	2583(13)	390(13)	8401(12)	118(8)
C(39)	3249(14)	1100(11)	8197(9)	85(6)

U(eq) is defined as one third of the trace of the orthogonalized U_{ij} tensor

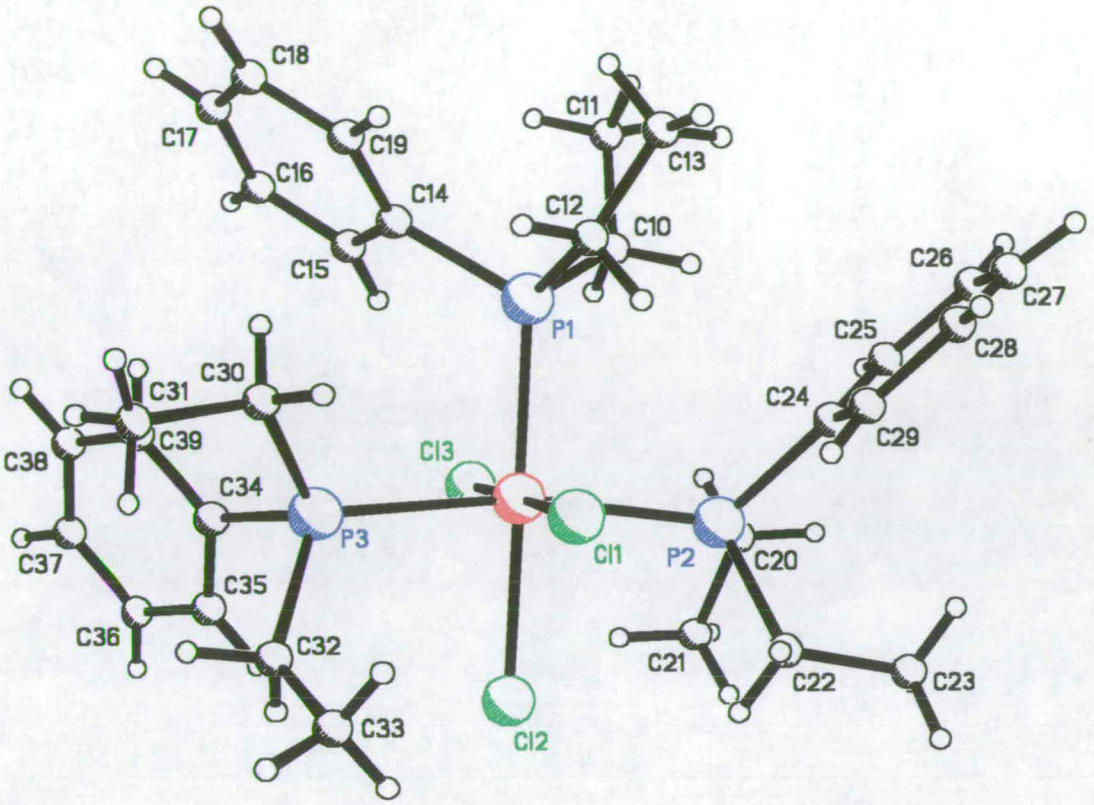

Figure *A*1.7 - Structure of *mer*-[$OsCl_3(PEt_2Ph)_3$]

Table *A*1.21A - Bond Lengths (Å) for *mer*-[$OsCl_3(PEt_2Ph)_3$]

Os(1)-Cl(3)	2.344(3)
Os(1)-Cl(1)	2.350(4)
Os(1)-P(1)	2.373(4)
Os(1)-P(3)	2.413(4)
Os(1)-Cl(2)	2.436(4)
Os(1)-P(2)	2.440(4)
P(1)-C(10)	1.826(12)
P(1)-C(12)	1.83(2)
P(1)-C(14)	1.86(2)
C(10)-C(11)	1.499(12)
C(12)-C(13)	1.446(13)
C(14)-C(19)	1.368(13)
C(14)-C(15)	1.376(12)
C(15)-C(16)	1.394(14)
C(16)-C(17)	1.337(13)
C(17)-C(18)	1.347(14)
C(18)-C(19)	1.392(14)
P(2)-C(22)	1.820(14)
P(2)-C(20)	1.833(15)
P(2)-C(24)	1.840(11)

C(20)-C(21)	1.507(13)
C(22)-C(23)	1.500(13)
C(24)-C(29)	1.380(12)
C(24)-C(25)	1.384(12)
C(25)-C(26)	1.389(13)
C(26)-C(27)	1.348(13)
C(27)-C(28)	1.350(12)
C(28)-C(29)	1.397(12)
P(3)-C(34)	1.835(14)
P(3)-C(30)	1.87(2)
P(3)-C(32)	1.88(2)
C(30)-C(31)	1.492(14)
C(32)-C33a	1.48(2)
C(32)-C33'b	1.56(6)
C(32)-C33"c	1.57(5)
C(34)-C(39)	1.370(13)
C(34)-C(35)	1.378(12)
C(35)-C(36)	1.385(13)
C(36)-C(37)	1.336(14)
C(37)-C(38)	1.342(14)
C(38)-C(39)	1.389(14)

Table *A*1.21B - Bond Angles (°) for *mer*-[$OsCl_3(PEt_2Ph)_3$]

Cl(3)-Os(1)-Cl(1)	179.0(2)
Cl(3)-Os(1)-P(1)	87.46(13)
Cl(1)-Os(1)-P(1)	93.4(2)
Cl(3)-Os(1)-P(3)	93.52(13)
Cl(1)-Os(1)-P(3)	86.82(14)
P(1)-Os(1)-P(3)	96.3(2)
Cl(3)-Os(1)-Cl(2)	87.2(2)
Cl(1)-Os(1)-Cl(2)	91.9(2)
P(1)-Os(1)-Cl(2)	174.6(2)
P(3)-Os(1)-Cl(2)	85.0(2)
Cl(3)-Os(1)-P(2)	91.73(14)
Cl(1)-Os(1)-P(2)	87.8(2)
P(1)-Os(1)-P(2)	94.58(14)
P(3)-Os(1)-P(2)	168.1(2)
Cl(2)-Os(1)-P(2)	84.60(14)
C(10)-P(1)-C(12)	107.6(7)
C(10)-P(1)-C(14)	98.9(7)
C(12)-P(1)-C(14)	107.0(9)
C(10)-P(1)-Os(1)	113.9(5)
C(12)-P(1)-Os(1)	110.0(6)
C(14)-P(1)-Os(1)	118.4(5)
C(11)-C(10)-P(1)	120.8(11)
C(13)-C(12)-P(1)	123(2)
C(19)-C(14)-C(15)	121(2)
C(19)-C(14)-P(1)	123(2)
C(15)-C(14)-P(1)	116.3(14)
C(14)-C(15)-C(16)	119.2(14)
C(17)-C(16)-C(15)	118(2)
C(16)-C(17)-C(18)	124(2)
C(17)-C(18)-C(19)	118(2)
C(14)-C(19)-C(18)	120(2)
C(22)-P(2)-C(20)	103.6(7)
C(22)-P(2)-C(24)	99.7(6)
C(20)-P(2)-C(24)	103.3(6)
C(22)-P(2)-Os(1)	111.9(5)
C(20)-P(2)-Os(1)	115.5(5)
C(24)-P(2)-Os(1)	120.5(5)
C(21)-C(20)-P(2)	115.5(11)
C(23)-C(22)-P(2)	117.0(11)
C(29)-C(24)-C(25)	117.9(11)
C(29)-C(24)-P(2)	118.5(9)
C(25)-C(24)-P(2)	123.5(10)
C(24)-C(25)-C(26)	120.4(12)
C(27)-C(26)-C(25)	118.5(13)
C(26)-C(27)-C(28)	124.4(14)
C(27)-C(28)-C(29)	116.1(13)
C(24)-C(29)-C(28)	122.4(12)
C(34)-P(3)-C(30)	108.7(9)
C(34)-P(3)-C(32)	98.3(7)
C(30)-P(3)-C(32)	102.9(8)
C(34)-P(3)-Os(1)	117.2(5)
C(30)-P(3)-Os(1)	114.3(5)
C(32)-P(3)-Os(1)	113.5(6)
C(31)-C(30)-P(3)	116(2)
C33a-C(32)-P(3)	130(2)
C33'b-C(32)-P(3)	114(3)
C33"c-C(32)-P(3)	109(2)
C(39)-C(34)-C(35)	118.2(13)
C(39)-C(34)-P(3)	122.1(13)
C(35)-C(34)-P(3)	119.7(13)
C(34)-C(35)-C(36)	120.8(14)
C(37)-C(36)-C(35)	119(2)
C(36)-C(37)-C(38)	122(2)
C(37)-C(38)-C(39)	119(2)
C(34)-C(39)-C(38)	120.4(14)

*A*1.8 - References

(1) G. M. Sheldrick, SHELXS-86, Programme for the Solution of Crystal Structures, University Of Göttingen, Germany.

(2) G. M. Sheldrick, SHELXS-86, Programme for the Refinement of Crystal Structures, University Of Göttingen, Germany.

(3) G. M. Sheldrick, SHELXTL/PC, Version 5.03 Siemens Analytical X-ray Instruments Inc., Madison, Wisconsin, USA, 1994.

(4) A. Altomare, G. Cascarano, L. Giacovazzo and A. Guaglirdi, SIR92, *J. Appl. Cryst.*, 1993, **26**, 343.

Courses and Conferences Attended

1. Crystal Structure Analysis, Postgraduate Lecture Course, Dr. A. J. Blake and Dr. S. Parsons
2. N.M.R., Postgraduate Lecture Course Dr. D. Reed.
3. 16th Annual Irvine Review Lectures, University Of St. Andrews, 12th November 1993.
4. Electrochem' 94, University Of Edinburgh, September 1994.*
5. Scottish, Dalton Meeting, Heriot Watt University, March 1994.
6. Butler Postgraduate Electrochemistry Meeting,
   June 1994, University Of St. Andrews
   June 1995, University of Strathclyde†
7. Royal Society of Chemistry Annual Congress, Heriot Watt University, April 1995.*
8. International ESR Conference, University Of Edinburgh 1996.

---

* Poster Presentation
† Oral Presentation